Géologie et géochimie des granitoides et des roches basique associées du Valsenestre : place dans la province magmatique varisque des massifs cristallins externes du Haut Dauphiné (Alpes occidentales françaises)

Richard Arthur Oliver

OLIVER (R.A)

THESE

PRESENTEE PAR

OLIVER Richard Arthur

POUR OBTENIR LE TITRE DE DOCTEUR

DE L'UNIVERSITE JOSEPH FOURIER - GRENOBLE 1

(ARRETES MINISTERIELS DU 5 JUILLET 1984 ET

DU 30 MARS 1992)

SPECIALITE: SCIENCES DE LA TERRE

GEOLOGIE ET GEOCHIMIE DES GRANITOIDES ET DES ROCHES BASIQUE ASSOCIEES DU VALSENESTRE: PLACE DANS LA PROVINCE MAGMATIQUE VARISQUE DES MASSIFS CRISTALLINS EXTERNES DU HAUT DAUPHINE. (ALPES OCCIDENTALES FRANCAIS)

Thèse soutenue le 25 novembre 1994 devant la commission d'examen:

M. M. PIBOULE	Professeur, Université Joseph Fourier, Grenoble	Directeur
M. J. DIDIER	Professeur, Université de Clermont Ferrand,	Rapporteur
M. J.A. PEARCE	Professeur, Université de Durham, Angleterre	Rapporteur
M. R.P. MENOT	Professeur, Université de Saint-Etienne	Examinateur
M.J. BRUANDET	Professeur, Institut des Sciences Nucleaires, Grenoble	Examinateur
M. F. DEBON	Chargé de Recherche, CNRS	Examinateur

THESE

PRESENTEE PAR

OLIVER Richard Arthur

POUR OBTENIR LE TITRE DE DOCTEUR

DE L'UNIVERSITE JOSEPH FOURIER - GRENOBLE 1

(ARRETES MINISTERIELS DU 5 JUILLET 1984 ET

DU 30 MARS 1992)

SPECIALITE: SCIENCES DE LA TERRE

GEOLOGIE ET GEOCHIMIE DES GRANITOIDES ET DES ROCHES BASIQUE ASSOCIEES DU VALSENESTRE: PLACE DANS LA PROVINCE MAGMATIQUE VARISQUE DES MASSIFS CRISTALLINS EXTERNES DU HAUT DAUPHINE. (ALPES OCCIDENTALES FRANCAIS)

Thèse soutenue le ** novembre 1994 devant la commission d'examen:

M. M. PIBOULE	**Professeur, Université Joseph Fourier, Grenoble**	**Directeur**
M. J. DIDIER	**Professeur, Université de Clermont Ferrand,**	**Rapporteur**
M. J.A. PEARCE	**Professeur, Université de Durham, Angleterre**	**Rapporteur**
M. R.P. MENOT	**Professeur, Université de Saint-Etienne**	**Examinateur**
M.J. BRUANDET	**Professeur, Institut des Sciences Nucleaires, Grenoble**	**Examinateur**
M. F. DEBON	**Chargé de Recherche, CNRS**	**Examinateur**

THESE

PRESENTEE PAR

OLIVER Richard Arthur

POUR OBTENIR LE TITRE DE DOCTEUR

DE L'UNIVERSITE JOSEPH FOURIER - GRENOBLE 1

(ARRETES MINISTERIELS DU 5 JUILLET 1984 ET

DU 30 MARS 1992)

SPECIALITE: SCIENCES DE LA TERRE

THE GEOLOGY AND GEOCHEMISTRY OF THE INTRUSIVE ROCKS OF THE VALSENESTRE REGION, AND THEIR CONTEXT WITHIN THE MAGMATIC PROVINCE OF THE HAUT DAUPHINE.

Thèse soutenue le ** novembre 1994 devant la commission d'examen:

M. M. PIBOULE	**Professeur, Université Joseph Fourier, Grenoble**	**Directeur**
M. J. DIDIER	**Professeur, Université de Clermont Ferrand,**	**Rapporteur**
M. J.A. PEARCE	**Professeur, Université de Durham, Angleterre**	**Rapporteur**
M. R.P. MENOT	**Professeur, Université de Saint-Etienne**	**Examinateur**
M.J. BRUANDET	**Professeur, Institut des Sciences Nucleaires, Grenoble**	**Examinateur**
M. F. DEBON	**Chargé de Recherche, CNRS**	**Examinateur**

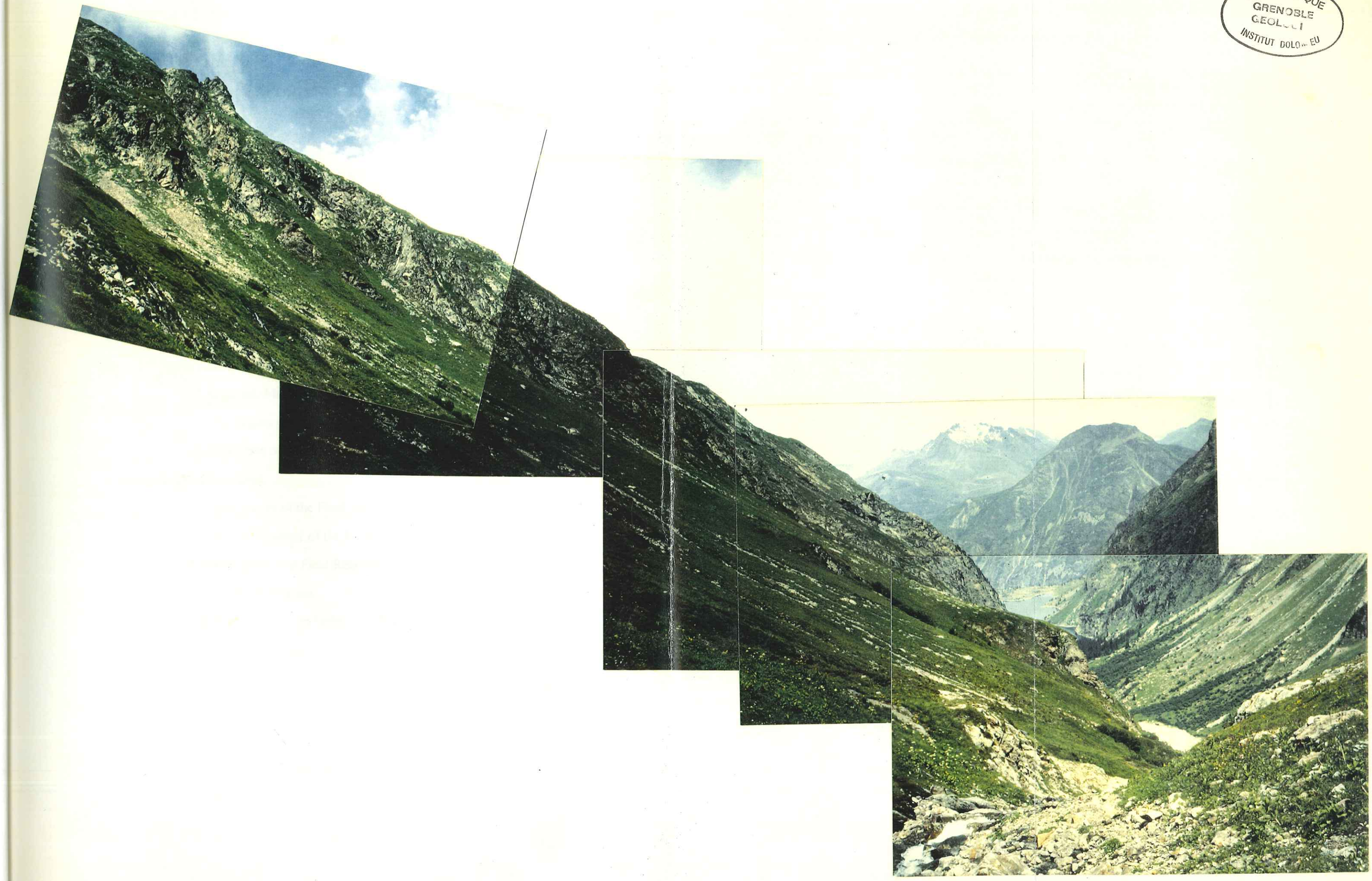

LIST OF CONTENTS

List of Plates

CHAPTER 1

THE WESTERN ALPINE MOUNTAIN CHAIN

1.1 INTRODUCTION

The western part of the Alpine Mountain complex forms an arcuate structure stretching for over a thousand kilometers from the Aar-Gotthard massifs in the north to Corsica in the south, and includes the massifs of Mont Blanc, Aiguilles Rouges, Belledonne, Grandes Rousses, Haut Dauphiné and Argentera. (see Fig 1.1)

These massifs consist of a series of crystalline rocks, mainly metamorphic in composition, but the central part of each of the massifs is formed by a series of intrusive igneous rocks for the most part granitic in composition. In general the nature of each of these massifs, consists of a central core made up of intrusive rocks ranging from granites to granodiorites with either monzonitic calc-alkaline or sub alkaline affinites(LeFort, 1973; Von Raumer, 1984; Vivier et al., 1984) to high-K syenites with probable alkaline affinites. These have been intruded, in two major phases, into a series of older volcano-sediments and granites which have been metamorphosed in general up to the greenschist-amphibolite facies but in some rare cases up to eclogite-granulite facies. These are surrounded by carbonates and sediments of the Upper

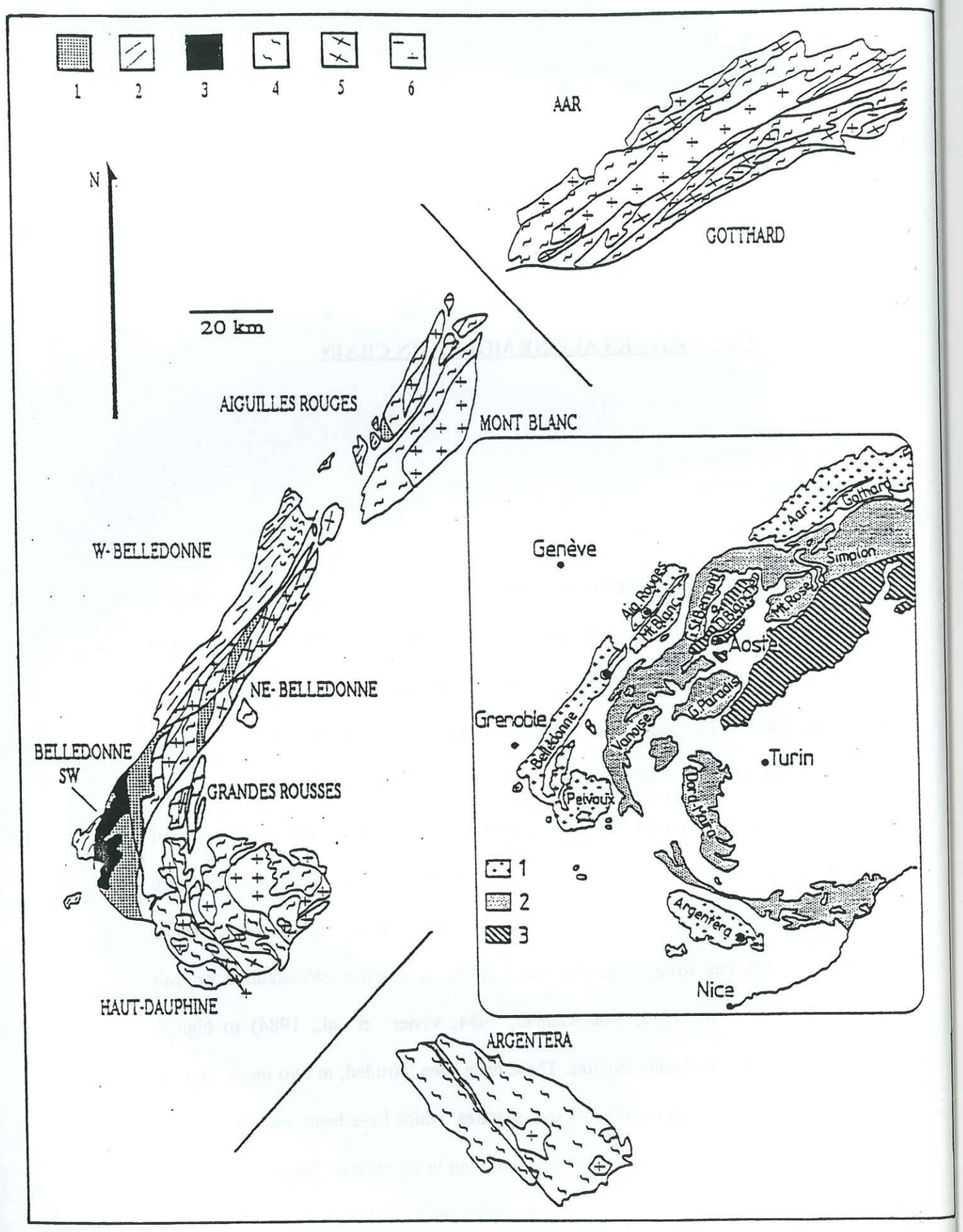

Figure 1.1 Structural and Lithological map of the ECMs: 1.Devonian to Lower carboniferous formations. 2. Metapelite Formations, Upper Proterozoic (?) to Lower Paleozoic. 3. Chamrousse Ophiolite (496 Ma) 4. Upper Proterozoic to Lower Paleozoic basement (Gneisses and amphibolites). 5.Lower Paleozoic to Upper Devonian Orthogneisses. 6. Lower Carboniferous granitoids.

Paleozoic-Mesozoic cover which have either slipped to the west along decollment planes (Siddens, 1983) to form the massifs of the pre-Alps e.g. The Bauges, Chartreuse, Vercors and Devoluy massifs in the south and west (Fig 1.2), or have been folded into immense nappes as in the case of the Morcles nappe in the Helvetic zone , or have been caught up in graben like structures, e.g. the Bourg d'Oisans syncline, which have subsequently undergone spectacular faulting and folding during the Alpine uplift period.(Barfety and Gidon, 1981,1983; Gratier and Vialon, 1980; Beach, 1981)

1.2 REGIONAL METAMORPHIC AND STRUCTURAL HISTORY

In the western part of the Alps, the basement relics occur in the Helvetic (Alpine external zone or Dauphiné zone) and the Penninic (Briançon and Piemont zones) domains. These are respectivly classified as the External and Internal Crystalline Massifs (ECMs and ICMs) and this summary will only deal with the ECMS, these being relevant to the subject of the thesis.

The ECMs appear as dome-like structures of crystalline basement unconformably covered by Upper Carboniferous (Westphalian D - Stephanian A), Permian and Triassic detrital sediments in an overstep sequence. They are considered as sub autochthonous and overriding their own sedimentary cover, towards the West and North-West (Bellieres, 1988). The overstep sequence consists of continental deposits (Debelmas and Kerckhove, 1980) associated with volcanics and pyroclastics of silicic and intermediate composition and having calk-alkaline affinities (Banzet et al., 1985; Shenker, 1986; Oberhansli et al., 1988; Mercolli and Oberhansli, 1988). These sequences express late Variscan rifting with pull apart and strike-slip tectonics related to the evolution of intramontane basins (Menard and Tapponnier, 1988).

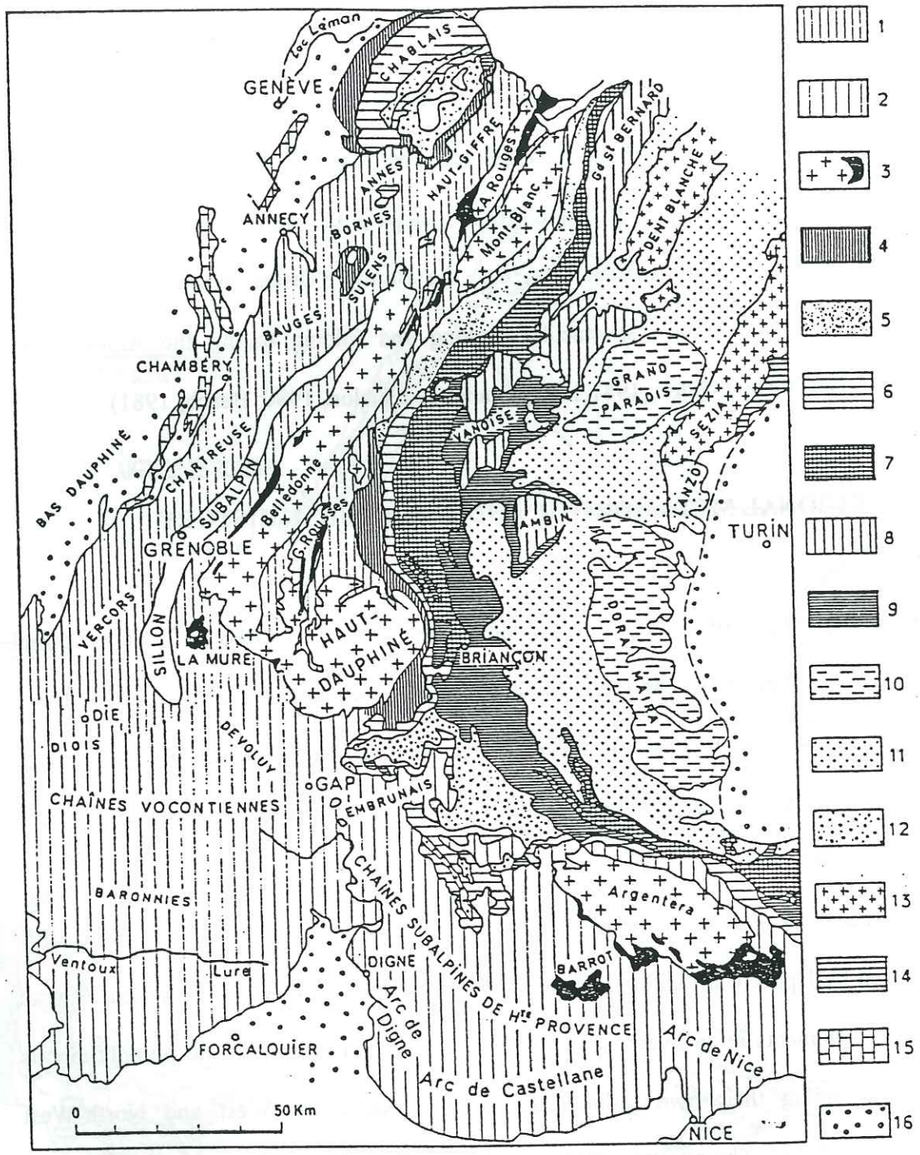

Figure 1.2 Structural map of the Western Alps: 1.2.9. Mezazoic sedimentary cover. 3. ECMs. 4. Ultra-Dauphinose 5.6.7.Brianconais formations. 10.13.14 ICMs. 11.12. Schistes Lustres and Flysch 15. Jura 16. Molasse deposits.

The Alpine overprint leads to anchizonal to episonal metamorphism (Monie and Maluski, 1983; Aprahamian, 1988) disturbing the Rb/Sr isotopic ratios of the Variscan paragenesis (Demeulemeester et al., 1986). Moreover a rejuvenation of the Variscan faults is testified to by the occurrence of Upper Paleozoic to Liassic tectonic slices.

PALEONTOLOGY AND LITHOLOGY

Paleontological data are scarce. Cambrian to Ordovician microfossils (Giorgi et al., 1979) have been reported from the black and green schists of the Huez formation (Grandes Rousses massif) whilst Visean palynological relics (Bellier and Streel, 1980) have been reported from metapelites of the South-Western edge of the Aiguilles Rouges. These can be compared with the Upper Visean microfaunas of the Taillefer series (southernmost part of the Belledonne) reported by Gibergy, 1968.. This Lower Paleozoic age for epizonal sediments, which are lithologically similar to the Visean schists of the Aiguilles Rouges and Taillefer (Southern Belledonne), highlights the weakness of correlations based only on comparisons between similar facies .

The majority of the Paleozoic sediments have suffered greenschist to amphibolitic grade metamorphism. As a consequence, a comparative lithostratigraphy of the Upper Proterozoic and Lower Paleozoic formations is quite difficult to define.

However recent comparisons (Von Raumer, 1984,1988) have shown that three evolutionary cycles may be tentatively distinguished in the ECMs within the pre Upper Carboniferous basement, these are respectively related to the A) Upper Proterozoic - Lower Paleozoic, B) Devonian and C) Lower Carboniferous periods.

A1- The oldest of these cycles is made up of a series of sediments and igneous rocks which have undergone a long lived orogenic event (Silurian to Visean), under deep crustal conditions and have been metamorphosed up to amphibolite grade. These conditions are testified to by the wide extent of migmatisation and the occurance of relict granulitic and /or eclogitic parageneses. These formations could contain some relics of an older basement found essentially in the Aar-Gotthard, Haut Dauphiné and possibly the Aiguilles Rouge massifs which are, as yet, poorly understood.

In the Aiguilles Rouges, Belledonne and Argentera massifs these gneisses and amphibolitic formations could represent a taphrogenic evolution from Cambrian to Ordovician times that led to a general Ordovician rifting. This is supported by an important sequence of bimodal volcanism (Liegeois and Duchesne, 1981; Von Raumer, 1987; Paquette et al., 1989).

A2- This series consists of Lower Paleozoic formations of a mainly amphibolitic nature, which have however undergone a less severe and younger series of metamorphic events during Upper Devonian to Dinantian times. The Chamrousse ophiolite is the most spectacular representative of such terrains, being overthrusted and overturned upon rocks of Devonian to Dinantian age (Carme, 1973; Scarenzi, 1984; Menot et al., 1987)

A3- A series of metapelitic formations deriving from flysch deposits which include the series of St Gervais, Serie Satinee, Sarenne and Valetta these last two being somewhat uncertain. Their age of deposition is badly constrained but is probably of Precambrian or Lower Paleozoic age (Carme, 1970; Simeon, 1979). The tectonic structure of these formations is related to supra-crustal conditions.

B- This group is of probable Upper Devonian age and has only been described and dated in the south-western area of the Belledonne massif (Riouperoux-Livet formations) (Scarenzi, 1984). Lower Carboniferous metamorphism grades up to epizonal and mesozonal conditions (Carme, 1965; Menot, 1986,1987; Menot et al., 1987). Its

southwards extension can be recognized within the Chaillol series (SW Haut Dauphiné). The Lac Blanc volcanic and plutonic complex (Grandes Rousses)(Giorgi, 1979b) has also been compared with the Riouperoux-Livet formations (Menot and Vivier, unpublished observations) but this correlation is still hypothetical. The Devonian bimodal volcanism and trondhjemitic intrusives (352 +/-56 and 365 +/-17 Ma; Scarenzi, 1984; Menot et al., 1988b) are considered as resulting from an aborted mechanism of continental rifting (Menot, 1987), whilst Carme (1975) and Carme and Pin (1987) argued for an active margin context.

C- This last group of Lower Carboniferous formations outcrops within the different massifs as a series of intercalated volcanic and sedimentary sequences, (bimodal volcanism with essentially clastic sediments) (Aar-Gothard: Marcolli and Oberhansli, 1988; S.Aiguilles Rouges: Laurent, 1968; Belieres and Streel, 1981, Bellieres, 1988; Belledonne: Bordet and Bordet, 1963, Gibergy, 1968, Carme, 1970, Vivier et al., 1987). These formations have been metamorphosed in epizonal conditions, sometimes showing a strong mylonitic fabric (NE Belledonne). They could represent syn to late orogenic basins of the pull apart type.

TECTONICS

The deformation and metamorphism displayed within the basement rocks of the ECMs can only be explained by a sequence of events during Paleozoic times.

The major tectonic structures consist of vertical to steeply dipping foliation planes, which are related to large scale upright folds, with horizontal axes (Von Raumer, 1984; Bogdanoff, 1986) and/or non-cylindrical shear folds, associated with regional strike slip zones (NE Belledonne: Carme, 1970; Vivier et al., 1987).

Late tectonic structures, essentially mylonitic zones associated with NE-SW lateral strike slip movments, occur in regions of epizonal metamorphic conditions and overprint former penine style folds and nappes which have been recognised in the Aiguilles Rouges (Von Raumer, 1984; Von Raumer and Menot, 1989), Argentera (Bogdanoff, 1980, 1986) and Aar massifs (Oberhansli et al., 1988).

The central and eastern parts of the Haut Dauphiné seem to be structurally more complicated as both gently dipping and subvertical formations co-exist within the pre-batholithic basement.

Finally some areas e.g. the south western edge of the Belledonne and the westernmost part of the Haut Dauphiné are characterised by monoclinal or broadly folded structures (Bordet and Bordet, 1963; Carme, 1973; Le Fort 1973; Menot, 1987).

METAMORPHISM

A Variscan multistage evolution has been described in most areas of the ECMs by a variety of workers a review of which is given by Von Raumer, (1984 a and b).

1. The earliest event is one of high pressure and temperature of late Silurian to early Devonian age, U/Pb dates of 425-395 Ma (Paquette, 1987, Paquette et al., in press), supported by relics of eclogitic and granulitic facies: Aiguilles Rouges 780°C/11Kb (Liegois and Duchesne, 1981), Argentera 710-760°C/12-14Kb and 710-760°C/9-11Kb (Latouche and Bogdanoff, 1987). Recent petrological observations have led to the conclusion that not only the ecloglites but also major parts of the basement had reached lower crustal conditions by this stage. (Von Raumer, 1988)

2. The subsequent evolution is expressed by a P-T path where early kyanite is followed by sillimanite bearing assemblages, and mineral assemblages with cordierite-K feldspar in anatectic melts and incongruent cordierite bearing melts which appear at the thermal

peak. 650-700°C/4-6Kb (Von Raumer, 1984b, 1987); A late growth of andalusite is locally recorded (Aig. Rouges: Von Raumer,1984: Mont Blanc: Oliver, unpublished observations). This general P-T-t path indicates a regional change towards higher geothermal gradients with amphibolite facies conditions being of Devonian age.(NE Belledonne 373 Ma, Demeulemeester, 1982; Argentera 375-350 Ma, Monie and Maluski, 1983).

This metamorphism is accompanied by structural transformation with early nappe tectonics being succeded by strike-slip shearing. The later being partly contemporanous with intrusions of lower Carboniferous granites (Carme, 1970; Vivier et al., 1987; Joye, 1989).

3. Epizonal retrogressive metamorphism related to strike slip movements during Lower to Mid-Carboniferous times (Carme, 1970; Demeulemeester, 1982; Bogdanoff, 1986; Vivier et al., 1987)

The interpretation of this sequence of events leads to a complicated paleotectonic model involving subduction-obduction, collision and hypercollision processes (nappe stacking, crustal thickening, uplift and strike -slip shearing), from late Silurian to Mid Carboniferous times. This type of evolution can be compared with that of the axial zone of the Variscan belt (Matte, 1986; Von Raumer, 1984; Bogdanoff, 1986; Von Raumer and Menot, 1989).

However, not all regions of the ECMs have undergone the same events, e.g. the SW part and the western edge of the Belledonne massif only shows evidence of a single metamorphic event. This major tectonic and metamorphic event is of Dinantian age (between 365 Ma and 324 Ma Menot et al., 1987). It shows evidence of syn to late metamorphic nappe piling in epi to mesozonal conditions (Carme, 1973; Menot, 1986; Menot et al., 1987; Carme and Pin, 1987). This event implies an increasing P-T evolution for most of the tectonic units.

The far corner of this southwestern region has only been involved in the orogenic event during Upper Devonian to Lower Carboniferous times (Menot, 1987) and probably represents an outer zone of the Variscan belt (Menot, 1987, 1988).

On the north western edge of the Belledonne massif and separated from it by a major fault plane, is a metapelitic formation with possible metavolcanic horizons (Vivier, 1987), this formation known as the "Serie Satinee" (see A3 above) has undergone a polymetamorphic evolution with successive events first in the upper amphibolitic followed by greenschist conditions. This latest event is related to lower Carboniferous shearing (Carme, 1970; Gasquet et al., 1981). No relics of higher grade assemblages having been found.

It is in the Aar-Gotthard, Haut Dauphiné and Argentera massifs, where the oldest metamorphic events have been recorded:

Following Arnold (1970) and Grauert and Arnold (1968) some formations from the Gotthard massif suffered successive metamorphic events under amphibolitic conditions with subsequent anatexis, followed by granulite (circa 450 Ma) facies conditions before being intruded by Caledonian granitoids.

In the central and south eastern parts of a) The Haut Dauphiné and b) The Argentera massifs, two successive anatectic stages have been observed (Le Fort and Pecher, 1971, Von Raumer, 1984; Bogdanoff, 1986). The second event post dates relics of staurolite-kyanite-garnet gneisses and of sillimanite-cordierite bearing orthogneisses (Le Fort, 1973; Bogdanoff, 1986). The two anatectic stages are considered as Cadomian or earlier and Variscan (Devonian to Carboniferous).

In conclusion, the majority of the formations from the different regions of the ECMs show striking lithological, tectonic and metamorphic similarities: the Upper Silurian to Lower Carboniferous time span is characterized by a long lived multi-event evolution, this is assuming that these formations were within the axial part of the orogenic terrain.

Within some of the massifs there is evidence to suggest that these events have been superimposed on an earlier event.

IGNEOUS ACTIVITY

Volcanic and Subvolcanic Events:

The products of this type of igneous activity consist of either basaltic or bimodal series, mainly representative of stages of crustal distension, which have occurred at different times.

Proterozoic and Lower Paleozoic metavolcanics: These consist of amphibolites included in the gneissic and amphibolitic basement of the ECMs. Several types can be distinguished using the criteria of origin and age of the protoliths, as well as by their subsequent tectonic and metamorphic evolution.

The oldest amphibolites (protolith age: circa 870 Ma) are known from the Gotthard massif and may be the result of active margin magmatism. The HP paragenesis being related to an early Ordovician event (468 Ma) (Gauber et al., 1988).

The most common type of protolith however is defined by retrogressivly metamorphosed eclogites and mafic granulites. These indicate a period of ensialic rifting (Aig.Rouges, Belledonne and Arenterra massifs), as shown by the bimodal igneous activity, and the geochemistry of the eclogitic protoliths, which indicate either N and T morb type compositions with a small crustal component, (Liegois and Duchesne, 1981; Paquette et al., 1989; Von Raumer et al., in press)or ocean relics (Aar-Gotthard: Oberhansli et al., 1988). Dating by U/Pb on zircons, and Sm/Nd whole rock isotope methods, gives Ordovician ages (475-450 Ma) for the magmatic event and Silurian ages (425-395 Ma) for the high grade metamorphic event. (Paquette et al., 1989)

The 496 Ma old meta-ophiolite of Chamrousse (Scarenzi,1984; Menot et al., 1988; Pin and Carme, 1987) differs from the previous amphibolites by the spectacular preservation of its primitive magmatic character and by the absence of any high pressure metamorphic assemblages. Its chemical evolution, which indicates a multistage accreation (Bodinier et al., 1981) has been explained as either a) the transition from an attenuated continental setting to a true oceanic domain (Menot, 1987; Menot et al., 1988a and 1988b) or b) an allocthonous accreation related to a subduction zone (Pin and Carme, 1987).

Metavolcanics of Middle Paleozoic age have only been reported from the South Western part of the Belledonne massif (i.e. the Rioperoux-Livet formations) (Menot, 1986) and consist of leptynitic and micaceous gneisses, acid and basic metavolcanics and trondhjemites. They are considered as a single plutonic and volcanic complex, separated into five main units (Menot, 1986).

The age of crystallization of the trondhjemitic bodies has been dated from 352 +/- 53 and 365 +/- 17 Ma (Scarenzi,1984; Menot et al., 1984 and 1988). Menot, (1987) ascribes these rocks to an aborted continental rift whilst Carme and Pin, (1987) prefere an active margin environment.

For the metavolcanics of Upper Paleozoic age only those of syn to late orogenic origin (e.g. Lower Carboniferous) are taken into account. Spilites, keratophyres and tuffs are associated with a series of sedimentary facies consisting of arenites, pelites and conglomerates. Visean microfaunas have been recognised on the southern edge of the Aiguilles Rouges massif (Bellieres and Streel, 1981) and in the southwest area of the Belledonne (Gibergy, 1968). The chemical signatures of these metavolcanics are ambiguous with both tholeiitic and calc-alkaline affinities being present (Carme and Pin, 1987; Menot, 1987; Mercolli and Oberhansli, 1988).

Plutonic Events:

Intermediate to silicic intrusive rocks can be related to two different phases. The first event, which is badly defined both in time and space, is of Upper Proterozoic - Lower Paleozoic age whilst the second occurred during Upper Devonian to Lower Carboniferous times.

Cadomian - Caledonian intrusives consisting of orthogneisses from the Aar-Gotthard (Arnold, 1970; Mercolli and Oberhansli, 1988), Aiguilles Rouges (Von Raumer, 1987), Haut Dauphiné (Le Fort and Pecher, 1971) and Argentera (Bogdanoff, 1986), sometimes bearing high grade paragenesis (sillimanite), are considered as part of the pre-Variscan basement. Recently, similar sorts of orthogneisses from the north of the Aiguilles Rouges massif have been interpreted as a series of effusives in conjunction with a sub-volcanic series (Favre, 1989).

The intrusive episode which commenced in Upper Devonian times is also marked by a series of orthogneisses. In the Belledonne chain, they are spacially and genetically associated with the "Devonian anatectic" stage (Vivier et al., 1987)They consist mainly of heterogeneous biotitic and amphibolitic granitoids, often porphyritic in texture, with associated diorites and leuco-gabbros. Locally, acid basic igneous associations are preserved. Geochemical patterns indicate both a mantle contribution and a crustal origin by partial melting of greywackes (Ploquin and Vivier, 1984). In other parts of the ECMs, where the late orogenic shearing is less marked, cordierite-bearing anatexites and granites (Von Raumer, 1984, 1987) represent time equivalents of the Devonian orthogneisses.

These early products of the Variscan plutonic suite are followed by discordant granitoids of Carboniferous age (often cordierite bearing), followed by calcalkaline and Mg-rich subalkaline granites. Their time related chemical evolution is characterized by an increasing mantle source componant and a correlative decrease of the crustal contribution (Ploquin and Vivier, 1984; Aumaitre et al., 1985; Vivier in press). The syn- to late kinematic intrusions were partly controlled by the Lower to Mid Carboniferous strike slip tectonics (Carme, 1970; Vivier et al., 1987; Belliere, 1988; Joye, 1989). The latest intrusions (circa 300 Ma) are post-kinematic and devoid of internal structuration (e.g. Argentera massif (Bogdanoff, 1986). In general the Carboniferous intrusives of the ECMs shows marked similarities to those of the innermost parts of the Variscan belt (Orsini, 1979).

1.3 THE REGION OF THE HAUT DAUPHINE

TOPOGRAPHY OF THE HAUT DAUPHINE REGION

The area which is the subject of this thesis,is a part of the western extremity of the Parc National des Ecrins. This national park encompasses the mountainous region of the massifs of the Haut Dauphiné (P.LeFort 1973). The topography of the Haut Dauphiné (Fig. 1.3), is amongst the most spectacular in Europe and until the uniting of the Savoie with France in the 1800's, contained the only French mountains over 4000 meters in altitude the Dome de Neige 4014 mts. and the Barre des Ecrins 4102 mts.. Its extremely high average altitude of 2280 meters (Blanchard 1943) is accentuated by the steep sided valleys which cut deep into the mountains (Fig. 1.4).On all sides from Bourg d'Oisans (724 m) in the North, Entraigues (806 m) in the West Gap (760 m) and Embrun (980 m) in the South and Briancon (1280 m) in the East, glacier cut valleys thrust deep into the heart of the massifs. At the heads of these valleys lie the remains of what was once an extensive glacial complex and these small remenants feed the now small streams and rivers which drain the massifs.

HYDROLOGY

All of the streams and rivers which flow out of the Haut Dauphiné have their origins in either glaciers or snow melt run off (Fig.1.4). This means that for a period of three or four months in late spring and early summer, these streams and rivers which are normally small and even sometimes non-exsistant, become raging torrents and this is the reason

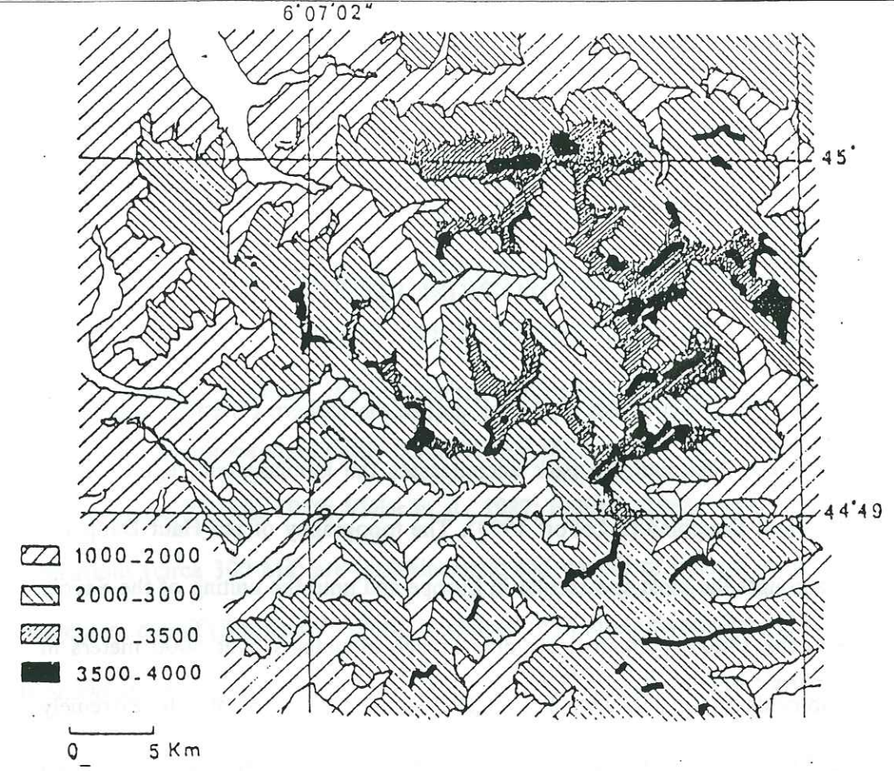

Figure 1.3 Topography of the Haut Dauphine (after Bellair, 1948)

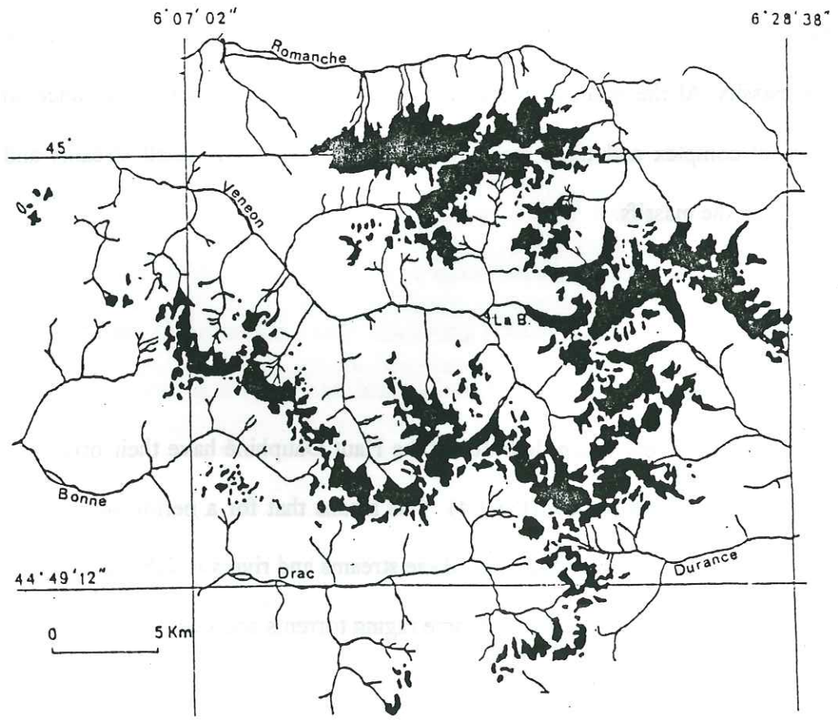

Figure 1.4 Rivers and glaciers of the Haut Dauphine (after Le Fort, 1973)

together with the ancient glaciers that the deep valleys have been incised into the rocks of these massifs.

The underlying strata has also played a large part in the depth to which these valleys have been able to reach, and a good example of this can be seen in the region of Bourg d'Oisan, where the river of the Romanche until then flowing through crystalline rocks suddenly comes in contact with softer folded shales and carbonates of Liassic age ,which have been trapped in the Bourg d'Oisan syncline (Barfety 1979). Here the river has cut a large flat bottomed valley which at one time formed a large lake. A few kilometers further on the river again cuts into rocks of the crystalline basement and the valley returns to a steep sided gorge.

The extent of the glaciation is today very limited with the firn level at about 3000 meters (Fig. 1.4). In 1973 the limits of the glaciation was in fact somewhat less than depicted occupying a surface area of approximatly 100 km2. Today in 1987 this area has undergone further erosion and the area now under glaciation is approximatley 60 km2.

The water run off of the Haut Dauphiné is grouped into five main channels. From the East and North the Romanche River drains westward where it meets the waters of the Veneon which drains the center of the massif, further South the river Bonne drains the Valley of the Valjouffrey, and the valley of the Valgaudmar is drained by the Severaisse. Both of these rivers run into the River Drac, which after draining the south of the massif runs north to Grenoble to meet the Isere, flowing south from the Savoie. The East and South of the massif is drained by the River Durance and its numerous tributairies, which flow south and west to join the Rhone south of Avignon.

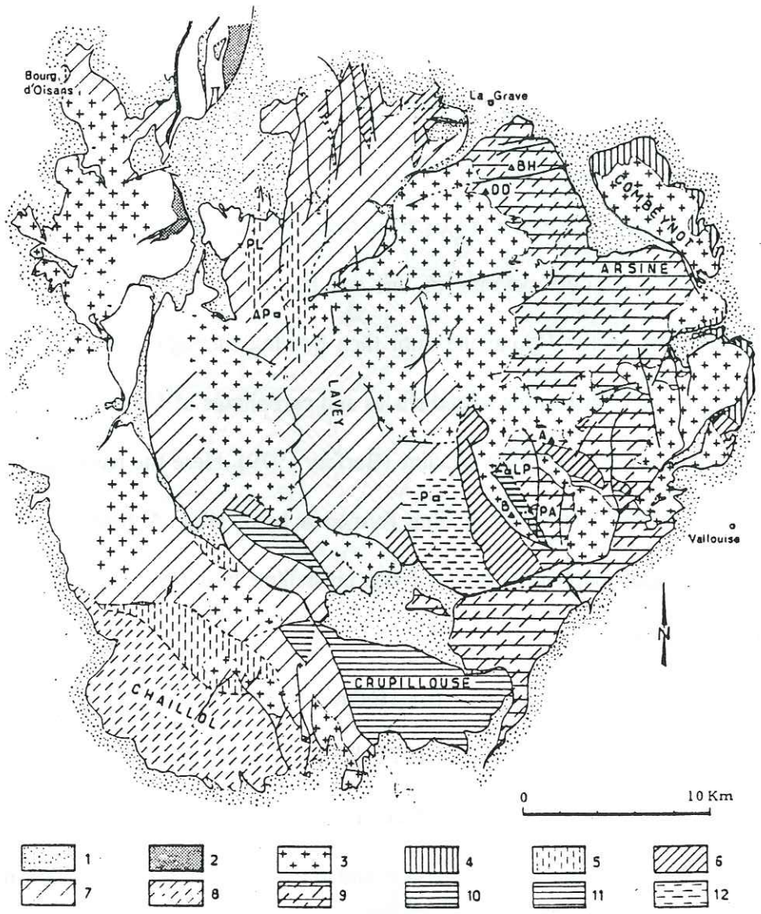

Figure 1.5 Structural and Lithological map of the Haut Dauphine (after Le Fort and Pecher, 1971)
1. Mesazoic sediments 2. Upper Carboniferous meta-sediments 3. Variscan granites 4.& 5.Acid volcanic detritus (c) 6.Basic volcanics (c) 7.& 8.Volcanic detritus 9.& 12. Volcano-sediments (migmatised) 10. Ancient foliated mylonites 11. Older granites.

Essentially then, the Haut Dauphiné forms a large highland area. This has formed the basement for at least two orogenic events, these being the Variscan and Alpine orogenys. Its topography is intimately linked to the effects of these events, as it is also to its geology.

STRUCTURE AND METAMORPHISM

STRUCTURE

The Haut Dauphine is structurally some what more complex than other parts of the ECMs. The oldest structures consist of a series of mylonitic zones, of which the "lineament de La Pilatte" situated in the centre of the massif, is typical.

This is followed by a period of complex deformation in which sub-vertical foliation planes co-exist with gently dipping folds (Pecher, 1970; Le Fort, 1973;). which are overprinted with large scale isoclinal folds with horizontal axes.

Late stage Variscan tectonics consist of regional ductial strike-slip zones, mainly in the west of the region.

This is followed by the onset of distention during Triassic times with the formation of Graben like structures and syn-sedimentary ensialic basins (Barfety et al., 1979).

The last tectonic event is linked to the crustal shortening engendered by the "Alpine orogony", and this is expressed as large scale thrusting towards the WNW with the development of imbricated basement-basement and basement-cover sequences (Butler et al., 1986)

METAMORPHISM

The basement rocks consist of a series of volcano-sediments and volcanics, which have undergone deep crustal metamorphism up to amphibolite grade, with subsequent migmatization and anatexis (Fig. 1.5). Le Fort (1973), distinguished three major series

a) A series of acid gneisses with rare horizons of amphibole, having suffered catazonal metamorphisme and intruded by gabbros and granites. b) The La Lavey and Chaillol series, consisting of volcano-sediments together with volcanic members, metamorphosed in the mesozone or catazone, with a general migmatisation and c) a series of slightly (epizonal) metamorphosed acid volcanics and volcano-detritus, cut by Variscan granites.

INTRUSIVE ROCKS OF THE HAUT DAUPHINE

The earlist intrusions of this period consist of a series of orthogneisses with porphyric textures, and outcropping mainly in the south-west of the region. The most important of these is the massif of Crupillouse Fig. 1.5. These are considered to be of probable Cadomian to Caledonian age (Le Fort and Pecher, 1971).

The granitoids of Devonian-Carboniferous age, consist of a number of plutons of varing size, which occcupy approximately half the surface area of the Haut Dauphiné region.

Their style of intrusion into the gneisses and migmatites of the basement rocks is relatively uniform, with very few traces of contact metamorphism, although in general the granitic intrusions show slightly chilled margins with finer grain sizes than the main body.

A number of the intrusions have been studied in the past by a variety of workers.(Buffiere, 1963; Ozocak, 1965; Barbieri, 1970; Pecher, 1970, 1971: Le Fort and Pecher, 1971; Bartoli, 1973; Le Fort, 1973; Barfety and Pecher, 1984; Vittoz et al., 1987), and their work has allowed the definition of the principal characteristics of the structure, petrology, mineralogy and to a lesser extent the geochemistry of these granites.

Pecher (1970) noted that the presence of sub volcanic to volcanic terms in the plutons of the eastern margin of the region, and their absence in the west and center. He interpreted this as the result of intrusion at different structural and metamorphic levels within the crust.

The granites which form the western border of the Haut Dauphiné region are distinguished by the association of a basic facies, rich in amphibole, biotite and sphene, and a leucocratic facies with essential biotite (Le Fort, 1973; Aumaitre et al., 1985; de Boisset et al., 1984; de Boisset, 1986; Banzet, 1987). In the south-west the basic rocks are relatively abundant and form large km2 intrusions (massives of Colle Blanche and Moutieres) and are associated with quartz monzonites and monzo-granites (Banzet, 1987). Further north in the massives of Peou de St Maurice, Quatre Tours/Belle Cote and Rochail the basic rocks are in the form of dykes and isolated enclaves within the main granitic bodies.

These types of association have been described within the potassium-rich sub-alkaline granites having shoshonitic affinities (de La Roche and Stussi, 1984), of the French Variscan domain (Ploumanac'h,(Barriere, 1977);Les Ballons, (Pagel and Leterrier, 1980)

To the east of a major Liassic suture, the granite complexes of Turbat-Lauranoure and La Berarde-Promontoire form two north-south trending axes of granitic intrusions which stretch for 20 kms within the center of the Haut Dauphiné. These are leucocratic granites, often porphyritic, lacking enclaves, where the biotite which never exceedes 10% is usually chloritised. Chemically they can be classified as calco-alkaline in type.

Further to the east within the structural unit of the Ultra-Dauphinois the hololeucratic granite of the Combeynot forms an independant massif. This massif consists of a subvolcanic annular ring complex with micro-granitic and rhyolitic dyke systems and two granitic plutons. (Costarella, 1987). The chemical nature of this complex is alkaline, even though the developed mineralogy is not strictly that of the alkaline granites. However

Bonin, (1987,1988 and in press) has recently demonstrated that this type of association is solely dependant on the H2O content of the melt.

1.4 OBJECTIVES OF THIS STUDY

The aim of this study is to:

a) Briefly describe the structure and general geology of the area between Lac Lauvitel and the Valsenestre valley, in the western part of the Haut Dauphiné region.

b) Describe the petrology, chemical mineralogy and geochemistry of the igneous rocks outcropping within the area.

c) Using geochemical, and mineralogical data including major and trace element, rare earth element (REE), zircon morphology and mineral geochemistry, define and differentiate the granite intrusions of the Haut Dauphiné in terms of their source and possible evolution.

CHAPTER 2

THE FIELD AREA

2.1 TOPOGRAPHY OF THE FIELD AREA

The field area is situated in the north-western part of the Haut Dauphiné massif (Fig.2.1), lying between the Valsenestre valley in the south and the Romanche-Veneon valley in the north. To the east, the escarpment of the Muzelle-Tete de la Muraillete forms the boundary whilst to the west a line running from the peak of Le Tete de Chétives to the peak of Le Rochail forms a natural and partial geological barrier. The region is extremely mountainous and rather difficult of access. Its average elevation is 2200 m and there are several peaks over 2700 m. The four highest points are the Signal de Lauvitel (SL) 2903 m., the Tete de la Muraillette 3020 m. the peak of Le Rochail 3023 m and the Pic du Clapier du Peyron (PCP) 3169 m.(Plate 2.1)

The area is dominated by a) The granite massif of Rochail in the north-west and b) the east-west ridge which, running from the Col de la Muzelle, rises to the Pic du Clapier du Peyron and passes via the Brèche de Valsenestre to the Signal de Lauvitel(Fig.2.1). This idge effectively divides the terrain into northern and southern parts, especially in terms of access.

As can be seen from Figure 2.1, the southern part of the area has three major valleys running towards the south, these being from east to west the vallons des Combes, Valsenestre and Combe Guyon. These three valleys drain into the Beranger river which runs through the Valsenestre valley to meet the River Bonne at La Chapelle en Valjouffrey . Between the Vallon des Combes and the Vallon de Valsenestre is a high ridge running northward from Les Quatre Tours via the peak of Ramu to the Pic du Clapier du Peyron. A second ridge, separating the Vallon de Valsenestre from that of the Combe Guyon again runs towards the north from les Peys via the peak of Alfrey to the Signal de Lauvitel. Several well developed glacial cirques can be seen, notably below the Pic du Clapier du Peyron and the Signal de Lauvitel (Plate 2.2) in the Vallon de Valsenestre, although only one small glacier still exists in the former.

The northern part has a single valley which runs from the PCP-SL ridge to Lac Lauvitel and is drained by a stream which finds its source in the glaciers of the Pisse below the PCP and drains into the lake. The eastern ridge runs from the PCP to the Tete de Muraillette, whereas the Western ridge runs from the Signal de Lauvitel via the peak of the Roche de la Selle to the Pointe de Confolant in the Rochail massif and from there up to the peak of Le Rochail in the heart of the Rochail massif.

2.2 GENERAL GEOLOGY OF THE FIELD AREA

Figure 2.2 is a generalized structural and geological sketch map of the field area from the Valsenestre valley to Lac Lauvitel, based on field observations and analysis of collected samples,(Fig.2.3) and shows the main geological details of the area. It can be seen that the region as a whole has undergone quite severe structural deformation.

Figure 2.1 Topographic map of the Lauvitel - Valsenestre region.

Figure 2.2

STRUCTURAL AND GEOLOGICAL SKETCH MAP OF THE LAUVITEL-VALSENESTRE REGION, HAUT DAUPHINE

SCALE 1: 20000

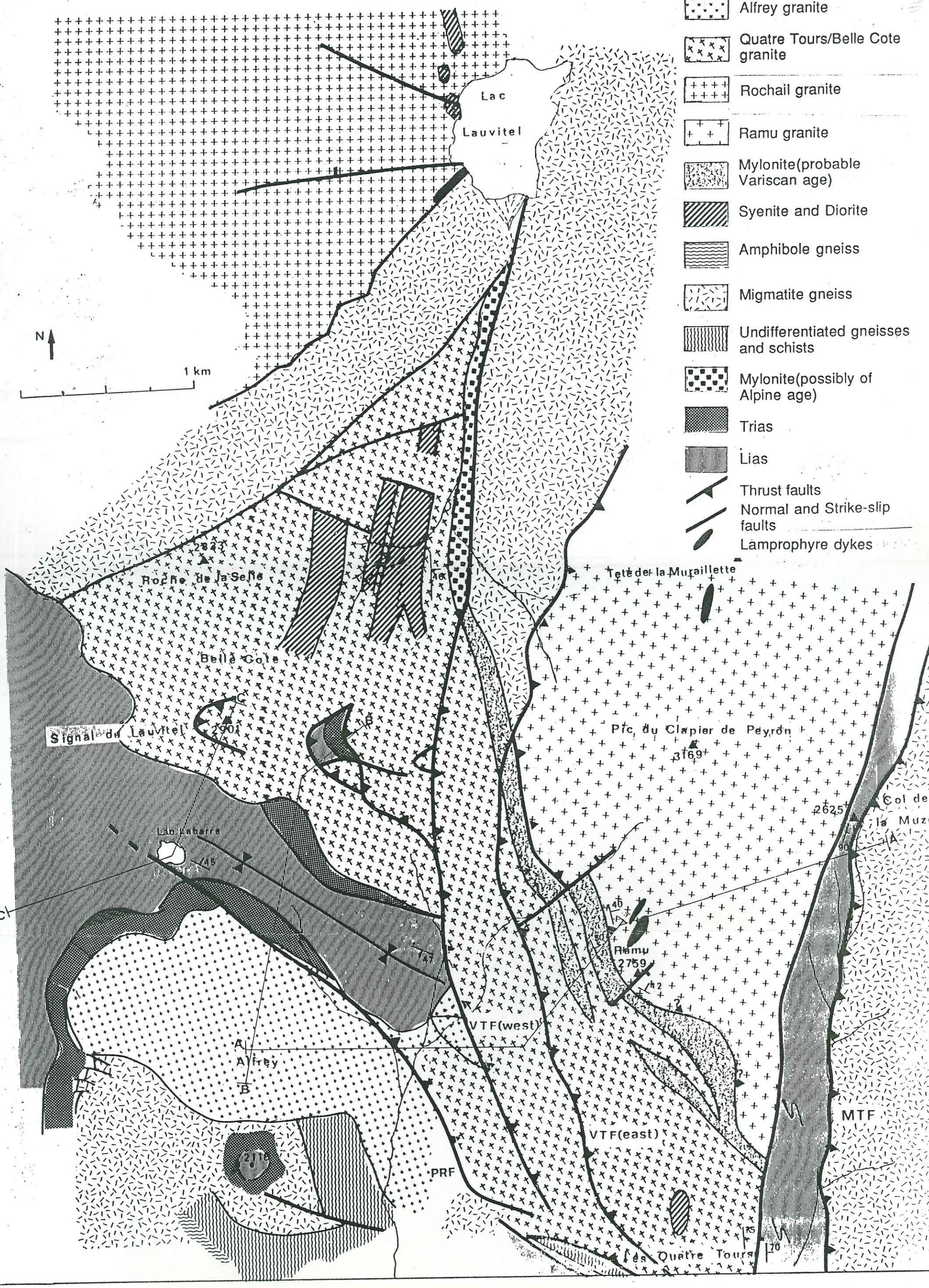

Figure 2.3 Sample location map

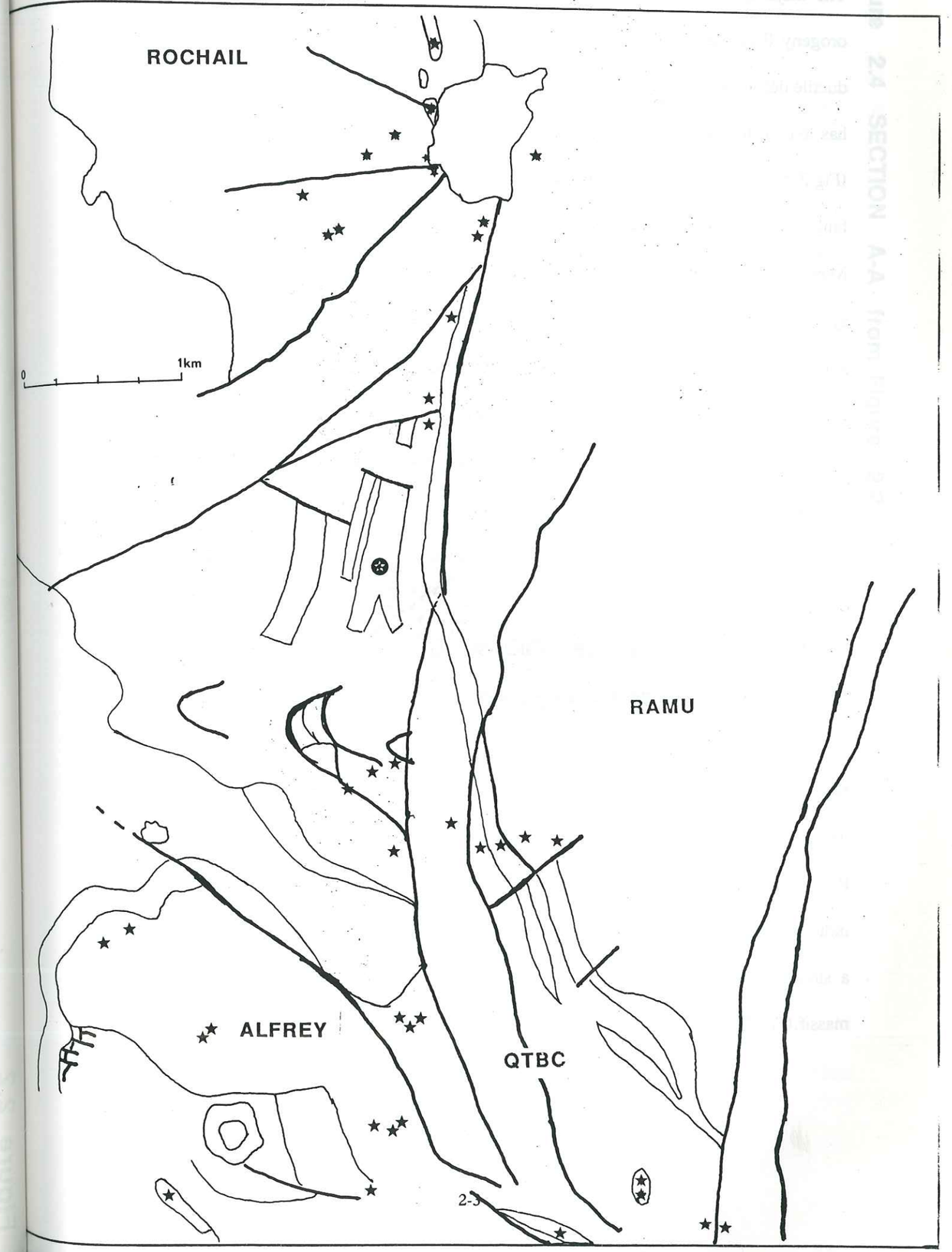

The majority of this deformation can be attributed to movements during the Alpine orogeny (infolding of Triassic and Lower Jurassic volcano-sediments), but some of the ductile deformation (mylonites) are of possible late Variscan age. Thrusting from the east has led to the formation of a series of thrust sheets stacked one on top of the other (Fig.2.4). At least four major thrust faults can be traced. In the east is the Muzelle thrust fault (MTF). This fault runs in a north-south direction passing through the Col de la Muzelle before swinging towards the east where it eventually joins the La Meije thrust system(Fig.1.*). The Eastern Valsenestre thrust fault (VTF(east)), commences in the south at the intersection of the MTF with a major east-west running fault, which follows the valley of the Beranger, offsetting the Valsenestre massif. The VTF(east) curves west and north to pass through the PCP-SL ridge and forms the feature of the Brèche de Valsenestre (Plate 2.3); this continues north eastwards under the Tete de la Muraillette (Plate 2.4) and disappears in the gneisses which form the ridge of the Draye de l'Embernard (Figs. 2.1,2.2).

The third thrust fault is the Western Valsenestre thrust fault or VTF(west) which also appears to branch from the southern extension of the MTF and runs almost parallel to the VTF(east) passing through the PCP-SL ridge, approximately 450 metres west of the Brèche. Between this point and the Signal de Lauvitel several inverted normal and minor thrust faults occur which have trapped a number of Triassic and Liassic blocks (Fig. 2.5, Plate 2.5). The presence of olistoliths in these blocks (Barfety et al., 1986) would indicate coeval movement during deposition; this type of structure has been described in a similar context by Gilchrist et al. (1987) further to the south, in the Valsenestre massif.(Fig 2.7)

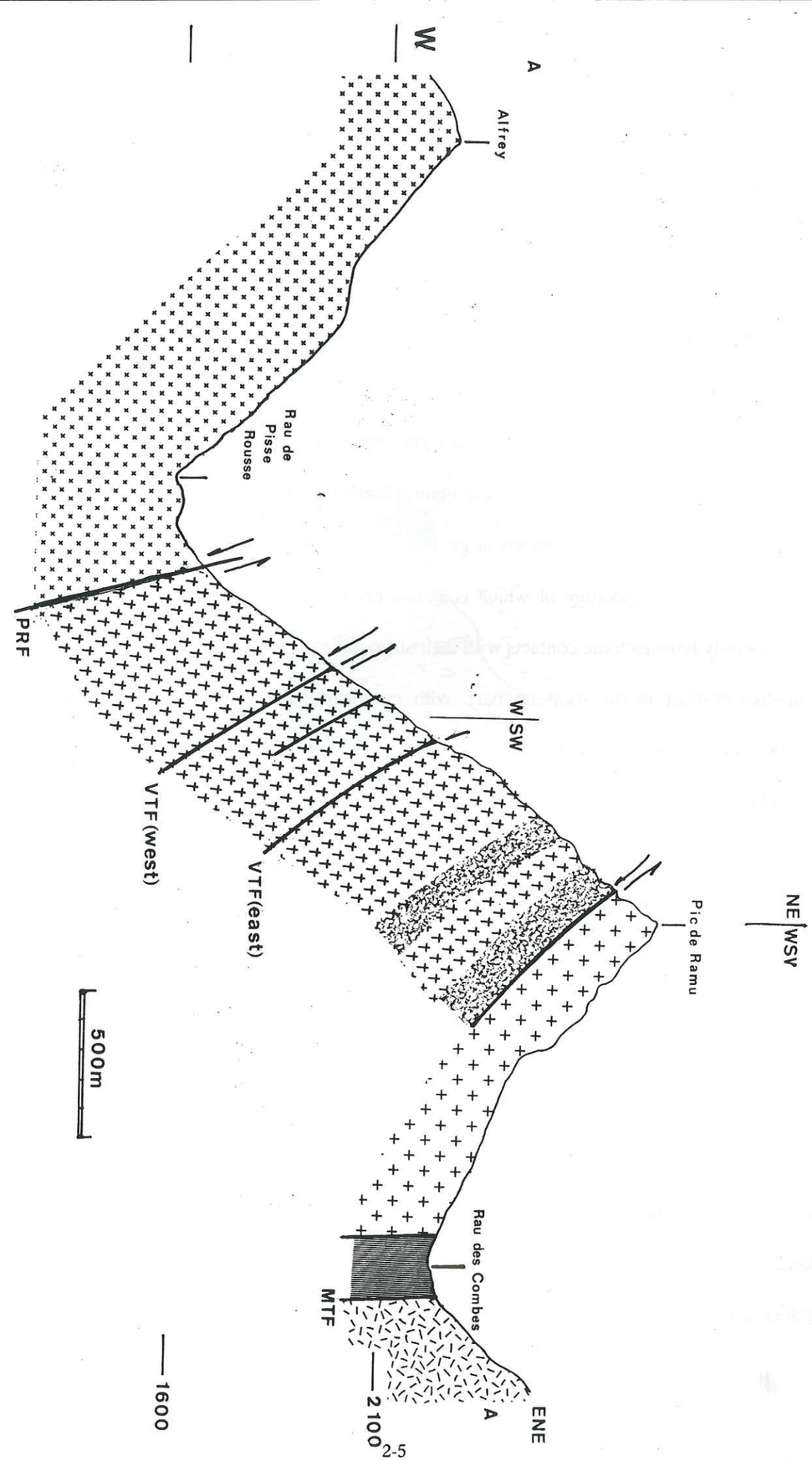

Figure 2.4 SECTION A-A from Figure 2.2

The fourth thrust fault is the Pisse Rousse thrust fault (PRF) which starts in the same manner as the two previous faults but progresses westwards along the southern limit of the Lac Labarre syncline. The nature of the fault appears to change in the west with thrusting becoming a composite of strike-slip and normal movement; the fault partially offsets the sediments of the basin, before it disappears under the Liassic cover (Plate 2.6,Fig. 2.6).

Within this area four tectonically separated granites crop out. The Ramu granite occurs in the east, the Quatre Tours/Belle Cote granite in the centre, the small Alfrey granite in the west and further to the north the large body (area of approx. 30 km²) of the Rochail granite, the general geology of which is shown on Figure 2.9. The QTBC and Ramu granites only have tectonic contacts with their surroundings, but the Alfrey granite has an intrusive contact in the southern part, with migmatites and amphibolites whilst the Rochail granite is intruded into similar types of rocks on its northern and western boundaries.

In the east the Ramu granite has been thrust over the Quatre Tours granite. The two are separated by a band of schists, gneisses and mylonites, (Figs. 2.2,2.4), which run northwards until meeting the VTF(west) in the Lauvitel valley. Champenois (1982) found that the ductile component of these mylonites showed a dextral movement towards the north, whereas the later cataclastic movement was to the west. This would seem to indicate that these mylonites are possibly of late Variscan age. Slates and shales of Liassic age have been faulted and folded against both the Ramu and the Quatre Tours granite in the Combes valley by the Muzelle thrust fault.(Plate 2.8)

Underlying the Ramu granite, and separated from it by a band of interleaved gneisses, schists and mylonitic rocks which vary from some tens to 200 to 300 metres in thickness,

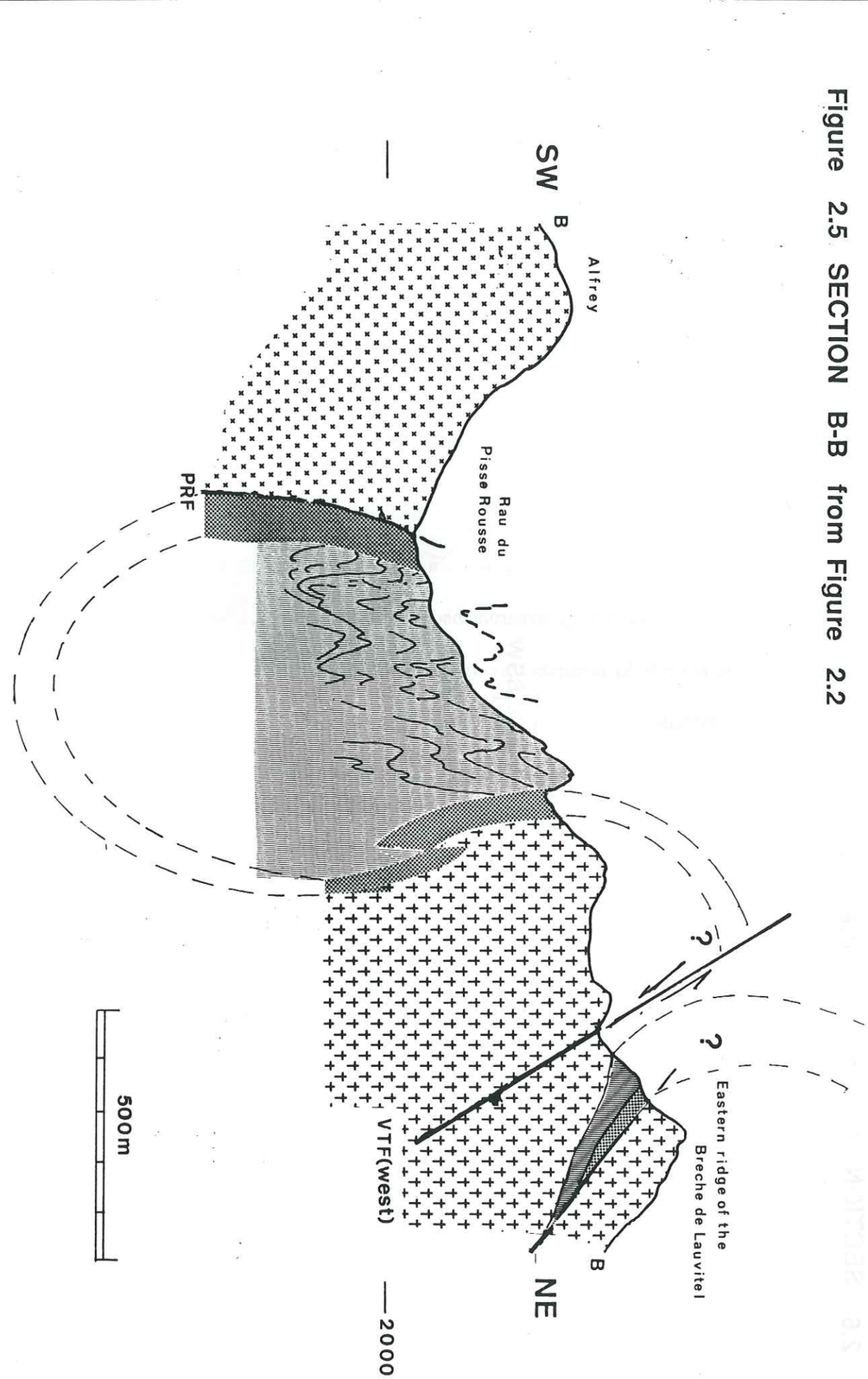

Figure 2.5 SECTION B-B from Figure 2.2

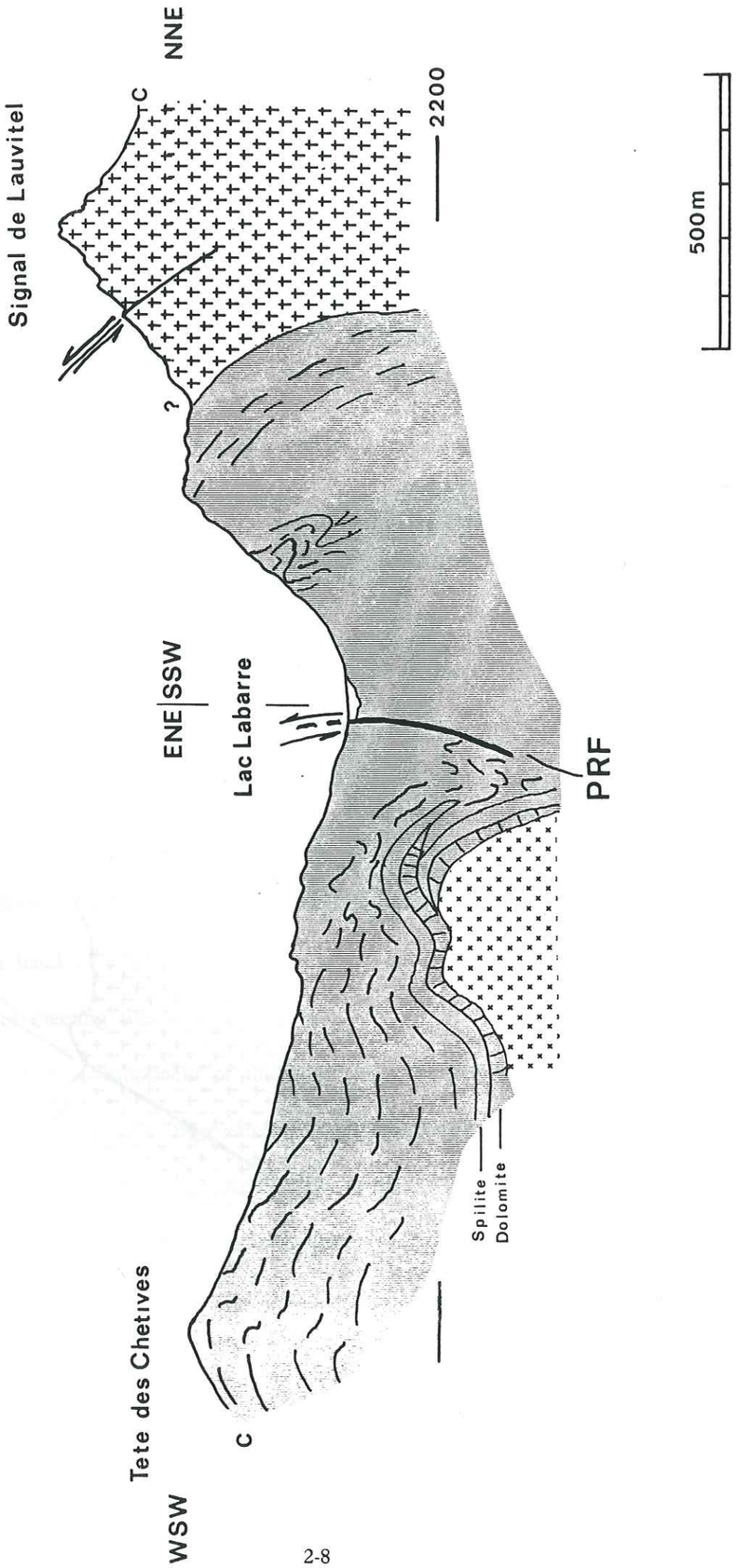

Figure 2.6 SECTION C-C from Figure 2.2

lies the Quatre Tours/Belle Cote granite (QTBC). In the south (Fig. 2.2)the QTBC is thrust over rocks of the metamorphic basement, but in the west is thrust over the Alfrey granite by the PRF. The granite is cut by the two segments of the VTF but north of the PCP-SL ridge it spreads to the west to fill the Combe de Belle Cote before disappearing under the cover of the Lac Labarre syncline.

On this side of the PCP-SL ridge, the zone of mylonitic rocks forming the horizon between the Ramu and QTBC granites, is hidden under glacial deposits but reappears and follows the valley of the Pisse Salle at least as far as Lac Lauvitel. In this section the mylonitic rocks show a greater degree of cataclasis, indicating that deformation here is possibly of Alpine age. To the west of the valley broad intrusive syenite dykes of the Combe de Belle Cote, themselves intruded into the northern extension of the QTBC granite, dominate the outcrop. The VTE (west) cuts back towards the east to disappear under glacial moraine and cover. Towards the north end of the valley several normal faults with a strike slip component, towards N120° cut both the granite and the syenite giving small offsets down the valley. This movement has in several places removed parts of the syenitic intrusions.

Migmatitic amphibolite gneisses form a structural barrier between the QTBC granite and the southern part of the Rochail granite (previously studied by Buffiere, 1963, and DeBoisset, 1986). The contact is everywhere faulted with the main fault direction at N55°. These again appear to be composite faults having both normal and strike-slip components. The gneisses are cut by veins of granite showing marked orientation and alteration of the ferro-magnesian minerals: chlorite after biotite. The veins cut the gneissic foliation which is sub horizontal, having a general direction of N010° and a dip of 25°.

Plate 2.1 Pic du Clapier du Peyron (alt. 3169m) seen from the southern ridge looking north.

Plate 2.2 Glacial cirque with the peak of the Signal de Lauvitel (alt.2900m) rising above, seen from the Ramu.

Plate 2.3 The Breche de Valsenestre, looking south from the Belle Cote. Here the two arms of the Valsenestre thrust fault create the saddle of the Breche.

Plate 2.4 The Valsenestre Thrust Fault, Below the Tete de la Murialette looking towards the east from the Belle Cote. Here the Ramu granite is thrust over the gneisses of the La Lavey formation.

Plate 2.5 Overturned olistolith, on the ridge between the Signal de Lauvitel and Lac Labarre. Granite in the bottom left is overlain by Liassic sediments which are in turn overlain by quartzites and spilites of Triassic age with granite in the extreme top righthand corner of the photograph.

Plate 2.1

Plate 2.2

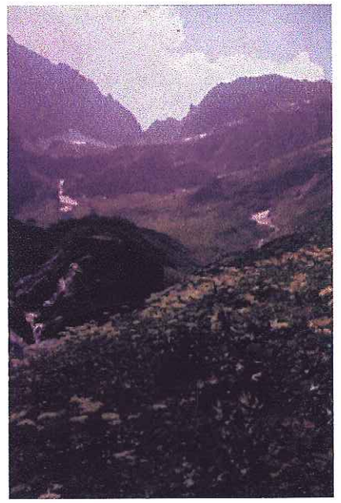

Plate 2.3

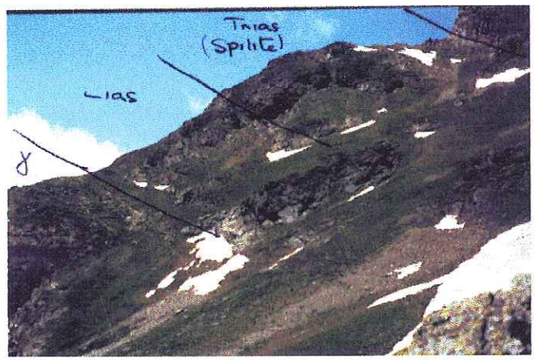

Plate 2.5

Plate 2.4

To the south and west of the Pisse Rousse Fault the Alfrey granite has been intruded into metamorphic rocks consisting of biotite schists, quartz-rich banded gneisses and amphibolite gneisses. To the south the intrusive contact is well displayed with granitic veins cutting across foliations in the metamorphic rocks; however no metamorphic aureole has been observed. This would indicate that either the temperature of the country rocks was at, or near, the temperature of the granite at the time of its emplacement or alternatively that the granite was dry. The presence of pegmatitic material would appear to favour the first hypothosis. To the north the Alfrey granite is overlain by the rocks of Triassic and Liassic age in the Lac Labarre syncline. The contact between the two is partly tectonic (Fig. 2.6) but in the west it forms an erosional surface (Barfety and Gidon, 1983) indicating that the granite had been exposed during Permian and Early Triassic times.

2.3 DESCRIPTION AND FIELD RELATIONSHIPS OF THE IGNEOUS ROCKS

2.3.1 RAMU GRANITE

The Ramu granite crops out west of the fault which passes through the Col de la Muzelle and includes the peak from which it takes its name as well as part of the Pic du Clapier du Peyron. Further north, the Ramu granite appears as isolated intrusions in the western part of the La Lavey formation which here consists of a monotonous series of acid migmatitic gneisses. The granite is in the form of an imbricated sheet at the Pic de Ramu Fig.2.4, and lies above a series of interleaved gneisses, schists and mylonites

Plate 2.6 The Pisse Rousse Fault in the region of Lac Labarre. The Lines mark movement planes with some directions. The fault at this point is composite with both thrust and normal components.

Plate 2.8 The Muzelle thrust fault below the Quatre Tours in the Vallon des Combes. Here Liassic sediments in the east have been thrust against The Quatre Tours Belle Cote granite to the west.

Plate 2.9 The leucocratic Ramu granite, at the Pic du Ramu looking north towards the Pic du Clapier du Peyron.

Plate 2.10a Large panals of gneiss (picked out on black) within the Ramu granite. Vallon des Combes looking north towards the Col de la Muzelle.

Plate 2.10b Contact between a block of gniess (top right) and the Ramu granite. Vallon de Valsenestre.

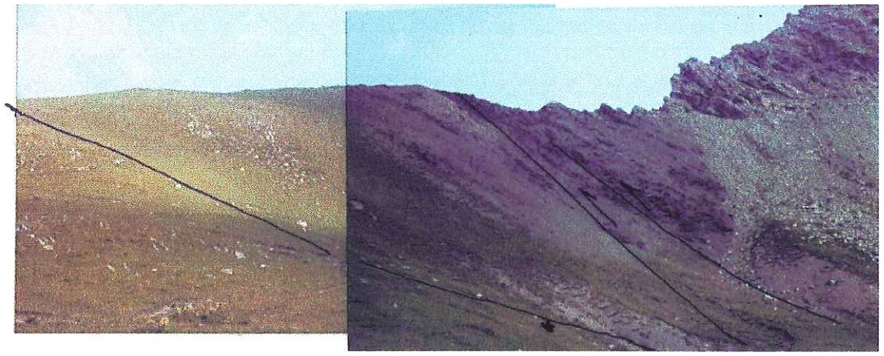

Plate 2.6

Plate 2.8

Plate 2.9

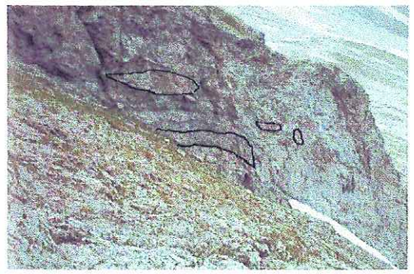

Plate 2.10a

Plate 2.10b

(Champenios, 1982), which outcrop in a sinuous band extending towards the north. At outcrop the Ramu granite is a very leucocratic two mica granite(Plate 2.9) with a preponderance of muscovite, having no preferred orientation, so does not appeared to have suffered to much from Alpine deformation. Biotite is generally altered to chlorite. Grain size is medium although locally it can become quite coarse. The granite is distinctive in that enclaves and panels of half-digested acid biotite gneiss are fairly frequent (Plates 2.10). Close to the summit of Ramu as well as on the south flank of the Pic du Clapier du Peyron a number of pegmatitic veins appears; these contain small spessartine garnets and a distinctive grey coloured highly perthitic potassium feldspar. The latter are very similar to the potassium feldspar described by Verjat (1980) and Vivier and Menot, (1987) from pegmatites in the Sept Laux granite, in the Belledonne massif (Fig 1.2). Bonet (1982) ascribed them a late anatectic origin, with formation of the feldspar crystals whilst under strain, such that the crystal growth was not uniform, thus giving them their distinctive colour.

On the eastern slopes, running up to the peak of Ramu, a number of lamprophyre dykes trending 040° can be seen. These are very fine grained sub-volcanic to volcanic textured rocks. The width of the dykes never exceeds two or three metres and tend to form lens shaped intrusions in the granite. It is not clear whether these are offset and boudinaged pieces of a single dyke, or infilling of local pull-apart features within in a zone of sheared granite. In mineralogy and texture they are similar to other lamprophyres described throughout the Haut Dauphiné (e.g. Vatin-Perignon et al., 1974,1977; Buffet and Aumaitre, 1973; Adeline, 1982). Their origins could be linked to the alkali volcanism of the Triassic period, but a more likely origin is as intrusions linked to pull apart textures, during the major strike-slip movements of late Variscan times. This is born out by the

general trend of these dykes throughout the External Crystalline Massifs, this being perpendicular or sub-perpendicular to the mylonitic zones .

The boundaries of the Ramu granite are everywhere formed by faults of some description with the exception of the small intrusions found to the north of the Col de la Muzzelle where they are intrusive in the La Lavey gneisses.

2.3.2 QUATRE TOURS/BELLE COTE GRANITE

South of the PCP-SL ridge, beneath the band of gneisses and mylonites, with which it is occasionally interleaved, the Quatre Tours/Belle Cote (QTBC) granite forms a linear outcrop, running south east-north west. The outcrop varies in width between 1 and 1.5 kms, this being dependent, locally on the position of the PRF and VTF(west). The QTBC runs from the pinnacles of the Quatre Tours,(Plate 2.11) from which it takes the first part of its name, through the PCP-SL ridge . North of the ridge it expands to form the western side of the Lauvitel valley, filling the Combe de Belle Cote (see frontispiece) and disappearing under the Mesozoic cover to the west. To the north it terminates at a faulted contact with the migmatite gneisses of the country rocks close to Lac Lauvitel. Its surface outcrop totals approximately 8 square kilometres. The QTBC granite includes a number of dioritic and syenitic enclaves in the form of rounded inclusions reaching some tens of square metres in surface area at outcrop, especially in the southern half. Further north, in the Combe de Belle Cote, syenite becomes a relatively major intrusive feature consisting of a number of dyke-like intrusions with widths varying from 30 to 80 metres and outcropping over distances of several hundreds of metres. (Fig.2.2)

Figure 2.7

Detailed map of part of the Syenite dykes Combe de Belle Cote

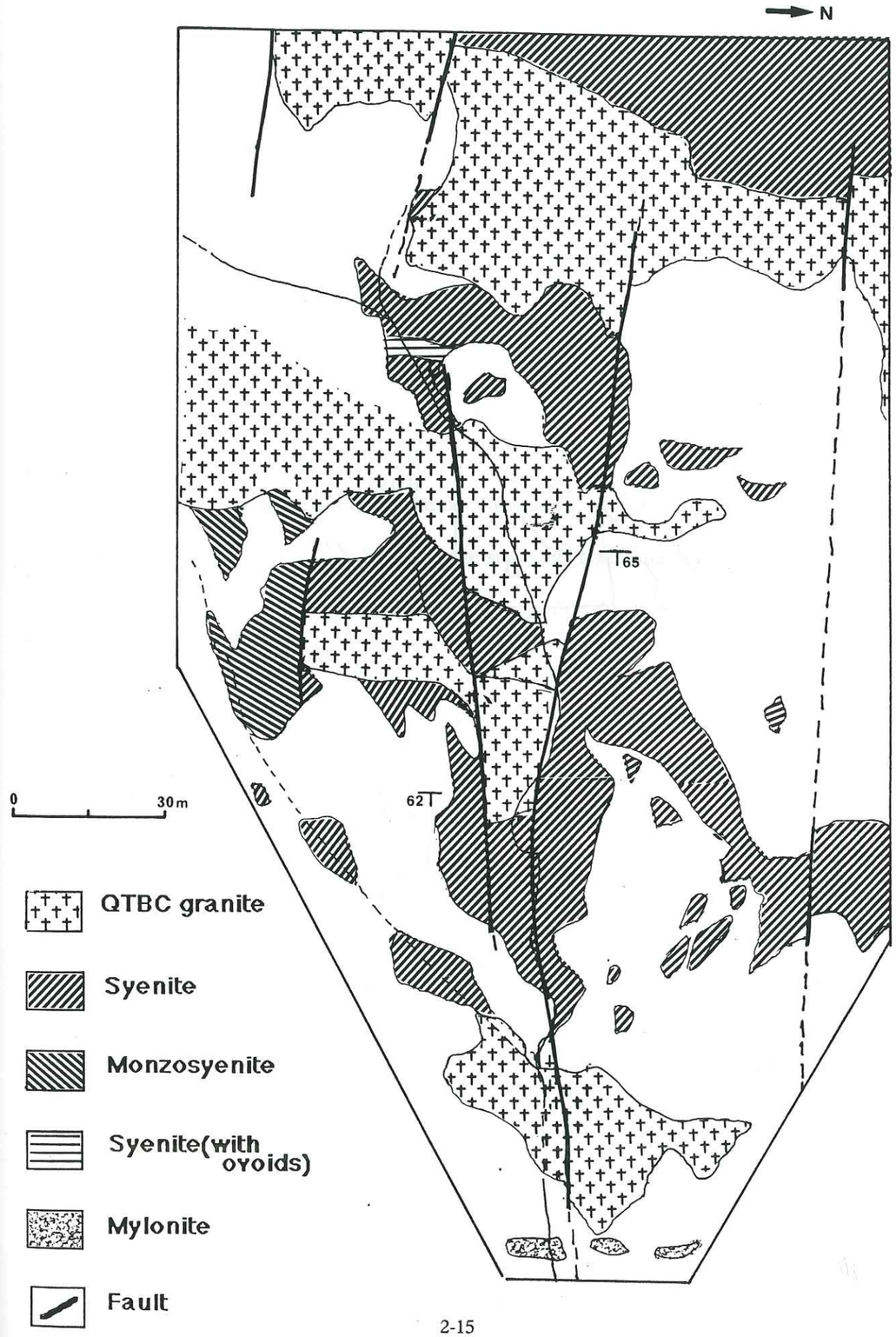

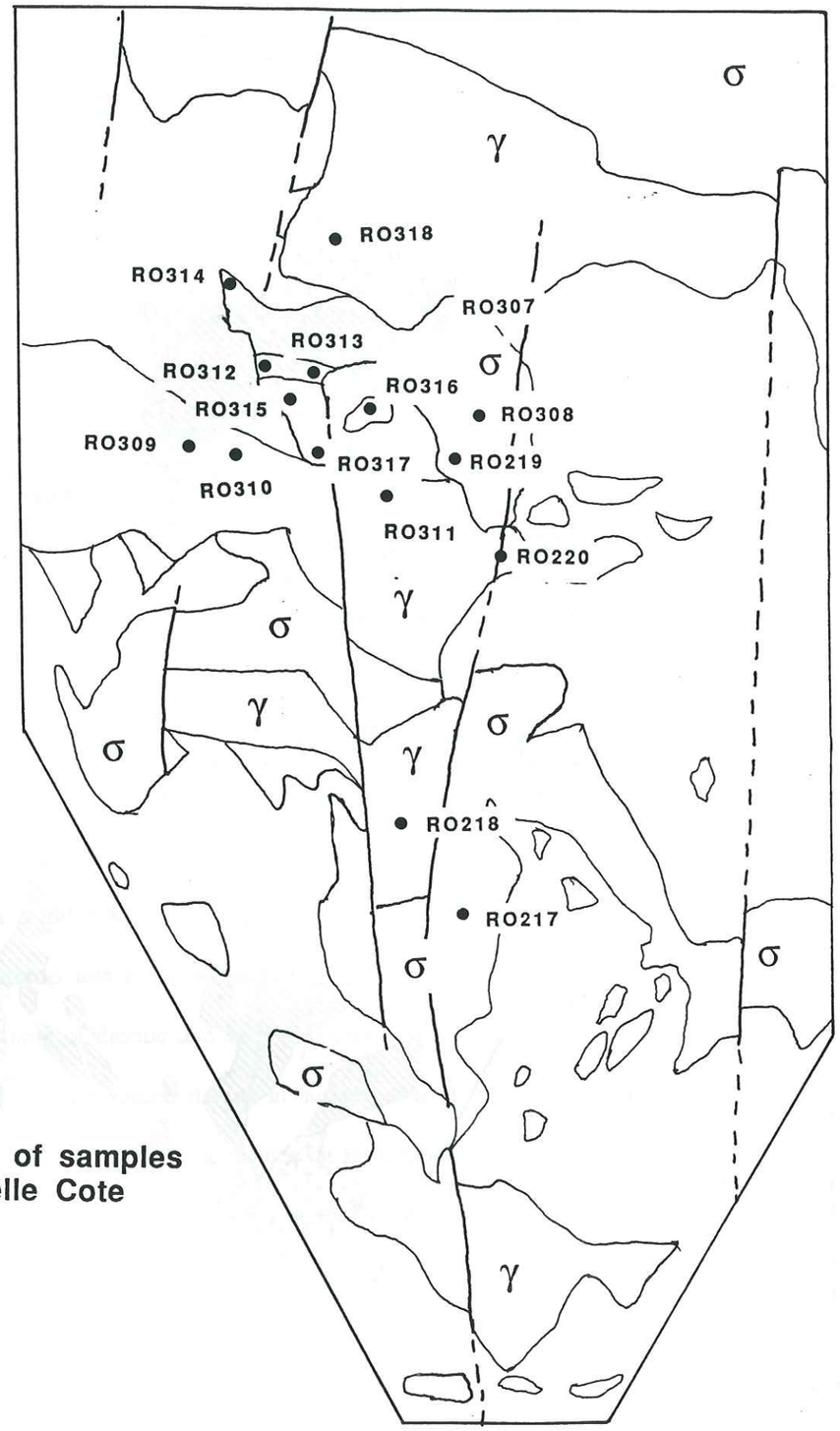

Figure 2.8

Location map of samples Combe de Belle Cote

In the south the QTBC granite is fairly leucocratic although, locally, accumulations of biotite in the form of schlieren give rise to a somewhat darker rock. In general it is a fine to medium grained granite, more or less porphyritic, except at its southern contact with the gneisses, with good euhedral phenocrysts of potassium feldspar of millimetre to centimetre size. Near the southernmost extremity, close to the faulted contact with the Liassic rocks, the ferro-magnesian minerals become strongly aligned with the apparent dip of the Muzelle fault. This is possibly a secondary metamorphic effect due to Alpine reactivation and movement along the MTF, this is supported by the almost total chloritization of the biotite together with a parageneses of albite, quartz and calcite close to the fault line.

Near the PCP-SL ridge, close to the Brèche de Valsenestre, the granite is cut by large pegmatite veins which are topaz (0.5 to 1 mm in size), and cordierite bearing, together with some veins of aplite. This would perhaps indicate that this part of the granite is within the roof zone. If this is indeed the case and taking into account that the thrusted base of the granite is found in the Beranger valley, the minimum volume of magma is of the order of 10 to 12 km^3 i.e. a moderate sized silicic magma chamber. North of the ridge the granite forms the cirque of the Combe de Belle Cote and the peak of the Roche de la Selle. Further to the west the boundary is formed by a sedimentary horizon when the granite disappears under the Mesozoic cover, whereas to the north and north-west it is fault bounded against the migmatites of the ridge which runs from behind the Roche de la Selle down to Lac Lauvitel. The eastern boundary is formed by a zone of mylonite, but from field relations it is difficult to ascertain whether the mylonite is of granitic i.e.QTBC origin or the migmatites of the La Lavey formation which form the eastern slopes of the valley. Whilst movement on the zone of faulting shows elements of thrusting, the latest

movements(striations and calcite/quartz mineral growth directions show right lateral movement in a northerly direction.

In the region of the Belle Cote the QTBC granite is very similar to the southern part, being a medium-grained slightly porphyritic rock. However, it is slightly more melanocratic, with a greater abundance of more or less chloritised biotite, especially within the vicinity of the basic intrusives. Near the contact with the basic dykes the ferro-magnesian minerals show a preferred orientation of 120°, abutting the contact at an oblique angle. The reasons for this are not totally clear, it could be argued that if the granite was not totally solid, but retained a certain plasticity, then this may account for this localized orientation, although the fact that the form of the intrusions are dykes indicates that the granite had a certain cohesion at their time of emplacement. This is born out by the sharp nature of the dyke-granite contact with no signs of mechanical interaction in the form of mixing.

Two distinct types of basic enclaves or intrusions associated with the QTBC granite have been identified. The first occurs as quite a large (tens of square metres surface) enclave, having a roughly ovoid shape and outcropping just to the north and above the pinnacles of the Quatre Tours. In hand specimen the rock is grey-green in colour, and has both a fine grained and a medium-grained equigranular facies. The principal minerals are hornblende and plagioclase feldspar with subordinate potassium feldspar, biotite and honey-coloured sphene: this is the dioritic type. The second type of basic rock is a syenite which occurs as small (3-5 metres surface area) enclaves, notably in the cliffs above and to the east of the Cabin de Valsenestre (Fig 2.1), and along the line of the VTF(west) in the Vallon, between 2000 and 2400 metres (not shown in Fig. 2.2). Similar rocks occur as large dyke-like intrusions as in the Combe de Belle Cote (Figs. 2.7,2.8).

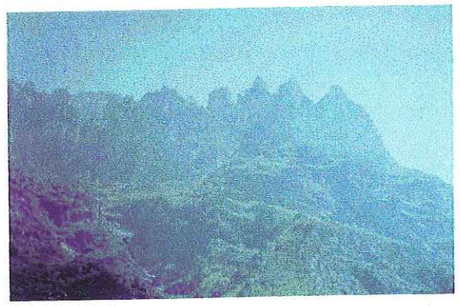

Plate 2.11

Plate 2.12

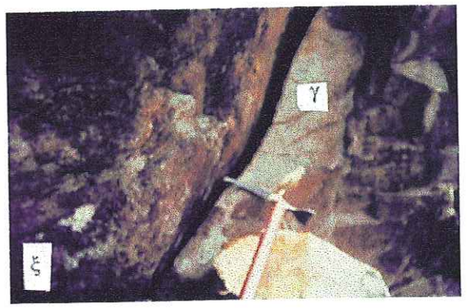

Plate 2.13

Plate 2.14

Plate 2.15

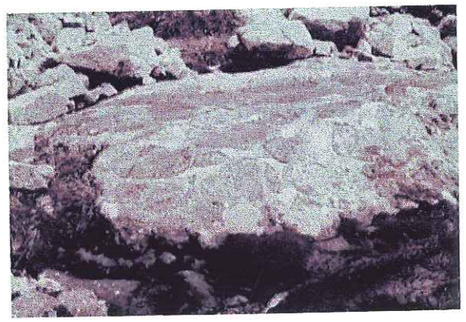

Plate 2.16

Plate 2.11 The Pinacles of Les Quatre Tours looking towards the east from Alfrey.

Plate 2.12 Facies containing ovoids from the centre of the largest syenite dyke, Belle Cote. The ovoids have an actinolite rim, with the centres being a mixture of biotite, amphibole, feldspar and opaques.

Plate 2.13 Fine grained granite vein of the Alfrey granite, intruding country rocks (gneisses), southern contact of the granite.

Plate 2.14 View of the Alfrey granite, here overlain by Mesazoic cover, Combe de Guyon looking south west.

Plate 2.15 Monzosyenite with a amphibole rich granite, erratic block from Les Gauchoirs, in the northern part of the Rochail massif.

Plate 2.16 Fractal enclaves of syenite within the granite, La Refuge des Sources, Rochail massif.

The dykes are sub vertical with a dip of 62° to 65° to the east (Fig.2.7). Here the rocks consist mainly of melanocratic syenites, showing a marked schistosity orientated in the direction 020° and having a dip of 35 to 40° to the east. This is either an Alpine overprint or might possibly be an original fabric. The mineral assemblage is hornblende, biotite, plagioclase feldspar, orthoclase feldspar, sphene, apatite and occasional calcite. There are also less extensive monzo-syenites with a similar mineralogy, but also including large, (several centimetres), poikolitic potassium feldspar phenocrysts. Towards the centre of the largest syenite dyke, a thin (1 to 2 metres thick) band of rock containing small ovoid inclusions occurs (Plate 2.12). These inclusions are aligned with the schistosity and have a radiating fibrous texture with a 1 to 2 mm border of biotite crystals. De Boisset (1986) considered these to be pseudomorphs after original olivine, but there is only a small amount of petrological evidence to support this (citop: Chapter 3).

2.3.3 ALFREY GRANITE

The Alfrey granite takes its name from the high point on the western ridge of the Vallon de Valsenestre, and has a surface outcrop of approximately 2.5 square kilometres. To the south and south-west the granite has been intruded into a series of banded gneisses, biotite schists and migmatite gneisses(Fig. 2.2), and whereas veins of granitic material cut the country rock,(Plate 2.13) no evidence of thermal metamorphism has been observed. This would therefore indicate that a) the country rock was at, or near, the temperature of the intruding granite and b) either the fluid phases remained within the confines of the intrusion or the Alfrey granite was relatively dry. The occurrence of a number of aplitic veins but very little pegmatitic material, within the contact region, and

the existence of pegmatitic material towards the supposed centre of the intrusion would indicate that the fluid phases remained within the confines of the intrusion.

The granite is overthrust at its eastern extremity by a thin band, (10 to 15 metres thick), of mylonite/gneiss, (not indicated on Fig. 2.2), which is undoubtedly part of the QTBC granite as it quickly grades into the QTBC granite, with no apparent contact. To the north the Alfrey granite is first faulted against, but then disappears under rocks of Triassic and Liassic age in the Lac Labarre syncline (Barfety and Gidon, 1983)(Fig. 2.5,2.6: Plate 2.14). Three or four kilometres further to the west a number of small stocks of granitic material have been mapped (with a total surface area of less than 0.5 km^2) (A.Pecher pers. comm and 1:50000 BRGM La Mure sheet, 1989.), these are very similar in appearance and make up to the Alfrey granite.

The Alfrey granite is medium grained, especially in the valley of the Combe Guyon where, locally, it can be quite dark with the development of a biotite-rich facies. Further towards the east and away from the contact zone the granite becomes porphyritic with the development of potassium feldspar phenocrysts, up to 2 or 3 cms in length which, in the region of the Pisse Rousse, show a preferred orientation of N090°. This facies is quite close to the PRF fault, and this prefered orientation could be evidence that this fault was active during the emplacement of the Alfrey granite but is most probably a primary magmatic flow texture, related to an emplacement direction. It is here in the centre of the AG, that some small veins of pegmatite appear, indicating that an exsolved fluid phase was more prevalent towards the centre of this small intrusion.

The Alfrey granite differs from the Rochail and QTBC granites in having no associated suite of basic rocks, apart from rare, small, highly altered and rounded xenoliths. These are made up, for the most part, of small crystals of plagioclase feldspar surrounded by

small lath-like crystals of chlorite after biotite. As well, the Alfrey granite unlike the QTBC and Ramu granites, shows evidence of its in situ emplacement.

2.3.4 ROCHAIL GRANITE

Lying to the north of the band of migmatitic basement gneisses which form the limit of the QTBC granite, and to the north and west of Lac Lauvitel is the Rochail granite. This is a large pluton with a surface area of greater than 30 square kilometres (Fig 2.9). This intrusion has been studied by a number of workers in the past (Giraud, 1952; Buffiere, 1963,1964; Giorgi, 1981; de Boisset, 1986). Here the observations are limited to that part of the granite which crops out within the immediate vicinity of Lac Lauvitel in the east and the Lac du Plan Vianney beneath the Brèche de Perier in the west (Fig 2.1).

The granite generally consists of a fine to medium-grained facies, grey in colour although, locally, biotite becomes sparse, giving rise to a more leucocratic rock. Close to the syenitic intrusions of the Cascade de Lauvitel (Figure 2.10 and Fig.2.11) and les Gauchoires (Fig.2.10) a facies with a light green hornblende and pink potassium feldspar is developed (Plate 2.15). It is limited to a band of one or two metres maximum width and some several metres long, and is clearly a reaction between the syenite and granite, perhaps indicating that at the time of intrusion of the syenite, the granite was not entirely solid. This hypothosis is further born out by the syenite intrusion at Les Sources (further to the northwest, Fig.2.10), where the granite and syenite display fractal textures,(Plate 2.16) and a certain amount of mixing of the two magmas has taken place. However, in general the granite is very homogenous. Tourmaline bearing pegmatites and aplites are fairly common, and some evidence of cross cutting was found in the vicinity

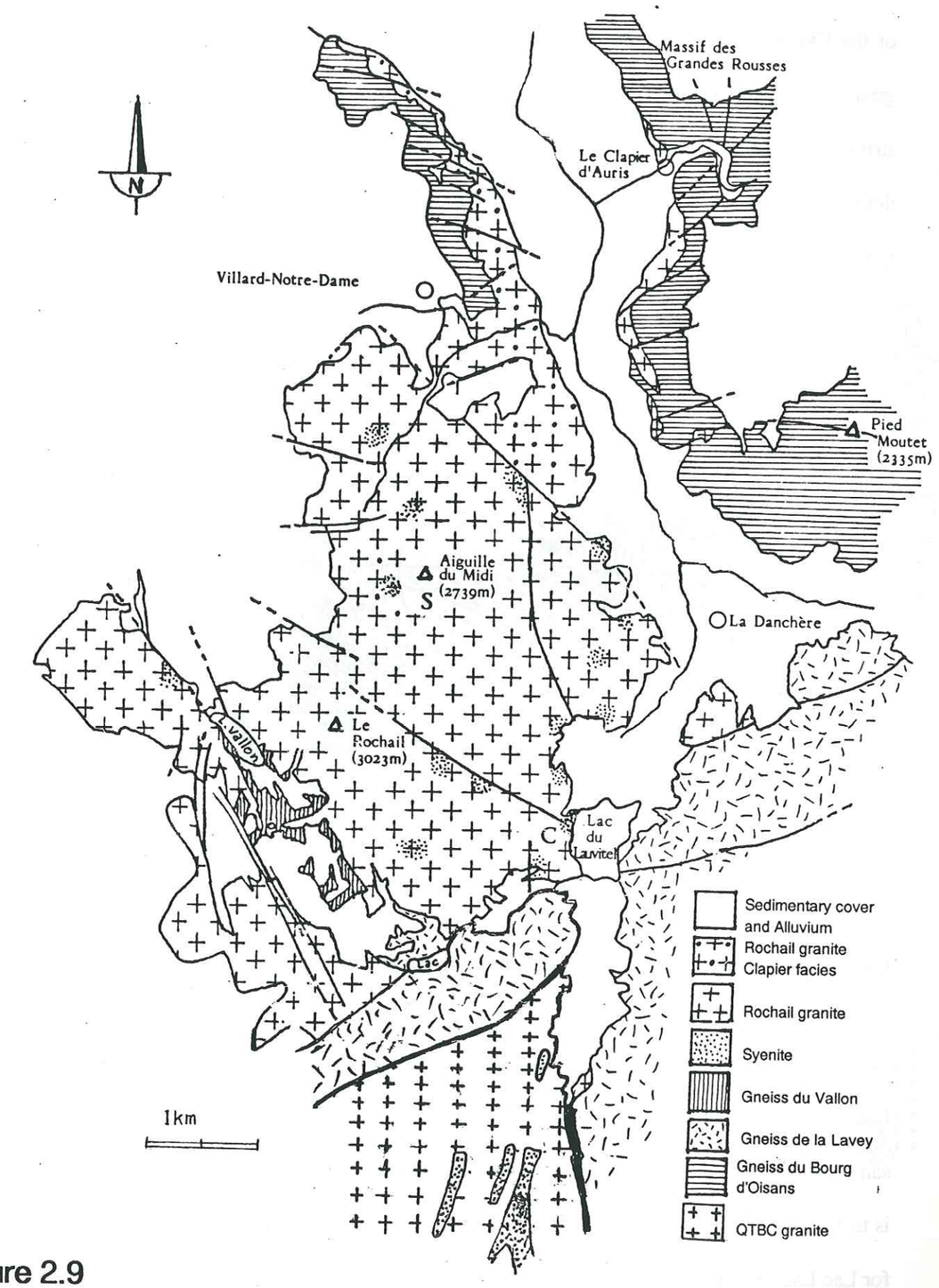

Figure 2.9

Generalised geological sketch map of the Rochail granite.

(After Buffiere, 1963)

of the Cascade, (Fig.2.11) indicating that the aplites are later than the pegmatites. The granite has suffered some late tectonic deformation with the development of normal and strike-slip faulting in a general east-west direction. Small cataclastic shear zones are also developed within the granite, and the accompanying mylonites and chloritization are typical of Alpine deformation.

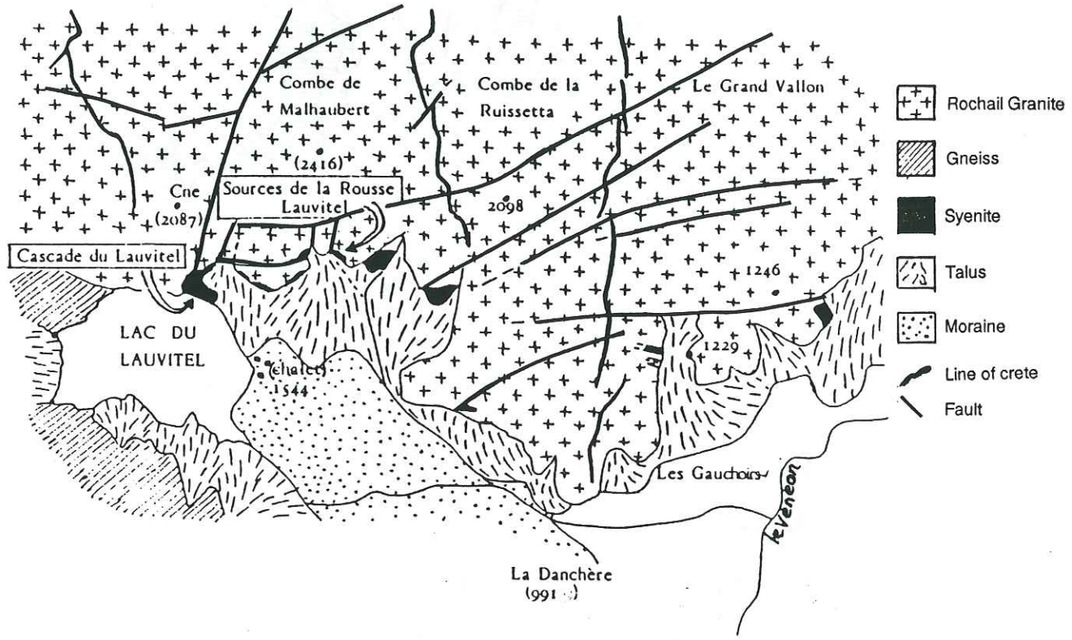

Figure 2.10 Detail of the Rochail granite in the region of Lac Lauvitel.
(after T. de Boisset,1986)

Several syenite intrusions appear in this part of the granite, notably at the Cascade de Lauvitel and Les Gauchiors (indicated on Fig. 2.2 and fig. 2.10), but do not attain the same dimensions as those found in the Belle Cote, although a fair amount of the material is to be found in the major rock fall which blocks the valley and makes the natural dam for Lac Lauvitel. The intrusion at the Cascade de Lauvitel is some tens of square metres

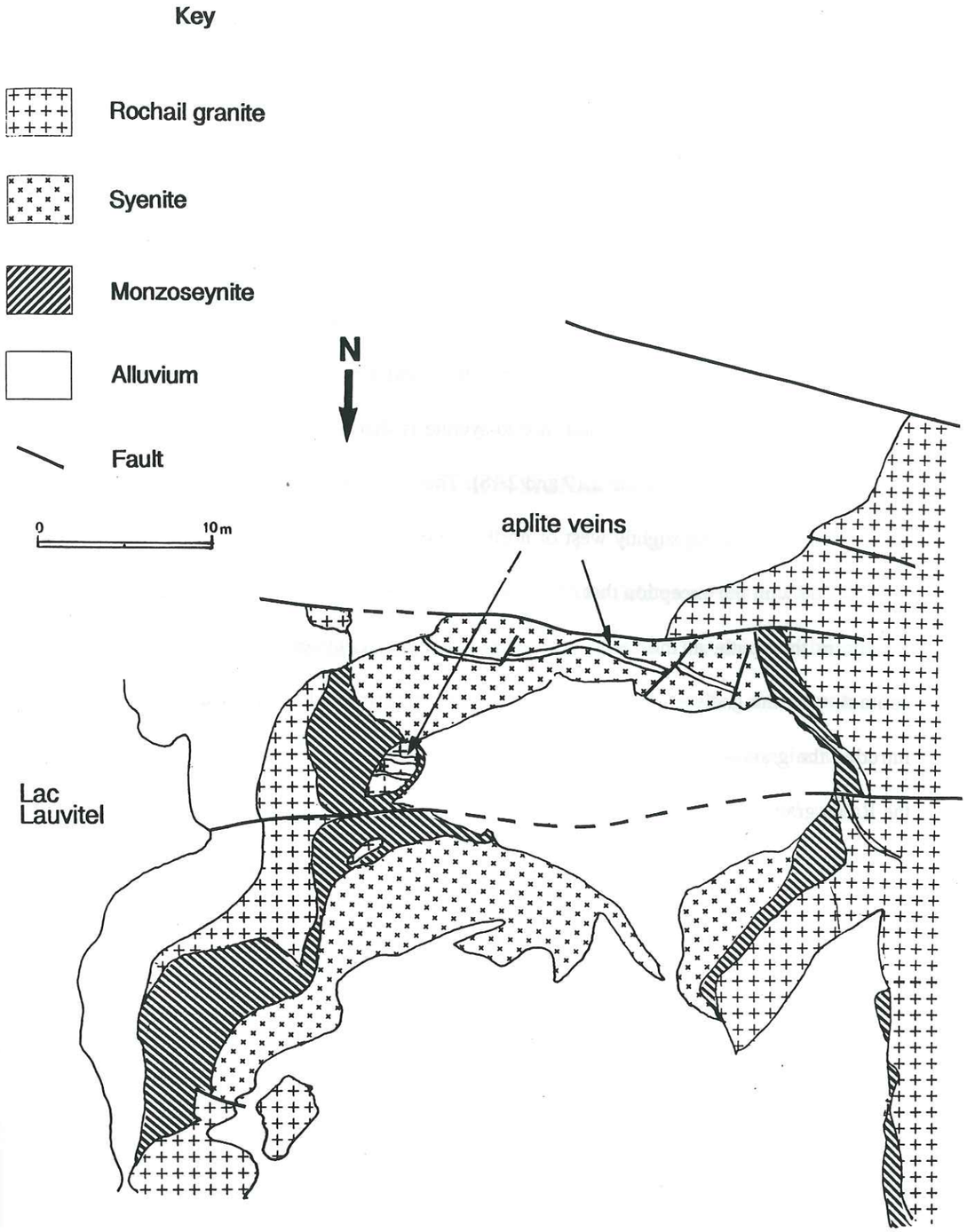

Figure 2.11
Detailed map of the syenite intrusion at the Cascade de Lauvitel

at outcrop and contains two different facies, these are detailed in Figure 2.11. The centre of the intrusion consists of a dark melanocratic, coarse grained, hornblende and biotite rich syenite, whereas the outer edge (2-5 metres thick) consists of a lighter coloured monzo-syenite with large (up to several cms) potassium feldspar crystals, poikolitically enclosing both amphiboles and biotites. As well, the monzo-syenite contains a number of enclaves or autoliths of the darker central syenite, and a number of granitic enclaves. The contact between the syenite and monzo-syenite is sharp, as is the contact between monzosyenite and granite (Plate 2.17 and 2.18). The intrusion at Les Gauchoirs is in the form of a dyke trending slightly west of north, the facies being very similar to those at the Cascade with the exception that no enclaves were seen.

Finally, in the south, at the south west corner of Lac Lauvitel, close to the faulted contact with the gneisses, a 4 to 5 metre wide lamprophyric dyke, trending N040°, has intruded the granite. This is in all respects similar to the lamprophyres observed within the Ramu granite, and elsewhere in the ECMs.

2.4 DESCRIPTION OF THE METAMORPHIC ROCKS

Here the metamorphic rocks considered are those of the basement, with a probable pre-Cambrian to Lower Proterozoic age.(See Chap. 1, Von Raumer, 1984, Menot et al, 1990)

2.4.1. SOUTH OF THE CLAPIER DU PEYRON SIGNAL DE LAUVITEL RIDGE

East of the Muzelle thrust fault the metamorphic rocks of this field area form the north-westward extension of the "Series Corticales" of the Haut Dauphiné. This series has been described by Termier (1901) and Le Fort (1973), while Le Fort (1971) and Bartoli (1973), gave detail on the principal formation of this series in the type locality, i.e. the valley of Le Lavey, where a thick sequence of acid migmatites interleaved with occasional but persistent horizons of amphibolitic gneisses occurs. These amphibolites, in turn, contain occasional but non persistent bands of marble or 'CIPOLIN'. The Series Corticales have been interpreted (LeFort, 1973) as a volcano-sedimentary sequence which has suffered at least two episodes of metamorphism and deformation. Hence these rocks can be interpreted as belonging to the A1 formations of Upper Proterozoic to Lower Paleozoic age (Chap. 1). As a minor point of interest, in the past the marbles have been commercially exploited (Carriére des Combes above Valsenestre: Barffety et al., 1989). Beneath the QTBC granite in the Beranger valley(bottom centre of Fig.2.2) is a small outcrop of this same series, thrust fault bounded above by the granite, and in the west, normally faulted against a small slice of Mesozoic rocks.

South of the Alfrey granite and forming the cliffs which dominate the village of Valsenestre (Plate 2.19), is a series of undifferentiated banded gneisses intercalated with more or less persistent horizons of biotite schist. A relatively thick (45 m) band of amphibolites occurs to the west of the point of Le Peys in the valley of the Combe Guyon (South Western corner of Fig.2.2), they show a complex deformation history with folds of both metric and centemetric wavelength (Plate 2.20). These amphibolites continue beneath the granite of Le Chalp on the south side of the Beranger valley (not shown on Fig. 2.2), but nowhere do these amphibolitic horizons achieve the same thickness or persistence as those outcropping in the La Lavey valley to the east of this region (Termier, 1901; Le Fort, 1973; Bartoli, 1973).

Lying above the amphibolite gneiss formation is a series of acid migmatite gneisses. The foliation in the acidic gneisses is made up of alternating bands of quartz plus feldspar with bands of amphibole and biotite. Frequent pods of folded granitic material occur, up to 2 metres in length, indicating that at one stage in their history these rocks had probably approached their fusion temperature.(Plate 2.21)

It is difficult to decide on mineralogical grounds whether or not this acid series can be correlated with the La Lavey gneisses or whether they are lower down in the sequence. However from structural data this would appear to be the case.

4.2.2.NORTH OF THE CLAPIER DU PEYRON-SIGNAL DE LAUVITEL RIDGE

In the northern sector in the Lauvitel Valley, the ridge running from behind the Roche de la Selle eastwards to the southern end of Lac Lauvitel (Fig. 2.1) consists of a series of

well amphibolitic banded gneisses. These show evidence of several phases of ductile deformation, in the form of refolded isoclinal folds. In general they are darker and more amphibolitic in nature than the acid gneisses which outcrop on the other side of the valley in the north eastern sector, but their relationship is not clear.

The leucosomes are made up essentially of quartz and potassium feldspar with occasional chlorite after biotite. The melanocratic layers consist of fine-grained biotite with subordinate amphibole, finely layered with occasional large crystals of plagioclase feldspar that show good deformation shadows, and rare broken and corroded garnet.

The gneisses which outcrop to the east of Lac Lauvitel and run southward under the Tete de la Muraillette, and over which the Ramu granite has been partially thrust, consist of a thick (at least 2 kms) and monotonous series of more or less migmatised acid gneisses. The development of quite extensive leucosomes, which frequently cross cut the schistosity, indicates a high P-T regime. They are very similar in many respects to the acid gneisses found to the south of the Alfrey granite (Fig. 2.2). The only difference is that in the north, alteration is well developed, with almost total chloritization of the ferro-magnesian minerals, and white mica is extensively developed at the expense of plagioclase feldspar. Deformation consists of a complex system of small scale folds (metre scale) and two foliations, one penetrative and concordant with the axial planes of the folding, whereas the second cuts across the first and is not penetrative. Again from the structural relationships these acid gneisses which form the base of the La Lavey formation appear to be higher in the sequence than the more amphibolitic gneisses as overthrusting is from the east. Stratigraphically, this makes sense in the context of an Upper Proterozoic volcanic arc.

Plate 2.17 Contact between the syenite facies (σ1) and the monzosyenite facies (σ2), Cascade de Lauvitel, southern part of the Rochail massif.

Plate 2.18 Contact between the Rochail granite (γ) and monzosyenite (σ2), Cascade de Lauvitel, southern part of the Rochail massif. (Note the aplite viens cross cutting the granite, but not themonzo-syenite, an indication that the granite was already in a solid state at the time of the intrusion of the basic rocks.

Plate 2.19 Undifferentiated gneisses and schists. Cliffs above the Village of Valsenestre.

Plate 2.20 Folded and tilted amphibolite gneisses, Combe du Guyon.

Plate 2.21 Folded granitic leucosomes in acid gneisses, 100 metres above plate 2.20, Combe du Guyon.

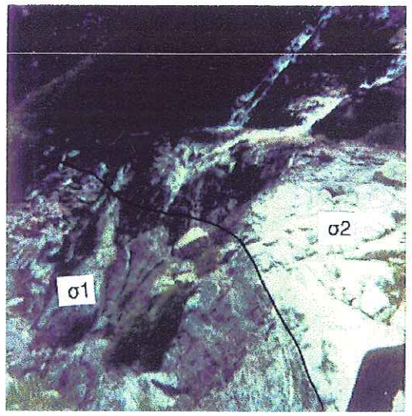

Plate 2.17

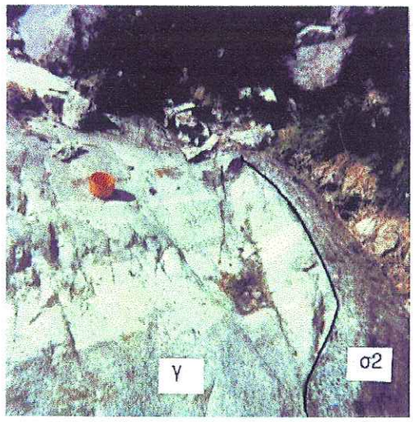

Plate 2.18

Plate 2.19

Plate 2.20

Plate 2.21

2.5 SEDIMENTARY COVER

Towards the end of the Carboniferous period this part of the Western Alps, became subject to deposition of sediments within a series of basins. Vestiges of rocks of Carboniferous and Permian age are found both to the west, where coal-bearing strata of Westphalian D or Stephanian age occur at La Mure (Sarrot-Reynauld, 1961,1963), and in the north where a thin band of mainly sedimentary rocks of Carboniferous age , including some acid volcanics (Lameyre, 1958), runs down the eastern side of the Grandes Rousse massif to terminate in the valley of La Lavey. These rocks have suffered Alpine deformation and metamorphism, and remain as small slices pinched in the Alpine fault system.

During late Permian and early Triassic times the region was involved in distension, peripheral to the opening of what would become the Tethyan ocean. This event was marked by the extrusion of thick sequences of basic spilitic volcanics (Vatin-Perignon et al., 1974,1977; Buffet and Aumaitre, 1973; Buffet, 1981; Adeline, 1982). It is probable that at least some of the lamprophyric veins which cut the basement where associated with this volcanism.

This period was followed by one of deposition in a series of ensialic basins and finally, in shelf sea and shallow oceanic conditions during Liassic times and onwards. At some later time the deposition of sediments ceased when the closure of the Tethyan ocean was in full spate, and the region was again involved in uplift and deformation. The first evidence of this is an increase in temperature, determined by Rb/Sr and K/Ar measurements, with a marked metamorphic event at 152+/-12 Ma (Vittoz et al., 1987, opcit, Chapter 5),

followed by several subsequent thermal events at 69+/-2 Ma, 39+/-7 Ma and 15+/-1.2 Ma (Demeulmeester, 1982). During the period dating from late Mesozoic times to the present day, the region has undergone a severe crustal shortening, with the result that not only have old Variscan normal, thrust and strike-slip faults reactivated in the crystalline basement, but also the soft sedimentary cover of the Lower Mesozoic has been spectacularly deformed and folded. The vestiges of this deformation appear as a number of synclinal and anticlinal structures, e.g. the Bourg d'Oisans complex (Carte Geologique de la France, Vizille, Series 1:50000).

In the field area the Mesozoic cover is limited in the eastern part to a thin band running north-south. This is the southern extension of the eastern arm of the Bourg d'Oisan syncline, which has filled in and then been shortened by the Muzelle fault zone (Barfety and Gidon 1981). In the west and forming a projecting west to east tongue across the Vallon de Valsenestre are the sediments of the Lac LaBarre syncline Fig.2.2 (Barfety and Gidon, 1983). This area is an eastwards extension of the Col d'Ornon structure (Barfety et al., 1989).

The sediments in the east have been compressed within the MTF, and consist entirely of grey slates. Whilst the sediments of the Lac Labarre syncline range from interleaved spilites, conglomerates and sandstones of Triassic age at the base, to fine grained calcileutitic shales at the top of the sequence.

2.6 SUMMARY AND CONCLUSIONS

The field area is a structurally complex region where crystalline basement in the form of Upper Proterozoic to Lower Paleozoic metamorphosed volcano-sediments have

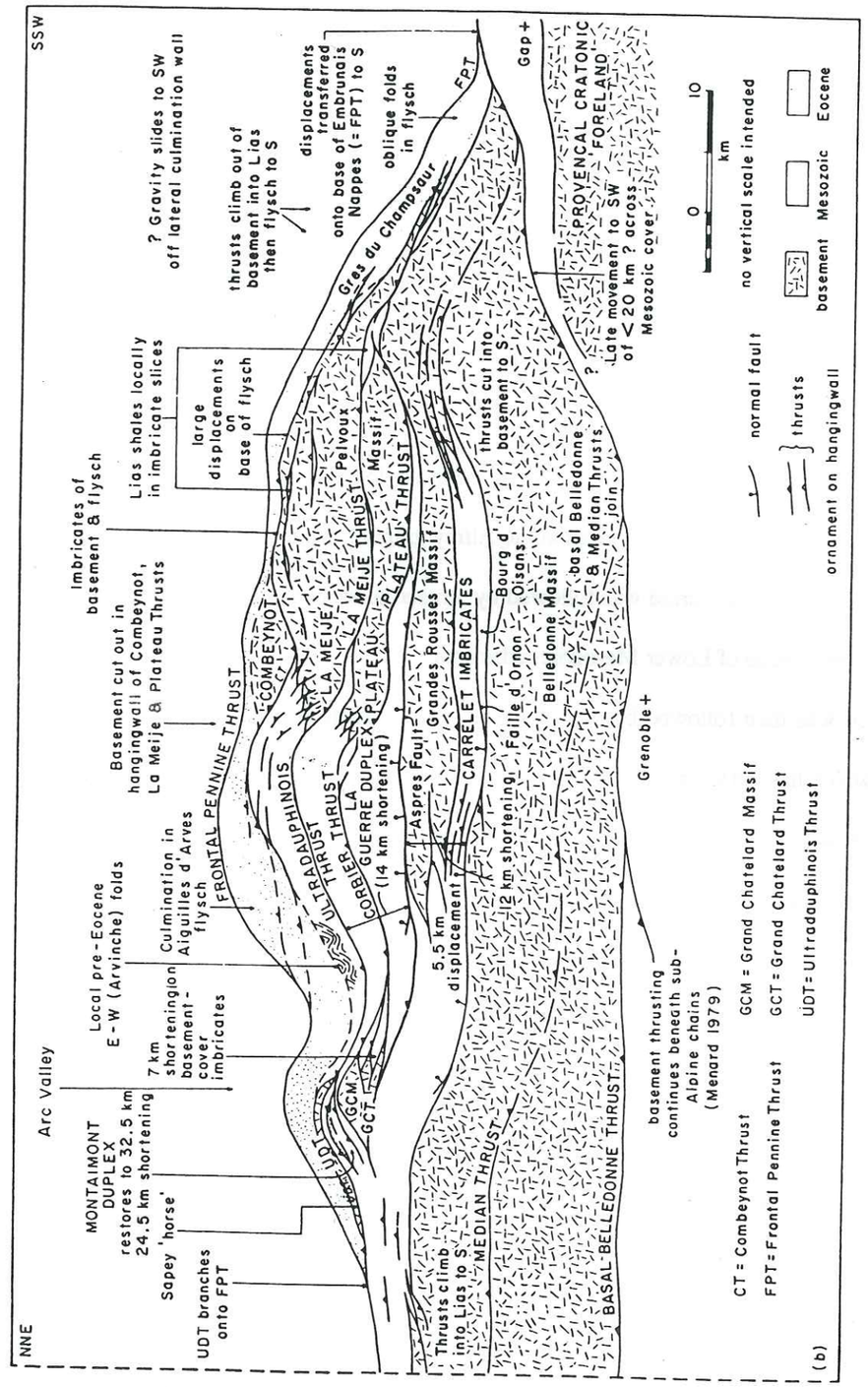

Figure 2.12 Part of a schematic longitudinal section along the North Western external Alpine Thrust Belt. (after Butler et al., 1986)

undergone polymetamorphism. These volcano-sediments have subsequently been intruded by a series of granitic rocks associated with a small suite of basic dykes and intrusions during Variscan times. Rb/Sr and K/Ar dates range from 340 Ma to 310 Ma (Demeulmeester, 1982: Vivier unpublished data and this thesis). During this period, syn-tectonic thrusting and possible strike slip movement have affected the region, and the major result of this deformation has been the creation of mylonitic zones often along the boundaries of allocthonous granite massifs. Following this period, the area suffered erosion (no evidence for deposition of Upper Carboniferous to Lower Permian sediments in this region has been found, although these do exist to the west and further north) and evidence of eroded surfaces in the Alfrey granite, which appears to be in situ exists (Plate 2.14). This period was followed by crustal extension, and the deposition of quite thick sequences of Lower Mesozoic sediments.

This period was then followed by one of severe crustal shortening, with thrusting from the east, which has led to the failure of the crystalline basement, essentially along existing lines of weakness, and the development of a series of thrust faults, which have resulted in the creation of a series of thrust sheets (Butler et al., 1986).(Fig 2.12)

Within the field area this has resulted in the overthrusting of the Ramu granite over the QTBC granite which has in turn been overthrust onto the Alfrey granite. Field relationships do not unequivocally demonstrate that this type of deformation was unique to the Alpine orogenic event. On the contrary it is probable that some of the observed deformation, in the form of strike-slip tectonics, was coeval with the emplacement of the intrusives, resulting in the creation of mylonitic zones in late Variscan times.

Subsequent deformation during Alpine metamorphic events has given a retrometamorphic overprint, especially close to the major fracture zones (Demeulmeester, 1982), whereas the Mesazoic cover has suffered intense deformation and mild metamorphism (slate grade).

CHAPTER 3

PETROLOGY AND MINERAL CHEMISTRY OF THE INTRUSIVE ROCKS

3.1 INTRODUCTION

The intrusive rocks of the Valsenestre region can be divided into two major types. The first, and in terms of surface outcrop and volume, the most important, are the granitic rocks. The second is a series of basic rocks which range from 49% SiO_2 to more intermediate varieties at 58% SiO_2. Termier (1980), who first described these rocks from an outcrop on the western side of Lac Lauvitel, called them syenites, whilst rocks, having somewhat similar mineralogy, chemistry and textures, have been described from the Massif Central (Lacroix, 1917; Couturie, 1977; Michon, 1979; Bellanger, 1980; Sabatier, 1980,1984) and been given the name of Vaugnerites after the village in the region of the Lyonnais where they were first described (Lacroix, 1917). (Vaugnerite; A dyke rock consisting of major amounts of biotite, pyroxene, hornblende and plagioclase feldspar with a little orthoclase; Le Maitre, 1989; Michon, 1979)

Similar rocks from the Vosges (Pagel and Leterrier, 1980; Pagel, 1981; Andre, 1983 for the Ballons pluton; and Hameurt,1968; Gagny, 1968; Fluck, 1980; Pagel, 1981 for the Cretes pluton) have been called durbachites. (Durbachite: fine to medium-grained melanocratic variety of syenite consisting of large flakes of biotite with hornblende and megacrysts of orthoclase in a groundmass of oligoclase and a little quartz.(Le Maitre, 1989). In fact the basic rocks of the QTBC-Rochail complex vary in composition, and whilst mineralogically they cannot be classified as vaugnerites, lacking pyroxene, they are also somewhat different chemically from durbachites. Following the classification of Streckeisen

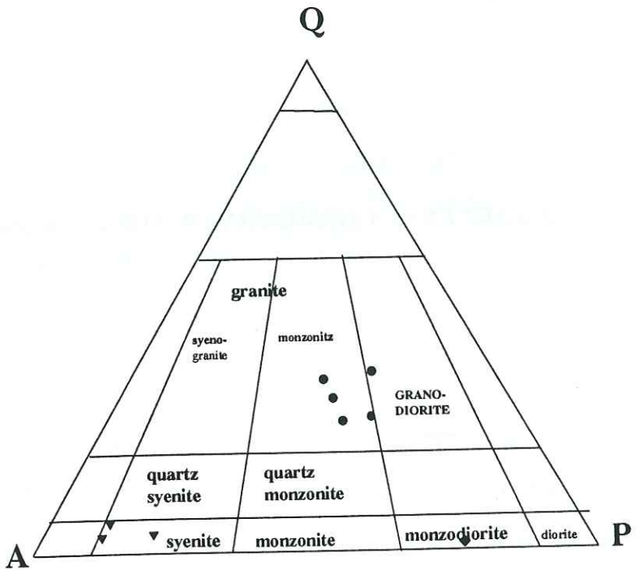

Figure 3.1 Modal classification of the igneous rocks from the Valsenestre suite.

(● granite ▼ syenite ● diorite)

(Fig. 3.1) these rocks fall in the domain of the syenites and alkali syenites. Therefore in this thesis, the term syenite will be used, unless the rocks have a definite dioritic mineralogy, as in the case of the large enclave found in the Quatre Tours region.

3.2 RAMU GRANITE

The Ramu granite is situated above and to the East of the Quatre Tours-Belle Cote granite and is separated from them by a major thrust fault, the VTF (East), together with a band of mylonites and gneisses, having a variable thickness of some tens up to a hundred meters. (see Fig. 3.2)

gure 3.2
STRUCTURAL AND GEOLOGICAL SKETCH MAP OF THE LAUVITEL-VALSENESTRE REGION, HAUT DAUPHINE
SCALE 1: 20000

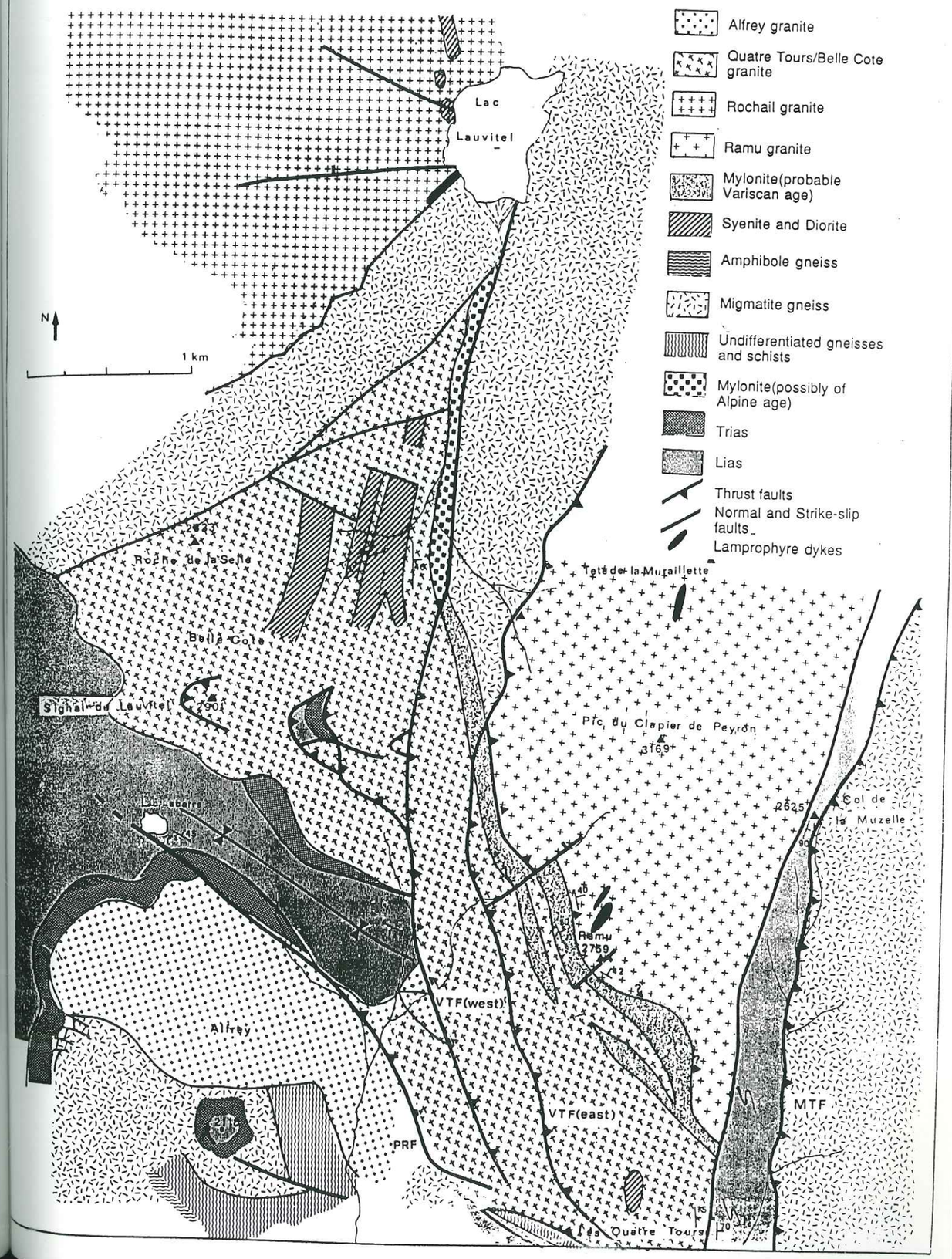

TEXTURE

The granite is generally a medium-grained leucocratic granite, with essential muscovite and subordinate biotite, usually chloritised. From time to time a coarser grained facies appears, this facies being characterised by the almost total absence of biotite/chlorite and the presence of very large (millemetric in size) crystals of muscovite Plate 3.1a.

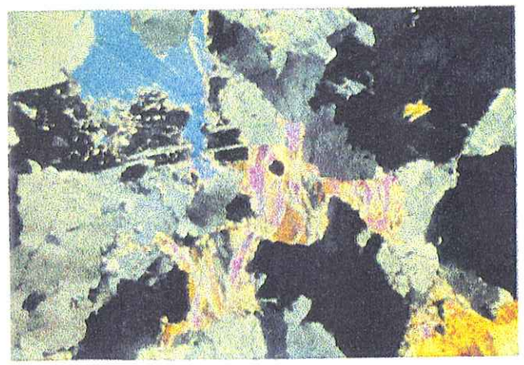

PLATE 3.1a Photomicrograph of large muscovite crystals in the coarse grained facies, Ramu granite.
(Crossed polarised light)

MINERALOGY

Plagioclase

Plagioclase feldspar, which makes up 34% of the rock, generally forms good euhedral crystals, frequently showing zoning, with the more calcium-rich bands being picked out by sericite. From time to time the edges show destabilisation textures with embayments and lobing especially when in contact with potassium feldspar. Small half digested crystals are sometimes found in the centre of potassium feldspar (Plate.3.1b) indicating the late growth of this mineral. The plagioclase is in general an oligoclase varying from An 12 to An 18 .

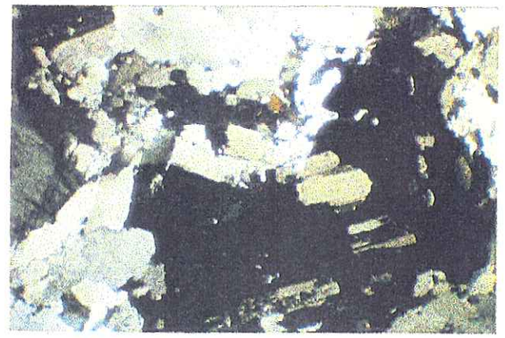

Plate 3.1b Photomicrograph of pöikolitic potassium feldspar with ingested, orientated plagioclase feldspar, Ramu granite.
(Crossed polarised light)

Potassium feldspar

This occurs either a) as relatively rare, large crystals of perthite having a pöikolitic texture and containing half digested crystals of plagioclase, with more rarely, small crystals of muscovite and occasional small laths and crystals of apatite or b) more normally, smaller euhedral crystals of microcline. Where the perthite is in contact with plagioclase, textures showing the destabilisation of the later are present. The lobes formed by this destabilisation show myrmekitic textures (Plate 3.1c) indicating that the two crystals were not in equilibrium. This would suggest either a low temperature and probable shallow depth of crystallisation for this granite, or alternatively a sub-solidus re-equilibration. Modally K-feldspar represents from 25 to 30% of the total.

Muscovite

This mineral occurs as small elongated laths, (e.g. Plate 3.2) within the finer-grained textured facies, sometimes associated with biotite, which has generally been altered to chlorite. Often the muscovite shows deformation with kinking and necking into interstitial positions, indicating its relative early formation.(with respect to K-feldspar and quartz). If it

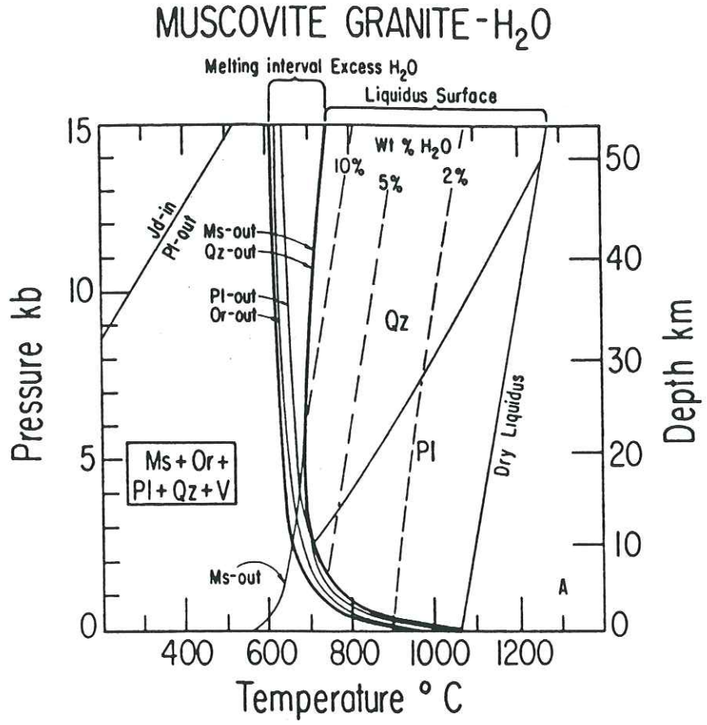

Figure 3.3 A) Phase diagram for a muscovite bearing granite, for pressures up to 15kbar. Based on experimental data.
B) Conditions for the fusion of rocks in the system gabbro - tonalite - granite - H_2O. Lines a toe indicate some depth - temperature paths estimated for rocks subjected to regional metamorphism (Turner, 1968), areas f and g are estimated P -T conditions for high grade metamorphism. From this it can be seen that the Ramu granite could have been generated from rocks as high as 10 km crustal depth.
(Figures from Wylie, 1983)

Plate 3. 1c Photomicrograph showing myrmakitic textures between feldspars, the coloured mineral in the centre is chlorite after biotite, Ramu granite.
(Crossed polarised light)

is a primary mineral, then the temperature of crystallisation must have exceeded 700°C at greater than 1.5 kbar (Deer, Howie and Zussman, 1960). These conditions can be obtained at relatively shallow depth (Wylie, 1983) Fig. 3.3 and may be considered as further evidence of the high level origins for this anatexic granite. In the coarser grained facies muscovite occurs as large (millimetre size) well formed crystals Plate. 3.1a, these tend to cut and infill fissures in the plagioclase whilst at the same time fissures in the muscovite are infilled by perthitic potassium feldspar.

Quartz

Quartz is the most abundant mineral (up to 40%) and generally takes up interstitial positions indicating its late development. It quite often shows signs of tectonic deformation with well developed mortar textures especially in the medium-grained facies. Larger but interstitial crystals in the coarser-grained facies show undulose extinction indicating their growth under conditions of strain (crystallisation during emplacement or re-crystallisation during later deformation?).

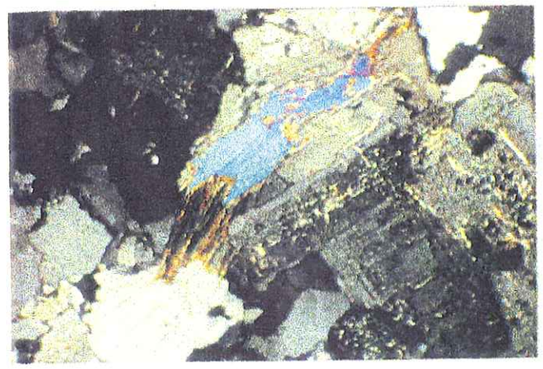

Plate 3. 2 Photomicrograph of the fine grained facies of the Ramu granite showing the interstitial lath-like habit of muscovite.

(Crossed polarised light)

Minor phases

Apatite occurs as rare small crystals and laths in association with potassium feldspar. Rare zircons, with metamict centres are associated with muscovite, these could be inferred as being relicts from the source rocks, but late stage crystallisation from post-magmatic fluids or eventual tectonic processes can not be ruled out, although this later hypothesis is somewhat fragile as no evidence of high grade metamorphism has been found in this granite.

CRYSTALLISATION SEQUENCE

	liquid	crystal mush	quasi-solid
Plagioclase	----------		
Perthite		----------	
Muscovite		----------	
Microcline			----------
Apatite		----------	
Zircon	----------		
Quartz			----------

Table 3.1 Possible sequence of crystallisation for the Ramu granite

Summary and Conclusions

The Ramu granite both from its texture and mineralogy lends itself to the hypothesis of a high level anatexic granite, but formed under conditions where P> 1.5 kb and T≈ 700°C. The probable order of crystallisation is plagioclase, perthitic potassium feldspar and muscovite together with apatite and finally quartz (Table 3.1). The close association of the granite with the acid gneisses of the westward extension of the La Lavey formation and especially the fact that half digested gneissic blocks are quite frequent, indicates the possible source rock for this anatexic end product.

3.3 THE QUATRE TOURS/BELLE COTE GRANITE

The granite forms an elongate slice from the pinnacles of the Quatre tours in the Vallon de Valsenstre in the south to the northern contact with basement gneisses in the Lauvitel valley (Fig 2.2 and 3.2). The QTBC granite shows some variation in texture over its length, and has a number of associated basic dykes and enclaves of both syenite and diorite. In the north, small veins of granite were observed cutting the gneisses in the western wall of the valley, at point 1 on Fig. 3.4. Subsequent geochemical analysis shows that these veins are very similar to the main body and are probably part of it.

TEXTURE

To the south and east, close to the contact with the basement rocks, the QTBC granite is a fine to medium grained equi-granular rock, showing a marked lineation of the ferro-magnesian minerals close to the faulted contact with rocks of Liassic age, further north and west however the granite becomes much coarser grained, eventually becoming quite porphyritic in texture. At the highest point of the granite, to the west of the Breche de Valsenestre the granite is cut by a number of veins of pegmatite, which contain small crystals of topaz and large crystals of early formed apatite . Aplites also occur, cross cutting

Figure 3.4 Sketch map of the northern part of the Quatre Tours/Belle Cote and the Rochail granite.

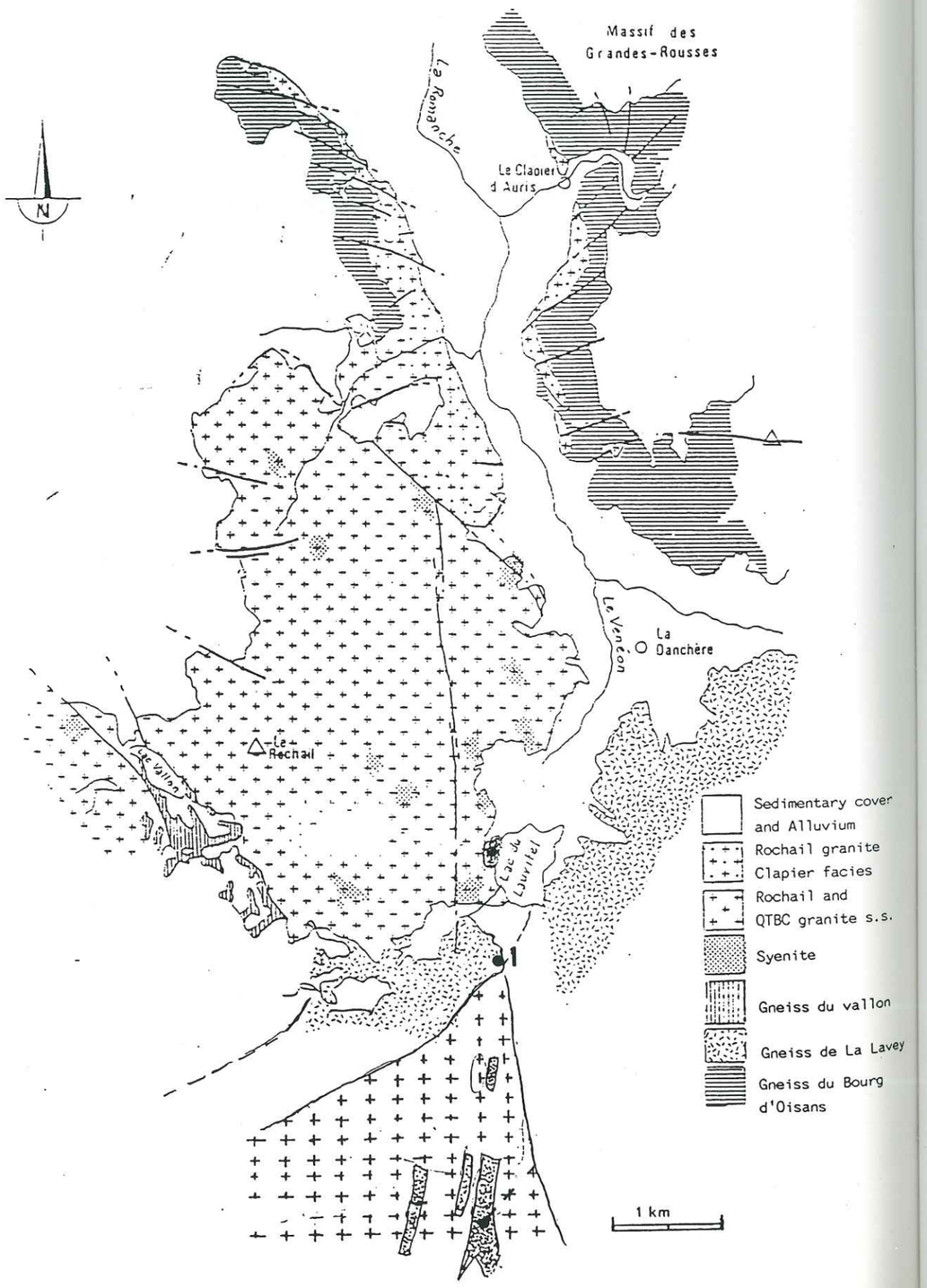

the granite and pegmatites. This would seem to indicate that the granite was fairly wet at least in its final stages of cooling.

The granite north of the PCP-SL ridge is a medium grained iso-granaular rock, with occasional phenocrysts of potassium feldspar, generally showing no preferred orientation. However the QTBC does show from time to time a marked lineation especially of the ferro-magnesian minerals. Here it has suffered a greater degree of relatively low temperature (i.e. Alpine) deformation, than that at the northern end of the valley, and this is reflected in the cataclastic nature of certain of the minerals e.g. potassium feldspar and more especially quartz which shows up microscopically in small shear zones with well developed mortar textures. These cataclastic textures tend to be particularly well developed adjacent to the thrust faults. Towards the northern end of the valley the grain size becomes progressively smaller and the phenocryst phase dies out all together. This may be a reason for the relative reduction in cataclastic textures, as the finer grained rock, being mechanically stronger will have better resisted tectonic forces. Ferro-magnesian minerals, biotite and chlorite after biotite, when close to fracture zones, show lineations, perpendicular to the fault plane, which may indicate that tectonic deformation was in progress during the emplacement of the granite.

MINERALOGY.

Due to the differences observed between the northern and southern parts of this granite, a separate mineralogical description has been made for the two halves.

1. QTBC North of the PCP-SL ridge

Plagioclase Feldspar

Plagioclase is well represented and is often the most abundant mineral (modal 35-40%). Crystals tend to be well formed (Plate 3. 3) and euhedral, indicating a facility of growth during their crystallisation. The plagioclase which is an Oligoclase (An 15 to An 20)

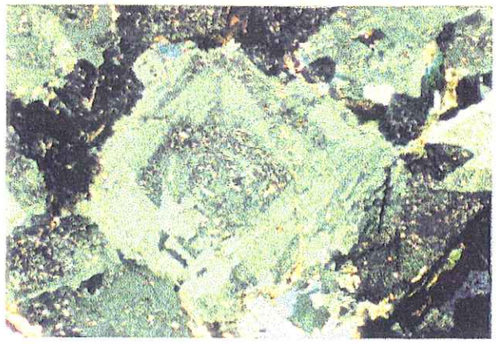

Plate 3. 3 Photomicrograph showing zoned plagioclase feldspar, QTBC granite. (Crossed polarised light)

frequently shows marked destabilisation textures with the formation of myrmekitic edges and a relatively strong degree of sericitisation. The formation of calcite in the centres of some crystals, may indicate the more basic nature of the early liquid or alternatively may be an indication of late stage CO_2 rich hydrothermal activity, although there is little other evidence of this.

Biotite

The majority of the biotite crystals (modal 3-5%), (which show extensive chloritization), have been squeezed into interstitial positions. The microscopic structure suggests the crystallisation of biotite associated with apatite and zircon, just before or perhaps contemporaneously with the potassium feldspar. This could explain the interstitial nature of the biotite crystals (Fig. 3.5) This is however petrologically and mineralogically difficult to envisage, and a more feasible explanation would be that the fast crystallisation of the potassium feldspar, whilst the granite was undergoing deformation during the later stages of crystallisation, has pushed the biotite crystals, which are relatively easy to deform, into these interstitial positions, this is born out by; a) where the rock is relatively free of K feldspar, the biotite remains undeformed and b) both biotite and plagioclase show kinking whilst quartz has well developed undulose extinction.

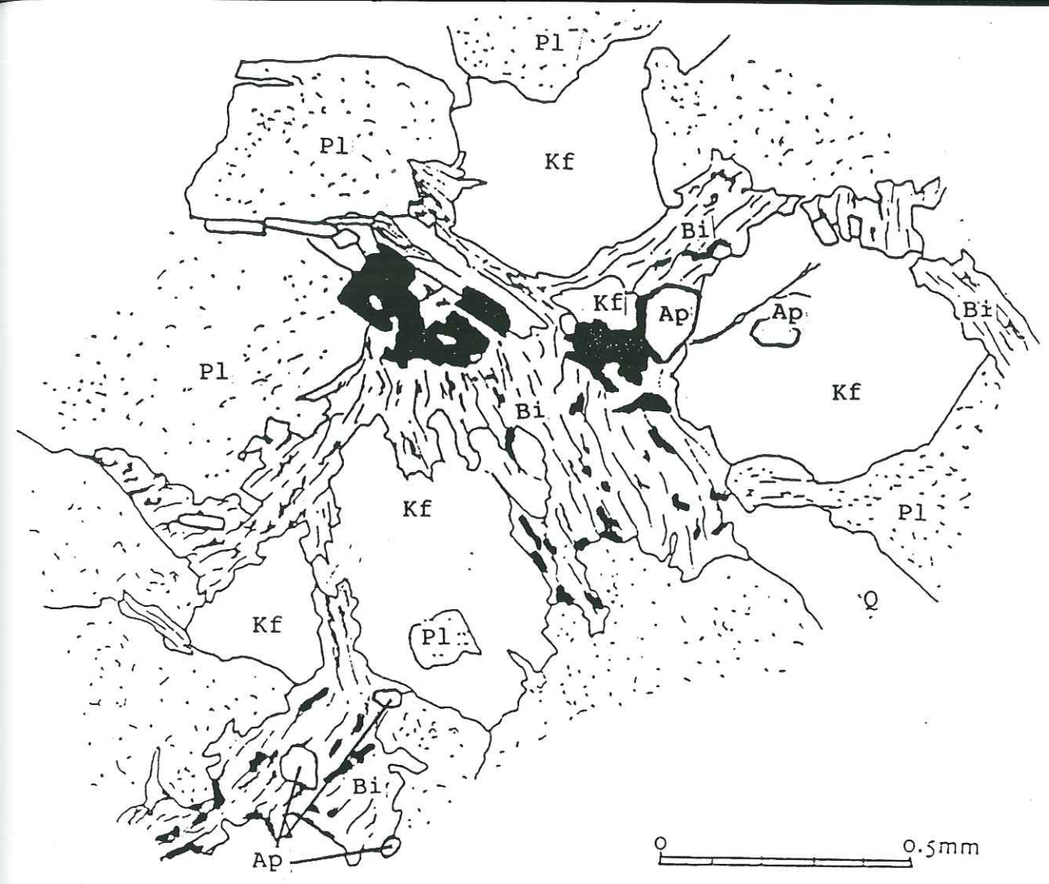

Kf = Potassium feldspar Pl = Plagioclase feldspar Bi = Biotite Ap = Apatite

Q = Quartz

Figure 3.5 Detail from a photomicrograph from the Quatre/Tours Belle Cote granite. (Northern Section).

Potassium Feldspar

Potassium feldspar (modal: 25-30%) is 85-90% Orthoclase and appears to be relatively late forming, probably coeval or just after biotite. It has generally a pöikolitic texture with small crystals of plagioclase being trapped inside (Plate 3. 4.). Phenocrysts, found in the more porphyritic variety, is generally perthitic and twinning is common. Microcline (10-15%) is usually very late, forming small sub-euhedral crystals associated with quartz.

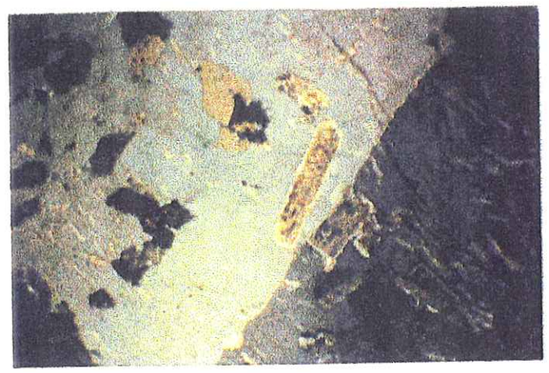

Plate 3. 4 Photomicrograph of pöikolitic potassium feldspar from the QTBC granite. (Crossed polarised light)

Quartz

Quartz (modal: 25-30%) is late stage and forms small interlocking crystals which show undulose extinction. Again this can be taken as an indication of the formation of this mineral under conditions of strain, which are undoubtedly due to the lack of room to grow in a crystal mush which is forcing its way into position in the surrounding country rocks.

Minor Phases

Apatite, Zircon and rare sphene are early forming minor phase minerals and are frequently found associated with and incorporated into later forming biotite.

CRYSTALLISATION SEQUENCE

Apatite	---------		
Zircon	---------		
Plagioclase	----------		
Biotite		----------	
Perthitic Orthose			----------
Microcline			----------
Quartz			----------
Phase	liquid	crystal mush	quasi solid

Table 3.2 Sequence of crystallisation for the QTBC granite (North)

2. Granite south of the PCP-SL ridge.

Although this is the same granite intrusion as that found north of the PCP-SL ridge it does have some notable differences which distinguish it from the later. It is bounded both above and below by thrust faults (VTF and Pisse Rousse) and has the Ramu granite thrust over it. Enclaves of syenitic material do occur, but it also contains enclaves of dioritic material. Further the granite develops a much more porphyritic texture than that north of the PCP-SL ridge. Both pegmatitic and aplitic veins occur whilst structurally it is somewhat more complex, having suffered major thrust faulting and shear deformation, It also appears to have been more affected by chloritization, undoubtedly due to the greater amount of brittle deformation during the Alpine event.

MINERALOGY

Plagioclase feldspar

This occurs as small, generally euhedral crystals, with a greater range of An values, from an oligoclase at An 20 to andesine at An 32 and is slightly more abundant (modal: 40-45%) than the northern sector. The plagioclase shows fairly extensive alteration to sericite, zoning of crystals is quite common and the sericite has often preferentially altered one or more zones within the crystal. Kinking of the albite twinning lamella is also common, indicating a strain regime during crystallisation.

Biotite

Biotite (modal: 3-5%), where it is relatively fresh forms small blebs but with no apparent alignment of the crystals except in the south east close to the faulting of the granite against the Mesozoic rocks (Fig. 2.2). However the degree of chloritization appears to be much more pronounced south of the ridge. This can be explained by the much greater degree of tectonic activity in the form of thrusting and faulting, bringing greater movements of oxidising fluids. Whilst some of this chloritization is certainly due to circulation of fluids

during Alpine movement, the hypothesis for late magmatic alteration cannot be excluded, as other similar granites, (Rochail:(Buffiere, 1963; de Boisset, 1986) Peta rel:(Le Fort, 1973) within the Haute Dauphine, show the same type of alteration, but have not suffered the same degree of tectonic deformation as the QTBC.

Potassium Feldspar

Potassium feldspar (modal: 20-25%) is 90-95% Orthoclase and again appears to be relatively late forming, probably also coeval or just after biotite. It has generally the same poikilitic texture as that north of the PCP-SL ridge. Phenocrysts are more common and somewhat larger, perthitic and twinning is again common. Microcline (5-10%) is usually very late, forming small sub-euhedral crystals associated with quartz.

Quartz

Quartz both modally (25-30%) and petrologically shows little difference from that north of the PCP-SL ridge, with the exception that mortar textures in small microscopic shear zones are more prevalent.

Minor phases

Zircon and apatite are again early forming minor phases with zircon being more abundant than further north of the ridge, both these minerals are generally found as inclusions in biotite although apatite as small laths and rounded inclusions also occurs in potassium feldspar. Sphene appears to be much less prevalent. Occasional monazite occurs as well developed crystals, but with fracturing and destabilisation along the crack boundaries (Plate 3.5).

Pegmatites and Aplites

Aplite veins which occur throughout the granite are generally quite small, up to some tens of cms in width, and cross cut the granite but without a preferred direction. They do tend to become more abundant in the region of the Breche de Valsenestre where they are associated with veins of pegmatite. The texture is very fine grained and the mineralogy is similar to that of the main body of the granite, with the exception, that plagioclase is less

Plate 3. 5 Photomicrograph showing a large (0.5mm) monazite crystal in orthoclase feldspar. The crystal shows evidence of de-stabilisation and leaching, QTBC granite. (Southern Section).

abundant and biotite is virtually absent. The pegmatites which crop out at the Breche are composed of large crystals of potassium feldspar (70%), quartz and albite intergrown, together with apatite and rare topaz and cordierite.

CRYSTALLISATION SEQUENCE

Apatite	----------		
Zircon	----------		
Plagioclase	----------		
Biotite		--------	
Perthitic Orthose		----------	
Microcline			-------
Quartz		----------	
Monazite		------ ?	
Phase	liquid	crystal mush	quasi solid

Table 3.3 Sequence of crystallisation for the QTBC granite (South).

Summary and Conclusions

The QTBC granite complex consists of an elongate slice of rock, mainly granite in composition, but with important associated basic rocks, described later in this chapter,

of syenitic and dioritic composition. The mineralogy is typical of a monzonitic type granite (de la Roche and Stussi, 1982; Barfety et al., 1989). The sequence of crystallisation shows some small differences between north and south and resumes are given in Tables 3.2 and 3.3.. DeBoisset (1986) thought that the QTBC granite formed part of the Rochail granite massif which lies just to the north, and is similar in appearance and chemistry. He thought however, that the "main body" may have had a more complex crystallisation history than the QTBC granite. He based this on observations, where quartz instead of being interstitial, as is the case for the QTBC, was a much earlier forming mineral, being anhedral and haloed by potassium feldspar. No evidence of this type of texture has been seen in the Quatre Tours granite, and further, the presence of cordierite and topaz in the pegmatitic phases would tend to place the QTBC granite in a similar category as the cordierite bearing granites which lie further towards the centre of the Haute Dauphine i.e. the Cretes granite (Pecher, 1973).

3.4 ALFREY GRANITE

The Alfrey granite forms a small elliptical shaped outcrop to the south of Lac Labarre (Fig.2.2 and 3.2). It has the merit of having a partially preserved intrusive contact with the surrounding basement rocks. The Alfrey granite is separated from the Quatre Tours granite by the Pisse Rousse fault, and is apparently in-situ. This is demonstrated by the normal intrusive contact with the country rock gneisses lying to the south and south-west, into which it has been intruded. Further, no large thrust faults have been mapped to the west (Carte de La France: 1:50000, La Mure, 1989). In the east it consists of a medium-grained porphyritic granite, with the K feldspar phenocrysts showing a preferred orientation. The ferro-magnesian mineral is biotite; muscovite occurs as a secondary mineral usually in zones of high deformation, generally replacing plagioclase feldspar. Towards the western extremity of the intrusion the porphyritic tendency diminishes and the quantity of biotite increases, associated with quite large (¼mm size) crystals of monazite as an accessory phase. This increase in biotite is accompanied by a decrease in quartz content, and quartz grains become much less interstitial in character.

MINERALOGY

Plagioclase Feldspar

Plagioclase feldspar generally consists of well-formed euhedral crystals, but with two distinct generations. The first consists of quite fresh andesine (An 32) which shows both albite and Carlsbad twinning. This accounts for about half of the total plagioclase. From time to time a zonation of these crystals can be observed, the zoning being picked out by small inclusions. The second is an oligoclase (An 15-25) which shows heavy alteration essentially to sericite. This would indicate two separate phases of crystallisation, the first being in a slightly more calcic environment than the second. This duality dies out towards the centre of the intrusion and the amount of potassium feldspar increases, all the plagioclase being an oligoclase in the porphyritic facies.

Biotite

Biotite makes up approximately 5% of the Alfrey granite and is generally more or less chloritised.

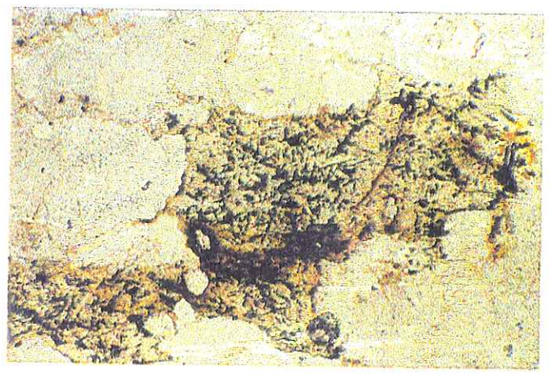

Plate 3. 6 Photomicrograph showing altered biotite with the development of acicular crystals of rutile as replacement minerals. Equigranular apatite and zircons are also present, Alfrey granite. (Plane polarised light)

In the biotite-rich facies, found to the south and west of the intrusion, the biotite forms good euhedral crystals although chloritization is pervasive. Apatite ,zircon and monazite are common inclusions together with fine shards of iron oxides and needles of rutile (Plate 3.6), a good indication that there was at some stage a circulation of high temperature fluids. Well developed crystals of muscovite are also associated with the biotite. Modally the biotite forms about 10%-15% of this darker facies. Further east in the porphyritic facies, chloritization is complete and the biotite has a tendency to be interstitial. As has been described for the QTBC granite (Section 3.3) biotite shows signs of deformation, quite often being draped around the phenocrysts of potassium feldspar.

Muscovite

This mineral appears in three forms. The first is a primary forming mineral associated with biotite in darker facies of the intrusion. Secondly, it sometimes appears as small interstitial laths between crystals of Andesine plagioclase in the non-porphyritic facies. The third form is as sericite in the alteration of plagioclase this phenomenon being pervasive throughout the granite. This again seems to indicate that late stage hydrothermal fluids have affected this granite.

Potassium Feldspar

In the non-porphyritic facies, potassium feldspar occurs as anhedral crystals of perthitic orthoclase or more rarely as microcline, which is much smaller and sometimes interstitial in character. Traversing to the eastern end of the intrusion, largish (up to 3cm long) phenocrysts of perthitic K-feldspar make their appearance. These are generally pöikolitic in texture, enclosing small crystals of plagioclase and chlorite. Carlsbad twinning is prevalent and the probable late stage growth of these crystals is evidenced by the fact that chlorite after biotite is deformed around the phenocrysts, alternatively this could be a deformation texture.

Quartz

Quartz is variable in character and modal quantity depending on the position within the intrusion, varying from 20-25% in the rim facies to 30-35% in the porhpyritic facies. In the

east, close to the faulted contact with the QTBC granite, quartz often occurs as small interstitial crystals, some times with sub-rounded edges, and showing undulose extinction patterns. It also occurs in micro shear-zones with well developed mortar textures. Further to the west, but still in the porphyritic facies, quartz tends to occur as small to medium automorphic crystals interstitial between potassium and plagioclase feldspar. This habit is also present in the biotite rich facies but here a second habit exists, with euhedral crystals sometimes showing basal hexagonal sections. This could indicate that at least some of the quartz is a primary and possibly early forming mineral in this particular facies. More likely this could indicate secondary growth of quartz from hydrothermal fluids. This second hypothesis fits well with the growth of muscovite and the destabilisation of Ti rich biotite.

Minor Phases

The minor phases consist of apatite and zircon, which are early forming, associated with and incorporated into later forming biotite, and monazite which forms quite well developed although fractured crystals. They are associated with biotite/chlorite and plagioclase feldspar, often within the matrix of the feldspar but also in interstitial positions between the feldspar crystals and biotite. Thorite is a very rare minor phase in the biotite-rich facies, forming small well shaped crystals having a good cubic shape. Strangely sphene was not observed, but its absence may be due to the biotite being Ti rich.

CRYSTALLISATION SEQUENCE

Apatite	----------		
Zircon	----------		
Monazite	----------		
Plagioclase	----------		
Biotite	----------		
Perthitic Orthoclase	----------		
Microcline			----------
Muscovite (Possible secondary mineral)	-------		----------
Quartz idem	--------		----------
Phase	liquid	crystal mush	quasi solid

Table 3.3 Possible sequence of crystallisation for the Alfrey granite

Summary and conclusions

The Alfrey granite shows a more varied cooling and post magmatic history than either the QTBC or Ramu granites and a possible sequence of crystallisation is given in Table 3.3. Whilst the case for two magmas cannot be entirely excluded, no evidence to support this was seen in the field. It can be seen from petrographic evidence that there are distinct facies changes within the body, from a slightly more basic non-porphyritic character at the western edge grading into a porphyritic granite at what was most probably the centre of this small granitic stock. The presence of four or five smaller intrusions, further to the west, (A.Pecher, personnel communication), would seem to indicate that the Alfrey granite is one of number of small stocks representing a larger and deeper lying batholith.

3.5 ROCHAIL GRANITE

As has been stated the Rochail granite is a fairly large batholith, covering an area of more than 30 km^2 (de Boisset T., 1986). A small part of this granite crops out in the study region (Fig. 3.4) and this account deals only with this part.

TEXTURE

The granite is generally a fine to medium-grained grey/green coloured granite, biotite is usually chloritised. It is normally homogenous and iso-granular, but locally may be affected by a schistosity with alignment of the chloritised biotite. Close to the syenite enclaves of La Gauchoire a facies with light green amphibole and biotite occurs but is never more than a metre wide.

MINERALOGY

Plagioclase

Plagioclase feldspar, in the form of oligoclase (An15), makes up to 45% of the rock and generally forms good euhedral crystals. Very little zonation of the feldspar was observed. Frequently the edges of crystals show destabilisation and disequilibrium textures with

embayments, lobing and myrmekitic textures, especially when in contact with potassium feldspar. Alteration, in the form of sericite, is prevalent.

Biotite

Biotite is not more than 5% of the rock and is more or less chloritised, and contains zircon, numerous crystals and laths of apatite as well as fairly numerous opaque oxides. When biotite is associated with large amounts of potassium feldspar, it shows deformation textures and takes up an interstitial position. This can be attributed to the fast growth of the K-feldspar in a crystal rich environment.

Potassium feldspar

Potassium feldspar makes up 20-25% of the rock and is mostly perthitic orthoclase with a little, (10% of the mineral) microcline. Occasionally observed with a rim of albite it is often pöikolitic with small crystals of plagioclase aligned along growth fronts. That it grew as a relatively late stage mineral is demonstrated by the way in which it has pushed biotite into interstitial positions.

Quartz

Quartz makes up 25-30% of the rock and generally takes the form of small interlocking crystals in interstitial positions indicating its late development. However, occasionally small quite well formed crystals of quartz are found included in crystals of potassium feldspar, indicating that at least some quartz had formed before the formation of the K-feldspar.

Minor phases

Apatite occurs as small crystals and laths in association with biotite. Zircons generally with radiation halos are also associated with this mineral. Opaque oxides, usually hematite and pyrite are relatively abundant.

CRYSTALLISATION SEQUENCE

Zircon	----------		
opaque Oxides	----------		
Plagioclase	----------		
Biotite	----------		
Perthitic Orthoclase		----------	
Quartz			----------
Phase	liquid	crystal mush	quasi solid

Table 3.4 Possible sequence of crystallisation for the Rochail granite

Summary and Conclusions

The Rochail granite, in the part studied, is a fine to medium grained granite, somewhat darker in hand specimen than either of the other granites within the sector, due mainly to the darker colour of the plagioclase feldspar. This darkening is caused by alteration, probably by the late stage circulation of hydrothermal fluids which have led to the chloritization of the biotite and seritization of the plagioclase. Demeulemeester, 1982 dated this late event to the late Variscan at 293 Ma (K/Ar ages from biotites). The mineralogy resembles that of the QTBC, but does not appear to have the same variety of textures, perhaps indicating a faster cooling history.

3.6 BELLE COTE SYENITE

The Belle Cote syenite occurs as a relatively large intrusion (> 0.5km^2 surface area) for this type of basic material, within this context, and consists of a series of dykes, running roughly north south (Figures 3.2 and 3.4). The dykes are fairly massive having widths which vary between 30 and 80 meters, and lengths of some hundreds of meters. They are everywhere in contact with the granite, except to the north, where they have been truncated by a series of en-echelon faults. The contacts show little evidence of chilled textures, so it would appear that the dykes were probably injected into a granite which was still very hot and was in all probability a fairly dense crystal mush. No real evidence of magma mixing

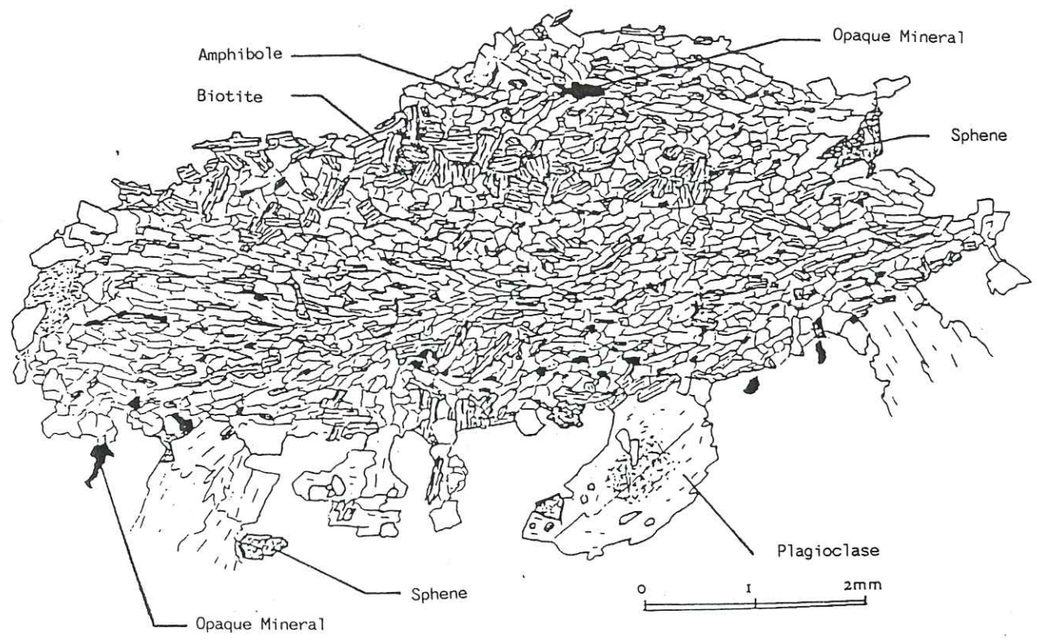

Figure 3. 6 Detail of an ovoid from the central part of the Middle syenite dyke, Belle Cote, showing fine grained intermingled amphibole and biotite. Note the alignment of the amphiboles with the long axis of the ovoid. (Drawing after de Boisset, 1986).

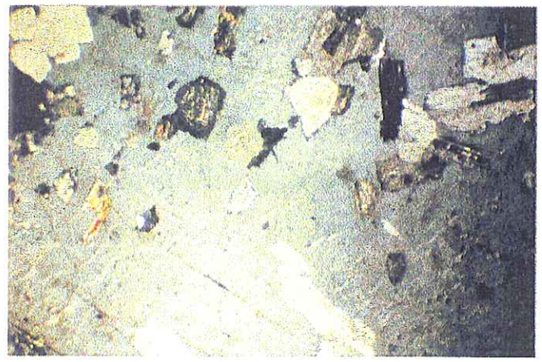

Plate 3.7 Photomicrograph of a large pöikolitic potassium feldspar crystal, Belle Cote syenite. (Crossed polarised light).

has been observed in the field, but further north within the Rochail granite (de Boisset 1986, Vittoz 1987), rocks having very much the same appearance and chemistry appear as fractal enclaves having been broken and invaded by the granite that was still liquid, and here there is evidence of mechanical mixing of the two magmas. Other outcrops of syenite within the QTBC granite, appear as angular blocks and panels, when unaffected by post emplacement deformation.

TEXTURE and MINERALOGY

The syenitic dykes of the Combe de Belle Cote show important internal mineralogical variations, essentially consisting of a series of facies, possibly making up what was originally a fractionation series. This hypothesis is based on the changing abundance of ferro-magnesian minerals, which run from a rock principally of amphibole with minor plagioclase and potassium feldspar at the centre of the dykes, with a possible cumulate texture, to rocks formed essentially from potassium feldspar with minor amphibole and biotite towards the outsides. All the facies making up these dykes have abundant sphene and apatite as minor phases. There are however two other possible alternatives for these variations, A) These textures could be the result of massive chemical exchanges between the dykes and the surrounding granite or B) due to a purely internal mechanical process within the dyke during its emplacement, appropriately called Flowage Differentiation. For A) to be a serious hypothesis, one would require evidence of either a two-way exchange across the syenite-granite interface with the formation of ferro-magnesian minerals within the granite. Small regions can be seen with this phenomena, but this rarely exceeds a strip of more than 1 or 2cms in width. Alternatively a massive one way exchange of elements, especially potassium would be required, with a subsequent greissening of the contact region, this has not been observed to any great degree in the field, being limited to a small region of pegmatitic type material, (consisting of large centimetre sized crystals of K-feldspar and biotite). Flowage differentiation has been simulated in laboratory experiments (Battacharji, 1967), and under certain conditions leads to the central concentration of solid

particles held in suspension in a liquid being intruded into a narrow vertical fissure. This effect can be attributed to the strong velocity gradients and turbulent flow near the margins of the intrusion, which cause the suspended particles to be rotated and to migrate towards the centre of the body. The textures as observed in the field, bear some similarities to this situation and may well be due to this type of emplacement mechanism. It is however very evident, that these intrusions have undergone an important thermal re-equilibration, with the replacement of primary mineral assemblages, probably Ca rich pyroxene, amphibole, phlogopite and plagioclase feldspar to amphibole phlogopite/biotite, plagioclase and K-feldspar with accessory sphene and apatite. As will be demonstrated later, this re-equilibration has taken place in a regime of moderate pressure (around 5 kbar) and fairly low temperature (<700°C). None the less the cumulate nature of the ferro-magnesian rich facies at the centre of the dykes, coupled with the highly potassic nature of the more leucocratic facies could still be considered as original features of a series which has undergone a closed system retro-metamorphism.

No clear cut internal margins were observed, the change in facies within the dykes tends to be gradual although occasionally a more leucocratic facies appears abruptly having only biotite as the dark mineral, but this is never very extensive, and tends to form small oval pods, with their long axes roughly parallel to the orientation of the dykes. The largest of the dykes at Belle Cote has a facies in its centre in which, a distinct alignment of small (2 to 3 cm long) ovoid shaped spheroids occurs (Plate 2.12). These spheroids consist of very fine interlocking fibrous crystals of amphibole and biotite (Figure 3.6). De Boisset,1986, thought that they could be pseudomorphs after original olivine, but no real petrological evidence supports this idea. The K-feldspar often forms large highly pöikolitic phenocrysts surrounding small ferro-magnesian minerals (Plate 3.7), with biotite 'draped' around the feldspar crystals, giving the rock the appearance of a melanocratic orthogneiss (Plate 3.8) , this being the so called 'lozenge facies'.

Plate 3. 8 Facies from the Belle Cote syenite showing biotite crystals draped around crystals of potassium feldspar.

Amphibole

Amphibole, is present in greater or lesser amounts in all of the facies, it is quite often the only ferro-magnesian mineral present and consists of essentially two varieties

1) A green or brown coloured actinolitic hornblende (see Table 3.6 for typical chemical compositions).

2) Pale green coloured actinolitic tremolite which tends towards the cummingtonite end- member on the diagram of Na+K against Si (Fig. 3.7 and 3.8)

This species sometimes occurs as small replacement features at the centre of the corroded actinolitic hornblende but, more normally as fresh pale green fringes around the edges. The first variety has two forms. The first of these often shows destabilisation of the centres with calcite + albite + quartz + opaque minerals being the essential breakdown products. Crystals are euhedral to sub-euhedral, sometimes showing twinning, and are normally quite corroded, often forming clots surrounded by K-feldspar. The centres sometimes show relict cleavages after pyroxene, with small blebs of albite and quartz, indicating the changing

equilibrium in the melt, probably during its emplacement into a still warm and partially molten granite. It is important to note that the relict pyroxenes are most abundant

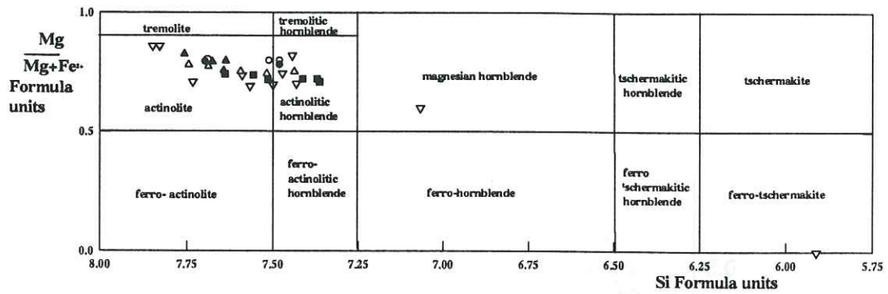

Figure 3. 7 Nomenclature diagrame for calcic amphiboles (Ca+Na)>>1.34, Na<0.67) for syenites from the Belle Cote. (Symbols ● RO312 ■ RO313 ▲ RO314 △ RO316 ○ RO317 ▽ RL313, RL317,RL318,RL319). (from B.E.Leake, 1978). Based on 23 Oxygens.

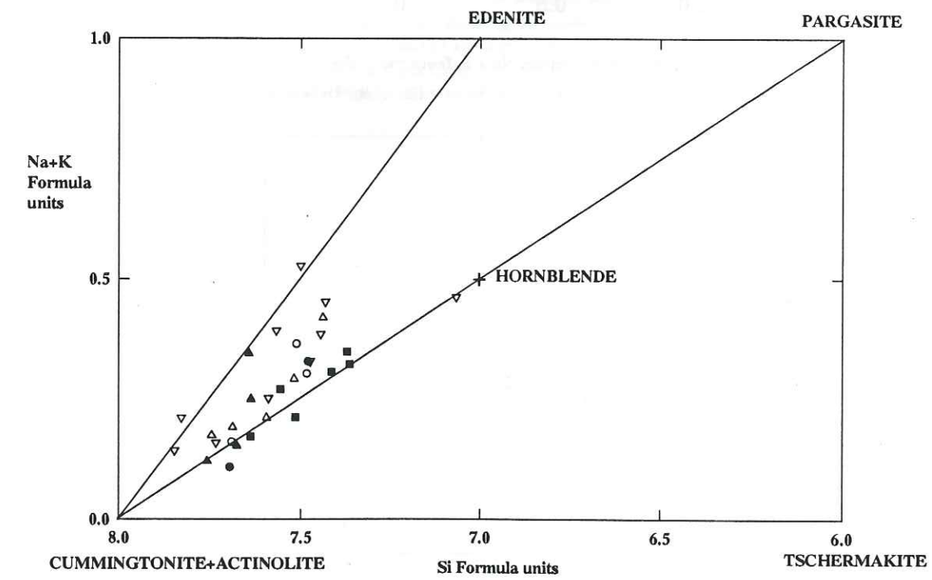

Figure 3. 8 Compositional variation in amphiboles (based on 23 oxygens), for the Belle Cote syenites. The majority of amphiboles plot within the cummingtonite-edenite-pargasite triangle, but a few plot below the cummingtonite-pargasite line being depleted in (Na+K), whilst two plot above the cummingtonite-edenite line and one sample plots in the hornblende field.

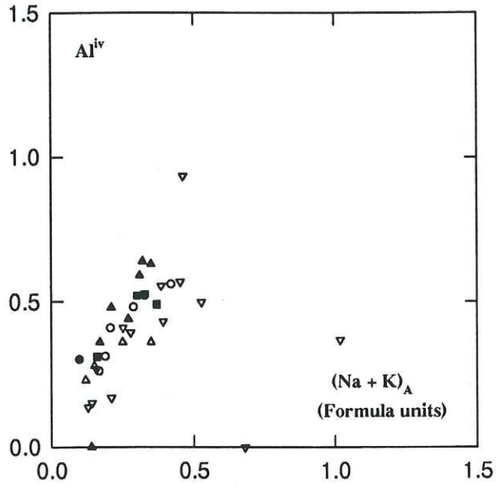

Figure 3. 9 Plot of Al^{iv} versus Na + K from the A site for amphiboles from the syenites of the Belle Cote.

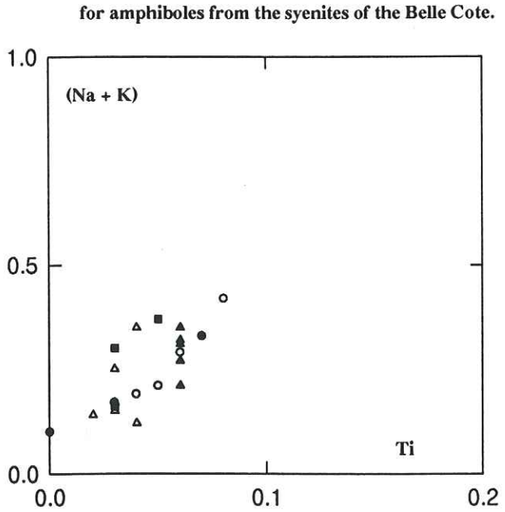

Figure 3.10 Plot of Na + K versus Ti for amphiboles from the syenites of the Belle Cote

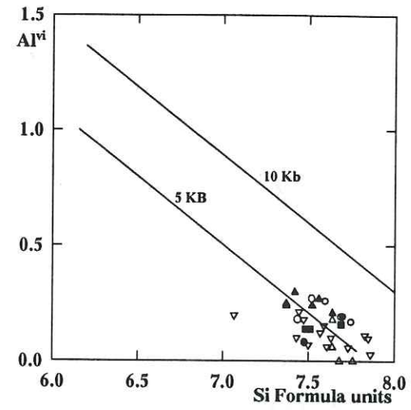

Figure 3.11 Plot of Al^{VI} versus Si for amphiboles from the Belle Cote syenite, showing the probable pressure of crystallization at around 5 Kb. (Pressure values are from Helz, 1973, 1982) (Symbols as in Figure 3.7)

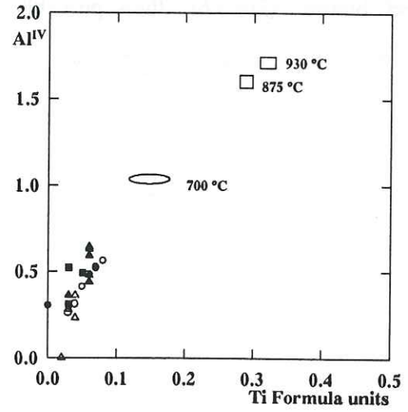

Figure 3.12 Plot of Al^{IV} versus Ti for amphiboles from the Belle Cote syenite, showing the probable temperature of formation. Values are from Helz, 1973 for calcic amphiboles obtained from experimental data at H_2O saturation and 1000 to 700 °C at 5 Kb. (Symbols as for Figure 3.6)

towards the centre of the dykes, in facies having high concentrations of amphibole or amphibole plus biotite, and are seldom observed in the lighter facies found towards the exterior of the dyke formations.

The second variety of amphibole is generally anhedral and has numerous inclusions, of apatite often relatively well developed, sphene, which is normally more or less corroded, and biotite. These later quite often show the same crystal orientation within a single hornblende, indicating that the amphibole has either partially replaced the biotite or that growth of the two minerals was contemporaneous.

Towards the exterior of the dykes, in the more leucocratic facies, the amphibole is not in equilibrium and shows reactions along the edges of individual crystals with the surrounding potassium feldspar, this reaction results in replacement minerals of calcite, albite and epidote developing along the cleavage planes up to the total replacement of the crystal.

Towards the centre of the largest dyke, bands of oval shaped formations occur (Plate 2.12), running roughly parallel to the edges of the dyke, the centres of these ovoids are filled with fibrous masses of actinolite and biotite (Fig.3.6), these probably represent the relics of original calcic and magnesium rich minerals, possibly augite. Similar types of aggregates have been described in vaugnerites from the Massif Central of France (Michon, 1979; Bellanger, 1980; Sabatier,1980; Montel et Weisbrod,1986) in durbachites (Holub,1977) as well as in some lamprophyres (Velde,1971; Sabourdy,1975). These have generally been interpreted as relics after olivine, the principal argument being the presence of small laths of chrome spinel. This may not be the case here, as the presence of chrome spinel amongst the opaque minerals has not been determined, however relict pieces of clinopyroxene have been determined, it is therefore more realistic to suppose that these are relics after clinopyroxene as opposed to olivine, although the under-saturated nature of these rocks cannot entirely rule out the possibility that olivine once existed.

Under normal circumstances amphibole is not an early forming mineral in basic rocks, crystallising after the formation of pyroxene, from the general aspect it can also be inferred that crystallisation was later than the apatite and the large corroded crystals of sphene. This would give a reaction of the type:

pyroxene (augite) + H_2O + K,Na = amphibole

On the whole the chemical range of these amphiboles is restricted (Table 3.6) and are included in the field of low Al amphiboles (1.42-5.24 wt. per cent Al2O3), this would appear to indicate that at least some amphiboles have crystallised below the solidus and have replaced original pyroxenes. These amphiboles are rich in calcium and magnesium and lie on a trend running from magnesian hornblende to actinolites (Figures 3.7 and 3.8). When they are zoned the centres are usually of magnesian hornblende whilst the exterior tends to be actinolite. This type of zonation has been described by Dodge et al.,1968; Czamanske et al.,1981; Letterrier and Pagel, 1980; Kawakatsu and Yamaguchi, 1987 Laporte,1987, and may correspond to the evolution of the physical and chemical conditions within the magma , or can be due to the deuteric action of late fluids and gases.

The changing nature of the amphiboles from magnesian actinolite to actinolitic tremolite is occasioned by a loss of Al_2O_3, Na_2O, K_2O, TiO_2 and a gain of SiO2 and MgO. FeO^t generally falls in value.

The structural formula for tremolite is given in Equation 3.2

A X Y Z

$- Ca_2\ Mg_5\ Si_8O_{22}(OH)_2$ (Equ.3.2)

Therefore the substitution must have been of the type

$(Na+K)A + Al^{iv} === - + Si$ (Equ.3.3)

$Ti + 2Al^{iv} === R2+ + 2Si$ (Equ.3.4)

(Where R2+ is a divalent cation in site Y)

and

Fe2+=== Mg2+

Table 3.6 Microprobe analysis of amphiboles for the seynites of the Belle Cote

Major elements (Oxides by wt%)

Sample	RO312	RO312	RO313	RO313	RO313	RO314	RO314	RO314	RO314	RO314	RO314	RO316	RO316	RO316	RO316	RO316	RO317	RO317	RO317	RO317	RO317
SiO2	54.12	52.41	53.70	52.50	52.22	52.50	53.62	53.35	51.73	51.07	51.36	56.05	53.64	54.46	53.16	57.30	54.20	53.34	52.63	54.71	51.84
Al2O3	2.92	3.54	2.76	3.72	3.91	4.30	3.41	4.24	5.24	5.20	5.13	1.42	2.54	1.70	3.14	1.54	3.02	3.93	4.46	2.57	4.40
FeO	8.26	9.01	7.83	8.30	8.21	11.22	10.41	10.45	10.99	11.52	11.06	7.09	8.91	8.82	9.74	8.67	9.19	9.92	10.19	8.97	9.92
MgO	17.80	17.83	17.83	18.37	18.19	15.93	16.74	16.35	15.95	15.67	16.12	20.30	18.66	18.97	16.99	16.97	17.54	16.88	16.41	17.90	16.77
CaO	13.09	12.65	12.88	11.49	12.63	12.52	12.54	12.36	12.02	12.29	12.22	13.10	11.97	12.87	11.99	11.99	12.42	12.14	12.10	12.36	11.95
Na2O	0.27	0.97	0.45	1.03	0.88	0.76	0.62	0.98	1.10	1.15	1.25	0.32	0.73	0.44	0.93	0.44	0.69	0.76	1.05	0.63	1.19
K2O	0.18	0.32	0.18	0.42	0.31	0.00	0.00	0.00	0.00	0.00	0.00	0.00	0.00	0.00	0.27	0.12	0.00	0.00	0.00	0.00	0.48
TiO2	0.02	0.65	0.27	0.45	0.24	0.51	0.31	0.56	0.55	0.58	0.58	0.40	0.24	0.30	0.37	0.15	0.40	0.47	0.59	0.32	0.70
MnO	0.34	0.20	0.21	0.24	0.00	0.00	0.00	0.00	0.00	0.00	0.00	0.25	0.26	0.85	0.22	0.22	0.00	0.00	0.00	0.00	0.27
Total	97.00	97.58	96.11	96.52	96.59	97.74	97.65	98.29	97.58	97.48	97.72	98.93	96.95	98.41	96.81	97.40	97.46	97.44	97.43	97.46	97.52
Formula units (Calculated for 23 Oxygens)																					
Si	7.70	7.48	7.69	7.51	7.48	7.52	7.64	7.56	7.42	7.37	7.37	7.76	7.64	7.68	7.64	8.05	7.69	7.60	7.52	7.75	7.44
Aliv	0.30	0.52	0.31	0.49	0.52	0.48	0.36	0.44	0.59	0.64	0.63	0.23	0.36	0.28	0.36	0.00	0.31	0.41	0.48	0.26	0.56
Alvi	0.19	0.08	0.16	0.14	0.14	0.24	0.21	0.27	0.30	0.25	0.24	0.00	0.06	0.00	0.18	0.26	0.19	0.26	0.27	0.17	0.18
Fe2+	0.98	1.08	0.94	0.99	0.98	1.34	1.24	1.24	1.32	1.39	1.33	0.82	1.06	1.04	1.17	1.02	1.09	1.18	1.22	1.06	1.19
Mn	0.04	0.02	0.03	0.03	0.00	0.00	0.00	0.00	0.00	0.00	0.00	0.03	0.03	0.10	0.03	0.03	0.00	0.00	0.00	0.00	0.03
Mg	3.77	3.79	3.81	3.92	3.88	3.40	3.56	3.45	3.41	3.37	3.45	3.88	4.19	3.96	3.64	3.56	3.71	3.58	3.49	3.78	3.59
Ti	0.00	0.07	0.03	0.05	0.03	0.06	0.03	0.06	0.06	0.06	0.06	0.04	0.03	0.03	0.04	0.02	0.04	0.05	0.06	0.03	0.08
Ca	1.99	1.93	1.98	1.76	1.94	1.92	1.91	1.88	1.85	1.90	1.88	1.94	1.83	1.94	1.84	1.81	1.89	1.85	1.85	1.88	1.84
Na	0.07	0.27	0.13	0.29	0.24	0.21	0.17	0.27	0.31	0.32	0.35	0.09	0.20	0.12	0.30	0.12	0.19	0.21	0.29	0.17	0.33
K	0.03	0.06	0.03	0.08	0.06	0.00	0.00	0.00	0.00	0.00	0.00	0.03	0.05	0.03	0.05	0.02	0.00	0.00	0.00	0.00	0.09
Total	15.08	15.30	15.09	15.25	15.28	15.17	15.13	15.16	15.24	15.29	15.31	14.83	15.45	15.19	15.24	14.87	15.11	15.13	15.19	15.10	15.32

Sample RO312 and RO313 are from the middle of the largest dyke.
Sample RO314 and RO316 are from midway between the middle and the edge, to the east and west respectively of the largest dyke.
Sample RO317 is from the eastern edge of the largest dyke.
(See Figure 2.8)

Microprobe analysis made at the Open University, U.K. by R.Oliver and G.Vivier. (see Appendix II).

Table 3.6 (Continued).

Major elements (Oxides by wt%)

Sample	**RL313**	**RL313**	**RL316**	**RL318**	**RL318**	**RL318**	**RL319**	**RL319**	**RL319**	**RL319**	**RL319**
SiO2	54.37	48.24	52.37	51.93	52.44	52.51	52.32	62.58	55.45	52.83	53.49
Al2O3	1.94	6.57	4.21	3.34	4.00	3.27	2.73	0.59	0.99	2.69	3.38
TiO2	0.12	0.96	0.61	0.60	0.60	0.42	0.41	0.07	0.10	0.53	0.45
FeO	12.17	15.26	10.11	11.99	12.36	12.37	10.46	7.23	9.22	9.90	10.74
MnO	0.32	0.25	0.25	0.36	0.44	0.28	0.27	0.31	0.32	0.26	0.27
MgO	16.44	13.04	16.52	15.55	16.14	15.50	16.77	14.58	17.94	17.15	16.72
CaO	12.73	12.08	12.03	11.57	11.69	11.67	11.53	9.96	12.36	12.04	12.12
Na2O	0.45	1.13	0.82	1.55	1.28	1.11	0.81	0.25	0.38	0.68	0.60
K2O	0.19	0.76	0.55	0.50	0.55	0.45	0.43	0.06	0.14	0.47	0.48
Total	98.72	98.29	97.47	97.39	99.50	97.58	95.73	95.63	96.89	96.55	98.25
Formula units (Calculated for 23 Oxygens)											
Si	7.73	7.07	7.47	7.50	7.43	7.57	7.63	8.69	7.86	7.61	7.59
Aliv	0.27	0.93	0.53	0.50	0.57	0.43	0.37	0.00	0.14	0.39	0.41
Alvi	0.06	0.20	0.18	0.07	0.10	0.12	0.10	0.10	0.03	0.06	0.16
Ti	0.01	0.11	0.07	0.07	0.06	0.05	0.05	0.01	0.01	0.06	0.05
Fe	1.45	1.91	1.21	1.45	1.46	1.49	1.28	0.84	1.09	1.19	1.28
Mn	0.04	0.03	0.03	0.04	0.05	0.03	0.33	0.04	0.38	0.03	0.03
Mg	3.48	2.85	3.52	3.30	3.41	3.33	3.65	3.02	3.79	3.68	3.54
Ca	1.94	1.90	1.84	1.79	1.78	1.80	1.80	1.48	1.88	1.86	1.84
Na	0.12	0.32	0.23	0.44	0.35	0.31	0.23	0.67	0.10	0.19	0.16
K	0.04	0.14	0.10	0.09	0.10	0.08	0.79	0.01	0.02	0.09	0.09
Total	15.14	15.46	15.17	15.25	15.32	15.22	16.22	14.86	15.31	15.16	15.14
mg*	0.70	0.59	0.74	0.69	0.69	0.69	0.69	0.77	0.72	0.75	0.73

Sample RL313 is from the contact of the upper dyke with the granite.
Samples RL316 and RL318 are from the coarse grained amphibole rich facies in the centre of the upper dyke.
Sample RL319 is from the pottasium rich feldspar facies from the upper dyke.

Values of Al^{iv} versus Na + K and Na + K versus Ti for the amphiboles from the Belle Cote dykes and the Rochail granite enclaves have been plotted in Figures 3.9 and 3.10 respectively, examination of these show that the proposed substitutions in Equations 3.3 and 3.4 are inter-linked, this means in effect that Ti^{4+} atoms extracted from the lattice are accompanied by an alkaline cation from the A site. This will give in this case:

$$1.3(Na+K)A + Ti + 5.6Al^{iv} === 1.2 + R2+ + 5.6Si \quad \text{(Equ.3.5)}$$

This increase in Si during crystallisation, accompanied by a relative diminution in Al^{iv}, Na, K, and Ti, would seem to indicate an overall increase of silica in the melt, which is a possible indicator of either, assimilation of a silica rich fluid from the surrounding granite, or a possible mixing with a more silica rich magma, or alternatively a fractionation mechanism .

The mg* number for all the amphiboles analysed (Table 3.6), mg* = $Mg/(Mg + Fe^T + Mn)$, are greater than 0.5 indicating their highly magnesian nature, this is due to a corresponding increase in the oxygen fugacity (fO2)(Wones, 1981; Kawakatsu and Yamaguchi, 1987). This increase in fO2 implies the formation of magnetite crystals with the resulting increase in the $Mg^{2+}/(Mg^{2+}+Fe^{2+})$ ratio (Andre, 1983).

All these factors could be due to the mixing of two magmas, but could also be due to absorption of crustal or crustally derived material. That some adsorption has taken place is evidenced by the presence of relict zircons, described in very similar rocks from the Colle Blanche granitic complex further to the south (Banzet, 1987).

The absence of substitution between Al^{IV} and alkali elements of site A in the crystal matrix, suggests that the pressure was quite moderate, approximately 5 kbar, (Figure 3.11) during the crystallisation of the amphibole (Leake,1965; Helz,1973,1982). From the experimental work of Eggler,1972; Helz,1973,1982 and Allen et al,1975, the temperature was probably of the order of 550-600°C (Figure 3.12). This is obviously well below the minimum solidus temperature of both basalt and granite emplaced at a shallow level (Tuttle and Bowen, 1958; Burnham, 1979; Burnham and Nekvasil, 1986). It therefore seems probable that the amphiboles have re-equilibrated under sub-solidus conditions, after having first formed from a reaction, from clinopyroxene (Dodge et al., 1968). Kawakatsu and Yamaguchi, 1987

ascribed this type of reaction to the circulation of late magmatic or hydrothermal fluids, and with the intimate association of the dykes with their granitic host. This has to be considered as a possible explanation for the formation of these rocks.

Biotite

Biotite, apart from a limited number of localised exceptions, is always less abundant than amphibole, and in the facies found towards the centre of the dykes, is generally less than five percent modal of the total, with some rare facies being almost totally free. When present, it is often rather altered, much more so towards the edges of the dykes. This alteration takes the form of chloritization around the edges of the biotite crystals, as well as exudation and breakdown along cleavage planes into opaque oxides. This is in all probability a fluid reaction with the enclosing granite.

Biotite appears in three forms 1) as large crystals, especially in the "lozenge" facies, (a local terminology, used to describe a facies which in appearance resembles flaser bedded sediments) (Plate 3.8) where it is draped around the K-feldspar crystals, 2) as small laths disseminated throughout the rock, and 3) as neo-formed, fairly fresh crystals associated with amphibole (Plate3.9) . It is frequently found as inclusions within both the K-feldspar and the green actinolitic hornblende, where it forms small islands all having the same optical

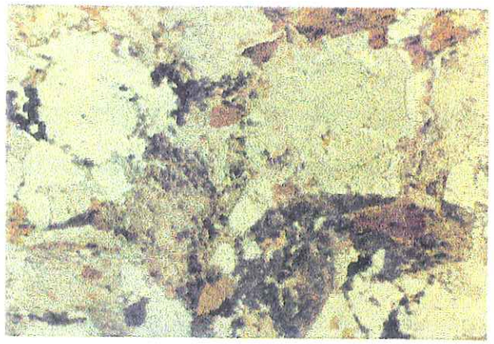

Plate 3.9 Photomicrograph of syenite from the Belle Cote central dyke, showing nucleation of fresh biotite within amphibole
(plane polarised light)

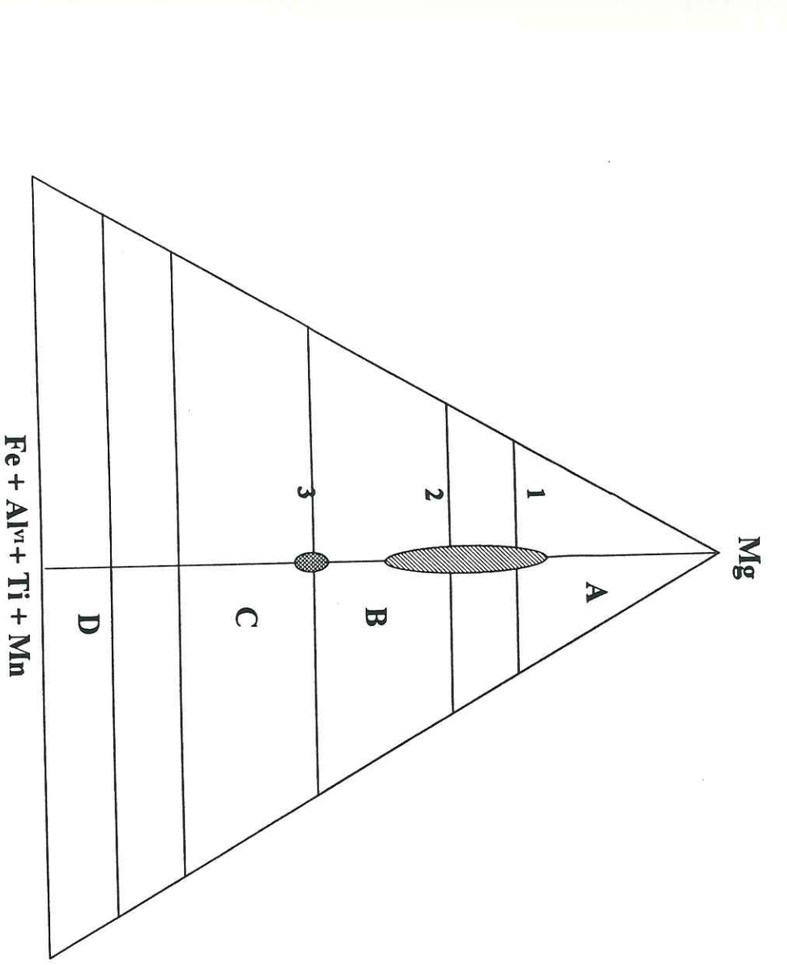

Figure 3.13 Diagram of biotite nomenclature after Foster, (1960)
A= Field of phlogopites, B= field of magnesian biotite
C=field of Iron biotite, D=Siderophilite and lepidomelene
1= biotite from the central facies, 2= biotites from the external facies
3= biotite from the surrounding granite

orientation indicating that it once formed part of the same mineral. This would seem to indicate that some of the biotite was an earlier forming mineral, than some of the amphibole, as well as some of the potassium feldspar; although the syn-crystallisation of some biotite and potassium feldspar is indicated by the presence of thin streaks of the latter, along cleavage planes within the biotite.

Inclusions within the biotite consist of apatite in the form of both laths and small angular crystals, rare zircon and small euhedral crystals of sphene running along the cleavage planes.

Chemically all the biotites are quite similar, but within this similarity, two types can be distinguished. The first type, corresponding to that found at the centre of the dykes, in general has an Mg/Fe ratio > 2:1; the second type which in general is found towards the edges of the d

Table 3. 7 Microprobe analysis of biotites from the Belle Cote syenite

Major elements (Oxides by wt%)

Sample	RO312	RO313	RO313	RO314	RO314	RO314	RO314	RO314	RO314	RO314	RO314	RO316	RO316	RO316	RO317	RO317	RO317	RO317
SiO2	38.03	38.61	37.61	38.79	38.34	38.94	39.66	38.71	38.95	38.49	39.48	38.26	37.57	37.67	38.93	39.50	38.87	38.32
Al2O3	16.11	14.88	15.33	14.61	14.38	15.28	14.48	14.78	14.62	14.89	14.72	13.78	14.22	13.29	13.11	13.74	13.76	13.69
FeO	13.03	13.06	14.10	14.36	14.98	14.48	14.19	14.32	15.77	14.28	13.39	14.62	14.96	14.31	13.22	14.06	14.28	14.54
MgO	16.10	16.57	15.38	14.53	14.28	14.41	15.51	14.41	13.98	14.40	15.46	16.35	15.68	15.20	16.59	15.57	15.10	15.59
CaO	0.00	0.00	0.00	0.02	0.00	0.00	0.07	0.00	0.00	0.00	0.46	0.00	0.00	0.01	0.01	0.00	0.00	0.00
Na2O	0.10	0.11	0.12	0.09	0.00	0.00	0.07	0.00	0.00	0.00	0.08	0.14	0.12	0.00	0.00	0.00	0.00	0.00
K2O	10.32	10.18	10.53	10.10	9.96	9.89	9.89	10.06	10.16	10.09	8.48	9.36	10.28	9.60	9.65	9.99	10.23	10.16
TiO2	2.57	2.53	3.31	2.78	2.32	3.09	2.16	3.16	2.90	2.55	2.69	2.41	2.01	3.01	2.17	2.95	2.98	3.10
MnO	0.28	0.12	0.19	0.14	0.14	0.11	0.18	0.18	0.23	0.14	0.06	0.17	0.13	0.14	0.12	0.19	0.18	0.14
P2O5																		
BaO																		
Total	96.54	96.06	96.57	95.42	94.40	96.20	96.21	95.62	96.61	94.84	94.82	95.09	94.97	93.23	93.80	96.00	95.40	95.54
Formula units (calculated for 22 Oxygens)																		
Si	5.56	5.67	5.54	5.77	5.79	5.73	5.84	5.74	5.76	5.76	5.81	5.69	5.66	5.74	5.85	5.82	5.80	5.72
Aliv	2.45	2.33	2.46	2.23	2.22	2.27	2.16	2.26	2.24	2.24	2.19	2.31	2.35	2.26	2.15	2.18	2.20	2.29
AlVI	0.33	0.24	0.20	0.33	0.34	0.38	0.35	0.33	0.31	0.38	0.36	0.22	0.22	0.13	0.17	0.21	0.21	0.12
Fe	1.59	1.60	1.74	1.79	1.88	1.78	1.75	1.78	1.95	1.79	1.65	1.82	1.88	1.82	1.66	1.73	1.77	1.81
Mn	0.04	0.02	0.02	0.02	0.02	0.01	0.02	0.02	0.03	0.02	0.01	0.02	0.02	0.02	0.02	0.02	0.01	0.02
Mg	3.50	3.63	3.38	3.22	3.21	3.16	3.32	3.19	3.07	3.21	3.39	3.63	3.52	3.45	3.72	3.42	3.36	3.47
Ti	0.28	0.28	0.37	0.31	0.26	0.34	0.24	0.35	0.32	0.29	0.30	0.27	0.23	0.35	0.25	0.33	0.33	0.35
Ca	0.00	0.01	0.07	0.00	0.00	0.00	0.00	0.00	0.00	0.00	0.00	0.00	0.00	0.00	0.00	0.00	0.00	0.00
Na	0.03	0.03	0.03	0.03	0.02	0.02	0.04	0.02	0.04	0.03	0.00	0.00	0.00	0.00	0.00			
K	1.92	1.91	1.98	1.92	1.92	1.86	1.86	1.90	1.92	1.93	1.59	1.78	1.97	1.87	1.85	1.88	1.95	1.93
P																		
Ba																		
Total	15.70	15.72	15.79	15.62	15.66	15.55	15.58	15.59	15.64	15.65	15.30	15.74	15.85	15.64	15.67	15.59	15.63	15.71
mg*	0.65	0.66	0.62	0.61	0.60	0.60	0.63	0.60	0.57	0.61	0.63	0.63	0.63	0.61	0.66	0.62	0.62	0.62

For the situation of samples refer to Table 3.6
Analysis performed at the Open University, UK.

Table 3. 7 (Continued)

Major elements (Oxides by wt%)

Sample	RO317	RL313	RL316	RL317	RL319	RL319	RL319	RL318	RL319	RL319	RL321	RL321
SiO2	38.97	36.83	34.95	38.61	38.38	39.84	38.71	38.27	38.01	37.97	38.27	38.60	38.61	37.86	38.40	38.29	37.21
Al2O3	14.13	13.20	13.68	13.63	13.67	14.00	13.43	13.12	12.90	12.90	12.43	12.52	12.83	12.39	12.54	14.38	14.44
FeO	14.32	21.63	24.59	14.14	14.35	9.02	8.84	18.77	16.84	16.83	14.21	14.52	14.80	15.66	15.91	18.39	18.26
MgO	15.50	11.17	10.95	16.39	16.16	20.55	19.81	13.75	14.22	14.22	16.31	15.53	16.05	15.36	14.54	12.67	13.07
CaO	0.00	0.03	0.11	0.00	0.00	0.02	0.06	0.02	0.07	0.08	0.14	0.10	0.05	0.06	0.08	0.06	0.08
Na2O	0.00	0.05	0.13	0.04	0.00	0.36	0.18	0.17	0.26	0.28	0.00	0.00	0.06	0.02	0.22	0.28	0.20
K2O	10.01	11.21	8.14	11.38	11.31	9.86	9.59	11.57	11.08	11.06	11.35	10.84	11.29	10.76	10.97	11.39	10.90
TiO2	2.03	3.12	1.92	2.63	2.84	1.35	1.32	2.66	2.92	2.93	2.54	2.33	2.76	2.41	3.09	2.42	2.35
MnO	0.14	0.28	0.25	0.20	0.15	0.16	0.05	0.21	0.31	0.31	0.17	0.14	0.15	0.27	0.25	0.31	0.37
P2O5		0.98	0.00	0.00	0.00	0.00	0.00	0.00	0.00	0.00	0.00	0.01	0.00	0.00	0.02	0.00	0.00
BaO		0.18	0.82	0.30	0.34	0.52	0.30	0.40	0.00	0.00	0.09	0.22	0.01	0.23	0.01	0.00	0.14
Total	95.10	98.67	95.53	97.31	97.18	95.69	92.30	98.94	96.60	96.57	95.44	94.81	96.61	95.00	96.00	98.20	97.02
Formula units (Calculated for 22 Oxygens)																	
Si	5.81	5.62	5.51	5.70	5.68	5.78	5.81	5.70	5.72	5.72	5.76	5.84	5.75	5.77	5.78	5.70	5.61
Aliv	2.19	2.37	2.49	2.30	2.32	2.22	2.19	2.30	2.28	2.28	2.21	2.16	2.25	2.22	2.22	2.30	2.39
Alvi	0.29	0.00	0.05	0.07	0.06	0.17	0.19	0.00	0.01	0.01	0.00	0.07	0.00	0.00	0.01	0.22	0.18
Fe	1.79	2.76	3.24	1.75	1.78	1.09	1.11	2.34	2.12	2.12	1.79	1.84	1.84	1.99	2.00	2.29	2.30
Mn	0.02	0.04	0.03	0.03	0.02	0.02	0.01	0.03	0.04	0.04	0.02	0.02	0.02	0.03	0.03	0.04	0.05
Mg	3.45	2.54	2.57	3.61	3.56	4.44	4.43	3.05	3.19	3.19	3.66	3.50	3.56	3.49	3.26	2.81	2.94
Ti	0.23	0.36	0.23	0.29	0.32	0.15	0.15	0.30	0.33	0.33	0.29	0.27	0.31	0.28	0.35	0.27	0.27
Ca	0.00	0.01	0.02	0.00	0.00	0.00	0.01	0.00	0.01	0.01	0.02	0.02	0.01	0.01	0.01	0.01	0.01
Na		0.01	0.04	0.01	0.00	0.10	0.05	0.05	0.08	0.08	0.00	0.00	0.02	0.01	0.06	0.08	0.06
K	1.90	2.18	1.64	2.14	2.13	1.83	1.84	2.20	2.13	2.13	2.18	2.09	2.14	2.09	2.11	2.16	2.10
P		0.01	0.00	0.00	0.00	0.00	0.00	0.00	0.00	0.00	0.00	0.00	0.00	0.00	0.00	0.00	0.00
Ba		0.01	0.01	0.02	0.02	0.03	0.02	0.02	0.00	0.00	0.01	0.01	0.00	0.01	0.00	0.00	0.01
Total	15.68	15.91	15.83	15.90	15.88	15.84	15.80	15.98	15.91	15.91	15.94	15.82	15.90	15.90	15.84	15.89	15.91
mg*	0.63	0.45	0.43	0.64	0.63	0.78	0.78	0.54	0.57	0.57	0.64	0.62	0.62	0.61	0.58	0.52	0.53

ykes, is much richer in iron, and has an Mg/Fe ratio less than 2 but usually greater than 1, indicating that these are still relatively rich in magnesium. After the classification of Foster, (1960), the first type can be classified as phlogopite, (Fig. 3.13), whilst the second type fall into the domain of the magnesian biotites. The fact that phlogopite is relatively abundant would indicate that the temperature of crystallisation was somewhat higher than the 550 to 600 degrees indicated by the amphibole, possibly at around 950 to 1000°C. It therefore, may well be that these phlogopitic biotites are primary minerals. Microprobe data for thirty six representative biotites measured at The Open University and The University of Clermont Ferrand are shown in Table 3.7.

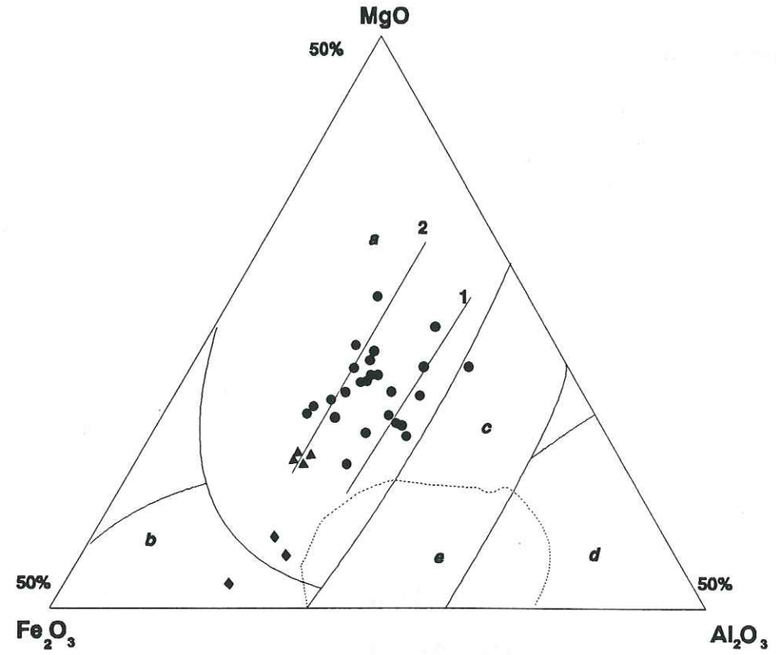

Figure 3.14 Plot of Fe_2O_3/MgO/Al_2O_3 (after Nockolds ,1947 and Leterrier, 1973) for biotites from the basic intrusions of the Quatre Tours - Belle Cote granite.

(● = Belle Cote syenite, ✹ = Fine grained Quatre Tours diorite, ▲ = coarse grained Quatre Tours diorite)

a = field of biotites associated with olivine or pyroxene; *b* = field of biotites associated with amphiboles; *c* = field of simple biotites; *d* = field of biotites associated with muscovite; *e* = field of metamorphic biotites.

Plotting these values for biotites on the triangular diagram of $Fe_2O_3/MgO/Al_2O_3$ (Nockolds, 1947) Fig. 3.14 reveals some interesting information. Firstly, with one exception, all the biotites plot into the field which Nockolds, (1947), and later Leterrier, (1973) defined as that, in which the biotite had crystallised in conjunction with either olivine or pyroxene, but not amphibole. In effect for this to have happened the ratio of iron to magnesium would have to be much greater.
Secondly, it reveals two distinct trends running more or less parallel to the Fe_2O_3-MgO couple.

1) The first trend is the most aluminous in character and includes those biotites found in the central facies of the Belle Cote dyke system.

2) The second trend includes biotites from all the other types of facies, including those from the contact facies with the granite.

The increase in total aluminium is correlated with a corresponding increase of Al^{IV}, which indicates a higher temperature of crystallisation (Deer Howie and Zusman, 1978). These two trends could be interpreted as a fractionation with falling temperature and pressure during the crystallisation of the basic magma. Alternatively, and quite probable, this indicates a reaction with the surrounding host granite, and can be classified as a retro-metamorphic phenomena.

Plagioclase Feldspar

Plagioclase is never very abundant in these rocks, rarely exceeding 10% of the total, and is always more or less altered. This usually takes the form of sericitic alteration along cleavage planes. It occurs either as small anhedral crystals, showing embayments of potassium feldspar or amphibole, or as partially digested crystals within the larger potassium feldspar phenocrysts.

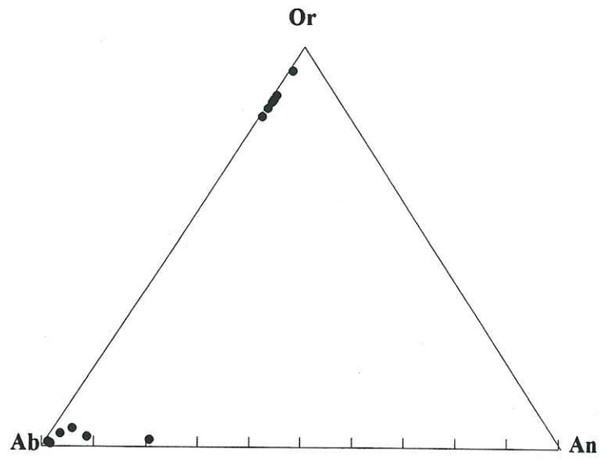

Figure 3.15 Or-Ab-An diagram for feldspars from the Belle Cote Syenitic dykes.

The chemical composition gives an oligoclase which can vary in composition from An 10 to An 25 (see Fig.3.15). Elsewhere within the European Variscan domain, similar types of intrusions give values for plagioclase of a much more basic nature. This difference has a possible explanation in that there has been loss of calcium during the re-equilibration process. This liberated calcium has then be incorporated into other minerals e.g. calcite and later forming sphene.

Potassium Feldspar

Potassium feldspar is variable in abundance depending on its position within an individual dyke. At the centre, the amount is relatively small, approximately 10 to 15%, but this increases as the edges are approached, where it can be as much as 30 to 40% of the total rock. It is generally perthitic orthose together with microcline which increases in percentage towards the exterior. It generally has two habits;-

1) This occurs in all facies and consists of a pervasive interstitial and late stage crystallisation, running from millimetre size up to crystals several centimetres across, and being highly pöikolitic. All the other minerals present, amphibole, biotite, plagioclase, sphene and apatite can be included within the boundaries of a single large crystal (Plate 3.10a and b). It is interesting to note that acicular apatite occurs only in these crystals of potassium feldspar.

2) In the more leucocratic facies found towards the exterior of the dykes, the feldspar becomes euhedral attaining sizes of several centimetres. From time to time small inclusions of plagioclase, relatively fresh, are found zoned around a centre of K-feldspar, having no inclusions at all, whilst small amphiboles, biotites and occasional sphene are grouped around the fringes of this ensemble. Therefore it can be concluded, that the crystallisation of potassium feldspar was always later than that of pyroxene, biotite, amphibole, sphene and apatite with hexagonal shape. Its relationship to plagioclase is more complex, as it would appear that in some facies crystallisation of the two plagioclases was synchronous, as evidenced by the epitaxic growth of plagioclase around an already crystallised K-feldspar.

Experimental work by Winkler and Schultes, (1982) has shown that euhedral crystals of potassium feldspar cannot continue to develop if the amount of liquid is inferior to 30%, whilst their appearance is a function of the rate of nucleation, divided by the speed of growth (Swanson, 1977), whilst one of the major factors controlling the speed of growth is the amount of H2O as well as P_{H2O} available to the crystallisation process. This means that the centres of the dykes were probably crystal rich mushes, due to the mechanical processes of the emplacement, whilst the edges, due to the lack of chilling from the margins (a heating effect can not in fact be excluded), would have increased the fluid content towards the exterior as well as increasing the P_{H2O}.

Quartz

Quartz when present (less than 3% of the total rock) is always interstitial in its habit, and appears in the last stages of crystallisation close to the edges of the intrusions, forming small grains between the crystals of potassium feldspar.

Minor Phases

Sphene and Apatite are the main minerals, in this category, together with minor Zircon, opaque oxides and rare allanite. The sphene which is quite abundant (up to 3%) is generally euhedral with frequent twinning and appears in two forms, first as large corroded crystals (see Plate 3.10), with inclusions of apatite, biotite and opaque minerals and secondly as quite small fresh crystals, often as inclusions in biotite, where they lie along the cleavage planes. From this it can be inferred that sphene was crystallising throughout the cooling of these dykes, although it has been interpreted as a product from the destabilisation of illmanite (Barriere, 1977; Orsini, 1980) but this would require a greater quantity of iron than is seen in these rocks (8%).

1) Euhedral hexagonal sections, but with a cloudy look, and often broken. These are found as inclusions in ferro-magnesian minerals (biotite, amphibole and sphene). The abundance decreases from the more basic facies at the centre towards the exterior.

2) Short prismatic crystals, normally associated with amphibole.

3) Long acicular crystals sometimes with hollow centres, indicating a rapid cooling history. These generally being associated with potash feldspar. This phenomena has been noted by a number of workers (Harisson and Watson, 1984). This could be due to a localised over saturation of phosphorus (Green and Watson, 1982) linked to the rapid growth of potassium feldspar and a very slow diffusion rate for phosphorus.

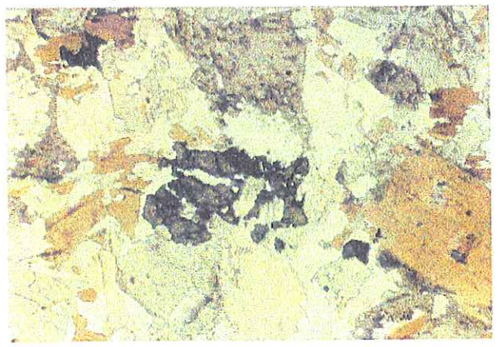

Plate 3.10 Photomicrograph of syenite from the Belle Cote central dyke, showing a large corroded crystal of sphene, partially replaced by amphibole and k-feldspar. Other mineral are biotite and apatite. (plain polarised light)

Apatite is ubiquitous as inclusions in other minerals with three types of habit:-

Summary and conclusions

The Belle Cote syenite consists of a number of parallel north-south running dykes, which show a complex mineral and petrological history. The absence of a chilled margin and no remelting textures in the surrounding granites indicates temperatures quite close to one another at the time of intrusion, although the viscosities would have been much different (Bebien et al., 1987). The mineralogy and petrology shows that the dykes have undergone a major re-equilibration during the cooling process, with the replacement of original clinopyroxene by magnesian rich amphibole, which has in turn undergone a later lower temperature re-equilibration to actinolitic tremolite. Some at least of the biotites appear to be primary minerals whilst it is possible that the late growth of K-feldspar may be due to exchange of fluids with the surrounding granite.

3.7 QUATRE TOURS DIORITE

The diorite associated with the southern portion of the Quatre Tours-Bellecote granite is much finer grained than the precedent syenite, and whilst there are facies changes within the diorites, the enclaves never develop the same textures associated with the syenites. The

largest outcrop occurs just above the pinnacles of the Quatre Tours and forms a dyke-like intrusion of some tens of meters long, by ten to fifteen meters in width. The more melanocratic, coarser grained facies occur towards the centre of the intrusion, and one could almost find reason to describe a chilled margin, at the contact with the granite, except that the contact is never really net. Further north, other smaller pods of a similar material are found, but almost without exception these are either partially or wholly tectonised by the Alpine movements.

TEXTURE and MINERALOGY

Generally these dioritic rocks are less rich in dark coloured minerals, sphene is much less abundant, and forms small prismatic crystals scattered throughout the rock (Plate 3.11), biotite is also generally confined to small laths and crystals scattered throughout the rock, although from time to time it forms small knots of crystals, in conjunction with green actinoltic hornblende, these having a star like formation; apatite also occurs as small laths and crystals, as inclusions in both biotite and amphibole. The overall texture is one of a fluid, which has been intruded into a quasi-solid, but has then suffered a re-heating process; as witnessed by the formation of small prismatic crystals of sphene, this being the result of a re-equilibration of plagioclase and amphibole.

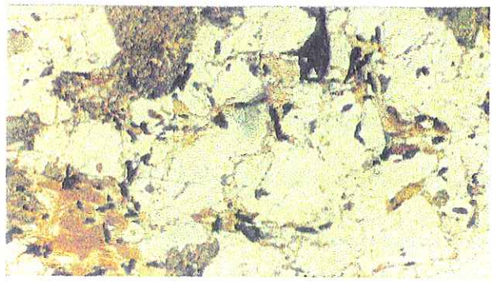

Plate 3.11 Photomicrograph from the Quatre Tours dioritic enclave. Sphene is a very prevalent accessory mineral. (Plane polarised light)

Plate 3.12 Three samples from the Quatre Tours diorite showing colouring of the feldspars.

Plagioclase

Plagioclase feldspar, consisting of andesine, with extinction angles of between 15 and 20° giving a composition of An 30 to 40, makes up about 55% of the total rock, (Plate 3.12), and consists of subhedral crystals, more or less altered to sericite. Where albite twinning occurs kinking of the lamella indicates that their formation took place under stress. Interaction and destabilisation by late forming potassium feldspar has given rise to small embayments and lobing, with the formation of myrmakitic textures. From time to time, zoned crystals occur, these having a tendency to be both larger than the norm and of good euhedral shape. The zoning is usually picked out by the formation of sericite in the more

calcium rich bands. A further phenomena is the systematic formation of a halo of potassium feldspar, usually microcline, around these crystals, indicating the late formation of this mineral.

Amphibole

Amphibole occurs as magnesian rich actinolite, normally green but sometimes brown. In the fine grained facies, it forms small clots of minerals, together with biotite, suggesting the syn-crystallisation of these two minerals. In the coarse grained variety, the two minerals again show some evidence of syn-crystallisation, but tend to take up interstitial positions between plagioclase and potash feldspar crystals. Microprobe data for thirteen amphiboles from the two different facies are displayed in Table 3.8. These data has been plotted on diagrams of Mg/Mg + Fe and Na + K against Si (Figs. 3.16 and 3.17) on which the fields for amphiboles from the Belle Cote syenites have also been plotted. In general the diorites plot nearer to the hornblende pole, but still within the cummingtonite/actinolite - pargasite - edenite triangle, and are classified as actinolites and actinolitic hornblendes (Leake, 1978; Tindle, 1982). On diagrams of Na + K versus Si and Na + K versus Ti (Figs. 3.18 and 3.19) the diorites fall well within the field of the Belle Cote syenites and no discrimination between fine and coarse grained varieties can be observed. On a diagram of Al^{VI} versus Si (Fig. 3.20) it can be seen that the pressure at which the diorites crystallised falls partially within the field of the Belle Cote syenites but in general below the line for 5 Kbars, on a diagram of Al^{IV} versus Ti (Fig; 3.21) this translates as a slightly higher temperature of crystallisation when compared to the Belle Cote syenites. These small differences can be explained by the differences in overall composition of the two rock types. Again these pressures and temperatures are well below the normal pressures and temperatures of solidification which would normally be associated with this type of magma, and as in the case for the syenites which outcrop further to the north these amphiboles have re-equilibrated under sub-solidus conditions.

Table 3.8 Microprope analysis of amphiboles from the Quatre Tours Diorite

Major elements (Oxides)

	Fine grained facies							Coarse grained facies					
Sample	**RO303**	**RO303**	**RO303**	**RO303**	**RO303**	**RO303**	**RO303**	**RO304**	**RO304**	**RO304**	**RO304**	**RO304**	**RO304**
SiO_2	50.27	48.43	50.27	48.51	49.65	51.43	47.85	48.32	48.87	51.39	51.26	49.27	50.47
Al_2O_3	4.25	5.34	4.03	5.82	4.90	3.97	5.43	5.45	5.91	3.56	3.58	4.88	4.08
FeO	13.10	13.31	13.13	14.20	14.38	13.43	11.46	13.56	13.57	11.83	11.91	13.04	12.53
MgO	14.91	14.73	14.47	13.58	13.83	14.88	13.54	13.71	14.02	15.19	15.38	14.32	14.96
CaO	11.76	10.98	11.61	11.47	11.47	11.57	11.3	11.42	11.52	11.74	11.84	11.04	11.33
Na_2O	0.78	1.24	0.77	1.15	0.88	0.83	1.17	1.05	1.28	0.74	0.69	1.23	1.05
K_2O	0.36	0.53	0.34	0.55	0.45	0.31	0.54	0.49	0.56	0.30	0.32	0.45	0.35
TiO_2	0.57	0.75	0.37	0.81	0.68	0.44	0.85	0.66	0.90	0.24	0.28	0.66	0.48
MnO	0.39	0.39	0.37	0.39	0.39	0.39	0.40	0.33	0.33	0.31	0.33	0.31	0.33
Cr_2O_3	0.03	0.37	0.02	0.03	0.33	0.02	0.42	0.18	0.02	0.02			
Total	96.42	95.7	95.73	96.5	96.63	97.28	92.54	95.32	96.98	95.72	95.77	95.22	95.6
	Formula Units (calculated for 23 Oxygens)												
Si	7.409	7.225	7.463	7.226	7.349	7.499	7.324	7.251	7.204	7.566	7.547	7.358	7.475
Al	0.738	0.939	0.706	0.987	0.855	0.683	0.979	0.963	1.207	0.618	0.622	0.859	0.708
Fe	1.615	1.661	1.629	1.769	1.800	1.638	1.467	1.702	1.673	1.454	1.467	1.629	1.516
Mg	3.275	3.276	3.202	3.016	3.052	3.235	3.090	3.067	3.080	3.333	3.375	3.188	3.303
Ca	1.857	1.755	1.847	1.831	1.819	1.807	1.853	1.836	1.820	1.852	1.868	1.767	1.799
Na	0.224	0.360	0.221	0.334	0.253	0.236	0.346	0.305	0.366	0.212	0.197	0.355	0.301
K	0.067	0.101	0.065	0.105	0.085	0.058	0.105	0.094	0.106	0.056	0.081	0.085	0.065
Ti	0.063	0.084	0.041	0.090	0.075	0.048	0.097	0.074	0.099	0.026	0.031	0.074	0.053
Mn	0.049	0.049	0.047	0.049	0.049	0.048	0.052	0.041	0.041	0.039	0.041	0.039	0.041
Cr	0.004	0.043	0.002	0.004	0.040	0.002	0.049	0.022	0.002	0.002			
Total	15.301	15.450	15.264	15.409	15.337	15.256	15.313	15.373	15.598	15.205	15.251	15.356	15.263
Mg*	0.66	0.65	0.66	0.62	0.62	0.66	0.66	0.63	0.63	0.69	0.69	0.65	0.68

Microprobe analysis made at The Open University, Great Britain.

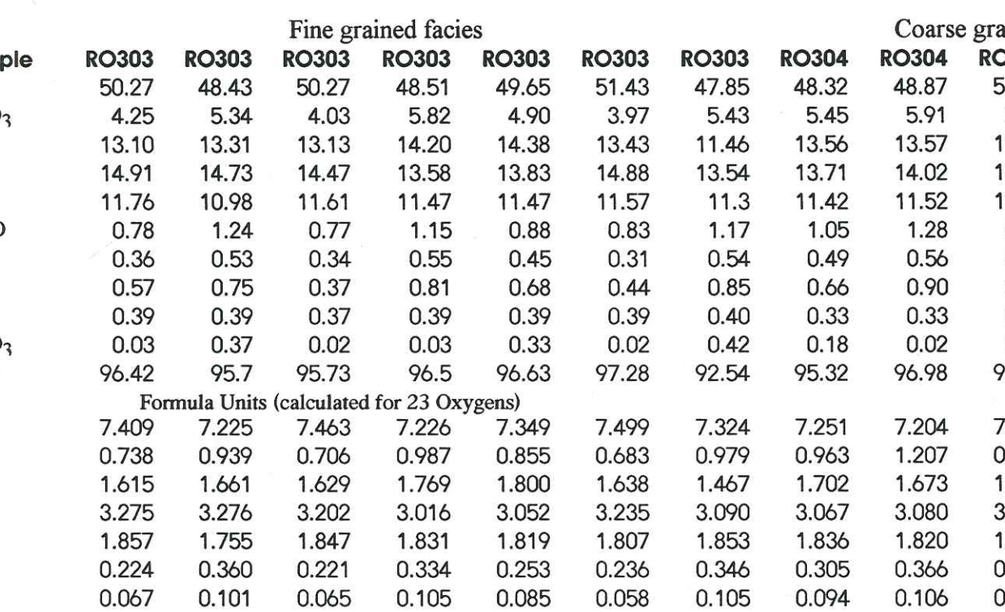

Figure 3.16 Nomenclature diagrame for calcic amphiboles (Ca+Na)>>1.34, Na<0.67) for for diorites from the Quatre Tours ◆ Fine grained diorite ▲ Coarse grained diorite (from B.E.Leake, 1978). Based on 23 Oxygens.

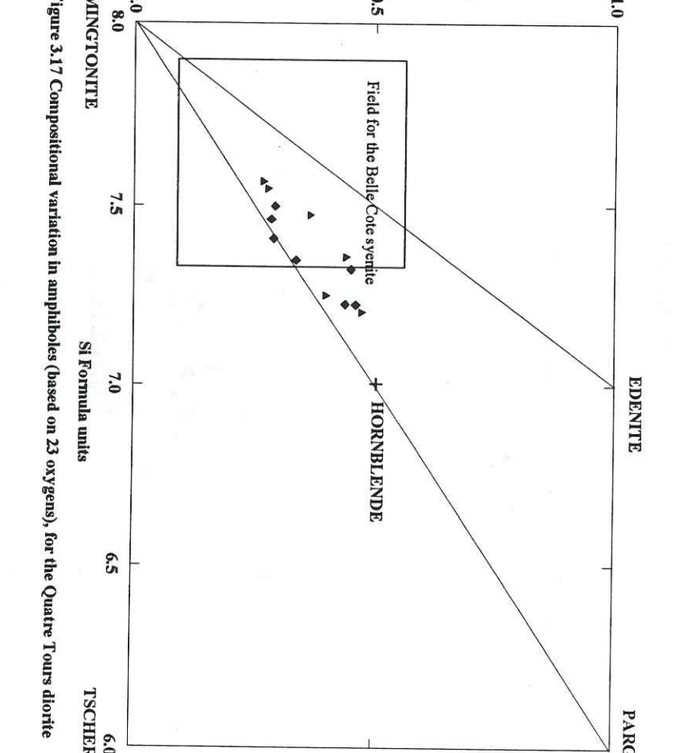

Figure 3.17 Compositional variation in amphiboles (based on 23 oxygens), for the Quatre Tours diorite

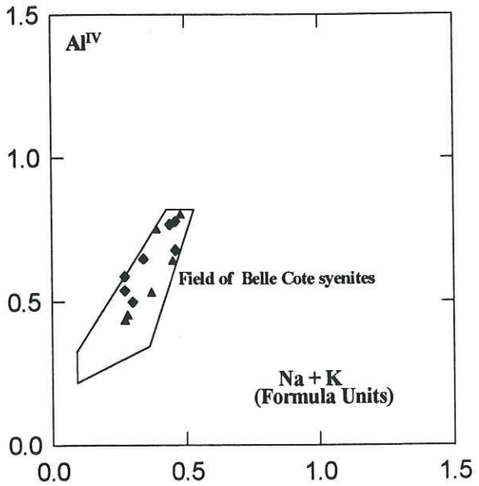

Figure 3.18 Plot of Al^{IV} versus Na + K from the A site for amphiboles from the Quatre Tours diorite (symbols as for Figure 3.16)

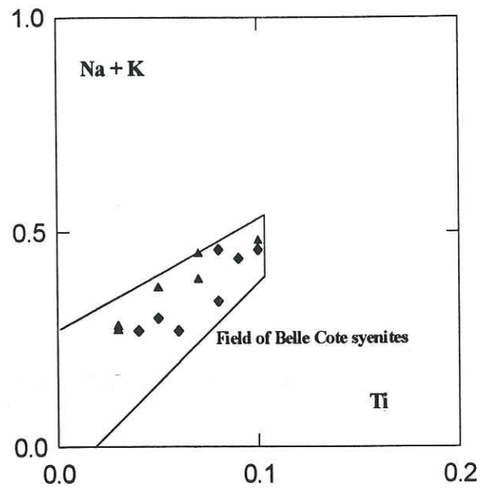

Figure 3.19 Plot of Na + K versus Ti for amphiboles from the Quatre Tours diorites (symbols as for Figure 3.16)

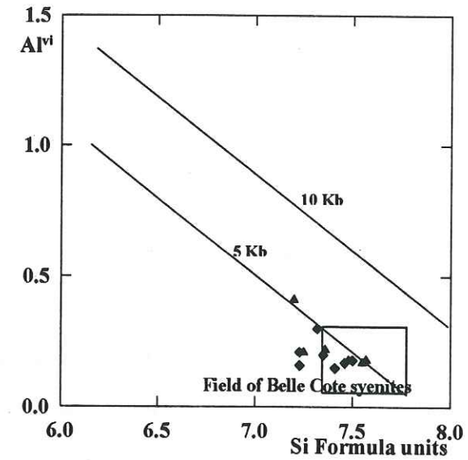

Figure 3.20 Plot of Al^{VI} versus Si for amphiboles from the Quatre Tours diorite, showing the probable pressure of crystallization at around 5 Kb. (Pressure values are from Helz, 1973, 1982) (Symbols as in Figure 3.15)

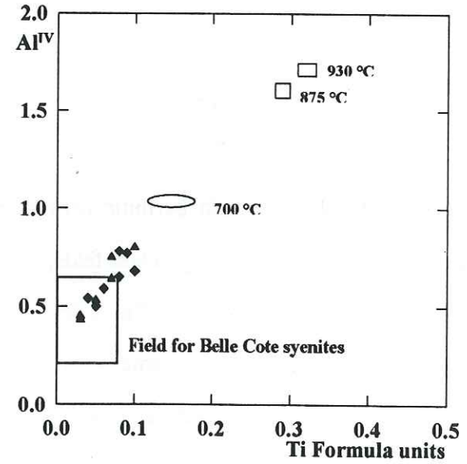

Figure 3.21 Plot of Al^{IV} versus Ti for amphiboles from the Quatre Tours diorite, showing the probable temperature of formation. Values are from Helz, 1973 for calcic amphiboles obtained from experimental data at H_2O saturation and 1000 to 700 °C at 5 Kb. (Symbols as for Figure 3.15)

Biotite

Biotite occurs in two forms, firstly as small clots, together with green hornblende; and secondly, as small sub-euhedral crystals scattered throughout the rock. The first is often partially chloritised.

Microprobe analysis data for seven biotites, from both the coarse and fine grained facies are displayed in Table 3.9.

These values have again been plotted on the triangular diagram of $Fe_2O_3/MgO/Al_2O_3$ (Nockolds, 1947) Fig. 3.14, which also shows the fields and trends for the Belle Cote syenites. It can be seen from this diagram, that those biotites from the coarse grained facies (solid triangles), plot on a prolongation of trend 2, being enriched in iron at the expense of magnesium. Biotites from the fine grained facies however, (solid diamonds), plot towards the edge of and even into region "b" of biotites formed in the presence of amphibole, whilst having an intermediate value of Al between the two trends. This highlights the difference in temperature, at the time of crystallisation, between these dioritic rocks and the more basic syenites further north.

Potassium feldspar

Occurs as small interstitial crystals of both perthitic orthose and microcline in the fine grained facies. From time to time crystals of plagioclase feldspar, more or less altered, have halos of potash feldspar, usually of microcline. The K-feldspar makes up about 15% of the total rock. This percentage is approximately the same in the coarse grained facies, but here the habit of the K-feldspar becomes similar to that described for the Belle Cote syenite, with large pöikolitic crystals (Plate 3.12), sometimes showing Carlsbad twinning.

Table 3.9 : Microprobe analysis of biotites from the Quatre Tours Diorite

Major Elements (Oxides)

	Fine grained facies			Coarse grained facies			
Sample	RO303	RO303	RO303	RO304	RO304	RO304	RO304
SiO_2	36.70	37.48	35.86	37.82	37.91	37.28	37.25
Al_2O_3	14.21	14.69	14.94	16.65	13.46	13.81	14.28
FeO	17.86	17.97	20.65	16.52	16.36	16.49	16.74
MgO	12.57	12.23	12.52	14.12	13.91	13.91	14.24
CaO	0.03	0.01	0.01	0.03	0.03	0.14	0.04
Na_2O	0.07	0.05	0.05	0.09	0.05	0.09	0.05
K_2O	8.68	9.15	9.07	9.52	9.29	8.37	8.51
TiO_2	-	-	-	-	-	2.40	1.82
BaO_2	0.37	0.41	0.40	-	-	0.37	0.25
MnO	0.25	0.23	0.23	0.19	0.22	0.20	0.22

Formula units (Calculated for 22 oxygens)

Si	5.829	5.857	5.550	5.902	5.948	5.722	5.682
Al	2.661	2.705	2.786	2.510	2.489	2.499	2.569
Fe	2.372	2.348	2.732	2.156	2.146	2.117	2.139
Mn	0.033	0.031	0.031	0.024	0.029	0.026	0.028
Mg	2.976	2.847	2.951	3.285	3.252	3.182	3.284
Ti	-	-	-	-	-	0.277	0.209
Ca	0.005	0.002	0.002	0.005	0.005	0.024	0.007
Na	0.022	0.016	0.017	0.026	0.016	0.026	0.016
K	1.758	1.824	1.830	1.895	1.859	1.639	1.658
Total	15.656	15.630	15.899	15.803	15.744	15.512	15.592
Mg*	0.56	0.55	0.52	0.60	0.60	0.57	0.58

Microprobe analysis made at The Open University, G.B.

Minor Phases

Sphene, Apatite, Quartz and Opaque oxides make up the majority of the minor phases, together with Zircon and occasional Allanite. Sphene is disseminated as small euhedral crystals throughout the fine grained facies, but occasionally, large somewhat corroded anhedral crystals also occur, associated with hornblende. This habit is the norm in the coarse grained facies, where the occurrence of sphene is much reduced.

Apatite occurs as crystals and laths associated with all the minerals in the fine grained facies, indicating the early formation of this mineral, but again, as in the case of sphene, it is much less abundant in the coarse grained variety.

Quartz

Quartz is never abundant and always exists as small interstitial crystals normally with undulose extinction.

Summary and Conclusions

The diorites, which outcrop in the southern part of the Quatre Tours Belle Cote granite, differ from the syenites found elsewhere within this and the Rochail granite, by the excess of plagioclase feldspar over potash feldspar; further, the chemical character of both amphibole and biotite shows small differences from that of the syenites, being for the first, poorer in magnesium and for the second richer in iron. This may be due to differences in the PT conditions at the time of emplacement, but a much more likely explanation is differences in the source material.

3.8 THE ROCHAIL SYENITES

The basic intrusions of the Rochail granite have already been described in some detail by T de Boisset, 1986, and only the essential information is reproduced here.

3.8.1 The Cascade de Lauvitel

The basic intrusions which crop out at the Cascade de Lauvitel can be subdivided into three distinct facies, which are, unlike the syenite dykes of the Belle Cote, separated spatially by a well determined contact.(see Figure 2.11)

The first facies was described by De Boisset as a porphyric monzo-syenite, with a preponderance of potassium feldspar, and constitutes about one third of the outcrop, forming an outer ring of from two to five metres thickness around the second facies. The contact with the granite is always very sharp and no modification to the texture is evident.

Several large (metric in size) blocks of granite, more or less rounded are found as enclaves within this facies. Both the granite and monzo-syenite are cut by a number of aplitic veins, which show dextral shear structures.

The second facies consists of a much more melanocratic rock than the monzo-syenite, with a much higher percentage of ferro-magnesian minerals, and of much finer grain-size, varying in thickness between one and three meters. Again the contact between this and the monzo-syenite, is generally quite sharp, but is never in contact with the granite. No enclaves were observed in this material, but as the contact with the central facies is approached, the occurrence of large potassium feldspar crystals becomes more and more frequent.

The third and most abundant facies, found towards the centre of the outcrop is somewhat heterogeneous in texture. In general, it contains large(several centimetres in length and breadth), highly pöikolitic crystals of potassium feldspar, separated by thin bands rich in ferro-magnesian minerals. Locally the syenite becomes more homogenous with a large grain size, in which individual biotite crystals can obtain centimetre size.

The whole of the outcrop is cut by a one to two metre thick band of leucocratic granite, which has been offset by post emplacement tectonics.

Mineralogy

Mineralogically there is little or no difference between the minerals developed at the Cascade and those already described at the Belle Cote. This presupposes therefore a common source for these two intrusions.

3.8.2 Les Sources

In the northern part of the Rochail granite (see fig. 3.4), the occurrence of syenitic intrusions are centred in the region of "Les Sources". Here the intrusions consist of a number of distinct bands of fractally developed enclaves, (Fig.3.22), varying from decimetric, up to several metres in size. These bands are aligned along a lineament of N150 to N160 between the refuge of Les Sources and the Aiguille du Midi. The outcrop here is approximately one

Figure 3.22 Detailed map of the syenitic intrusion, "Refuge des Sources" in the north of the Rochail granite.

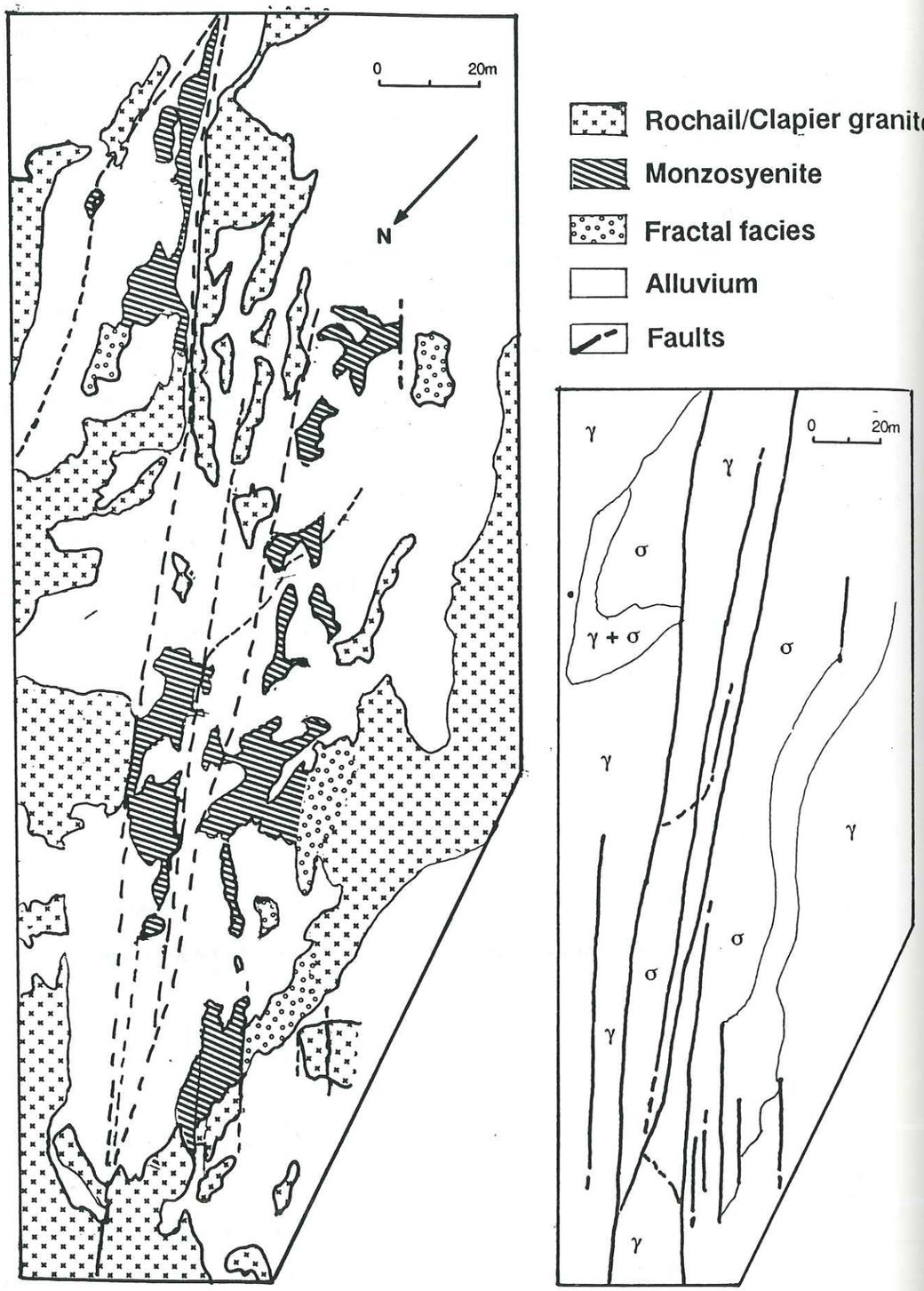

hundred metres long and the enclaves are bound in a porphyritic granite matrix. These can be divided into three distinct zones; 1) here the enclaves are massive (metric to pluri-metric in size) and angular in shape, with small veins of quartz and feldspar at the contact with the surrounding granite. This zone leads progressively into 2) where the enclaves are variable in size and become less angular and more oval in shape, but diminish progressively in size on approaching zone 3) here the enclaves are well rounded and oval in shape, although the contact with the surrounding granite is in all cases very sharp. All the enclaves consist of a leucocratic syenite with an abundance of large crystals of potassium feldspar.

Here, in contrast to the intrusions at the Belle Cote and perhaps also the Cascade de Lauvitel, the syenite appears to have been in a solid or quasi-solid state at the time of its contact with the granite magma. This is born out by the way in which the syenite has fractured in a brittle manner and then been incorporated as enclaves within the crystallising granite. This leads to the idea that the syenitic material has reacted with the intruding granites at different structural levels within these granite massifs.

Mineralogy

The Mineralogy of the outcrop has been described by T. de Boisset (1986) and I reproduce here his observations.

Texture

The monzo-syenite of the refuge des Sources is generally fine grained and has the look of a leucocratic diorite. Modally it comprises 35-40% K-feldspar, 30-35% plagioclase feldspar (oligoclase), biotite (Mg/Mg+Fe=0.59-0.60) 10-15%, hornblende (tremolitic) 10-15%, late forming quartz 3-5%, sphene 1% and prismatic apatite 1% plus traces of zircon. The quantity of potassium feldspar can attain 60-70% in certain facies, with some rare crystals having a pöikolitic texture. The alteration of the ferro-magnesien minerals and sphene is important, with biotite showing deformation and chloritisation. Amphibole has sphene and apatite as inclusions, and has suffered a partial alteration with chlorite + calcite ± epidote forming along cleavage plains.

3.9 LAMPROPHYRES

These exist as small veins and dykes of metric size, disseminated throughout the region, becoming more prevalent towards the south and west of the Haute Dauphine. The only examples found in the studied terrain are a) a number of lens shaped inclusions on the summit and eastern slopes of the Ramu peak, and b) a dyke of one to two meters width at the southern end of Lac Lauvitel in the Rochail granite. The origins of these lamprophyres are thought to be twofold firstly as intrusions of Permian age (Laurent, 1993) and secondly as the feeder dykes, for the alkaline volcanism that was prevalent during Triassic times within the region (Vatin-Perignon et al., 1973; Buffiere and Aumaitre, 1973; Adline, 1982). It seems probable that at least some of these intrusions are linked with the former, and it is probably true for those outcrops at the Ramu peak as well as the cross cutting dyke in the southern Rochail, as this has a trend roughly NW which would imply emplacement during very Late Carboniferous to Early Permian times.

Texture

They are everywhere very fine grained grey coloured rocks, being totally aphyric in hand specimen, although further south in the Valsenetre granite similar veins and dykes show phyric textures, with the presence of elongate crystals of chlorite after biotite Figure 3.21.

Mineralogy

The rocks are highly altered, but consist of small laths of plagioclase feldspar, crystals of chlorite after biotite, some times showing euhedral shapes and preserving the original cleavage, and very occasional highly corroded pyroxenes, in a glassy groundmass. Opaque oxides are very prevalent, associated mainly with the biotites, which may indicate an excess of iron in these later, or alternatively the degree of oxidation of the replacing chlorite minerals.

3.10 SUMMARY AND CONCLUSIONS

Within the Valsenestre region the intrusive rocks consist essentially of four separate granites, with or without an associated coeval basic component.

The Ramu granite presents a mineralogy and texture, which can be associated with the leucogranites of other collision zones, and may be attributed to a process of migmatisation of the gneissic material, with which it is associated; the event having taken place at a relatively high level in the crust.

The Alfrey granite may well be the oldest, and is certainly "in situ", as evidenced by the marked contact with the country rocks, preserved in the south and south-west margins of the intrusion. Like the Ramu granite it has no associated basic suite, but does show a regular mineralogical evolution from the margins, in towards the centre, indication of an in situ fractionation.

The Quatre Tours/Belle Cote granite complex has been imbricated and stacked over the Alfrey granite, and displays only tectonic margins. Relatively homogenous in character, it is noted for the variety of rock types in its associated basic suite, ranging from diorites at the southern end to syenites at the northern end.

The Rochail granite, the largest in both surface outcrop and volume, is mieralogically very similar to the Quatre Tours /Belle Cote granite, and also displays a suite of basic dykes and enclaves, mainly syenite in character, but with a much wider variety of textures to those found in the Quatres Tours/Belle Cote.

CHAPTER 4

GEOCHEMISTRY OF THE IGNEOUS ROCKS

4.1 INTRODUCTION

The purpose of this chapter is to detail the geochemistry of the granitic, syenitic and monzodioritic rocks associated in the Valsenestre-Lauvitel region and to attempt to gain some knowledge as to their origins, within the context of the Variscan collision event. For this purpose over 100 intrusive and metamorphic rock samples from the region were analysed by energy dispersive x-ray fluorescence (EDXRF) techniques at The Open University and the University Joseph Fourier, Grenoble. Subsets of these samples were also analysed by Instrumental Activation Analysis (INAA) at the Institut Max Von Laue-Paul Langevin, Grenoble following the procedures detailed in Oliver et al., 1981, and conventional wavelength dispersive x-ray fluorescence (WDXRF) at the University Claude Bernard, Lyon. A further small subset of samples were analysed for Boron by the method of Prompt Gamma Activation Analysis at the Institut Laue, Langevin, Grenoble(Oliver et al., 1987, Vittoz et al., 1986). The elements determined being Si, Al, Fe, Mn, Mg, Ca, Na, K, Ti, P, Ba, Rb, Sr, Y, Zr (by XRF); La, Ce, Nd, Sm, Eu, Tb, Yb, Lu, U, Th, Hf, Ta, Sc and Cr (by INAA); B (by PGAA); V, Ni, Cu, Zn and Nb (by EDXRF). The details of the analytical techniques used are documented in Appendices 1 to 3.

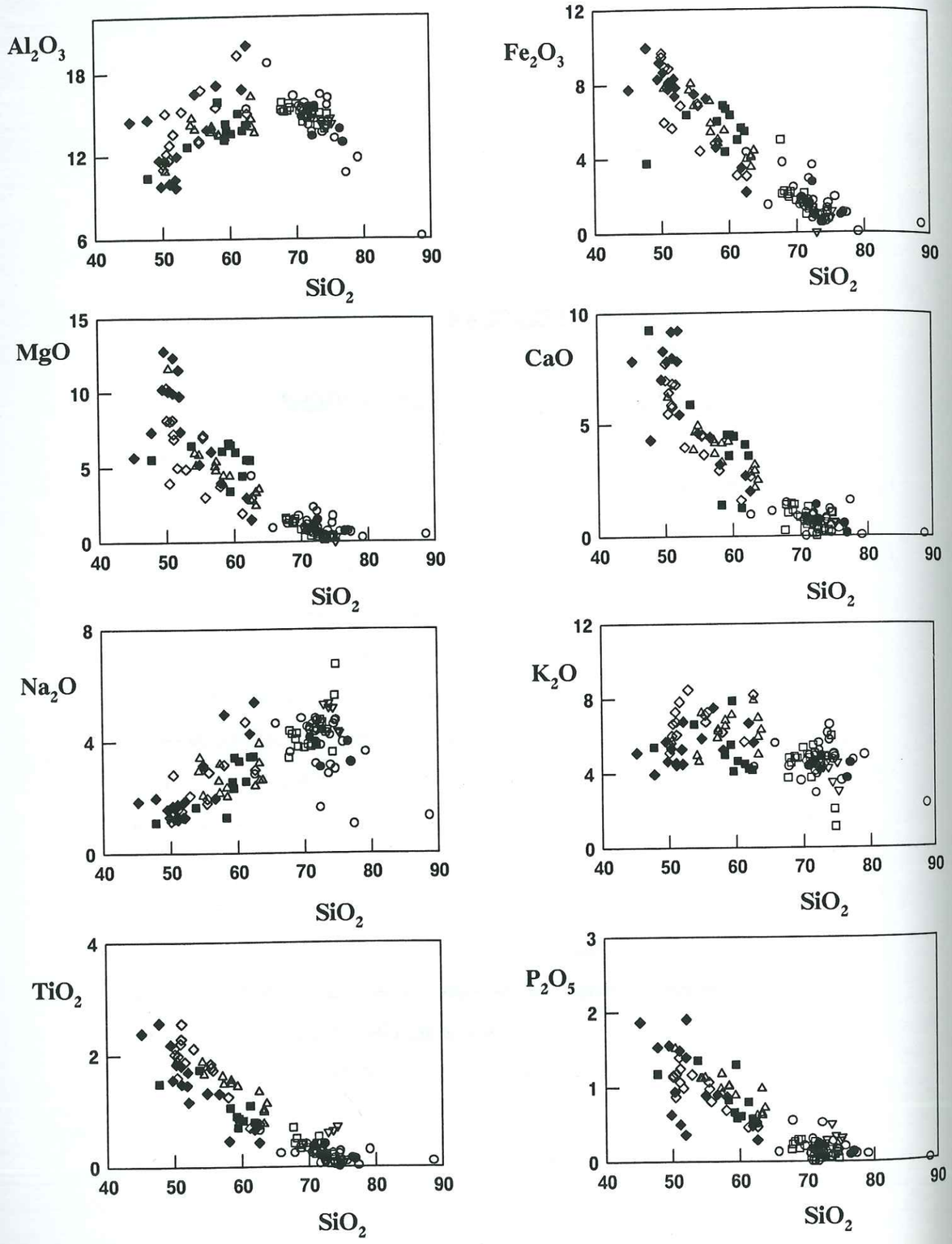

Figure 4.1 Major element discriminant diagrams of SiO_2 versus selected elements, for the intrusive rocks of the Valsenestre region, Haut Dauphine.

(○ Quatre Tours/Belle Cote granite, ● Alfrey granite, ▽ Ramu granite, □ Rochail granite, ■ Quatre Tours monzodiorite, ◆ Belle Cote syenite, ◇ Cascade de Lauvitel syenite, △ Refuge des Sources syenite.)

4.2 MAJOR AND TRACE ELEMENT VARIATIONS FOR ALL ROCKS

The major and trace element data for all rock types are illustrated in four ways. Firstly major and trace element analyses are listed in Table 4.1 and Table 4.5 (see Appendix 4). Secondly both major and trace elements are plotted against SiO_2 (Figure 4.1 4.4, 4.13, 4.16, 4.26 and 4.29). In the third case major elements are used in mineral/chemical discriminant diagrams after De La Roche, 1976, 1978 and Debon and Le Fort, 1982. In the fourth case trace elements are used in a variety of discriminant and comparative diagrams.

4.2.1 MAJOR ELEMENTS

Selected major elements plotted against SiO_2 for all types of igneous rocks are presented in Figure 4.1. The important features of these SiO_2 co-variation diagrams are as follows.

1) There is no real continuum of composition for the igneous rocks, but rather they form two distinct groups with SiO_2 values ranging from, for:-

a) Group 1 from 45 to 63% This group is formed by syenites, monzodiorites and some intermediate facies from the syenites.

b) Group 2 from 68 to 78% This group consists entirely of granites and related rocks, with one pegmatite at 88%.

2) Of the major elements Fe_2O_3, TiO_2 and P_2O_5 have an apparently linear trend, but show a large scatter, although P_2O_5 for the syenites around 50% SiO_2 could be said to show a vertical trend.

3) Aluminium shows two distinct trends, one positive for the basic to intermediate rocks and the second negative for the granite group.

4) K_2O are high for all the rock types, with values ranging from around 3% up to nearly 9%. Scatter within basic to intermediate rocks is much larger than for the granites, as are the overall values. Each group shows a fairly flat lying trend. Na_2O has

Figure 4.2 Nomenclature diagram for common igneous rocks after Debon and Le Fort, 1982 for rocks from the Valsenestre suite.
The paramaters are expressed as gram-atoms x 10^3 of each element in 100g of material.
Key: 1 (gr) granite, 2 (ad) adamellite, 3 (gd) granodiorite 4 (to) tonalite, 5 (sq) quartz syenite, 6 (mzq) quartz monzonite 7 (mzdq) quartz monzodiorite, 8 (dq) quartz diorite, 9 (s) syenite 10 (mz) monzonite, 11 (mzgo) monzogabbro, 12 (go) gabbro.
(Symbols are the same as for Figure 4.1)

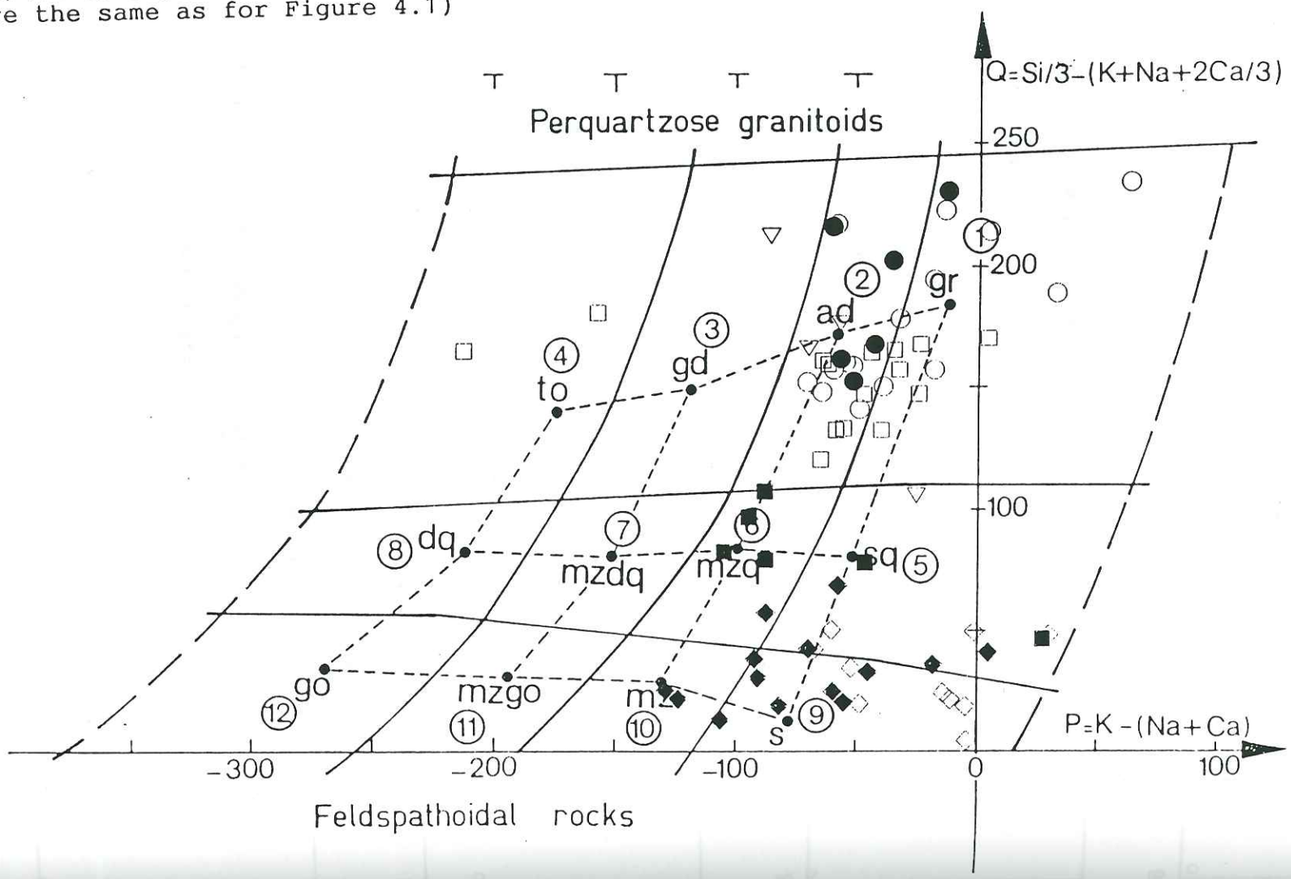

Figure 4.3 "Characteristic mineral" diagram (Debon and Le Fort, 1982) for the Valsenestre suite.
Parameters are expressed in milli-atoms x 10^3 for 100g of material.
I= muscovite>biotite, *II*= biotite>muscovite, *III*= ± biotite, *IV*= ± biotite ± hornblende ± Opx ± Cpx ± olivine, *V*= ± Cpx ± hornblende ± biotite. Numbers refer to regression lines for individual units.
(Symbols are the same as in Figure 4.1)

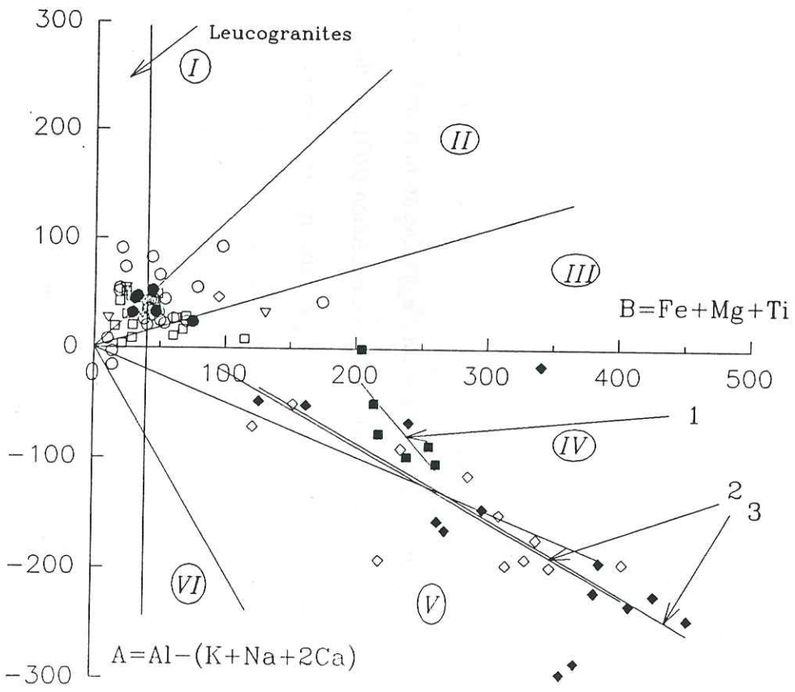

a positive trend for Group 1, but again with a large degree of scatter, whilst Group 2 forms a fairly homogenous group with no apparent trend.

5) Both MgO and CaO show a vertical trend for syenites with SiO_2 less than 55% and a slightly negative trend for syenites and intermediate rocks, which could be tentatively described as possible fractionation trends. Group 2 data is relatively incoherent.

4.2.2 CHEMICAL/MINERAL DIAGRAMS

Results have been plotted onto the Chemical-mineralogical diagrams of De la Roche, 1976, 1978, which were later modified by Debon and Le Fort, 1982. The usefulness of these types of diagram are to allow the mineralogical interpretation of igneous rocks from their bulk chemistry, whilst avoiding the tediousness of a modal analysis.

Figure 4.2 is a plot of Q=(Si/3-(K+Na+(2Ca/3)) versus P=K-(Na +Ca). the main object of this diagram is to indicate a typology for each sample based on its major element chemistry. It can be seen that the acid rocks plot into the granite and adamellite (monzogranite) spaces with one pegmatite in granodiorite space and two samples in the tonalite space. The basic rocks plot into the bottom right hand corner of the diagram with, in the main the syenites from Belle Cote plotting into the syenite and monzonite space whilst with one exception (RO125) the monzodiorites of the Quatre Tours plot into quartz syenite and quartz-monzonite space. The syenites of La Cascade show essentially higher K values than their Belle Cote counterparts and plot well into the bottom right hand corner and in effect make a continuum with the Belle Cote syenites.

Figure 4.3 is a plot of A=(Al-(K+Na+2Ca) versus B=(Fe+Mg+Ti). Of these two parameters, the first differentiates between rocks of a peraluminous (rich) or metaluminous (poor) character, whilst the second is entirely related to the dark minerals within the rocks, and is a reasonable indicator of the minerals present.

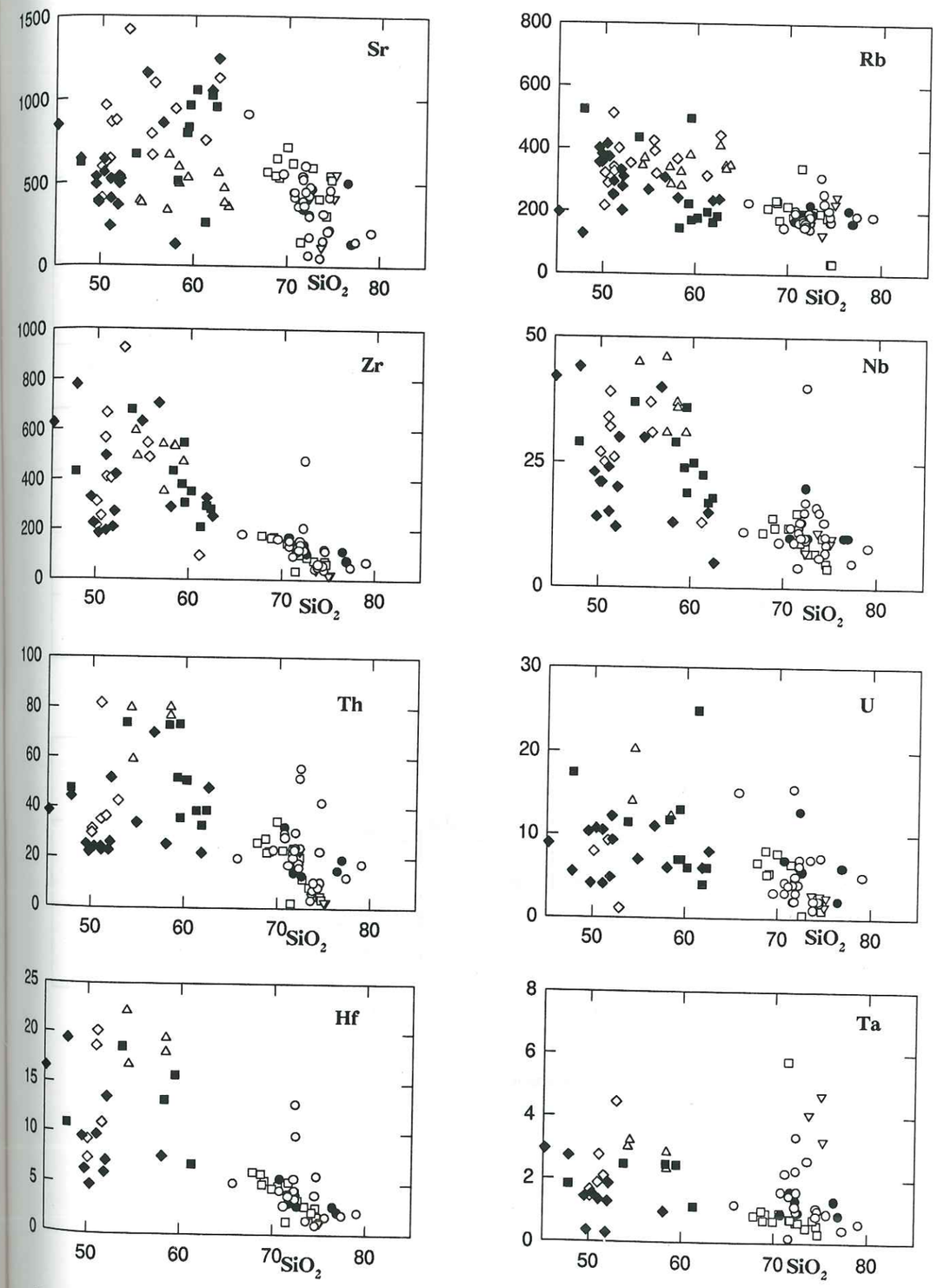

Figure 4.4 Trace element discriminant diagrams of selected trace elements versus SiO_2, for intrusive rocks of the Valsenestre region.

(Symbols are the same as for Figure 4.1)

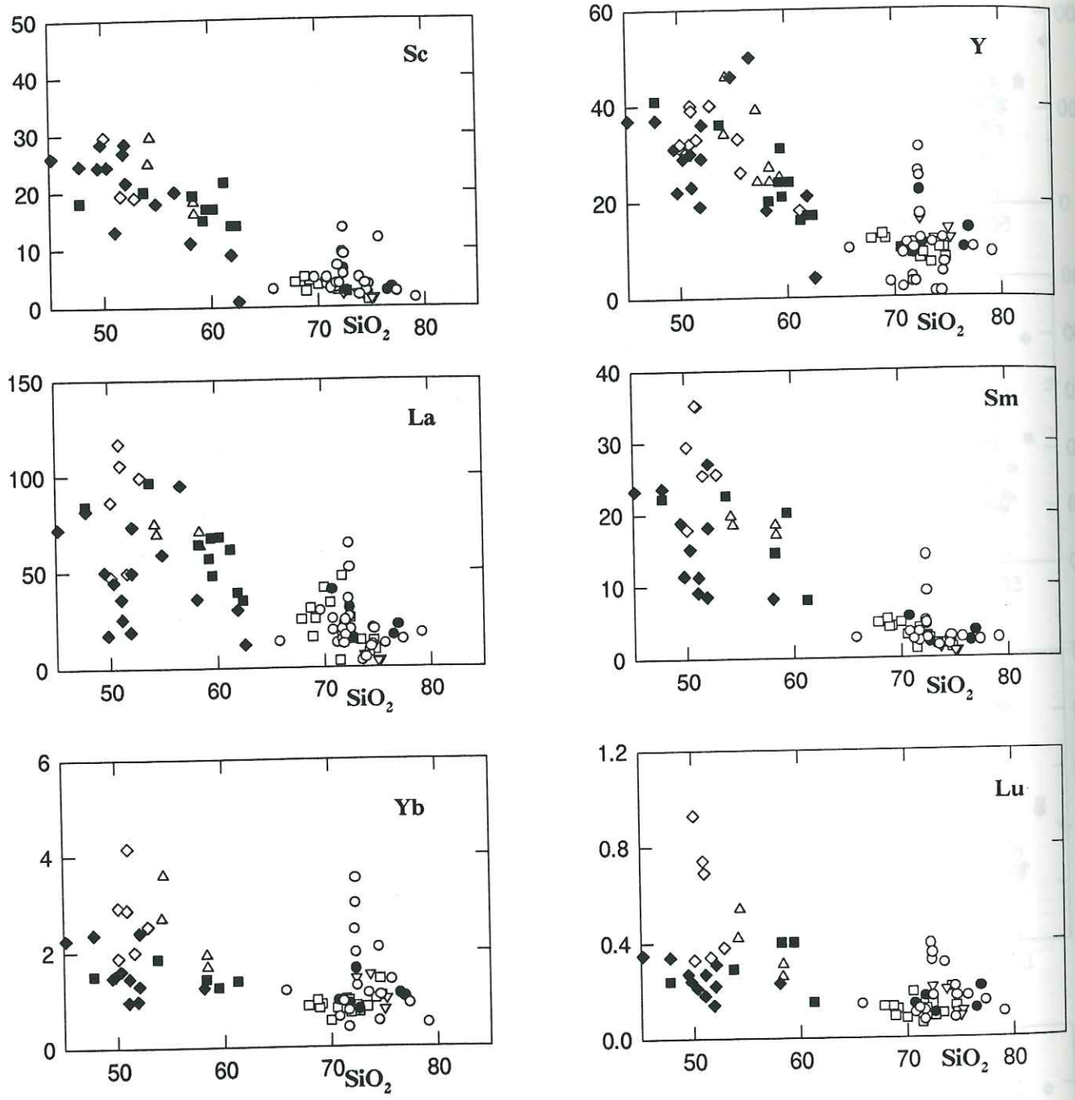

Figure 4.4 (Contd.) Trace element discriminent diagrams of selected trace elements versus SiO_2, for intrusive rocks of the Valsenestre region.

The majority of the granites fall above the origin in the peraluminous domain, and lie in either field *II* with biotite in excess of muscovite or field *I* with muscovite in excess of biotite. The mafic rocks show trends in the metaluminous domain. the Belle Cote and La Cascade syenites have very similar trends (regression line 2 and 3 on Figure 4.3) running from field *IV*, ± biotite ± hornblende ± Opx to field *V*, ± Cpx ± hornblende ± biotite. The Quatre Tours monzodiorite however has a somewhat different trend (regression line 1 on Figure 4.2) and lies wholly in field *IV*. All these basic rocks will contain primary sphene and or epidote and this is in fact the case (see Chapter 3).

4.2.3 TRACE ELEMENTS

Trace element discriminant diagrams for selected trace elements are displayed in Figure 4.4. The chosen elements being Sr, Rb and Th for the mobile elements, Zr, Nb, Hf, Ta and Y for highly incompatible elements, La and Sm for the light to medium rare Earths and Yb and Lu for the HREE.

The essential information to be gathered from these diagrams is that in general, as could be expected, the two groups have quite different concentrations of trace elements with the exception of U, Ta and the HREE. Further the values for the basic suite of rocks show larger degrees of scatter, the concentrations for the majority of the granite samples being quite well constrained.

TRACE ELEMENT CO-VARIATION DIAGRAMS

Figure 4.5 is a plot of MgO versus MgO* (MgO/FeO^T+MgO), this diagram demonstrates the essential differences between the two suites of rocks. The basic rocks have a large variation in MgO content for a well constrained MgO* number, whilst the reverse is true for the acidic rocks.

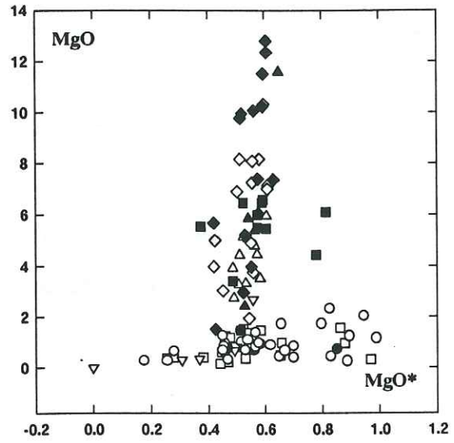

Figure 4.5 Plot of MgO versus MgO* for all intrusives from the Valsenestre region.
(symbols as for Figure 4.1 + ▲ les Gauchoirs syenite)

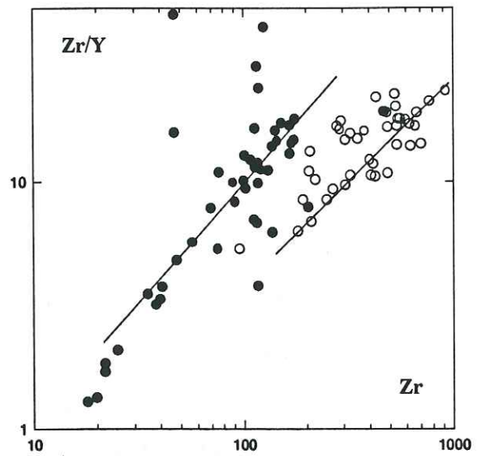

Figure 4.6 Diagram of Zr/Y against Zr for the intrusive rocks of of the Valsenestre region, Haute Dauphine.
(● granites, ○ diorites and syenites)

Figure 4.6 is a multi-element variation diagram of Zr/Y versus Zr as the discriminating factor . This type of diagram shows essentially the evolution of rock series with respect to fractionation and degrees of partial melting, Zr being less incompatible than Y. It can be seen that the two rock types are again well separated with two distinct

trends the remarkable event being the high Zr content of the basic rocks with respect to the acidic rocks, a reversal to that which might be expected. It is therefore evident that the basic rocks associated with the granites of the Valsenestre region have a somewhat complex chemistry and this will be examined in greater detail, further on.

4.2.4 BORON GEOCHEMISTRY

Boron, as a geochemical indicator has recently become of interest, due to its chemical and physical characteristics (Curtis and Gladney; 1985).

Geological Setting	Rock type	Concentration Boron (ppm)	Error
Rift	Peridotite	0.2	± 0.1
	Eucrite	0.8	± 0.2
	Allivalite	0.2	± 0.1
	Foliated gabbro	0.3	± 0.3
	Epigranite	1.6	± 0.3
Within Plate (Oceanic)	Alkali basalt	1.6	± 0.3
	Alkali gabbro	3.6	± 0.3
	Monzonitic gabbro	6.0	± 0.3
	Monzonite	3.1	± 0.2
	Nephaline syenite	5.7	± 0.3
	Alkaline granite	5.1	± 0.3
Within Plate (Continental)	Biotite granite	2.5	± 0.5
	Peralkaline granite (1)	1.5	± 0.3
	Peralkaline granite (2)	8.2	± 1.5
	Fayalite granite	1.7	± 0.3
Active Continental margin	Glassy Tuffs	172.0	± 2.5
	Pyroclastic flows	38.7	± 1.5
Syn-collision	Granite	28.0	± 1.3
	Tourmaline granite	475.0	± 5.5
Post Collision	Granite	13.4	± 1.2
	Granite (altered)	57.6	± 1.5
	Granite (Greissen)	342.0	± 4.0

(1) Riebeckite bearing (2) Arfvedsonite bearing

Table 4.2 Boron concentrations in differing rock types from a variety of tectonic environments. (Measurements made at the Institut Laue-Langevin, Grenoble.) (stated errors are 1σ and include both statistical and systematic uncertainties.)

Measurements made at the Institut Laue-Langevin (Oliver et al., 1989) indicate that rocks from different tectonic environments have differing Boron contents (Table 4.2).

Sample	Provenance	SiO_2	Al_2O_3	K_2O	B
RL102 Biotite	Cascade de Lauvitel Monzosyenite	37.80	13.39	10.01	1.40
RL102 Amphibole		50.19	5.05	0.68	0.20
RL103 K-Feldspar	Cascade de Lauvitel Potassium rich syenite	63.65	19.03	16.50	3.10
RL103 Biotite		39.30	13.69	10.09	2.10
RL103 Amphibole		52.60	3.82	0.37	14.00

Table 4.3 Major oxide and elemental abundances for mineral separates from two samples of syenite from the Cascade de Lauvitel intrusion.

Sample	Provenance	SiO_2	Al_2O_3	K_2O	Boron
RO124	Quatre Tours granite	72.48	14.95	4.46	12.9
RO125	Quatre Tours monzodiorite	59.40	14.23	7.88	3.4
RO257	Alfrey granite	72.69	15.53	4.93	23.1
RO258	Alfrey granite	72.39	13.33	4.21	28.2
RO303	Quatre Tours monzodiorite	59.94	13.29	3.77	12.2
RO304	Quatre Tours monzodiorite	58.28	14.81	2.82	7.3
RO309	Belle Cote granite	70.82	15.26	4.93	29.1
RO311	Belle Cote granite	71.23	15.78	4.52	13.9
RO312	Belle Cote syenite	51.88	10.27	5.29	9.0
RO314	Belle Cote syenite	50.33	11.63	5.34	7.7
RO501	Quatre Tours granite	74.56	15.59	4.94	15.5
RO502	Quatre Tours granite	74.68	16.13	4.84	14.5
RO508	Ramu granite	73.69	14.49	4.70	13.4
RO513	Alfrey granite	70.77	14.73	4.36	32.0
RL101	Rochail granite	70.56	15.18	4.98	15.5
RL104	Cascade de Lauvitel syenite	58.89	15.18	8.48	6.4
RL105	Cascade de Lauvitel syenite	50.96	11.64	7.31	5.0
RL106	Cascade de Lauvitel syenite	51.14	11.80	6.07	12.0
RL203	Refuge des Sources granite	67.82	15.79	4.81	13.9
RL205	Refuge des Sources syenite	58.38	13.48	6.53	6.4

Table 4.4 Major oxide and elemental abundance's for selected rocks from the Valsenestre region, Haute Dauphine. (Boron measurements made at the Institut Laue-Langevin Grenoble following the methods of Oliver et al., 1988 (see Appendix)).

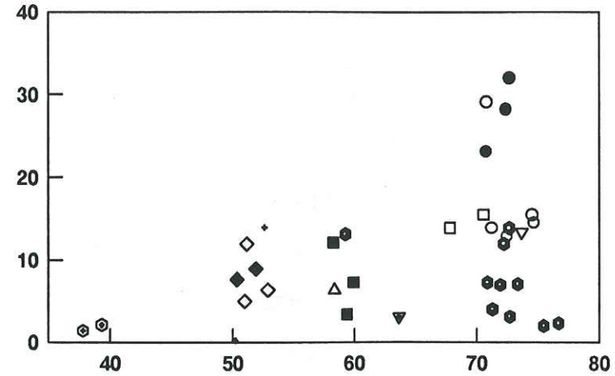

Figure 4.7 Plot of SiO_2 against Boron for selected granitic and basic samples from the Valsenestre Region, Haute Dauphine.
(symbols as for Figure 4.1 + • amphibole, ⊛ biotite, ▼ feldspar).

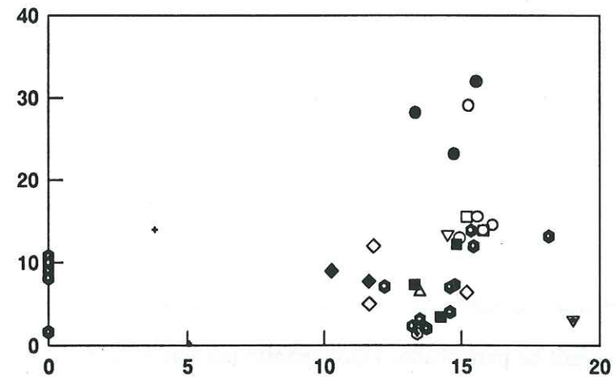

Figure 4.8 Plot of Al_2O_3 against Boron for selected granitic and basic samples from the Valsenestre region, Haute Dauphine.
(symbols as for Figure 4.7)

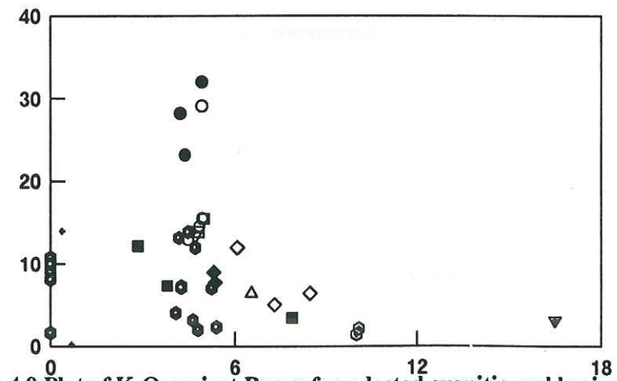

Figure 4.9 Plot of K_2O against Boron for selected granitic and basic samples from the Valsenestre region, Haut Dauphine.
(symbols as for Figure 4.7)

It is therefore possible to use Boron as a discriminant element to determine the differences in source materials and evolutionary history. Boron measurements (see Annexe 2) have been made on a small subset of samples from the Valsenestre region, as well as a set of mineral separates from two syenite samples from the Cascade de Lauvitel, RL102 and RL103 and the results obtained are shown in Tables 4.3. and 4.4. Granites show boron values ranging from 12.9 ppm to 32 ppm, average 19.81 ppm, whilst the monzodiorites range from 3.4 ppm to 12.2 ppm, average 7.6 ppm and the syenites range from 5 ppm to 12 ppm, average 7.75 ppm. Values for the monzodiorites and syenites show very similar abundances and it is within the granites that the largest spread is observed with the Alfrey granite showing somewhat higher values than the other granites.

These data are displayed in Figures 4.7, 4.8 and 4.9. Mineral data is not conclusive, with marked differences showing between the amphiboles of the two samples, but this may be explained by the very small data set available. The whole rock data is however, much more interesting especially Figure 4.7 where SiO_2 discriminates not only granitic rocks from Basic and intermediate rocks but also discriminates between different granite intrusions. Hence the Alfrey granite and one sample from the Quatre Tours granite, which may in fact be part of the Alfrey granite (sample is from the tectonised border zone between the two granites), plot well clear of the other granites. Further the Alfrey data shows boron values increasing from the contact facies towards the centre, indicating the in situ fractional crystallisation that has taken place within this small granite stock.

Summary and Conclusions

The general geochemistry of the intrusive rocks demonstrates the presence of two distinct types of magma, one acid and the other basic, showing distinctive geochemistry's, but which appeared to have occupied the same space time continuum.

This type of association is not unusual in collision zone environments (Fowler, 1988; Pitcher, 1993), especially in the post collision phase (Harris et al., 1986). The overall tectonic regime is possibly one of local extensions, giving rise to crustal thinning with the consequent release of pressure, occasioning the fusion of mantle material at moderate (circa 1100 °C) temperatures (Odling, 1994), which provides the heat source for melting the overlying thinned crust.

The geochemistry of the two different rock types will be developed separately to try to understand the very different magma generation processes and source regions which pertained.

4.3 GRANITE GEOCHEMISTRY

4.3.1 Major Elements

Representative samples from the different granites have been plotted on SiO_2 co-variant diagrams Fig. 4.10. The silica dioxide content of the granites ranges essentially from 68 to 78 wt% with one pegmatite sample at 88 wt%. Of the major elements only Al_2O_3, TiO_2 and perhaps Fe_2O_3 show slightly negative linear trends, this would seem reasonable in the circumstances. Of the other elements MgO and CaO form incoherent groups, with large scatter, both as an ensemble and within the individual granite bodies. The most plausible explanation for this being heterogeneity's within the source rocks from which the different granites were generated, but it should be noted that the majority of samples have values for Mg which bring them into the category of "high magnesien " granites as defined by Debon and Lefort (1988). Na_2O, K_2O and to a lesser extent P_2O_5 have flat lying trends. This may well be an indication

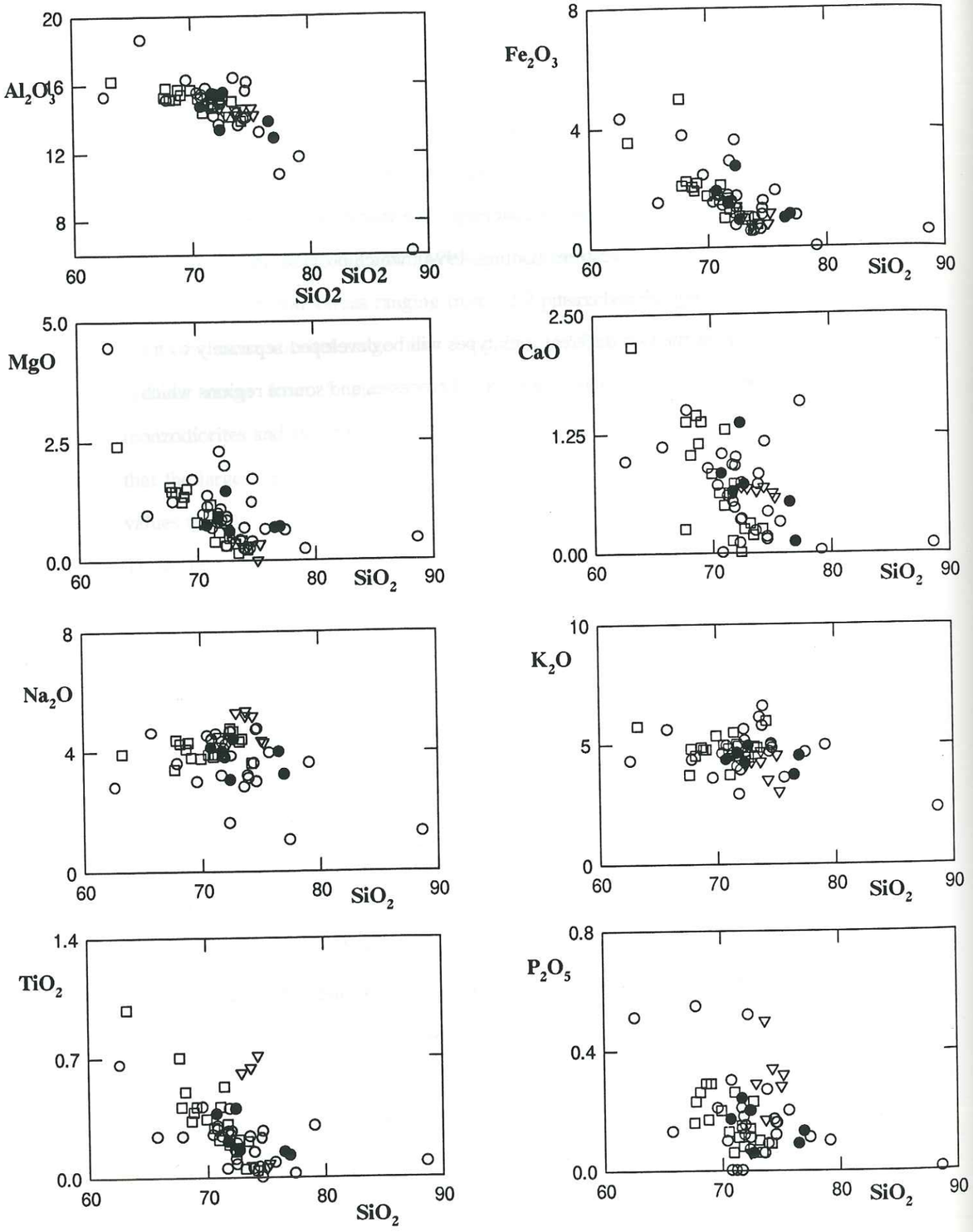

Figure 4.10 Major element discriminant diagrams of SiO_2 versus selected elements, for granites of the Valsenestre region, Haute Dauphine.

(○ Quatre Tours/Belle Cote granite, ● Alfrey granite, ▽ Ramu granite, □ Rochail granite)

of alteration suffered due either to the circulation of late stage magmatic fluids, of which there is some mineralogical evidence (op cit. Chapter 3), or alternatively could be attributed to circulation of alkali rich fluids during the Alpine orogenic event and the proximity of the major fault zones with which the whole area is associated, again some evidence for this also exists from K/Rb isotope data (op cit. Chapter 6).

The major element geochemistry of the four granites is very similar but some minor differences do occur, notably for sodium, where:

1. The Ramu granite may be distinguished by

a) a generally higher level of Na_2O >4.5 wt % and b) a low total Fe_2O_3 content <1 wt%.

2. The Quatre Tours-Belle Cote granite shows a wide spread of Na_2O values but has generally lower values.

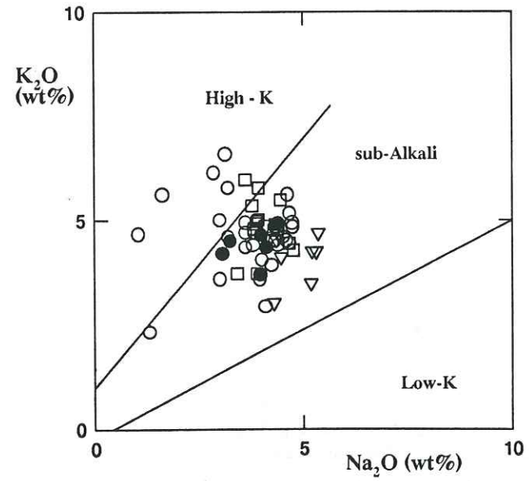

Figure 4.11 Na_2O versus K for the granites of the Valsenestre region.
(symbols as for Figure 4.10)

3. The Rochail and Alfrey granite have general values for Na_2O between the Ramu and Quatre Tours-Belle Cote granite.

To try to typify the granites they have been plotted on a diagram (Figure 4.11) of K_2O versus Na_2O. The majority of the granites plot into the sub-alkaline field, with the

exception of six samples from the QTBC granite and two from the Rochail granite, which plot into the High-K field. This excess of potassium may be explained either by proximity to fault zones, RO208 and 209, proximity to the roof zone of the QTBC granite, RO132 and 133, proximity to the monzodiorite enclaves of the Quatre Tours, RO652, and RO675A or the syenite of Les Gauchoirs, RL402 or an aplite vein crossing the syenite enclave of La Cascade, RL100.

In terms of the possible sources of granites Chappel and White,1974; White and Chappel, 1977; 1988, and Chappel and Stevens, 1988 suggested that granite intrusives of the Lachlan Fold belt, South Australia, could be subdivided on the basis of mineralogical, petrological and isotope characteristics into two different types, I types having igneous, or S types having sedimentary rocks as their source.

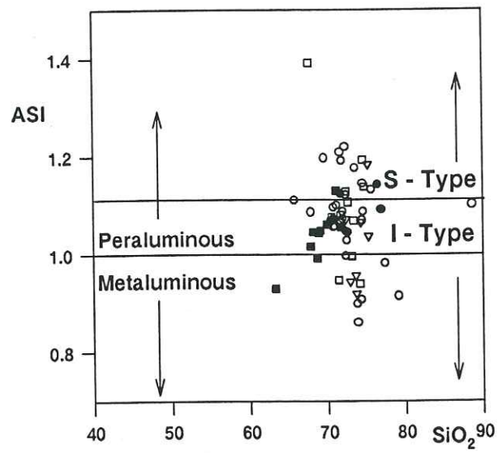

Figure 4.12 Plot of $Al_2/(Ca+Na_2+K_2)$, or alumina saturation index (ASI), versus SiO_2, for granites of the Valsenestre region.

These two different source types have since been studied by numerous workers in many different contexts and various chemical characteristics have been proposed. A major discriminatory indicator between S and I type has been determined as being a function of the alumina saturation. The Valsenestre data have been plotted on a diagram of this type (Figure 4.12) where it can be seen that two thirds of the samples

plot into the field of I-type granites. Of these several fall below the dividing line between peraluminous and metalouminous granites but there does not seem to be any distinction between granite types. The samples which fall into the domain of S-type granites show the same criteria i.e. no distinction between the four granites nor a distinction in terms of evolutionary trends.

4.3.2 Trace Elements

Trace elements can be helpful in specifying a number of parameters about magmas and their sources. For incompatible trace elements, i.e. those with crystal-liquid partition coefficients considerably less than one, e.g. Rb, Zr, Ba, U, light REE etc., even relatively small degrees of melting (10%) of the source will produce a liquid which incorporates the majority of these elements, and the ratio's of these elements in the melt will be very similar to those in the source (Gast, 1968; Schilling, 1971). This means that ratios of elements in the source material will be close to the initial ratios found in the derived melt. Only in the case where there are very small degrees of melting i.e. <5%, where the residue might contain a refractory phase, effective at fractionating elements such as Rb and Sr (e.g. amphibole or phlogopite) will these ratios in the melt be significantly different from that in the original source.

The granites have been plotted on a series of trace element discriminant diagrams in order to define,

a) Their inherent differences if any.

b) Their possible source

A number of trace elements Sr, Rb, Zr, Nb, Th, U, Hf, Ta, Sc, Y, La, Sm, Yb and Lu have been plotted on Harker type diagrams with SiO_2 as the discriminant factor (Figure 4.12). Sr, Zr, Th, Hf, Ta, Sc and Sm have slight negative trends, whilst Rb, Nb, U, Y, Yb and Lu have generally flat lying trends. La shows no particular trend but is disseminated in a cloud of points.

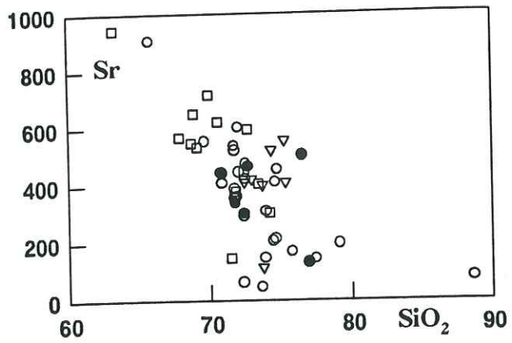

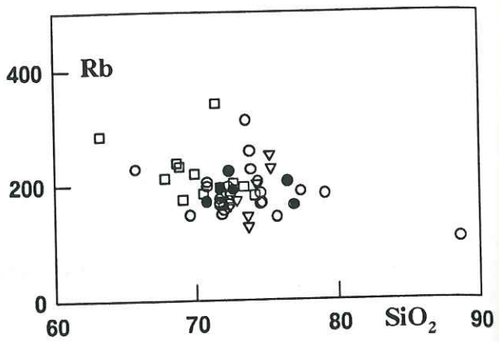

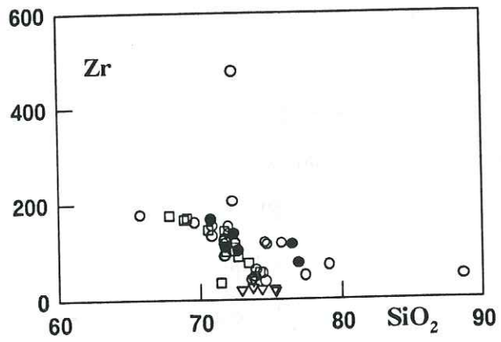

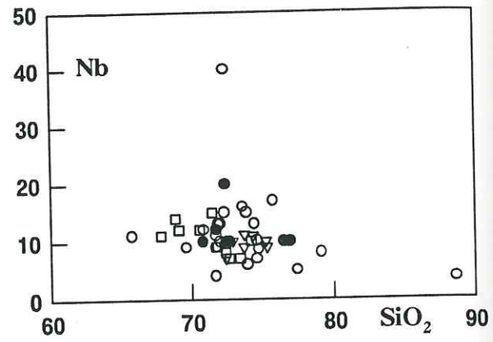

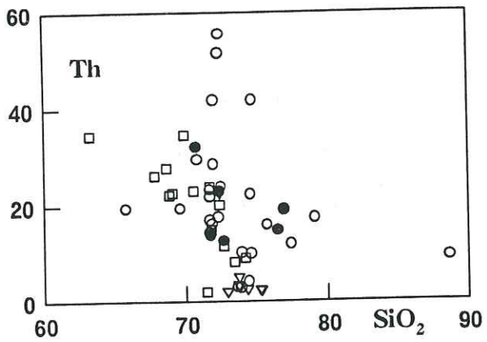

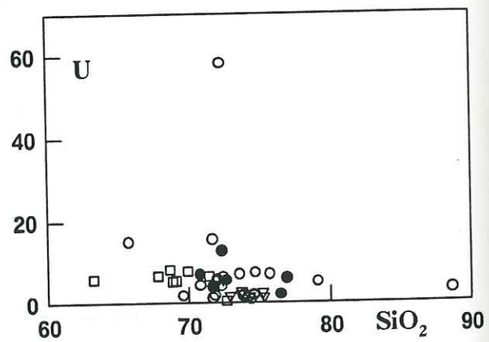

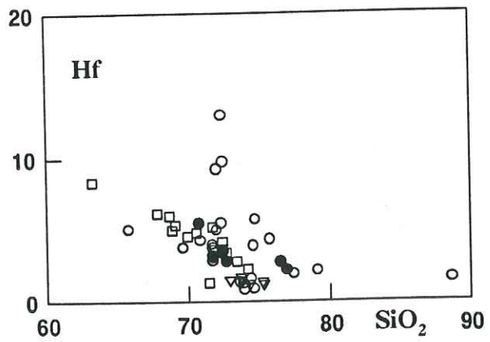

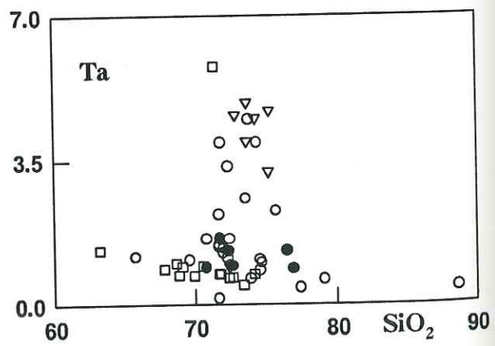

Figure 4.13 Trace element discriminant diagrams of SiO_2 versus selected elements for granites of the Valsenestre region, Haut Dauphine.
(symbols as for Figure 4.10)

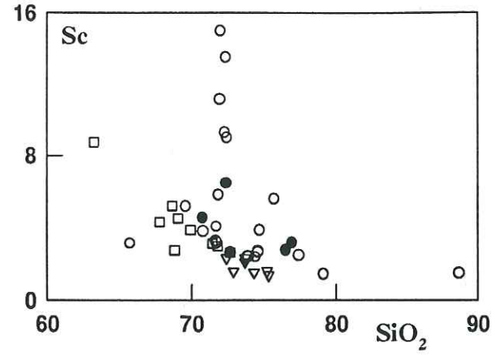

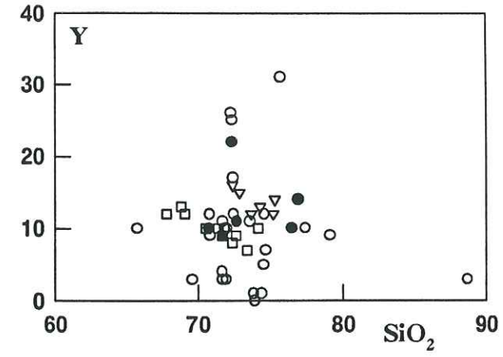

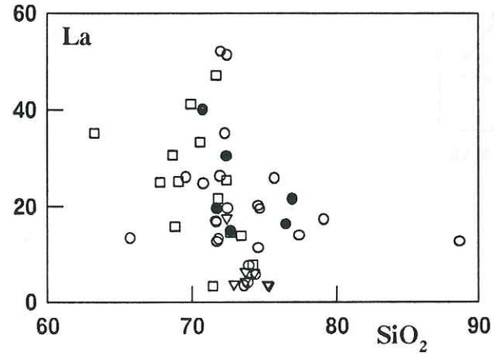

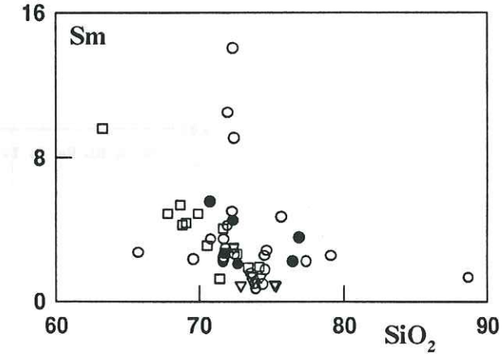

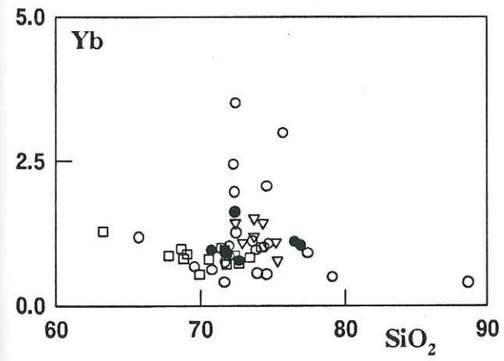

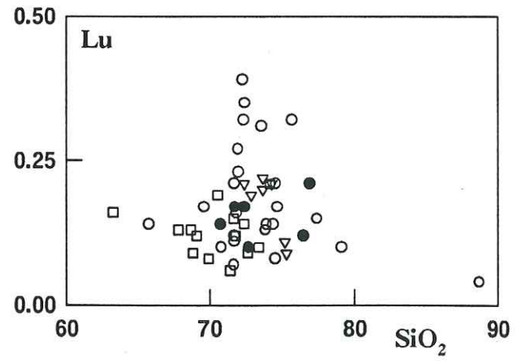

Figure 4.13 (cont.) Trace element discriminant diagrams of SiO_2 versus selected elements for granites of the Valsenestre region, Haut Dauphine.
(symbols as for Figure 4.10)

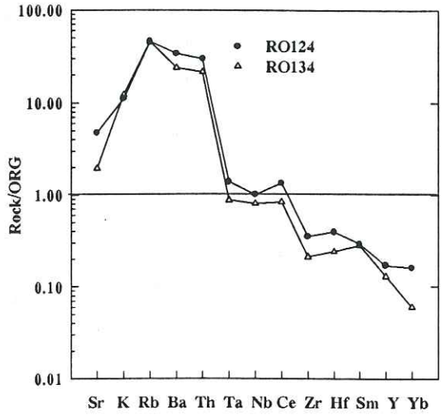

Figure 4.14a
Representative spidergrams of the Quatre Tours/Belle Cote granite. (southern sector)

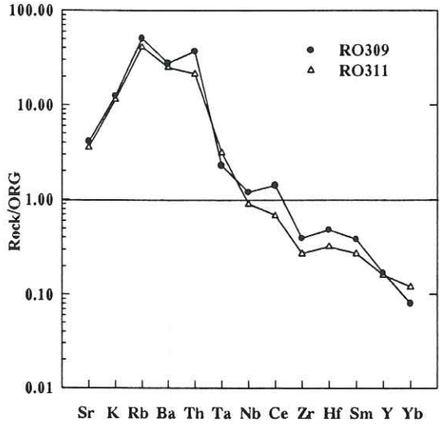

Figure 4.14b
Representative spidergrams of the Quatre Tours/Belle Cote. granite. (northern sector)

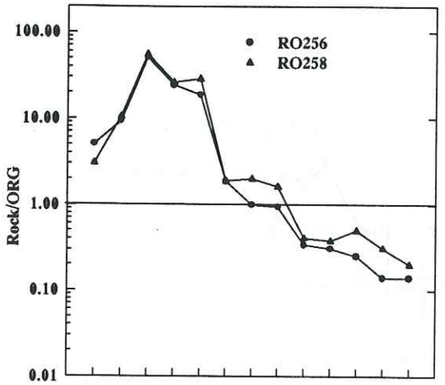

Figure 4.14c
Representative spidergrams of the Alfrey granite.

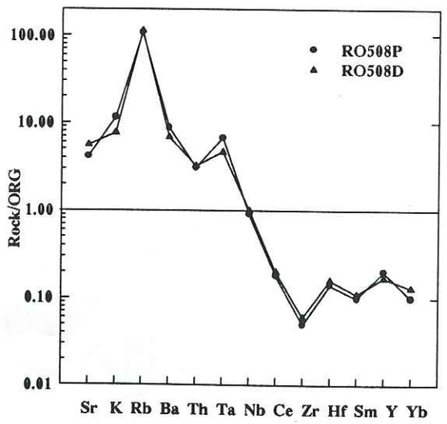

Figure 4.14d
Representative spidergrams of the Ramu granite.

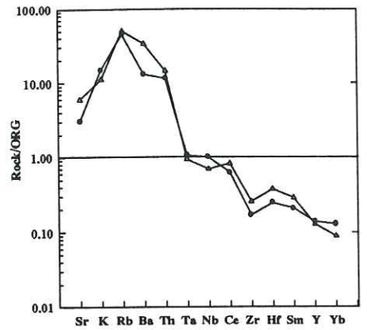

Figure 4.14e
Representative spidergrams
of the Rochail granite.
(Cascade de Lauvitel sector)

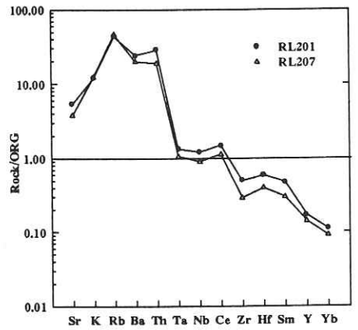

Figure 4.14f
Representative spidergrams
of the Rochail granite.
(Refuge des Sources sector)

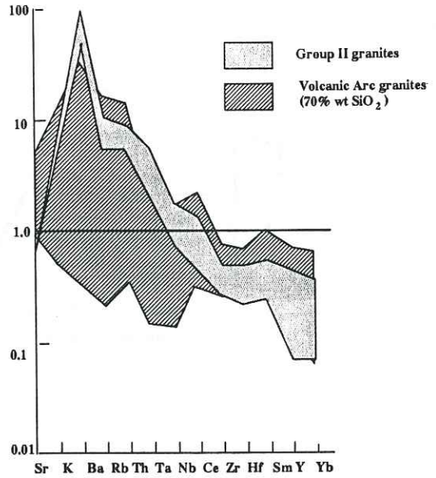

Figure 4.14g Multi-variant trace element diagram for Group II granites, (Himalayas, Hercynides and the Alps) and volcanic arc granites (Pearce et al., 1984) (after Harris et al., 1986).

Representative multi-variation diagrams of the separate granites have been plotted in Figure 4.14, using the normalising values of an hypothetical ocean ridge granite given by Harris et al., 1986.

(Sr = 100, K_2O = 0.4%, Rb = 4, Ba = 50, Th = 0.8, Ta = 0.7, Nb = 10, Ce = 35, Zr = 340, Hf = 9, Sm = 9, Y = 70, Yb = 8).

Comparing the patterns for the different granites, it can be seen, that whilst there are minor differences between the patterns for the granites of Alfrey, QTBC north and south and the Rochail massif, the overall patterns are very similar to each other and also show similarities with trace element patterns of granites from both Volcanic Arc and post-collision environments.. However, a major difference is shown by the Ramu granite, with the LIL elements, with the exception of Rb, being much reduced, but with a strong positive Ta anomaly and strongly negative HFS elements, these abundance's are consistent with the idea that the Ramu granite is a fairly high level, anatexic granite. Comparison with the average profiles for Volcanic Arc and Group II (collision zone) granites of Harris et al., 1986 (Fig4.14g) indicate that the granites of Quatre Tours/Belle Cote, Alfrey and Rochail resemble the former, whilst the Ramu granite has a profile closer to that of the Group II granites. Group II granites tend to be enriched in Rubidium and Tantalum but depleted in heavy rare earth elements (HREE) and high field strength elements (HFS) (Harris et al.,(1986)).

Ba and Sr are two elements which are constrained by the major phases (Biotite, amphibole, feldspar etc.), from a diagram of Ba versus Sr (Figure 4.15) it can be seen that the major control of these two elements is due to feldspar, which is in accordance with the relative importance of this phase especially with respect to biotite. Rb versus Sr (Figure 4.16a), as might be expected shows a well defined trend, line **b** in Figure 4.16a, of Sr enrichment with respect to Rb, with the samples from Les Sources, Belle Cote and Les Gauchoirs having the highest values of Sr, and this may well be due to some degree of interaction between the basic dykes and the granites. combining these two diagrams gives the Sr-Rb-Ba triangular diagram of Figure 4.16b, from this it can be seen that the majority of the granites lie below the line of Rb-Ba separation and

tend towards the Ba pole, re-affirming the S-type characteristics of these granites being of the HiBaSr type. (Tarney and Jance, 1994).

Collision magmatism is of necessity complex, as the production and source of magmas will change during the period of the collision (Tindle and Pearce, 1981; Harris, 1982; Radain and Fyfe, 1982 and Pharoah and Pearce, 1984). The granites of the Variscan of SW Europe have been defined and divided into two general groups (Didier and Lameyre, 1969;), a first phase of syn-tectonic intrusions from 340-300 Ma and a second later phase of late to post-tectonic intrusions emplaced circa. 280- 260 Ma, whilst Bonin et al., (1993) defined a suite of Lower to Middle Carboniferous high K calc-alkaline intrusions and a late Carboniferous near alkaline suite for the Variscan Alps.

Pearce et al. (1984) defined a number of trace element discriminate diagrams in order to determine, in an empirical way, (although petrogenitic criteria can be invoked for most of the discriminating boundaries) the differences between the provenance of granites within different tectonic regimes.

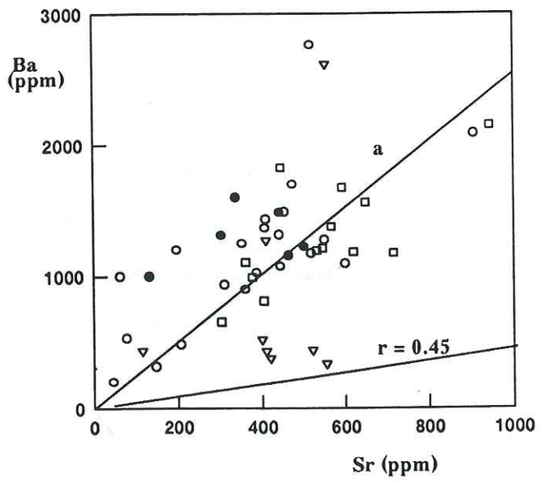

Figure 4.15 Plot of the LIL elements Ba versus Sr for the granites of the Valsenestre region, Haute Da
(line r=0.45 is ratio of ORG, a= full data regression symbols as in Fig.4.10)

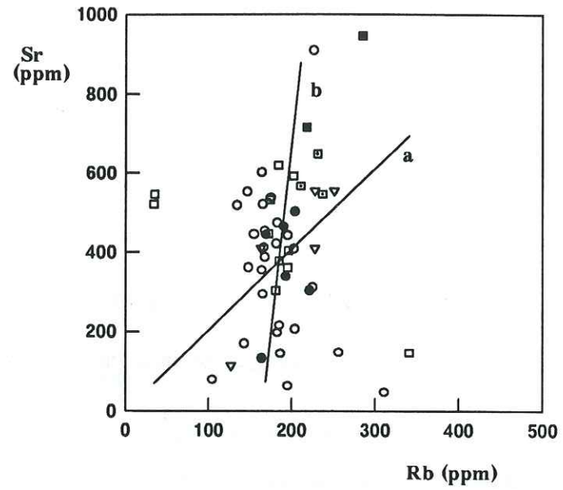

Figure 4.16a Plot of the LIL elements Sr versus Rb for the granites of the Western Haute Dauphine
(line a = data regression line, line b = trend, drawn by eye. symbols as in Fig. 4.10)

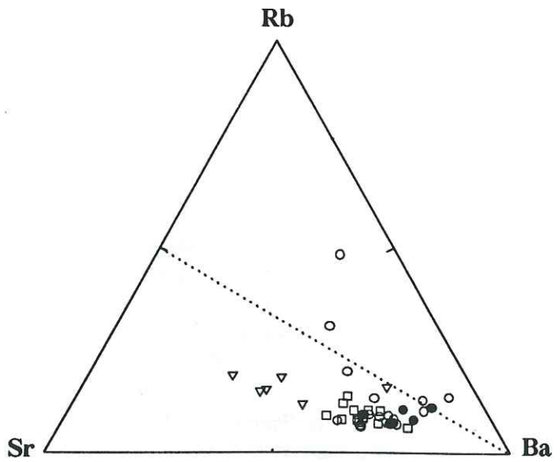

Figure 4.16b Triangular diagram of Rb-Sr-Ba for the granites of the Valsenestre region, Haut Dauphine.
(symbols as for Figure 4.7)

Two of these diagrams are Ta against Yb space and Rb against Y + Nb space. The former can be shown to discriminate effectively for syn-collision and volcanic arc

granites, and the latter, whilst in theory achieving the same type of discrimination should be somewhat easier to explain in petrogenetic terms. Data from the four granites plotted onto a Rb-Y + Nb diagram (Figure 4.17) clusters around the separation between the syn-collision and volcanic Arc granites. Again the Ramu granite due to its excess of Rb plots slightly away from the other three well into syn-collision space. When the data is plotted onto the diagram of Ta against Yb (Figure 4 .18) separation is somewhat better defined with the Ramu granite and a few samples from the Quatre Tours/Belle Cote granite plotting across and into syn-collision space

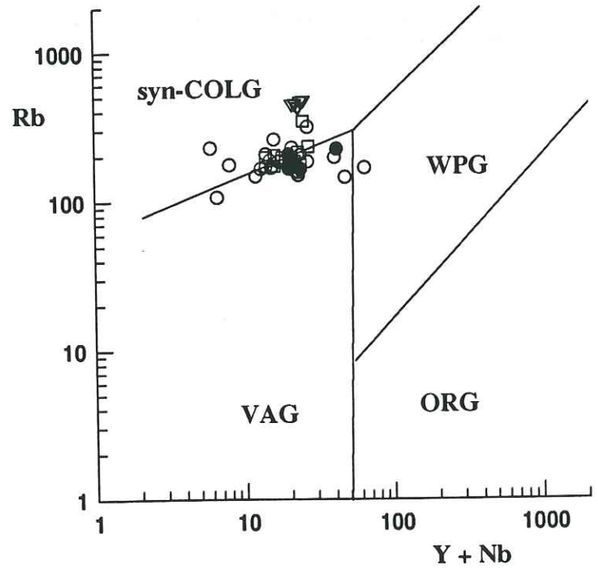

Figure 4.17 Rb against Y + Nb discriminant diagram for the granites of the Valsenstre region, Haute Dauphine. (after Pearce et al., 1984)
(symbols as in Figure 4.10)

whilst the rest plot essentially into volcanic arc space. This seems to indicate that source regions for the granites are essentially crustal, but that whilst the Ramu leucogranite behaves as a true syn-collision granite the sources of the Alfrey, Quatre Tours/Belle Cote and Rochail granites are to be found somewhat lower in the crust and may well be reworked granitic or granodioritic material generated during a former, possibly Acadian, period of subduction related magmatism.

Harris et al., (1986) defined a fourfold classification on geochemical criteria. Group I, intrusions pre-dating collision and having essentially the characteristics of calc-alkaline volcanic arc type magmatism. Group II, intrusions emplaced syn-tectonically commonly consisting of leuocgranites with an S-type signature (Chappell and White, 1974). Group III, intrusions of calc-alkaline infinity with rock types from gabbro to granites but dominantly tonalites and granodiorites and often containing enclaves of

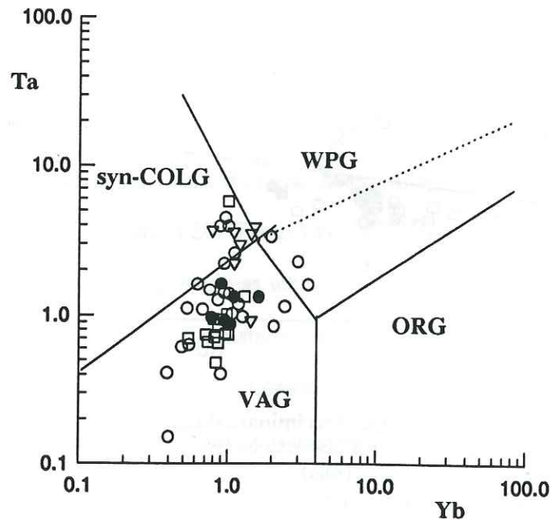

Figure 4.18 Ta-Yb discriminant diagram for the granites of the Valsenestre region, Haut Dauphine. (after Pearce et al., 1984)
(symbols as in Figure 4.10)

basic material., they differ from group I intrusions by having been emplaced after the

collision event. Group IV intrusions form small high-level plutonic suites of alkali to shoshonitic composition which are emplaced well after the end of the collision event. Data from the Valsenestre granites have been plotted onto a diagram of Rb/Zr versus SiO_2 (Figure 4.19) and this shows that indeed the Ramu granite follows quite closely the criteria for Group II granites with SiO_2 being greater than 70 wt% confirming the syn-collision nature of this granite. Some of the Quatre Tours samples as well as one sample RO207 from the Rochail granite also plot into the group II space and whilst for sample RO207 the excess of Rubidium may be explained to its relative proximity to a major fault zone, the Quatre Tours samples are somewhat more difficult to explain, as in only one case RO133 can an excess of Rb due to possible fluxing of late stage fluids be invoked. The other samples have relatively low values of Zirconium which may

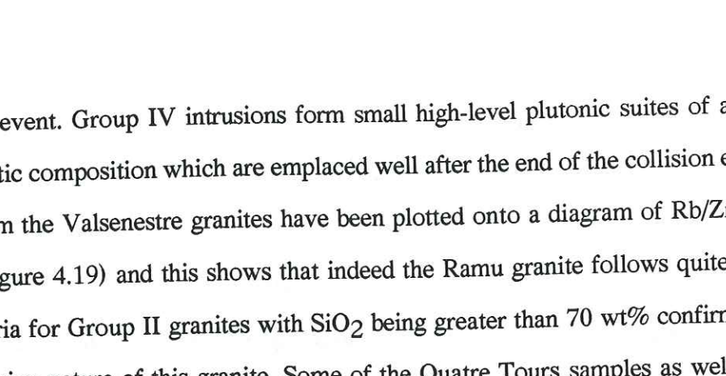

Figure 4.19 Rb/Zr against SiO2 discriminant diagram for the granites of the Valsenestre region, Haut Dauphine. (after Harris et al., 1986)
(symbols as for Figure 4.10)

reflect either a possible interaction between the basic dikes and enclaves or a more fractionated facies of the granite.

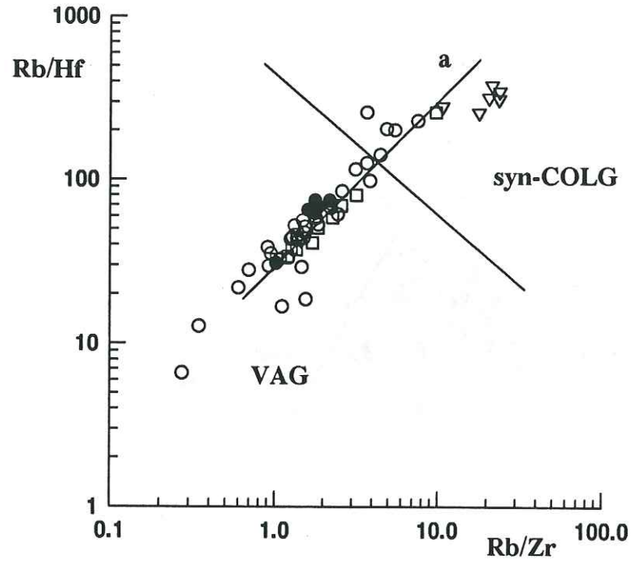

Figure 4.20 Multi-variant diagram of Rb/Zr against Rb/Hf for the granites of the Valsenestre region, Haut Dauphine.
(symbols as in Figure 4.10)

The majority of points from the Quatre Tours/Belle Cote, Rochail and Alfrey granite plot into the region which is ascribed to Group III and Volcanic Arc granites with calc-alkaline signatures. The data have also been plotted on a multi-variant diagram of Rb/Zr against Rb/Hf (Figure 4.20) These two HFS elements are normally depleted in syn-collision crustally derived magmas when compared to magmas derived either from mantel sources or mixed mantel crustal materiel. A regression line drawn through the majority of the data indicates a fractionation relationship, with the exception of the majority of samples from the Ramu granite which show an excess of Hf with respect to Zr.

The discrimination between Group I and Group III granites is not easy, as their geochemistry tends to be very similar, however it has been noted (Pitcher and Berger,1972; Harris et al., 1986; Hamidullah and Bowes, 1987) that post-collision

granites are often associated with small bodies of pyroxene-hornblende-biotite monzodioritic,

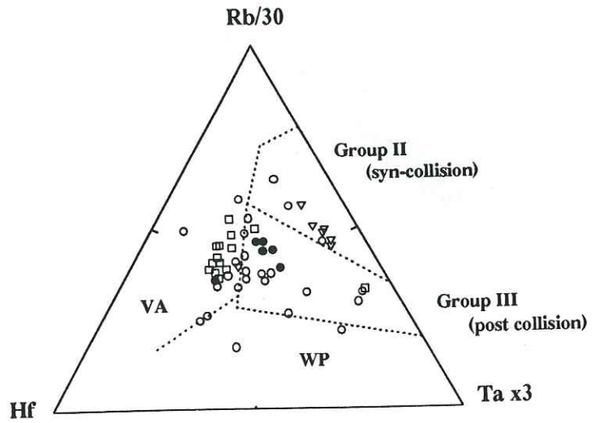

Figure 4.21 Diagram of Rb/30/Hf/Tax3 for the granites of the Valsenestre region, Haute Dauphine.
(symbols as for Figure 4.10)

syenitic and hornblende gabbroic bodies in a close space-time relationship, which is clearly the case for the Quatre Tours/Belle Cote and Rochail granites. Plotting these data on a triangular diagram of Rb/30/Hf/Tax3 (Figure 4.18), this particular diagram is quite useful, as the discrimination between these three elements allows the separation of both Volcanic Arc and Within Plate granites from the collision granites, it can be seen that data for the Ramu granite, with one exception again plot into the Group II region. The majority of the points from the Quatre Tours/Belle Cote and the Alfrey granites either plot into Group III space or close to the dividing line between this and volcanic arc space, whilst the majority of points from the Rochail granite plot further away, well into volcanic arc space.

4.3.3 Rare Earth Elements

Representative normalised plots of the REE for the different granites are shown in Figure 4.22 a -f. The most striking difference can be seen between those for the Ramu granite and the Quatre Tours/Belle Cote and Alfrey granites. The profiles of the

Ramu granite are in general quite flat with small LREE enrichments compared to the other granites, with quite marked negative Europium anomalies and relatively flat to positive HREE slopes. Both sectors of the Quatre Tours/Belle Cote and the Alfrey granite have very similar looking profiles with marked enrichments of the LREE, slight negative Eu anomalies, with one exception for the Alfrey granite from the more evolved central facies, and less steep HREE profiles. The Rochail granite profiles are somewhat different with those from the Cascade sector having moderate enrichments of the LREE very slight negative Eu anomalies and fairly flat HREE, whilst the Refuge des Sources sector has marked enrichment of the LREE and MREE with an abrupt flattening of the HREE. This may indicate the much greater extent of the mixing with the syenitic material of this part of the massif. Six samples from the Ramu granite have very low La/Yb ratios, ranging from 3.4 to 4.36 and total REE from 14.4 to 28.5 ppm. Two samples RO511 and RO512 which are from a much darker facies, containing a number of gneissic panels and enclaves, have much higher values with La/Yb at 12.26 and 15.43 and ΣREE of 71.28 and 92.38 ppm.

The Quatre Tours/Belle Cote granite shows a wide variation in its La/Yb ratios from 2.95 to 50.58, the mean being 22.05, however if the intrusion is split into northern and southern parts then the values obtained give 22.85 for the south and 20.69 for the north. The Rochail massif has a slightly higher value at 26.75, but if the massif is broken up into sectors, then the southern part of the massif has ratios very close to the northern part of the QTBC with a value of 20.67 whilst the northern part shows a slightly elevated value of 27.71. This may be due to the sampling which was made within the proximity of the syenitic intrusions and may be an indication of the greater amount of mixing that has obtained or alternatively it may be an indication of the greater degree of fractionation of this part of the granite, which following Giraud, (1956) and Giorgi, (1982) was emplaced somewhat later than the southern part of the massif.

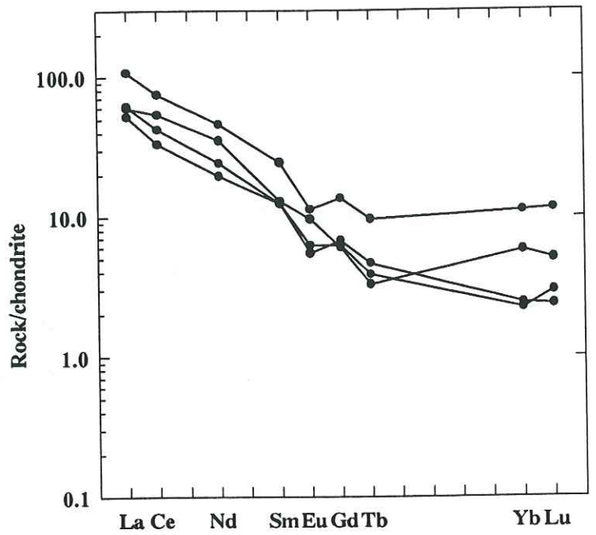

Figure 4.22a Rare earth patterns for the Quatre Tours/ Belle Cote granite. (Southern sector)

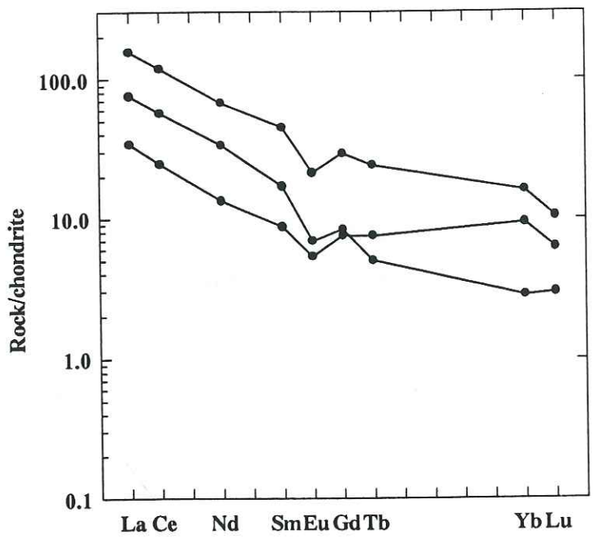

Figure 4.22b Rare earth patterns for the Quatre Tours/ Belle Cote granite. (Northern sector)

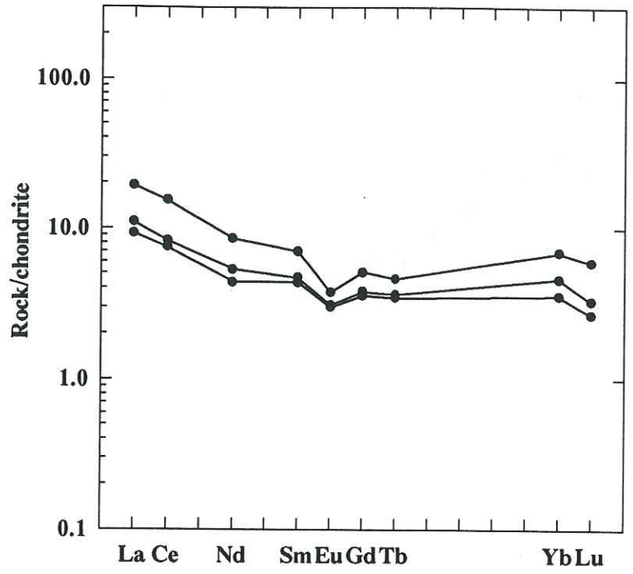

Figure 4.22c Chondrite normalised rare earth patterns for the Ramu granite.
(normalising values from Nakamura, 1974)

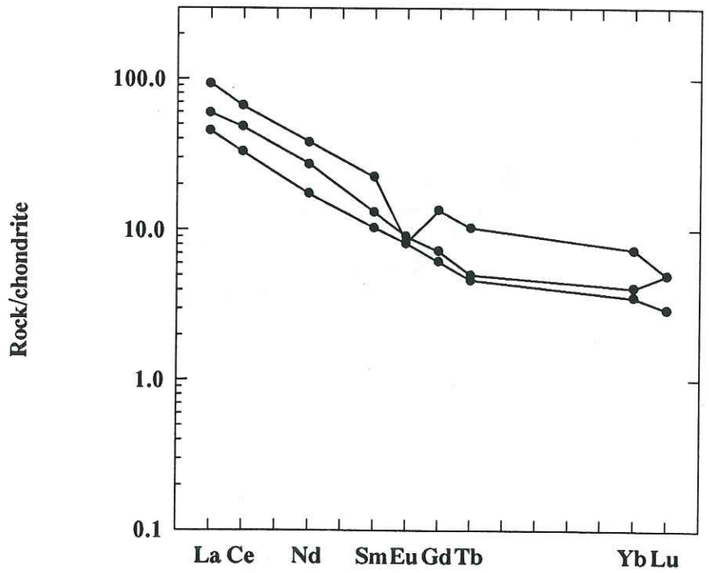

Figure 4.22d Chondrite normalised rare earth patterns for the Alfrey granite.
(normalising values from Nakamura, 1974)

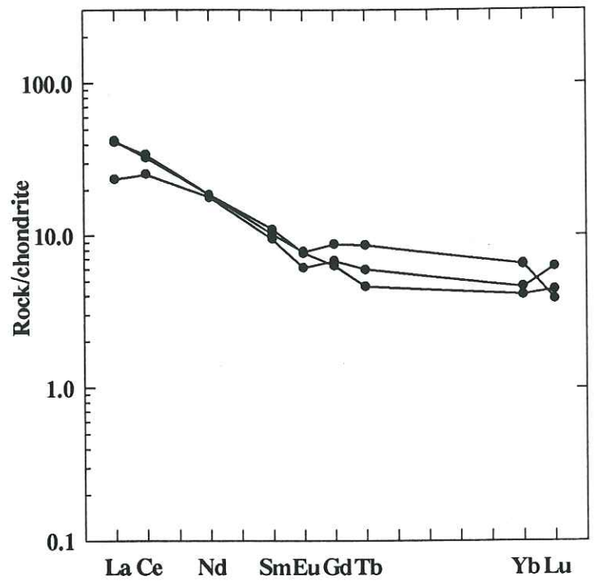

Figure 4.22e Chondrite normalised rare earth patterns for the Rochail granite (Cascade de Lauvitel)
(normalising values from Nakamura, 1974)

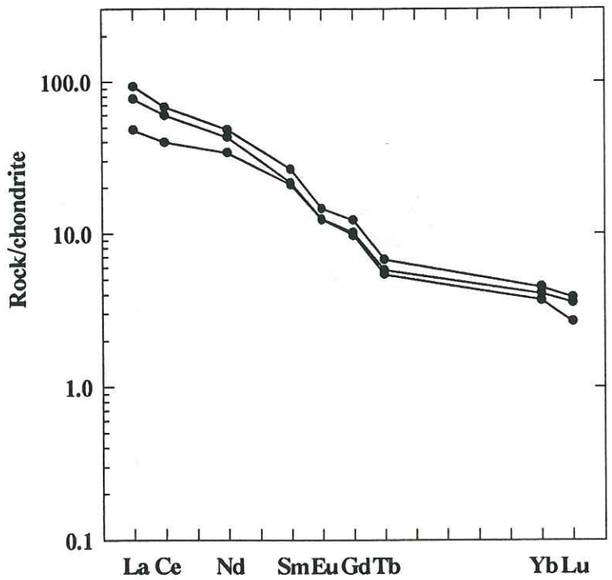

Figure 4.22f Chondrite normalised rare earth patterns for the Rochail granite. (Refuge des Sources)
(normalising values from Nakamura, 1974)

Total REE for the QTBC granite vary from 23.86 to 214.05 ppm with an average of 92.94 ppm, and these values are very similar to those of the Rochail massif which range from 20.46 to 173.49 with an average of 94.76. The Alfrey granite has La/Yb ratios ranging from 14.73 to 41.74 with an average value of 22.76 whilst ΣREE range from 57.61 to 145.85 ppm with an average close to that of the previous two of 93.09 ppm. An interesting point however is the fact that both the La/Yb ratios and the ΣREE increase from the contact facies in towards the central porphyry facies, tending to confirm the hypothesis (op cit. Chapter 3) that this particular granite stock cooled and fractionated from the outside inwards and is almost certainly in its emplacement

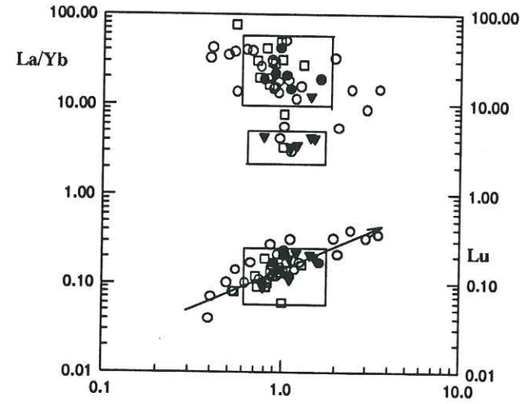

Figure 4.23 Composite diagram of La/Yb and Lu versus Yb for the granites of the Valsenestre region, Haut Dauphine.
(o QTBC granite, ● Alfrey granite, ▼ Ramu granite, □ Rochail granite.)

position. These data have been summarised on a diagram of La/Yb and Lu against Yb as the discriminant factor. For the factor La/Yb this shows an excellent discrimination for the granites of Alfrey and Ramu but both the QTBC and the Rochail granite show a large dispersion. The Factor Lu has a somewhat different behaviour with the Alfrey, Ramu and for the most part, the Rochail granites grouped together in the same space but the QTBC shows a marked linear evolution.

4.3.4 Discussion

Figure 4.24 and Figure 4.25 show the Multi-element variations and chondrite normalised rare earth patterns for some of the gneisses associated with the granites. Sample RO126 being a banded gneiss from below the Quatre Tours granite at its southern extremity, samples RO202, RO205 and RO211 are gneisses from the block, which effectively separates the northern part of the QTBC complex from the southern extremity of the Rochail massif, whilst sample RO510L and RO510P are from just below the Ramu granite.

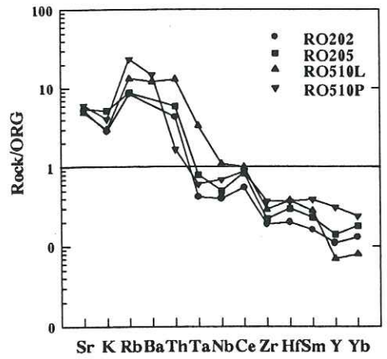

Figure 4.24 Multi-element variation diagram for four gneisses, from the Valsenestre region, Haut Dauphine. (normalised to ORG, values from Harris et al, 1986)

The multi-element diagram for three of the gneisses show some similarities with those patterns for both the QTBC and Rochail granites (Figure 4.14) although the LIL elements show an order of magnitude difference and the negative anomalies of Ta and Nb are more pronounced. Following these data it would not be impossible to generate a magma such as the Rochail granite, but it is evident that some extraneous source of LIL elements would have to be added, even if fusion rates were quite small.

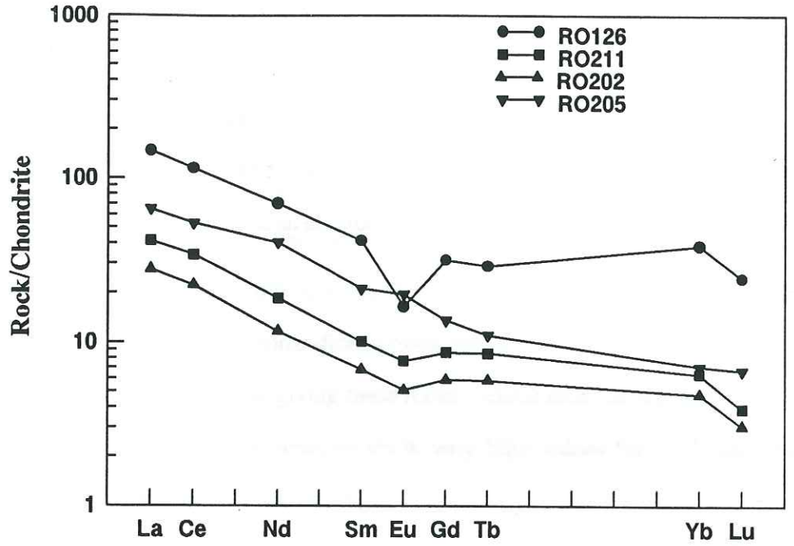

Figure 4.25 Chondrite normalized Rare Earth distribution patterns for gneisses from the Valsenestre region, Haut Dauphine. (normalising values from Nakemura, 1974)

With the exception of sample RO216, which appears to have affinities with arc-type magmas the rare earth patterns are a-typical for acid type gneisses and not to dissimilar to those for the southern part of the Rochail massif. It is therefore possible that these gneisses could in part at least be a source for the Rochail granite

4.3.5 Summary and Conclusions

The geochemistry of the granites demonstrates their essential sub-alkaline affinities but with small differences between the four different massifs. From these it has been possible to differentiate the Ramu granite from the rest and to assign a possible origin as a syn-collision type granite of the Group II of Harris et al., (1986). Of the three other granites the Alfrey and Quatre Tours/Belle Cote granites have affinities with the post-collision granites, but the Rochail granite appears to have greater affinities with granites from a volcanic arc type environment. This however does not accord well

with data from other domains (see chap 6). It is therefore a possibility that a) the Rochail granite was generated from material having a volcanic arc origin and or b) has suffered greater contamination from the associated basic rocks. It should also be added that the major part of the Rochail samples come essentially from within the vicinity of the Basic intrusions. Comparison with geochemical signatures of the associated metamorphic rocks shows some marked similarities between these and essentially the Rochail granite, making these then a possible candidate as a source rock.

4.4 BASIC ROCKS

4.4.1 Major Elements

Analytical data for the different outcrops of syenites and monzodiorites are displayed in Table 4.5 a - d. The SiO_2 content of the basic rocks varies from 45% for the most basic facies of the Belle Cote to almost 64% for the seynites of the Refuge des Sources. Within these limits the Belle Cote syenite ranges from 45% to 62%, the Cascade de Lauvitel from 50% to 62%, the Refuge des Sources syenite from 54% to 64% and the Quatre Tours monzodiorite from 58% to 62%. The ratio of Al_2O_3 to the alkalis is always less than one giving these rocks a metaluminous signature. However it should be noted that several analysis show very high values for LOI, and these are accordingly treated with some caution.

The major oxides have been plotted onto Harker discrimination diagrams (Figure 4.26) and show a number of variations:

1) The scatter of points both in general and within individual units is quite wide. None the less, overall fractionating trends can be seen, notably for AL_2O_3 (positive), Fe_2O_3, TiO_2 and P_2O_5 (negative).

2) Na_2O has a slight positive trend whilst K_2O is flat lying.

3) MgO and CaO look very similar with a group of high values for the samples for the Belle Cote and some from the Cascade de Lauvitel around 50% SiO_2 whilst above this figure the trend is generally slightly negative.

The geochemistry of the basic rocks indicates a possible source within the mantle. To determine if this is so the data of basaltic makeup i.e. those rocks with an SiO_2 content less than 54% have been plotted on a screening diagram of Al_2O_3 against TiO_2 (Figure 4.27). This diagram has the merit not only to distinguish those rocks having a genuine basaltic affinity but also to determine the presence of a cumulate phase as well as indicating a possible contamination or fractionation. The data for the Valsenestre rocks shows that with a few exceptions these rocks fall into the last case i.e. that they

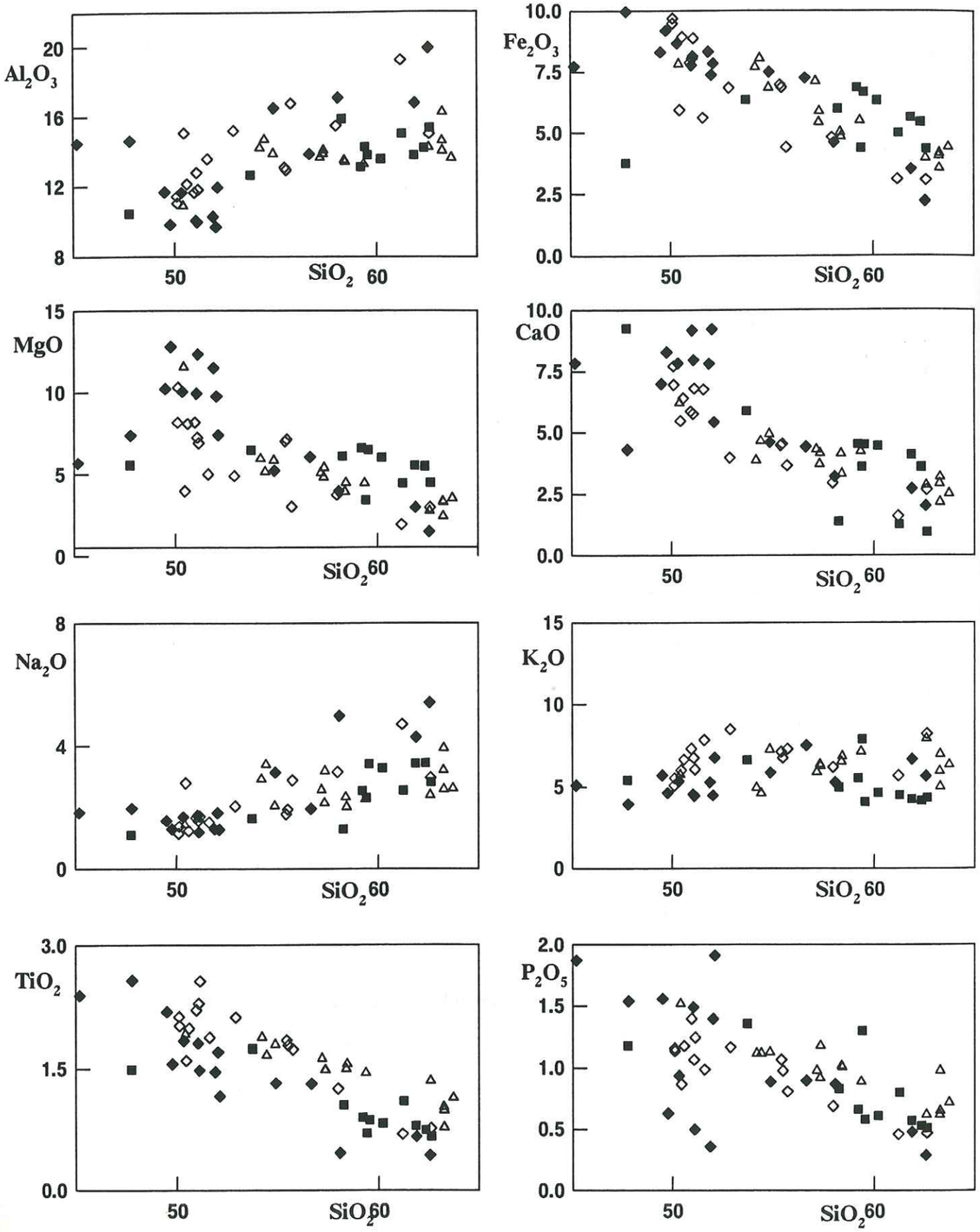

Figure 4.26 Major element discrimination diagrams of SiO_2 versus selected major elements, for the basic and intermediate rocks from the Valsenestre region, Haut Dauphine.

(■ Quatre Tours monzodiorite, ◆ Belle Cote syenite, ◇ Cascade de Lauvitel syenite, △ Refuge des Sources syenite,)

have undergone either a fractionation process or alternatively have assimilated crustal material. the exceptions to this being samples RO213,RO219 and RO313 from the Belle Cote syenites which plot into cumulate space and samples RL104,RL120 and RL131 from the Cascade de Lauvitel, which plot into basalt space.

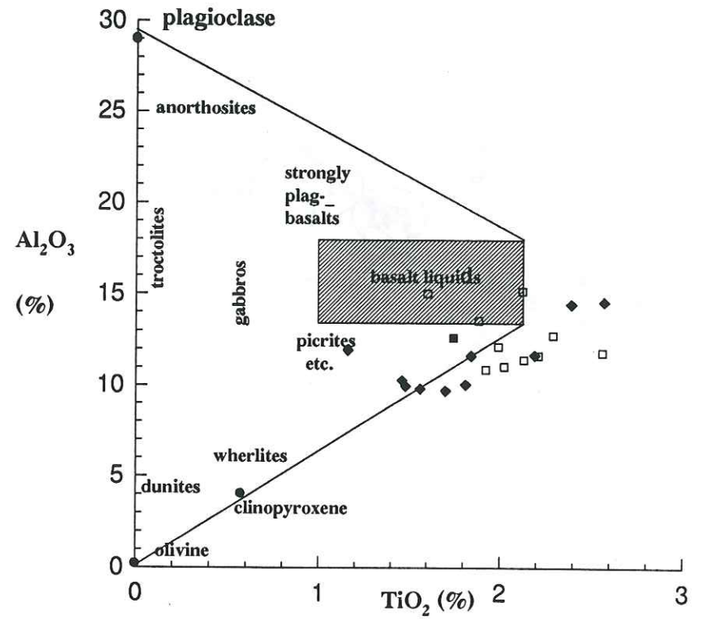

Figure 4.27 Screening diagram of Al_2O_3 against TiO_2 for rocks of mantle origin. Data from the Valsenestre region are for rocks with SiO_2 content less than 54 wt%.
(Symbols as for Figure 4.26)

Eliminating those samples with high LOI values, the rocks of mafic composition for the four outcrops show a range of composition from a high of 12.79% down to 4.91% MgO. On a CaO against MgO plot (Figure 4.28) they show some scatter about a trend which can be interpreted as a control due to amphibole ± clinopyroxene. It is interesting to note that values for amphiboles from the two different types of basic rocks are well separated, with the amphiboles from the monzodiorites of the Quatre Tours falling into the field of amphiboles described for the Mount St Helens 1980

eruption (Macdonald et al., 1986). All the rocks shown on the diagram are relatively enriched in Ni and Cr and can be considered as slightly accumulitic, the high values of P2O5 and the petrographic evidence (Chapter 3 op.cit) confirm the accumulation of apatite. This is further born out by the relative enrichment of Sr, Ce and Y known to concentrate in the apatite phase (Irving,1978; Green, 1981).

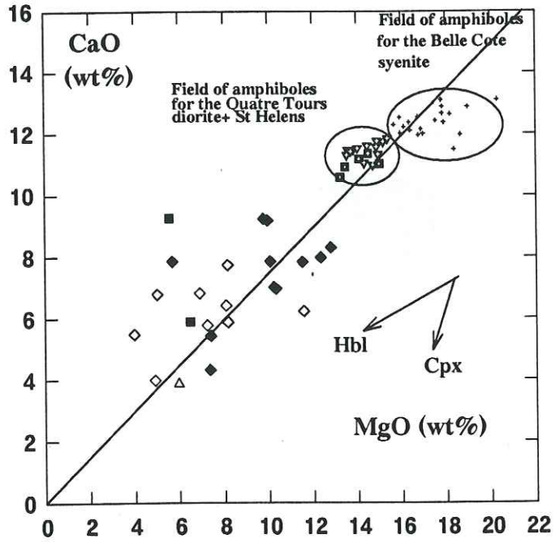

Figure 4.28 Variation diagram of CaO against MgO for basic rocks from the Valsenestre region, Haute Dauphine. Fields for amphiboles from the Belle Cote syenite, the Quatre Tours diorite and the Mt. St. Helens dacites are shown. The trends for hornblende and clinopyroxene are taken from MacDonald et al., 1986.
(symbols as for figure 4.26)

4.4.2 Trace Elements

Selected trace elements have again been plotted against SiO_2 (Figure 4.29). Scandium is the only element to show a real overall trend, having an expected negative correlation with rising silica content.

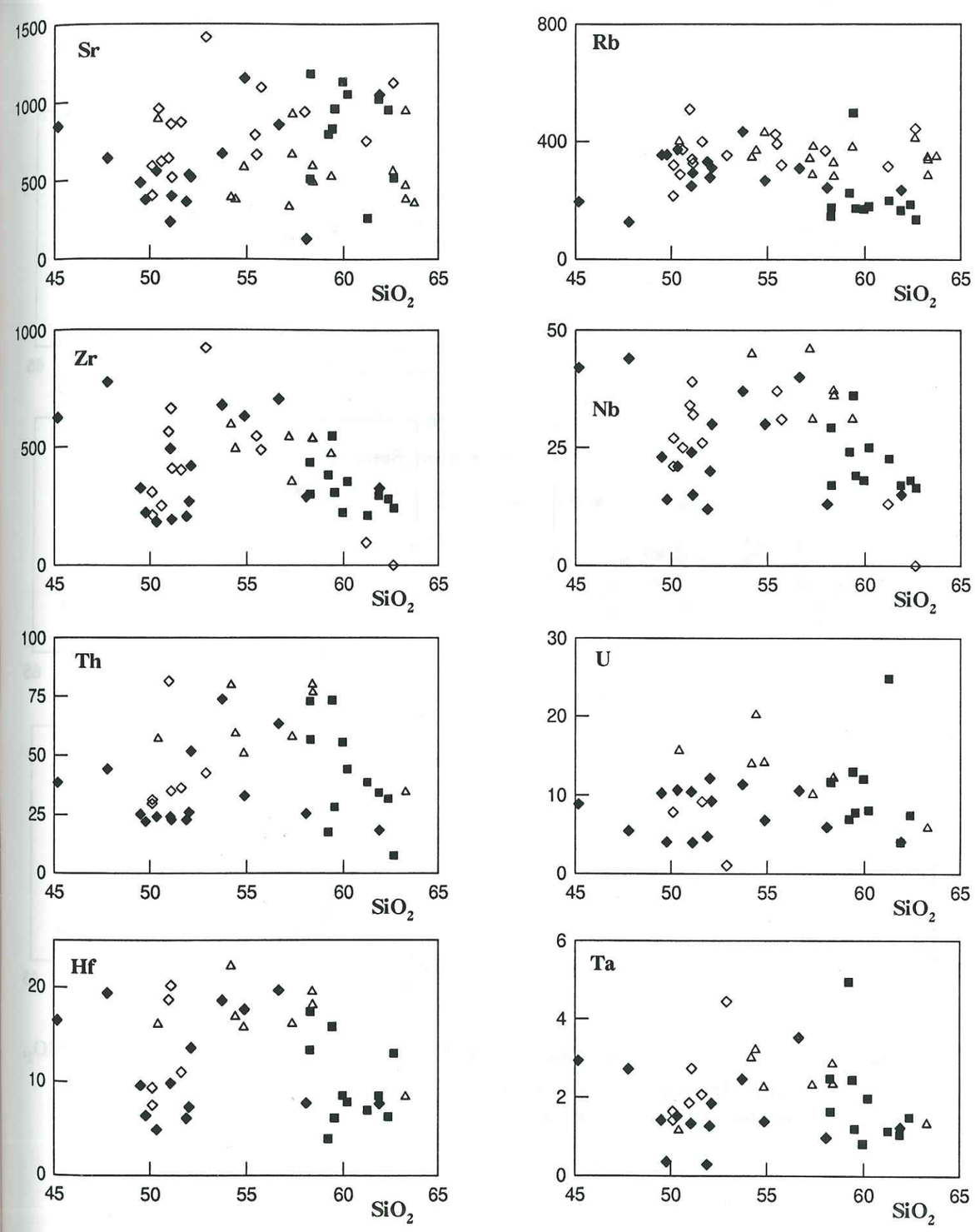

Figure 4.29 Trace element discriminant diagrams of selected trace elements versus SiO_2, for basic to intermediate rocks of the Valsenestre region, Haut Dauphine.
(symbols are the same as for Figure 4.26)

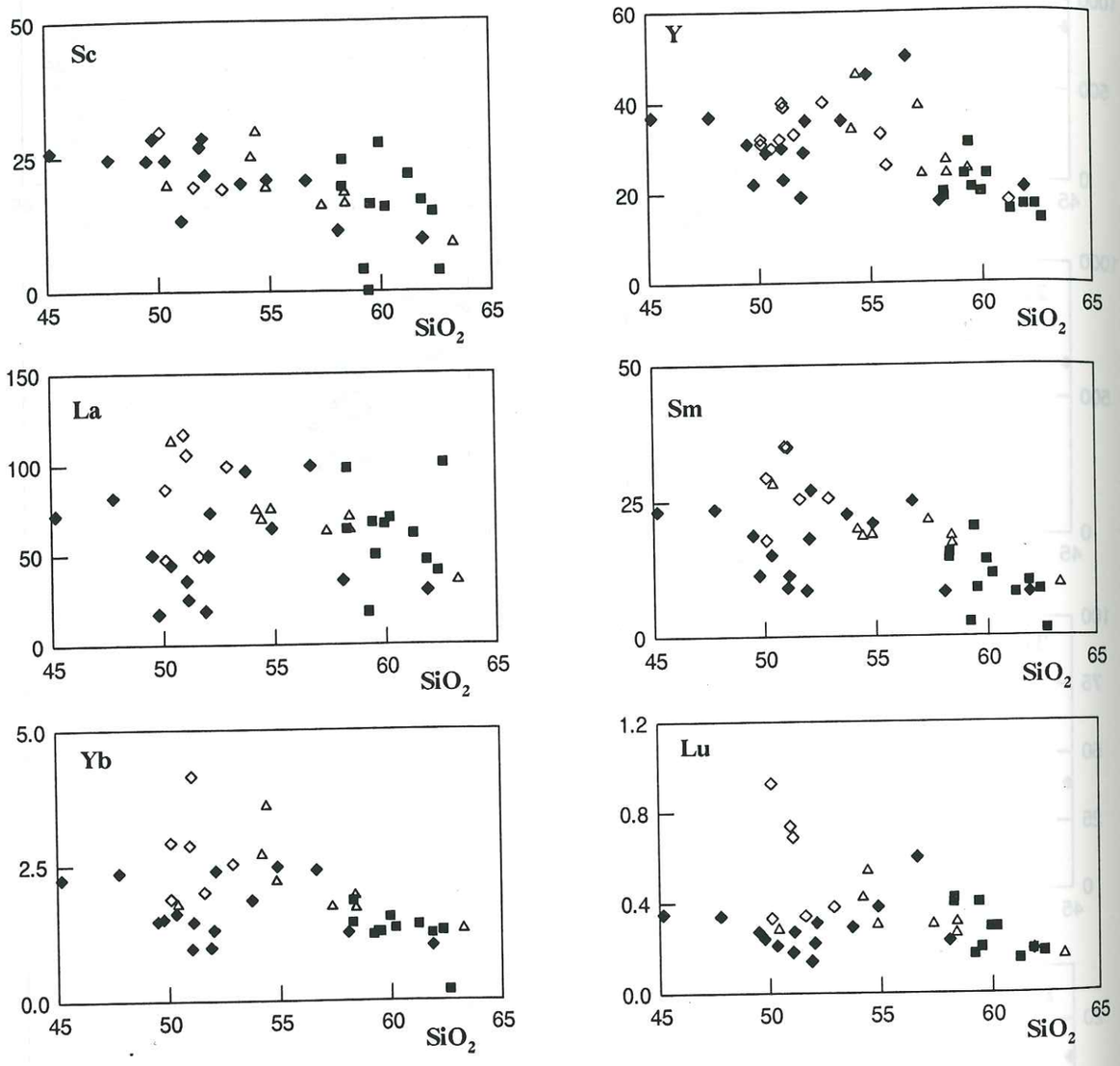

Figure 4.29 (Contd.) Trace element discriminant diagrams of selected trace elements versus SiO_2, for basic to intermediate rocks of the Valsenestre region, Haut Dauphine.
(symbols are the same as for Figure 4.26)

Thorium and possibly Hafnium, show a positive correlation with increasing SiO_2 for the samples from the Cascade de Lauvitel (open diamonds). Zirconium, Niobium and Yttrium, show a complex relationship, with an overall increase in abundance up to 55% SiO_2 wt % and a negative trend from 55% onwards. This may well be a fractionation type trend which would account for Thorium, Hafnium and Zirconium if zircon is a crystallising phase, but may also be due to the incorporation of sphene and apatite. Niobium and Yttrium are more difficult to explain but may well be due to the initial precipitation of pyroxene with the subsequent partition of these elements into later forming amphibole after pyroxene, especially in rocks of more intermediate composition (Lambert et al., 1974; Pearce et al., 1990).

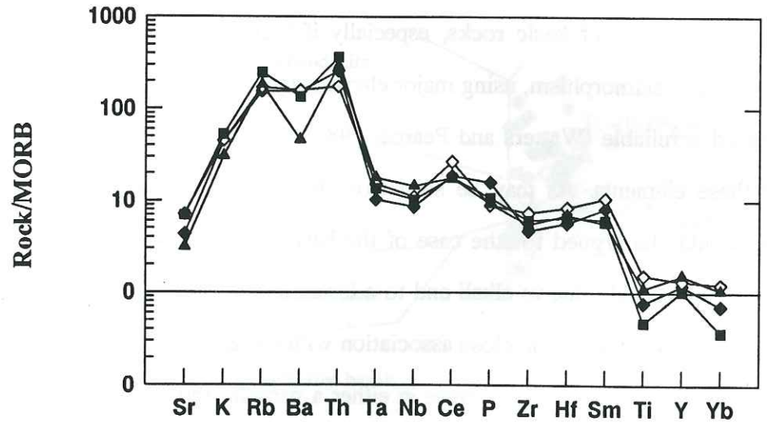

Figure 4.30 Multi-element variation diagram for representative basic rocks from the Valsenestre region, Haut Dauphine.
(MORB values after Pearce, 1983)
(symbols as for Figure 4.26)

Figure 4.30 is a Multi-trace element variation diagram for representative samples from the Valsenestre basic suite. All of the samples show very similar patterns, with the exception of the sample from Les Sources, which shows a negative Ba anomaly with respect to the others. However, all the samples show typical patterns of within plate

type magmatism, with marked enrichment of Rb, Ba and Th, Ta and Nb are enriched as are all the elements to Sm whilst Ti, Y and Yb show no enrichment or even slight depletion with respect to MORB. The patterns are not dissimilar for those of the lamphrophyre suite of the Caledonides (Macdonald et al., 1986) although somewhat more enriched in the LIL and certain of the HFS (High field strength) elements. The abundance's of Ti, Y and the HREE suggest that a mantle source of the depleted type could be responsible, (Macdonald et al., 1985) whilst the enrichment of the LIL elements may represent a subduction zone component, possibly a result of metasomatism of the mantle sources by aqueous fluids, generated by subducted ocean crust. This would suggest a complex, possible multi-source for the origins of these magmas. Crustal contamination may be a contributing factor, but for the moment this needs to be quantified.

Characterisation of suites of basic rocks, especially if they have undergone a post emplacement retro-metamorphism, using major element and derived normative data, is often considered unreliable (Watters and Pearce, 1987) due to the ready mobilisation of many of these elements. As may be seen from the major element versus silica diagrams this could be argued for the case of the basic rocks from the Valsenestre region. This being probably due to alkali and to a lesser extent, silica mobility, during the cooling of these rocks whilst in close association with the granites, into which they have been emplaced whilst these later were in either a partially molten or early post-crystallisation state with the subsequent circulation of large (relative) quantities of magmatic fluids.

Ratios between Y and Nb however have been shown to provide a means of identifying the petrologic character of igneous rock suites (Pearce and Cann, 1973, Pearce, 1984, Harris et al, 1988, Pearce et al, 1987) and the usefulness of co-variations between the immobile element ratios Zr/TiO_2 and Nb/Y in the characterisation of metamorphosed igneous suites has been demonstrated by Floyd and Winchester (1978). In a diagram, Figure 4.31, using these ratios, Zr/TiO_2 serves as a differentiation index whilst Nb/Y is used as an indicator of alkalinity. An effective separation of sub-alkaline and alkaline

trends can be made as well as an indication of the rock type. The Valsenestre data plotted on this diagram show medium to high Nb/Y ratios, characteristic of alkaline basalt and plot into this field for those rocks with fairly low SiO_2 values and into the field for trachy-andesites. It is note worthy that the suites of the Belle Cote and La Cascade plot close to the dividing line with sub-alkaline space, and this may be an indication of an eventual contamination through contact with the associated sub-alkaline granites.

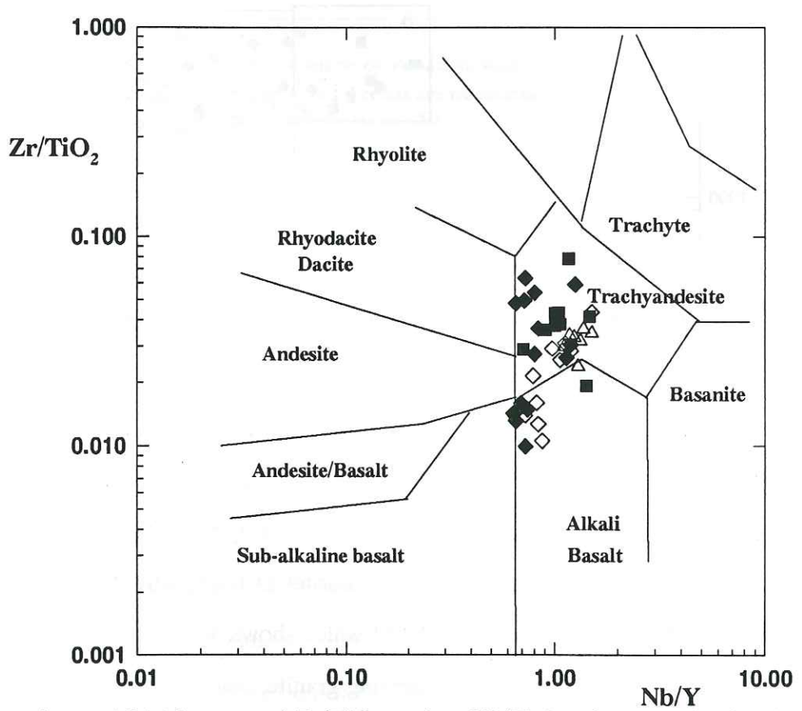

Figure 4.31 Diagram of Zr/TiO_2 against Nb/Y showing the distribution of the diorites and syenites from the Valsenestre region related to the fields for volcanic rocks. The field boundaries are from Winchester and Floyd (1977).
(symbols as for Figure 4.26)

Petrogenetic modelling based on the chemistry of the large ion lithophile elements (LIL) of Ba, Sr, and Rb has been well demonstrated (e.g. Macarthy and Hasty, 1976;

McCarthy and Groves, 1979; Tindle, 1982). These elements are particularly useful as they are found almost exclusively within the major silicate phases and will define fractionation trends followed by these elements. To this end LIL data from the basic rocks have been plotted on co-variation diagrams of Ba versus Rb (Figure4.32a) and Ba versus Sr (Figure 4.32b).

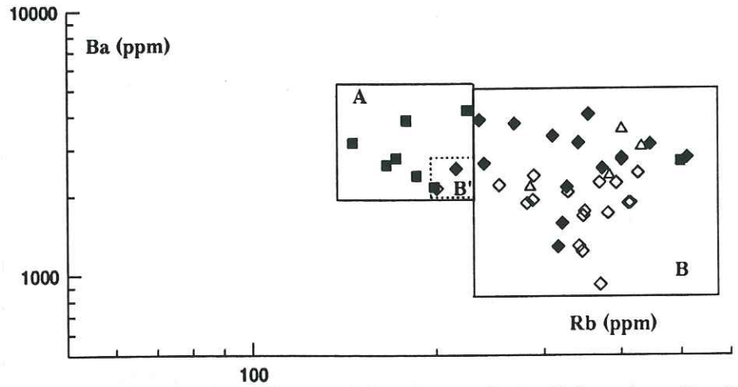

Figure 4.32a Ba versus Rb co-variation diagram for the Valsenestre suite of basic rocks.
(symbols as for Figure 4.26)

In Figure 4.32a Rb shows no particular fractionation type trend but rather a disseminated cloud. However as can be seen the two rock types with one or two exceptions constitute two distinct fields, the monzodiorites of the Quatre Tours, with the exception of one fine grained sample (RO125) which shows an excess of Rb, and may be explained to its proximity to the surrounding granite, being defined as field A whilst the syenites are delimited by field B, with the exception of two samples which make up field B' which falls into field A. Barium Strontium space however defines two distinct trends for the two rock types (Figure 4.32b). The trend for the syenites is slightly steeper than that of the monzodiorites, but never the less, both trends can be explained by the fractionation of variable amounts of biotite and amphibole.

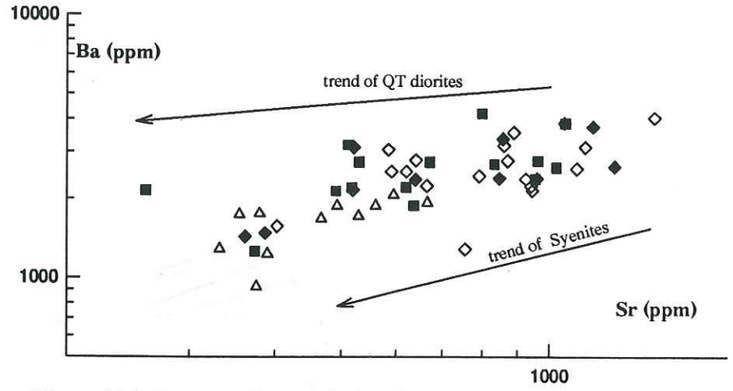

Figure 4.32b Ba versus Sr co-variation diagram for the Valsenestre suite of basic rocks. Trends are calculated least squares regressions.
(symbols as for Figure 4.26)

4.4.3 Rare Earth Elements

The behaviour of the Rare Earth elements are summarised in representative, chondrite normalised (normalising values from Nakamura, 1974), rare earth patterns for the basic rocks which have been plotted and are displayed in Figure 4.33. For comparison REE patterns of some lamprophyric rocks of Hercynian age from the Vorgesen massif, Switzerland (Oberhansli, 1986) have been included. The rare earth element patterns for the basic rocks, in general, have patterns, where the light REE are enriched by factors up to more than 200 times chondritic abundance's whilst the Heavy REE are more flat lying and enriched from 10 to 20 times chondritic values. The patterns in general follow an alkali basaltic trends (Chauvel and Jahn, 1984). Total Rare Earths are high and vary from 82 ppm to 484 ppm for the Quatre Tours monzodiorite with La/Yb ratios which vary from 15.04 to 56.03. For the Belle Cote syenite these values are ΣREE from 128 ppm to 462 ppm and La/Yb ratios of 11.48 to 38.19, for the Cascade

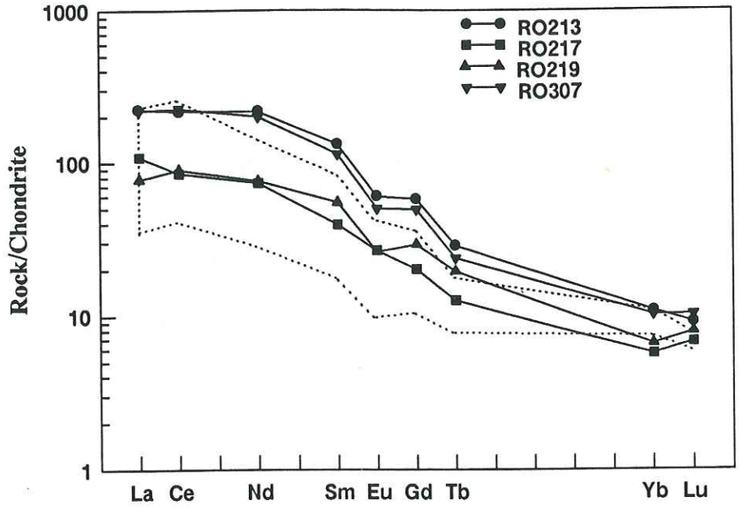

Figure 4.33a Chondrite normalized Rare Earth distribution patterns for the syenites of the Belle Cote, Valsenestre region, Haute Dauphine.
(Outline is for values of lamrophyric rocks from theVogesen massif, Switzerland after Oberhansli, 1986)

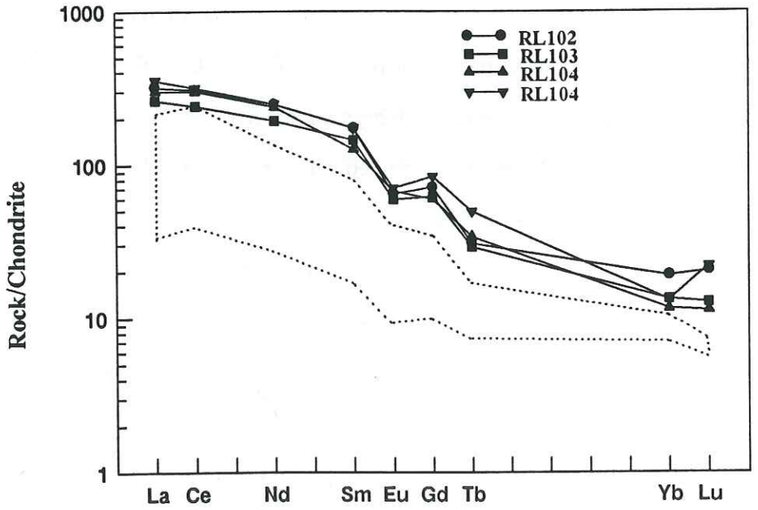

Figure 4.33b Chondrite normalized Rare Earth distribution patterns for the syenites from La Cascade de Lauvitel, Valsenstre region, Haute Dauphine.

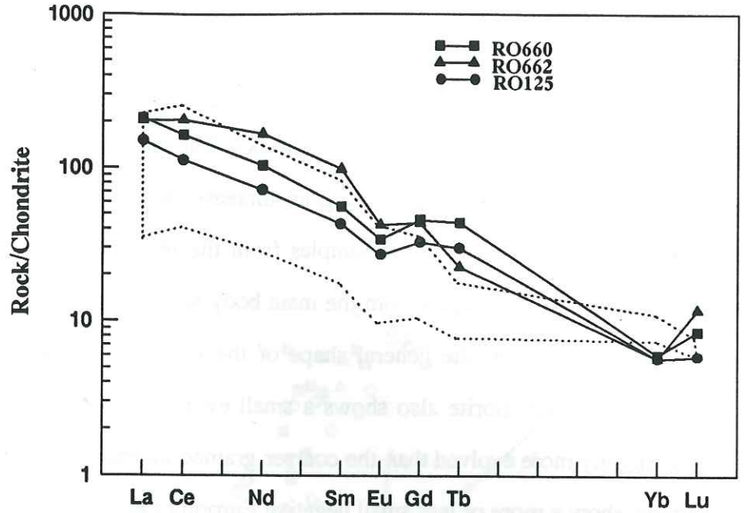

Figure 4.33c Chondrite normalised Rare Earth distribution patterns for the diorites of the Quatre Tours, Valsenestre region, Haute Dauphine.

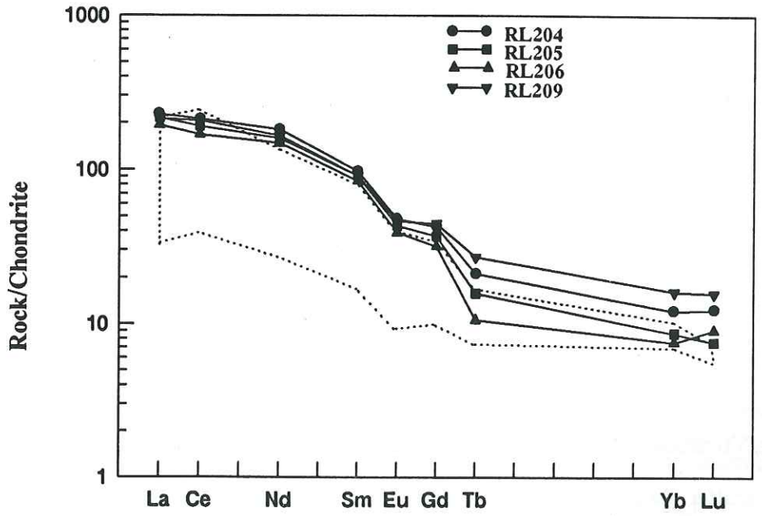

Figure 4.33d Chondrite normalised Rare Earth distribution patterns for the syenites from Le Refuge des Sources, Valsenstre region, Haute Dauphine.

de Lauvitel ΣREE vary from 292 ppm to 594 ppm with La/Yb ratios of 24.75 to 40.71 and for the Refuge des Sources ΣREE vary from 333 ppm to 412 ppm with La/Yb ratios of 19.36 to 37.63. They have both greater overall abundance's and steeper slopes than those of the Vorgesn massif and this is probably due to the elevated amphibole and apatite content associated with these rocks. The patterns from the Belle Cote syenite are the most interesting showing an increase in concentration of both trivalent and divalent REEs between two samples from the internal, amphibole rich facies of the central dyke, and samples from the main body with the development of a negative Eu anomaly, however, the general shape of the patterns remains very similar. The Quatre Tours monzodiorite also shows a small evolution, but the outer fine grained facies is slightly more evolved than the coarser grained internal facies. The majority of the patterns show a more or less small negative Europium anomaly arguing for at least some fractionation of plagioclase feldspar in the evolution of these rocks.

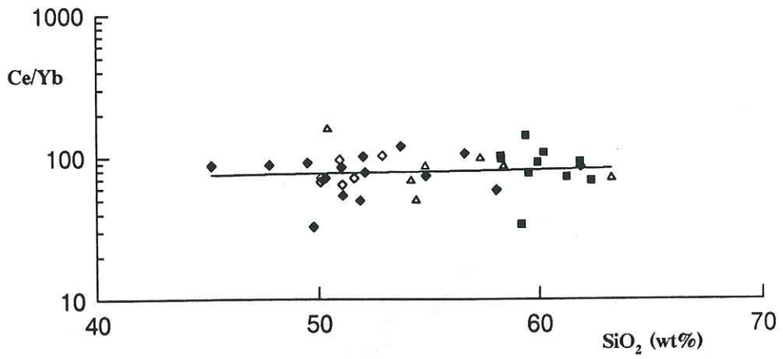

Figure 4.34 Variation of the ratio Ce/Yb with SiO_2 content for the basic rocks from the Valsenestre region, Haut Dauphine.
(Symbols as for Figure 4.24)

A plot of Ce/Yb ratios against SiO_2 as a discriminating factor is shown in Figure 4.34. Whilst some scatter about a regression line is evident, this diagram shows that, there is no overall major fractionating trend nor does there appear to be trends within the individual units, this indicates that the major silicate phases do not appear to affect the

evolution of the REE, and therefore this must be due to the abundant minor phases sphene, apatite and zircon present in these rocks (op cit. Chapter 3).

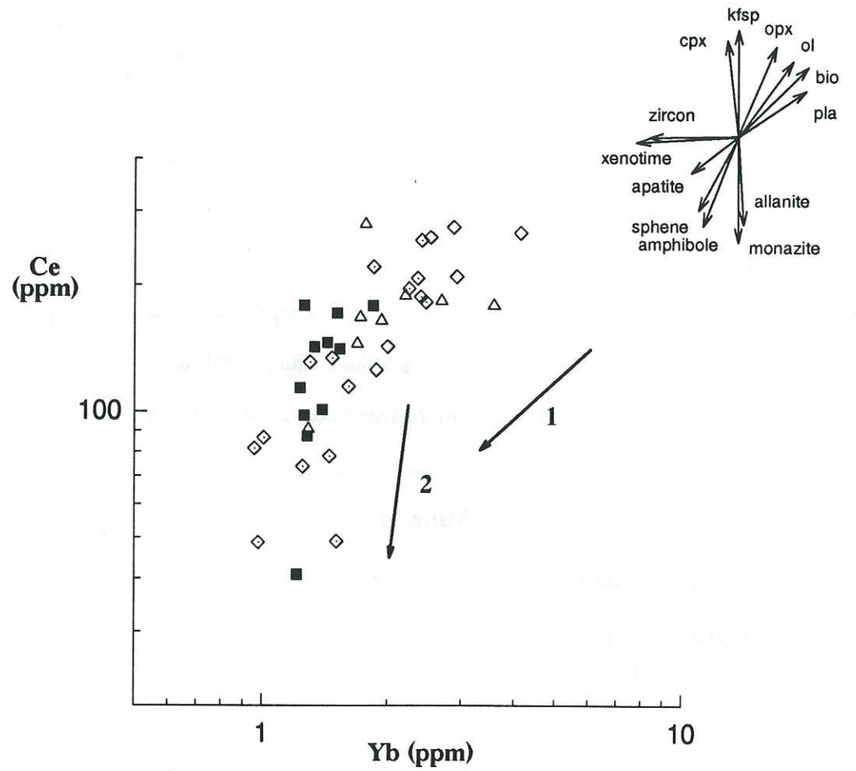

Figure 4.35 Ce-Yb co-variation diagram for the intrusive basic rocks of the Valsenestre region.
Numbers refer to trends, see text.
(symbols are as for Figure 4.26 except Belle Cote ◇)

The analysed samples have been plotted on a co-variation diagram of Ce against Yb Figure 4.35. A set of fractionation vectors have been drawn using the distribution coefficients from Table 4.6. The vectors which are based on single mineral phases, indicate that, with the exception of amphibole, the major phases should cause an increase in Ce and Yb values within the residual melt. From the plotted data two separate trends have been defined from least squares data. Trend 1 refers to the syenites of Belle Cote, La Cascade de Lauvitel and Les Sources whilst Trend 2 refers to the monzodiorites of the Quatre Tours. Both trends could be explained by assuming

some degree of hornblende fractionation, (e.g. Arth and Barker, 1976; Frey et al., 1978). . However for trend 1 this would not hold true as the majority of amphiboles in all the syenites are actinolites, which clearly result from the sub-solidus alteration of pyroxene, and therefore cannot be considered as primary crystallising phases. However these rocks are rich in both sphene and apatite, data from mineral separates of these two minerals are shown in Table 4.7. When these two minerals are taken into consideration then it can be seen that Trend 1 could be almost entirely controlled by apatite fractionation

Trend 2 is much steeper and lies well away from both amphibole or sphene or apatite fractionation trends. Minerals which could produce this trend are monazite and allanite, but these have not been observed in thin sections, or in microprobe studies.

Element	Mineral						
	ol	opx	cpx	pl	bio	amph	kspr
Ba	0.010	0.008	0.079	0.36	6.36	0.04	6.12
Rb	0.098	0.012	0.032	0.048	3.26	0.01	0.34
Sr	0.014	0.013	0.318	2.94	0.12	0.02	3.87
Ce	0.007	0.087	0.33	0.24	0.037	1.2	0.044
Yb	0.014	0.60	1.10	0.077	0.179	6.2	0.012

Element	Mineral					
	apatite	zircon	sphene	allanite	monazite	xenotime
Ce	25	3	80	5000	10000	700
Yb	25	250	60	100	200	10000

Table 4.6 Mineral-liquid distribution coefficients derived from Arth (1976) and Condie (1978) and Tindle (1982). Olivine (ol) values for basic to intermediate compositions; orthopyroxenes (opx), clinopyroxenes (cpx), plagioclase (pl), biotite (bio) and amphibole (amph) are for intermediate compositions. Values for minor phases are of an order of magnitude only.

	La	Ce	Pr	Nd	Sm
RL103a	3970	3320	430	2320	
RL103b	1100	5370	780	5500	
RL105		3410	190	2550	

Table 4.7 Microprobe analysis for selected mineral separates (sphene) from the syenites (RL103, Rl105) of the Cascade de Lauvitel

The explanation for this phenomenon must therefore lay elsewhere, possibly in the removal of REE by volatile phases or metasomatic exchange. In any case it would appear that the origins of the two rock types differ somewhat, although in some respects the possibility of a similar source rock being emplaced at different structural levels cannot be totally excluded. This idea is in fact further born out by the fact that the Quatre Tours monzodioritic outcrops all show a finer grained boundary zone or chilled margin, suggesting that emplacement was into a granite already solid or quasi-solid and that the amount of subsequent metamorphic re-equilibration was limited to alteration of the pyroxenes, whilst the syenites were injected into a medium which was somewhat hotter and the re-equilibrium took place over a much greater time period with a subsequent movement of REE into the minor phases of sphene and apatite. This again is born out by the evident minor fractionation of the REEs in the largest of the Belle Cote intrusions.

4.4.4 Discussion

The geochemistry of both the syenitic and monzodioritic rocks are characterised by the overall abundance of trace elements. In particular the high values of Ni, Cr and Sc indicate a strong participation from mantle derived material, whilst others as Ba, Rb, Sr and the LREE could imply a certain component of crustal material in their make-up. This type of geochemical association is comparable to a number of similar basic ultra-potassic rocks reported by a variety of different workers (Bailey, 1982; Thompson et al., 1984; Venturelli et al., 1984; Rock et al., 1986; Foley et al., 1987; Mitchell et al., 1987). The concentrations for MgO, K_2O and Na_2O of the basic suite associated with the granites of the Valsenestre region are in line with the definition of

Foley et al., (1987) for rocks of the ultra- potassic association i.e. MgO and K_2O > 3% and the ratio K_2O/Na_2O > 2. The relatively weaker concentrations of Ba, Nb, Ti, and La are more reminiscent of Mediterranean type lamprophyres (Foley et al., 1987 which are characteristic of post-collision environments (Thompson et al., 1984; Foley et al., 1987).

Trace element profiles (Thompson et al., 1984; Pearce J.A., 1983) are good discriminant diagrams with which to contrast the geochemical affinities of suites of rocks, and allow in part, the determination of the different components which have influenced the magmas, especially those associated with subduction,(Pearce, 1983) the principal indicators for this type of contamination being negative anomalies of Nb and Ta both of which are seen in these rocks (Figure 4..

It is generally recognised that ultrapotassic basic magmas are generated by partial melting of the upper mantle (Sabatier et al., 1980; Thompson et al., 1984, Venturelli et al., 1984, Montel and Weisbrod, 1986; Rock et al., 1986; Esperanca and Holloway, 1987; Foley et al., 1987). But most authors agree that even with a large element of crustal contamination it is necessary to invoke an enrichment of both incompatible and Large Ion Lithophile elements, either within the source material or during the ascent and crystallisation of these magmas, to explain their chemical make-up.

For the basic syenites and monzodiorites of this part of the Haute Dauphine, it seems unlikely that there has been more than peripheral interaction with the host granites, with the one notable exception in the region of the Refuge des Sources in the Rochail granite massif, (Chap 3 op.cit). Therefore the chemistry of these basic rocks can only have undergone limited modification and are in general unchanged, at least from a point early on in their history. The source or sources of enrichment must therefore be situated within the upper mantle or possibly the lower crust.

Fractional crystallisation of clinopyroxene and garnet from a basaltic magma, generated by the partial fusion of a garnet lherzolite under high pressure conditions (>30 Kb), (Foley et al., 1987), can give a product with abnormal enrichment of certain

incompatible elements whilst the residual liquid has an enhanced K_2O/Na_2O ratio. (Clarke et al., 1983). The high values of these incompatible elements indicates a large degree of fractional crystallisation which would exclude the high values of Cr, Ni and Magnesium which are also characteristic of these rocks.

Crustal contamination of a mantle derived magma, at depth within the lower crust, is in accordance with the 'hybrid' character of these rocks (Rock et al., 1986) as well as the elevated Sr^{87}/Sr^{86} ratio (Venturelli et al., 1984; Banzet, 1987). This does not however explain the high K_2O/Na_2O ratio as well as the low values for Na_2O. Foley et al. (1987) underlined the fact that this sort of hypothesis does not allow an explication of the abundance's of certain elements and consequently the geochemical interpretation remains difficult.

Further to the south of the Valsenestre region, in suites of similar rocks, Banzet (1987) determined the presence of corroded, inherited zircons characteristic of the rare granulite facies found amongst the basic metamorphic rocks of the Haute Dauphine. It could therefore be construed that a certain amount of contamination of these basic magmas has taken place, probably at an early stage in the emplacement process, but this contamination is a relatively minor contribution to the geochemical characteristics of these ultrapotassic basic rocks (Esperanca and Holloway, 1987; Foley et al., 1987). Supporting this hypothesis is the fact that those enclaves showing the greatest enrichment of incompatible elements are not necessarily the most silicic, whereas the effect of early contamination would be to increase the SiO_2 content.

If in fact these magmas originate within the upper mantle then the concentrations of incompatible elements, require a very small percentage of partial melting, less than 1% (Sun and Hanson, 1975; Hanson, 1978; Mitchell et al., 1987) and the difficulty arises in the segregation of the liquid phase. It therefore seems imperative that the partial fusion has taken place within a mantle which has undergone an enrichment process of the incompatible elements, this process has been largely envisaged by other workers.(Bailey, 1982; Peccerillo et al., 1984; Thompson et al., 1984; Venturelli et al.,

1984; Esperanca and Holloway, 1987; Foley et al., 1987; Mitchell et al., 1987; Banzet, 1987).

Metasomatic processes have been described by various workers (Bailey, 1982; Esperanca and Holloway, 1987; Foley et al., 1987; Mitchell et al., 1987), in lherzolite xenoliths from diatremitic volcanic rocks, indicating abnormal compositions, especially the alkali elements, replaced during the changes in mineralogy. The principal minerals concerned in these reactions being phlogopite, amphibole and the carbonate minerals, see Fig,4.36 for stability fields of these minerals for typical mantle pressures and temperatures.

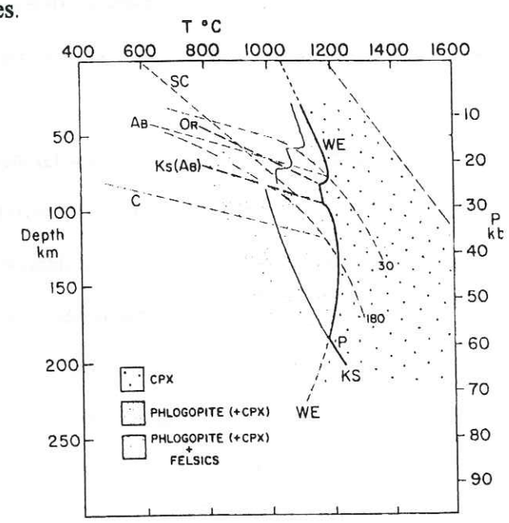

Figure 4.36 *P-T* relationships of mineral stabilities, solidi and geotherms.
Solidi: PSD - peridotite vapour absent solidus, KS- Kimberlite solidus, OE - peridotite solidus with H_2O and CO_2 present, WE - $KAlSiO_4$ - MgO - H_2O - CO_2 system which gives a measure of phlogopite stability in peridotite mantle.
Mineral stabilities: C = coesite, Ks = kalsilite, Ab = albite+ nephiline, (Ab) = albite (jadite + quartz), Or = K- feldspar, SC = solvus crest for alkali feldspar.
(after Bailey, 1987)

Elements are moved through this media by the action of fluids and volatiles whose probable provenance is either from the dehydration of a subducted plate or from out-

gassing from sources deeper within the mantle itself. Possible sites for the passage of these fluids are the deep crustal faults associated with collision zones with associated metasomatic processes and eventual fusion.(Bailey, 1982). The high K_2O/Na_2O ratio is a good indicator as this would be expected from the fusion of a lherzolite mantle rich in phlogopite, however the high values of HREE within the basic syenites and monzodiorites associated with the granites of the Valsenestre region would suggest an absence or at best only a small presence of garnet within the source rocks.

Some workers, basing their arguments on either isotopic data (Allibert et al., 1986) or geochemical (Thompson at al., 1984;Oberhannsli, 1986,Venturelli et al., 1987) suggest that subduction processes are a major element in the genesis of these ultra-potassic basic rocks. Following Thompson et al.,(1984) the origins for these ultrapotassic magmas is from deep within the upper mantle but with major contributions from the melting of subducted slabs, up to several millions of years after continental collision has taken place. This accounts for occasional negative Eu anomalies found in these types of rock, as their bulk compositions are to silica under saturated for feldspar to have precipitated.

These types of rock are considered as being characteristic of post orogenic phases within collision zones (Folley et al., 1987) and are emplaced after the last regional deformation episode (Thompson et al., 1984).

4.5 General Summary and Conclusions

The four granites of the Valsenstre to Lauvitel region show some marked differences in their chemical make up. The Ramu granite is distinguished by trace element and Rare Earth patterns which place it amongst the high level leucocratic granites. This is born out on multi-variant and discriminant diagrams, where following the classification of Harris et al., 1986, it falls into the Group II granites. The other three granites, Alfrey, Quatre Tours and Rochail are geochemically quite similar, but showing minor variations, and on a plot of Rb/30-Tax3-Hf (Figure 4.21) the Rochail granite plots

into volcanic arc space, whilst the Quatre Tours and Alfrey granites are generally within Group III space although the former shows quite wide dispersion. Whilst it is evident that all the granites are the result of crustal melts, there particular source rock types are not easily defined. The Ramu granite could possibly be considered as the result of the fusion of the La Lalley gneisses, over which it has been thrust, more especially as it contains numerous large, half digested panels of this materiel, however the geochemical arguments for this are too sparse to be taken into account.

The Rochail granite as similar looking trace and REE patterns to those of the analysed gneisses, although overall abundances differ by an order of magnitude, however the granite body as a whole shows evidence (Giorgi, 1982; Buffiere, 1960) of emplacement textures, certainly around its northern border, so its source material must be further down in the crust. It is however probable that a certain quantity of the gneisses into which it has been intruded have been assimilated and so play some part at least in the makeup of this granite.

The Quatre Tours granite has only tectonic boundaries and is therefore not "in situ", but its overall geochemistry is not very different from that of both Alfrey and Rochail and therefore the same type of source may be ascribed to this granite.

The Alfrey granite lies in situ and has a geochemistry very similar to both Rochail and Quatre Tours, but does show a small fractionation trend from the outside inwards, as demonstrated by the rare earth patterns.

The Mg* - B classification of Debon et al, (1994) puts the Quatre Tours and Rochail granites well within their syn-collision context and to a lesser extent the Alfrey granite, (Debon, personnel communication) however the boron data tends to disagree with this idea , as the Alfrey granite which has much higher values than other two, would appear to be situated within a syn-collision context, as opposed to a possible post-collision context for Rochail and Quatre Tours.

CHAPTER 5

ISOTOPIC GEOCHEMISTRY AND GEOCHRONOLOGY

5.1 INTRODUCTION

The purpose of this chapter is to review the isotope geochemistry and geochronology, carried out to date on the Rochail granite and the associated syenites from the intrusion at the Cascade de Lauvitel, and the QTBC granite with the associated syenites at the Combe de Belle Cote as well as to present new Rb/Sr data on the later.

Isotope geochemistry and geochronology have been performed on the Rochail granitic complex; in the first instance by Bonhomme and co-workers in 1963, who gave ages for the Rochail granite, from Rb/Sr data (corrected), of 317+/-9 and 327+/-16 Ma, aligned to an initial 87Sr/86Sr ratio of 0.712. Demeulmeester (1982) presented data both for K/Ar and Rb/Sr; from the former he obtained an age of 373 +/- 30 Ma, whilst

Rb/Sr determinations indicated an age of 331 +/- 31 Ma for the Rochail granite, with an initial 87Sr/86Sr ratio of 0.7049.

K/Ar data were presented by Vittoz et al (1987) in which two age determinations were made. The first, on amphiboles and biotites established an age of 324 +/-22 Ma for the cooling of the basement rocks, whilst the second gave an age of 160 +/-5 Ma for a thermal event which affected the K-feldspars of the igneous rocks. New Rb/Sr data for the Quatre Tours/Belle Cote granite and associated syenite dykes are presented. When these data are added to those of Demeulmeester a new age of 317 +/- 11 Ma is obtained with an initial 87Sr/86Sr ratio of 0.706088. This gives a somewhat younger age than previously published results on the Rochail massif and adds to evidence for a post-collision emplacement for the Rochail and Quatre Tours/Belle granites.

5.2 K/Ar ISOTOPE DATA

Demeulemeester (1982) published K/Ar data on amphiboles, from the northern part of the Rochail massif, which gave for this mineral a closing age of 373+/-30 Ma (Figs. 5.1 and 5.2), Whilst this data does not give a definite isochron, it did allow him to draw the conclusion, that the northern sector of the Rochail granite and its surrounding basement had not suffered to any great extent from the Alpine metamorphic event. Further he ascribed the apparent difference between this age and the general closing date of 324 Ma as due to an excess of radiogenic argon, whilst the amphiboles were in a closed system.

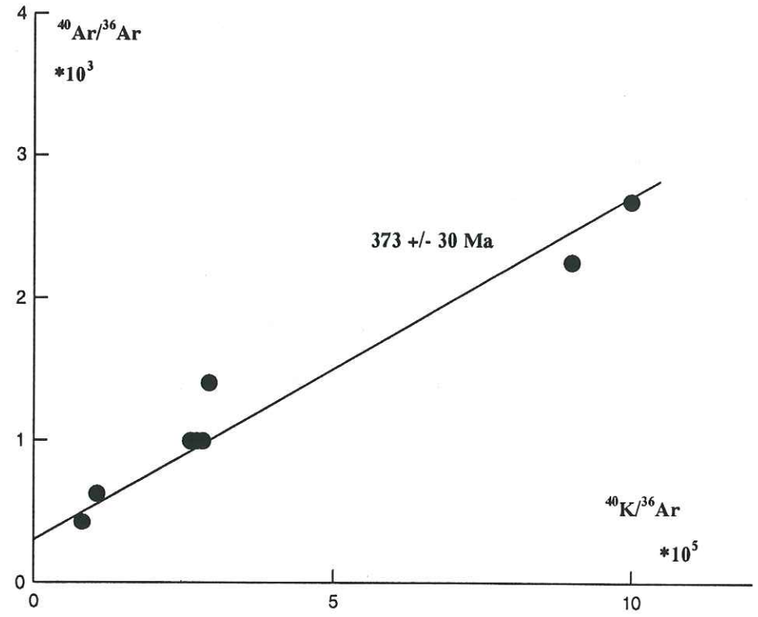

Figure 5.1 40Ar/36Ar versus 40K/36Ar for the northern part of rhe Rochail massif. (from Demeulmeester, 1982)

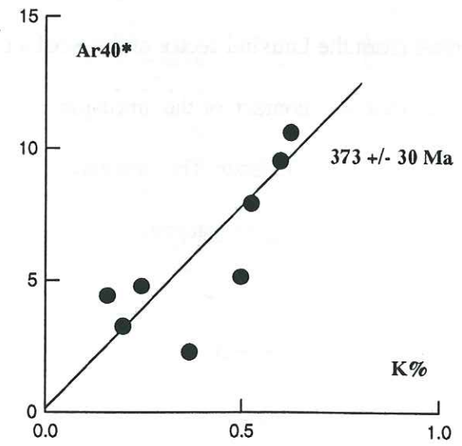

Figure 5.2 Plot of radiogenic Ar versus K% for amphiboles from the Rochail massif. (from Demeulmeester, 1982)

K/Ar dating of mafic minerals from the igneous rocks of the Quatre Tours/Belle Cote and Rochail intrusions (Vittoz et al., 1987), confirms the intrusion of these rocks during Variscan times, whilst the feldspars show evidence of a thermal event during the Jurassic.

The study was made on the following samples:

1) A fine grained equigranular sample of granite (RO309) from the Belle Cote section of the QTBC. This sample is relatively rich in biotite/chlorite.

2) Two syenites from the Belle Cote sector, one from the centre of the largest basic dyke (RO316) containing amphibole as the mafic phase. The second (RO317) from a position closer to the contact with the granite contains both amphibole and biotite as mafic phases.

3) Two biotite rich syenites from the Lauvitel sector of the Rochail granite, one (RL102) from the monzosyenitic contact of the intrusion containing large phenocrysts of perthitic potassium feldspar. The second (RL103) from the centre of the basic intrusion containing megacrystals of poikilitic microcline.

The locations of the samples are shown on Fig. 5.3.

Analyses were performed on separated fractions. For the granite (sample RO309) only K-Feldspar was analysed, as the plagioclase feldspar was too altered and the

Figure 5.3 Sketch map of the Rochail/QTBC sector of the Haute Dauphine, showing the location of samples used in the various studies.
RT= Demeulemeester RL & RO= This chapter
(map after Buffiere, 1963 and Demeulemeester, 1982)

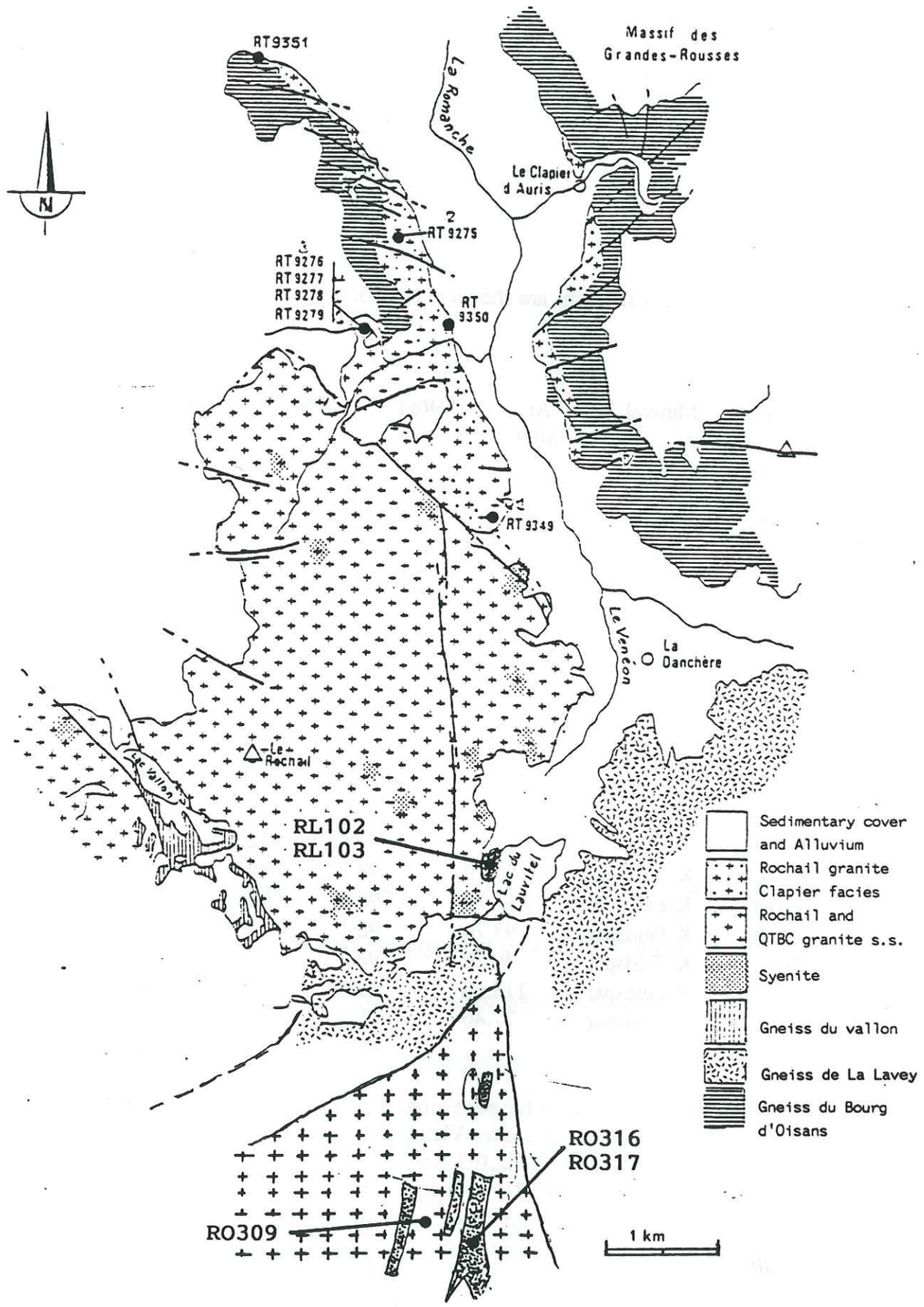

biotite too chloritised for sensible analysis. For the mafic samples, amphibole, biotite and potassium feldspar were analysed for all samples; but plagioclase feldspar could only be measured for sample RL103, from the cascade de Lauvitel, due to the high degree of alteration of this mineral in the other samples.

5.3 RESULTS

The analytical results are shown in table 5.1

Sample	Mineral	^{40}Ar (nl/g)	%Rad.	K%	$^{40}Ar/^{36}Ar$	$^{40}K/^{36}Ar$ ($*10^3$)	Age Ma (± 2 sig)
RL102	Biotite	95.80	98.7	6.91	22908	1092.1	325 ± 6
RL102	Biotite	89.90	96.9	6.74	9984	464.2	314 ± 4
RL103	Biotite	76.80	98.7	6.86	23333	1376.3	267 ± 12
RO316	Biotite	95.40	98.0	7.40	15078	767.9	304 ± 6
RO317	Biotite	99.20	98.2	7.53	16427	819.4	310 ± 6
RL102	Amphibole	5.48	83.4	0.39	1777	71.5	326 ± 8
RL102	Amphibole	5.72	87.6	0.42	2388	102.7	321 ± 11
RL103	Amphibole	4.46	83.3	0.33	1766	71.8	322 ± 20
RO316	Amphibole	4.87	84.4	0.32	1898	71.3	350 ± 18
RO317	Amphibole	5.53	89.9	0.34	2921	107.4	378 ± 18
RL102	K-Feldspar	73.90	97.8	10.83	13293	1274.6	167 ± 2
RL103	K-Feldspar	80.20	98.2	13.25	16437	1784.6	149 ± 4
RL103	K-Feldspar	81.10	98.7	13.25	23086	2493.1	151 ± 4
RL103	K-Feldspar	93.70	98.1	13.25	15627	1451.1	173 ± 6
RO309	K-Feldspar	49.20	98.2	12.46	16554	2756.0	99 ± 2
RO316	K-Feldspar	113.60	98.5	11.51	19551	1305.7	238 ± 4
RO317	K-Feldspar	77.40	98.5	11.90	20287	2055.6	160 ± 6
RL103	Plagioclase	11.67	86.4	1.83	2171	196.5	157 ± 4

Table 5.1 K/Ar data for separated minerals from the QTBC and Rochail intrusives. (After Vittoz et al., 1987)
RL102 and RL103 Rochail
RO309, RO316 and RO317 Quatre Tours/Belle Cote
Errors for ages are given as 2 sigma
Constants are taken from Stieger and Jaguar, (1977).

All the amphiboles gave ages in excess of 320 Ma, with RO316 at 350 Ma and RO317 at 378 Ma. The biotites range from 267 to 325 Ma.

Three of the five potassium feldspars, which were analysed, gave ages of approximately 160 Ma, whilst one (RO316) gives an older age at 238 Ma and the granite RO309 gives a much younger age of 99 Ma. The unique plagioclase analysed gives an age of 157 Ma comparable to that found for the potassium feldspars.

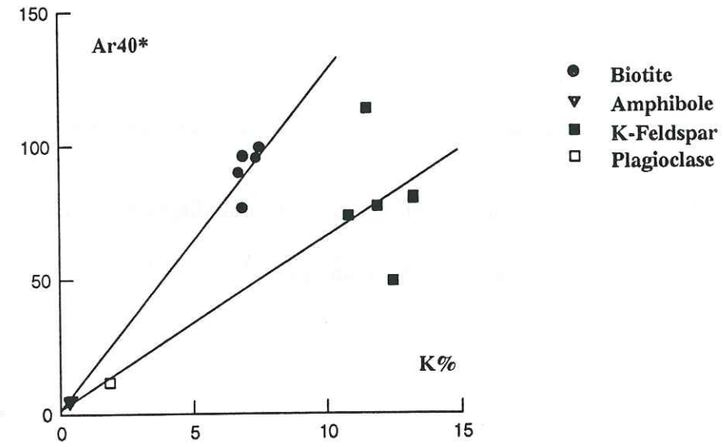

Figure 5.4 ^{40}Ar versus ^{40}K for intrusives from the Quatre Tours/Belle Cote and Rochail massifs.

These results have been plotted on a 40K versus 40Ar diagram (Fig. 5.4). The amphiboles and one biotite give a reasonable alignment on a regression line passing through the origin, indicating that no loss or excess of argon has affected these samples. Data have also been plotted on a 40K/36Ar versus 40Ar/36Ar diagram (Fig. 5.5). The results obtained are almost identical to those for the 40K/40Ar data with the isochrons passing through a point close to 300. This gives an age of 324+/-22

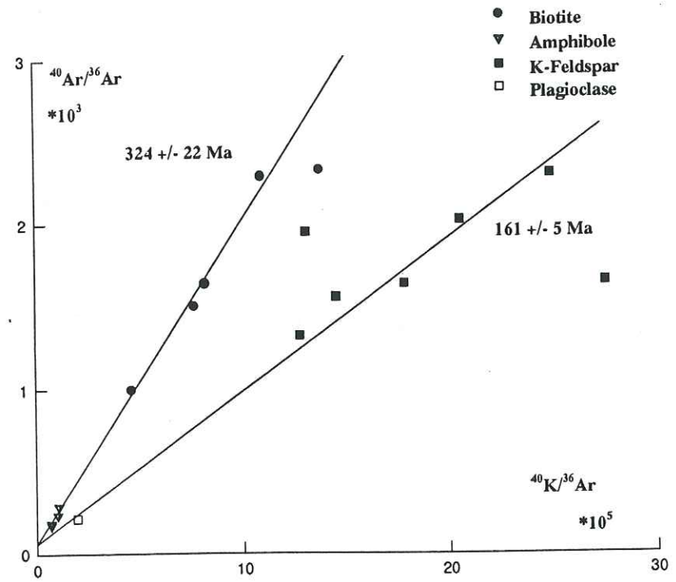

Figure 5.5 $^{40}Ar/^{36}Ar$ versus $^{40}K/^{36}Ar$ for intrusives from the Quatre Tours/Belle Cote and Rochail massifs.

Ma for the biotite/amphibole line. On the same diagram four of the feldspars also give a fairly reasonable alignment and an age of 161+/-5 Ma.

5.4 DISCUSSION

The age obtained of 324 +/- 22 Ma for the amphiboles and one biotite is much less than that found by Demeulemeester, (1982) for the northern part of the Rochail massif, but is comparable with earlier data obtained by Bonhomme et al., (1963) and with amphiboles for the basement gneisses in the Romanche valley, which have a K/Ar age of 324 +/- 12 Ma (Menot et al., 1988).

All three of the above mentioned authors interpreted these data as giving the age of cooling of the tectano-metamorphic block, during the Sudetean phase of the Variscan

orogenisis. This corresponds with the westerly directed, lateral tectonic event, of the internal part of the Belldonne Taillfer massif and with the end of the thrusting episode in the north-east of the internal part of the Belledonne massif (323 Ma), given by Demeulemeester, 1982.

The ages for the amphibole for RO316 and RO317 dated at 350 and 378 Ma respectively can most probably be explained by a local excess of radiogenic argon. Demeulemeester invoked this hypothesis to explain similar enrichments for amphiboles in the Grandes Rousses and Belledonne massifs. In this case a petrological and mineralogical explanation may be invoked . Both samples were taken from the largest of the syenite dykes in the QTBC granite at Belle Cote, which was intruded at a time when the whole (granite and basement) were still hot. This has resulted in an almost total re-equilibrium of the primary mineralogy of these dykes under thermodynamic conditions comparable with amphibolite facies metamorphism (see Chapter 3). It has been demonstrated (Tougarinov, 1965) that pyroxenes often contain an excess of radiogenic argon; and it is therefore conceivable, that during the transformation of primary pyroxene to amphibole, an excess of radiogenic argon remained. This hypothesis is enhanced, if, as is likely, the re-equilibration took place under closed system conditions, as is suggested by the mineralogy and geochemistry.

Results for the biotites give ages ranging from 257 to 314 Ma. These results are very close to those obtained by Demeulmeester (1982) for partly chloritised biotites from the Clapier zone of the Rochail granite e.g. 313 +/- 9 Ma and 290 +/- 8 Ma by Rb/Sr methods, and 293 +/- 13 Ma by K/Ar mass spectroscopy.

This author, in a study of the ages, obtained by analysis of biotites in the massifs of the Belledonne and Haute Dauphine, demonstrated the increase in the Alpine metamorphic event from west to east. This can be related to a progressive loss

of radiogenic argon as a function of the increase in metamorphic grade. From these studies Demeulemeester concluded that the western part of the Haute Dauphine had been relatively shielded from the Alpine metamorphism, this is born out by the large amount of brittle fracture in this region, as well as the values obtained on the biotites. It is interesting to note that, it is not necessarily those biotites that have suffered the most chloritization, which show the largest loss of argon, as one (RL102) lies on the isochron, whilst another (RO317) is dated at 310 Ma, very close to the date of crystallisation, therefore arguing for a late magmatic process for this effect.

Four of the potassium feldspars and the single sample of plagioclase give ages close to 160 Ma, whilst one K-feldspar gives an age at 238 Ma and another 99 Ma.

These results can be interpreted in the same way as the biotites, i.e. in terms of a greater or lesser loss of radiogenic argon but in this case as a function of the intensity of some later thermal event. In this case, the fact that the ages of five of the feldspars are close to 160 Ma is significant. Had the Alpine event been of a sufficient intensity to reset the feldspars, then it should have affected the chloritised biotites. Further, Bonhomme et al (in preparation), have shown that in the Belledonne massif and in the region of La Grave (central zone of the Haute Dauphine) fine clay fractions in the Liassic cover give dates of 40 to 50 Ma for the height of the Alpine metamorphic event, whilst closer to the studied region in the Bourg d'Oisan syncline, the fine clay fractions give an event at 26 Ma (Grand et al., in preparation). The temperature of crystallisation for these fine fragments, (approximately 200°C), is roughly equal to that for the opening of feldspar, and if they had indeed been subjected to these events then they should have shown comparable ages. This is not the case and we must therefore look for another explanation.

The regression lines for the feldspars on the 40K/40Ar and the 40K/36Ar versus 40Ar/36Ar diagram pass close to zero and 300 respectively. This indicates that their crystallisation, re-crystallisation or simply their thermal opening, with respect to radiogenic argon, took place in an environment that had no excess pressure with respect to argon (Bonhomme et al.,1988), and that all the feldspars, with the exception of the syenite RO316, were thermally reset at 160 Ma. Apparently the granite RO309 was either affected by an event at 99 Ma or lost argon by some other method, perhaps a partial opening during the Alpine event.

A general diagenetic event, took place in the sedimentary cover, over practically the whole of south-eastern France at 160-170 Ma (Bonhomme and Millot, 1987), and these workers demonstrated that this event was mainly thermal. Potassium feldspar is a good thermal thermometer, as the opening temperature with respect to argon lies between 170 and 200°C. It is therefore probable, that the age of 160 Ma found for these feldspars, is due to a reaction of the basement rocks to this diagenetic event.

5.5 SUMMARY AND CONCLUSIONS

The K/Ar isotope geochemistry has shown that, the intrusion of the granitic complex and its accompanying suite of basic rocks, of the western Haute Dauphine took place in the late Variscan at approximately 324 Ma. The analysed ages of the amphiboles, indicate the probable cooling history of the tectono-metamorphic block, during the Sudetean phase of the Variscan orogenisis. The chloritization of the biotites corresponds to a late Variscan episode at 314 Ma, whilst the ages obtained on the feldspars, indicates the effect of a diagenetic event within the overlying sedimentary cover during the Dogger.

5.6 Rb/Sr ISOTOPE DATA

Demeulemeester, (1982) presented Rb/Sr whole rock data on the northern part of the Rochail granite intrusion. The locations of the samples are shown on Fig. 5.3. whilst the analytical data he obtained is reproduced in Table 5.2

Sample						
1 (RT9275)	204	391	1.5094	.0302	0.7128	0.0005
2 (RT9276)	322	380	2.4590	.0492	0.7169	0.0005
3 (RT9277)	268	239	3.2574	.0651	0.7195	0.0005
4 (RT9278)	313	149	6.0963	.1219	0.7342	0.0005
5 (RT9279)	268	199	3.9046	.0781	0.7220	0.0005
6 (RT9349)	0.35	3.61	0.2806	.0056	0.7056	0.0005

Table 5.2 Rubidium Strontium Isotope data for the Northern part of the Rochail massif from Demeulemeester, 1982

The resulting isochron is shown in Fig 5.6

This gives a Rb/Sr age of 331 +/- 31 Ma with an 87Sr/86Sr initial ratio of 0.7049. Whilst these data correspond very well with those dates established by Bonhomme and co-workers, 1963, When the data is examined more closely some discrepancies come to light. Demeulmeesters data is in fact a mixture of samples from both basic and granitic rocks. The granites are 1,3, and 6 whilst 2,4 and 5 are rocks of basic to intermediate composition. In chapter three we demonstrated that the two rock types have different affinities, it seems therefore logical to separate the data.

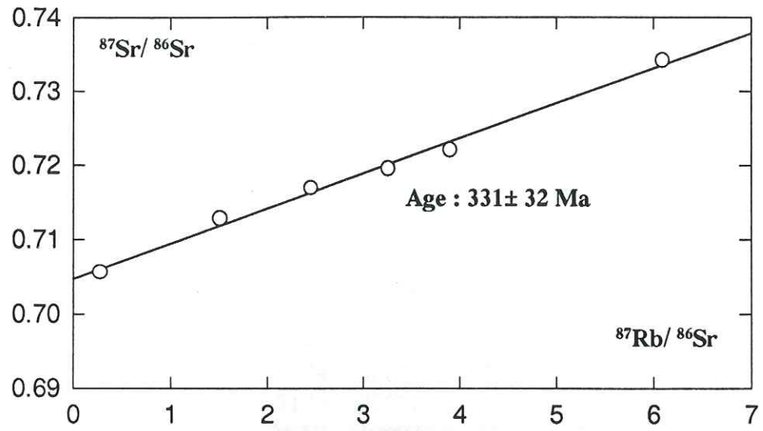

Figure 5.6 Plot of $^{87}Sr/^{86}Sr$ vs $^{87}Rb/^{86}Sr$ for the northern part of the Rochail massif. (Data from Demeulemeester, 1982)

5.7 RESULTS

New Rb/Sr data have been obtained on rocks from the QTBC granite complex. The samples consist of two granites, one syenite from the Belle Cote dykes and one diorite from the outcrop at the Quatres Tours, the localities for which are shown on Fig. 5.7.

1) Sample RO124 is a fine to medium grained granite from the southern end of the QTBC granite. The biotites are partially chloritised but otherwise the sample was quite fresh.

2) Sample RO125 is a fine grained diorite from the outcrop underneath the pinnacles of the Quatres Tours.

3) Sample RO213 is a medium grained syenite from the central dyke of the Belle Cote dyke system. The minerals being quite fresh.

4) Sample RO132 is a fine grained granite from the Vallon de Valsenestre, and is quite rich in biotite, which shows little alteration.

the data from these samples are displayed in Table 5.3

Sample	Rb	Sr	$^{87}Rb/^{86}Sr$	Err	$^{87}Sr/^{86}Sr$	Err
RO124	153	470	0.943	.009	0.710668	+/-12
RO125	467	796	1.699	.017	0.715302	+/-13
RO213	311	521	2.016	.020	0.717230	+/-19
RO132	300	54	5.575	.056	0.730601	+/-15

Table 5.3 New Rb/Sr Isotope data from rocks of the QTBC granite complex

(Analyses made at the Open University)

To make a resonable data set, these new data for rocks of granite composition, have been added to the existing data set. These are displayed in Table 5.4

Sample	Rb	Sr	$^{87}Rb/^{86}Sr$	Err	$^{87}Sr/^{86}Sr$	Err
RO124	153	470	0.943	.009	0.710668	+/-12
RO132	300	54	5.575	.056	0.731241	+/-15
RT9275	204	391	1.5094	.0302	0.7128	0.0005
RT9277	268	239	3.2574	.0651	0.7195	0.0005
RT9349	0.35	3.61	0.2806	.0056	0.7056	0.0005

Table 5.4 Isotope data from The Quatre Tours and Rochail granites used in Figure 5.7

These data are plotted on a new five point isochron which is displayed in Fig 5.7 This gives an age of 317 ± 23 Ma with an initial value of 0.705413. This is some 14 Ma younger than the previous value given by Demeulmeester.

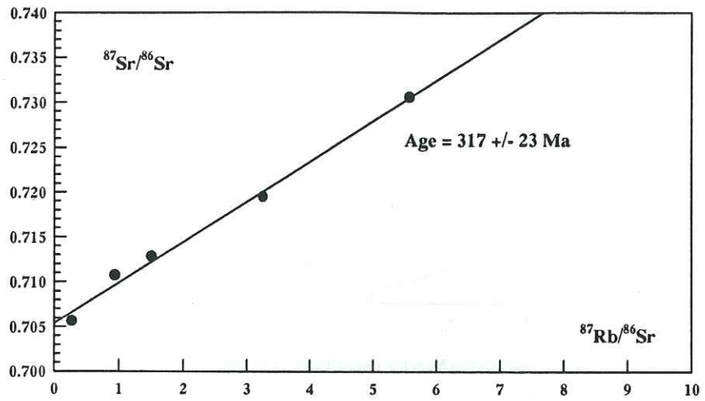

Figure 5.7 Isochron of granites from the Quatre Tours and Rochail.

The data from the basic intrusives are regrouped in Table 5.5 and these data have been plotted up in Fig 5.8.

Sample	Rb	Sr	$^{87}Rb/^{86}Sr$	Err	$^{87}Sr/^{86}Sr$	Err
RO125	467	796	1.6990	.0170	0.715302	+/-13
RO213	311	521	2.0160	.0200	0.717230	+/-19
RT9276	322	380	2.4590	.0492	0.7169	0.0005
RT9278	313	149	6.0963	.1219	0.7342	0.0005
RT9279	268	199	3.9046	.0781	0.7220	0.0005

Table 5.5 Data for basic and intermediate rocks used in diagram 5.8.

These data give a five point errorchron with an age of 304 ± 98 Ma, the large error being due to the amount of scatter. Whilst these new presentations of existing and new measurements should be regarded with some caution , especially those for the basic rocks, due to the amount of scatter in the data, it none the less appears that the Quatre Tours and Rochail granite is somewhat later than has previously been thought, and that the age of the associated basic to intermediate rocks could have been intruded some 10 Ma later. This accords quite well with field observations.

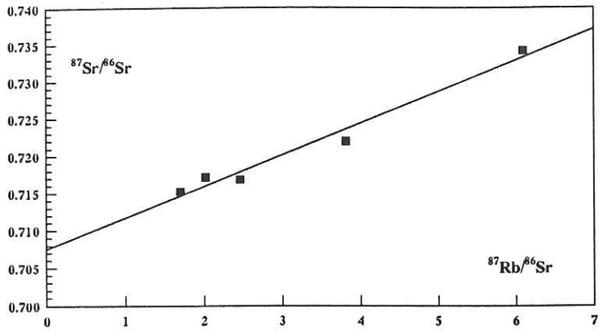

Figure 5.8 Isochron of syenites and diorites from the Rochail and QTBC intrusions.

To test the possibility that the isochrons for these data are due to the mixing of magmas the data have been plotted on a diagram of $^{87}Sr/^{86}Sr$ versus Sr, (Figure 5.9)

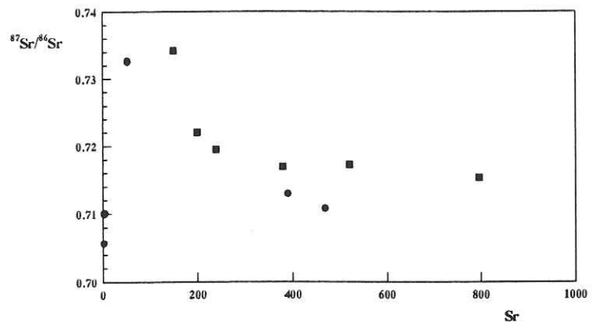

Figure 5.9 Plot of 87Sr/86Sr versus Sr for the intrusive rocks from the Valsenestre region Haut Dauphine. (Data from Demeulmeester, 1986 and new data)
(● granite ■ syenites + diorites)

this diagram has been shown to indicate magma mixing with the data from hybrid rocks, following a hyperole. (Bell et al., 1968,1969; Faure and Powell, 1972; Volmer, 1976, Du'Thou, 1982).

This is almost the case here, however to correlate this the same data on a diagram of $^{87}Sr/^{86}Sr$ versus $1/^{86}Sr$ (Bernard-Griffiths, 1975; Duthou, 1982) should if there is mixing,

describe a straight line, with the equation $R_m = f(1/Cm)$. From Figure 5.10 it can been seen that no straight line regression can be drawn, but on the contrary there is a dispersion of points for both types of rock, and it may therefore be concluded that there has been no effect of mixing in this case.

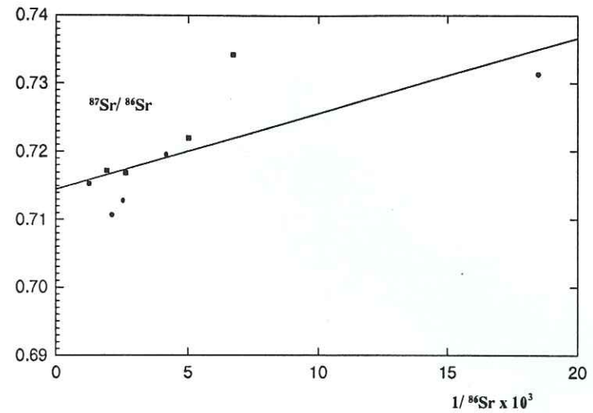

Figure 5.10 Plot of $^{87}Sr/^{86}Sr$ versus $1/^{86}Sr$ for the intrusive rocks of the Valsenestre region, Haut Dauphine. (Data source as for Figure 5.9.)
(symbols as for Figure 5.9)

5.8 SUMMARY AND CONCLUSIONS

The isotope geochemistry performed to date on the granitoids of the western part of the Haute Dauphine, demonstrate that the intrusion of these, together with their accompanying suites of basic rocks took place in mid to late Variscan times. K/Ar data for the QTBC basic suite gives 324 Ma whilst Demeulmeester, (1983) found 373 Ma for the Rochail granite. Rb/Sr data for the Rochail and Quatre Tours intrusives have been revised and together with some new data, now gives an age of 317 ± 23 Ma somewhat later than the age of circa 330 Ma found on what was mixed data by Demeulmeester, for the northern part of the Rochail granite. If this new age is correct then it puts the Rochail

and Quatre Tours granites within a period which is perhaps neither syn-collision, circa 330 Ma or post collision 300 Ma (Debon et al 1994) but somewhere between the two, this may be an explanation of its mixed geochemistry. The later errorchron for the basic to intermediate intrusions could indicate a later date for the intrusion of the basic rocks in the form of dykes.

CHAPTER 6

GEOCHEMISTRY OF THE IGNEOUS ROCKS OF THE HAUT DAUPHINE

6.1 INTRODUCTION

The region of the Haut Dauphine has been intruded by a number of granitic plutons (Figure 6.1) of various shapes and sizes. In general, the granitic material makes up about one half of the exposed surface of the region. A number of workers have undertaken studies of these intrusions (notably Buffiere, 1964; Ozocak,1965; Barbieri, 1970; Pecher, 1970,1971; LeFort et Pecher, 1971; Bartoli, 1973; LeFort, 1973; Barfety et al., 1984; Costerella, 1986; de Boisset, 1986) and these have elucidated the main structural, petrological and mineralogical characteristics, as well as providing a limited amount of geochemical information. These geochemical data have given rise to a number of interpretations and classifications of the granitic intrusions, these have been summed up by Stussi et al., 1983, in which, in conclusion these authors classified the granites using major element analysis. These data are presented in Table 6.1.

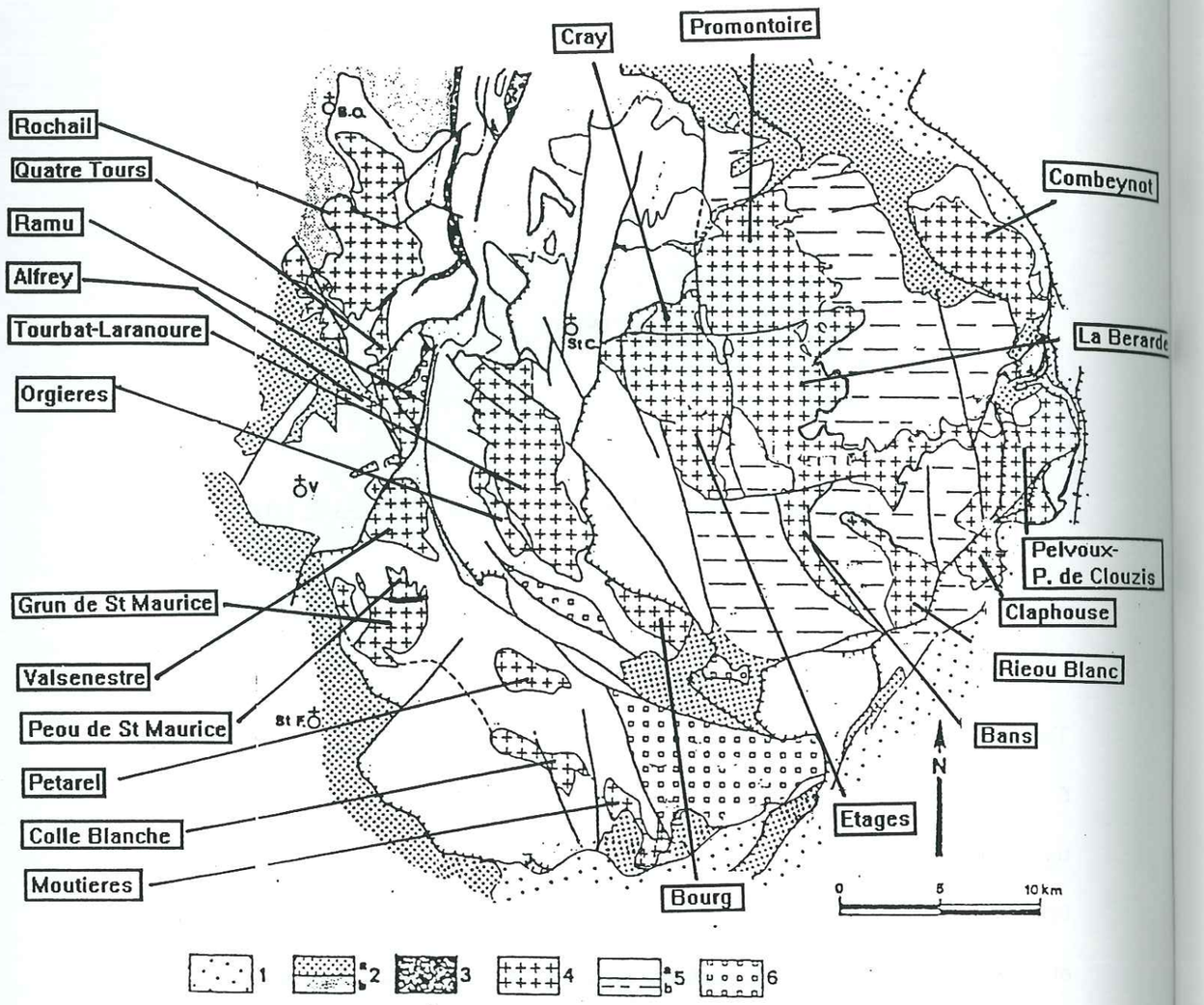

Figure 6.1 Structural map indicating the emplacement of the granites of the Haut Daupnine province, western French Alps.
(Key: 1. Eocene deposits 2. Mesozoic cover 3. Carboniferous deposits 4. Variscan granites 5. a) Migmatite gneiss b) Gneiss 6. Orthogneiss

		SiO2	Al2O3	Fe2O3	MnO	MgO	CaO	Na2O	K2O	TiO2	P2O5	LOI
Subalkaline granites												
Combeynot	n=4	74.41	13.04	1.83	0.04	0.60	0.55	2.92	5.35	0.20	-	1.08
		1.41	0.66	0.51	0.02	0.23	0.36	0.79	0.64	0.11		0.10
La Bérarde-Promontoire	n=46	75.24	12.85	1.41	0.05	0.40	0.43	3.94	4.49	0.12	-	0.74
		1.54	0.71	0.48	0.01	0.07	0.08	0.07	0.09	0.03	-	0.08
Etages	n=43	74.35	13.08	1.57	0.04	0.46	0.50	3.39	4.93	0.15	-	0.87
		0.50	0.19	0.21	0.01	0.07	0.24	0.36	0.13	0.04		0.10
Cray	R4G4	75.36	13.03	0.94	0.03	0.42	0.24	3.31	5.34	0.06	-	0.83
Graou	R2G6	70.10	13.73	2.38	0.05	1.15	1.34	3.48	4.39	0.31	-	1.40
Giobernay	SD32	73.30	13.10	1.63	0.05	0.49	0.39	3.67	5.15	0.22	-	0.90
Bans	B420	68.10	15.30	3.55	0.10	1.60	1.75	3.50	4.65	0.35	-	1.10
Pelvoux-Pic de Clouzis	n=10	73.16	13.26	2.01	0.05	0.65	0.55	3.69	4.44	0.31	-	1.21
		1.10	0.79	0.21	0.03	0.36	0.41	0.22	0.71	0.15		0.17
Rochail fin	n=12	72.35	14.70	1.37	0.02	0.60	0.42	3.96	4.79	0.20	-	-
		1.23	0.48	0.38	-	0.32	0.34	0.50	0.51	0.10		
Rochail gros.	n=15	65.67	15.42	3.11	0.06	2.09	1.80	3.61	5.60	0.48	-	-
		2.88	1.27	1.01	0.02	0.84	0.84	0.69	1.22	0.31		
Ramu	P6K1	75.60	13.82	0.85	0.04	0.21	0.50	3.83	4.25	0.17	-	1.03
Quatre Tours	n=6	72.06	14.85	1.41	-	0.80	0.33	4.35	4.18	-	-	-
		1.26	0.56	0.32		0.24	0.25	0.36	0.41			
Pointe Marcelline	P7T4	73.48	14.19	1.19	0.05	0.39	0.44	3.68	4.04	0.03	-	1.35
Combe Guyon	312882	72.39	13.33	2.72	0.06	1.45	1.37	3.06	4.21	0.40	-	-
Valsenestre	n=4	66.80	15.54	3.91	0.06	1.19	1.75	3.50	4.09	0.60	-	-
		0.96	0.61	0.35	0.01	0.11	0.33	0.23	0.43	0.07		
Chapelet	MX13	66.85	15.85	5.29	0.09	2.07	0.85	2.68	4.08	0.77	-	1.82
Entraygues	APE1	72.21	13.60	2.92	0.04	0.68	0.38	3.57	3.21	0.35	-	1.64
Péou St Maurice	n=11	72.13	14.89	1.44	0.04	0.52	0.80	3.96	4.53	0.23	-	-
		0.92	0.51	0.28	0.01	0.26	0.40	0.40	0.60	0.07		
Turbat-Lauranoure		73.30	13.42	1.27	0.04	0.52	1.01	3.26	4.89	0.23	-	0.89
	n=34	0.94	.035	0.26	0.01	0.12	0.29	0.08	0.15	0.06		0.15
Orgières	n=6	62.76	16.55	5.00	0.09	2.22	2.48	3.56	3.88	0.65	-	2.04
		2.79	0.99	0.76	0.01	0.51	1.29	0.74	0.89	0.11		0.48
Bourg	n=6	66.57	15.13	3.64	0.08	1.47	2.45	3.24	4.42	0.50	-	2.25
		1.44	0.48	0.38	0.01	0.19	0.32	0.18	0.27	0.09		0.31
Moutières Colle-Blanche	PV31	60.90	14.50	6.27	0.10	4.54	3.58	2.76	3.92	0.68	-	3.27
Alumino-potassic granites												
Grun de St Maurice	P3U1	71.58	15.29	1.35	0.03	0.40	0.58	4.03	4.75	0.18	-	1.20
Pétarel		75.00	12.30	2.37	0.07	0.59	0.34	3.40	4.34	0.15	-	1.32
Rieou Blanc	n=4	69.69	14.66	2.62	0.03	1.34	0.82	3.81	4.38	0.33	-	1.65
		1.92	0.47	0.48	0.03	0.72	0.29	0.25	0.23	0.10		0.35
Claphouse	n=5	70.70	14.31	2.85	0.03	1.34	0.47	3.48	4.28	0.52	-	1.70
		0.79	0.50	0.27	0.03	0.34	0.42	0.08	0.16	0.14		0.13

6.2 PRINCIPAL CHARACTERISTICS

In general, the Variscan granitoids of the region show high levels of K_2O (see Table 6.1). Using mineralogical and geochemical criteria Debon and LeFort (1983) concluded that two distinct magmatic trends could be distinguished (Figure 6.2). The first, of which the granites of the Berarde-Promontoire, Rieou Blanc, Quatre Tours, Grun de St Maurice, Peou de St Maurice and Rochail (see Figure 6.1), are amongst the most typical, make up an "alumino-sodique" trend, generally characterized by the presence of muscovite and the albite-rich nature of the plagioclase feldspar. The second trend, termed "monzonitic" is distinguished by the rarity of muscovite, the presence of oligoclase and the appearance of hornblende in the most melanocratic members of the series. The principal granites of this series are those of Col Blanche, Moutieres, Bourg, Turbat-Laurenore, Etages and the Pic du Valsenestre.

It is, none the less, somewhat difficult to separate the most leucocratic members of the two series; Barfetey et al., (1984), used the abundance of Na2O as a distinguishing criterion, with Na O being less than 3.65 wt% in the monzonitic trend and more than this figure for the alumino-sodic trend (Figure 6.3).

In general,using these criteria, the majority of the granitic intrusions can be classified into these trends with some notable exceptions, these being a)the Combeynot granite, with a very high potassium content and b) the Claphouse granite which lies in between the two defined trends. However this type of classification should be treated with great caution as the mobility of Na_2O in situations of low grade metamorphism and hot fluid circulation is very high.

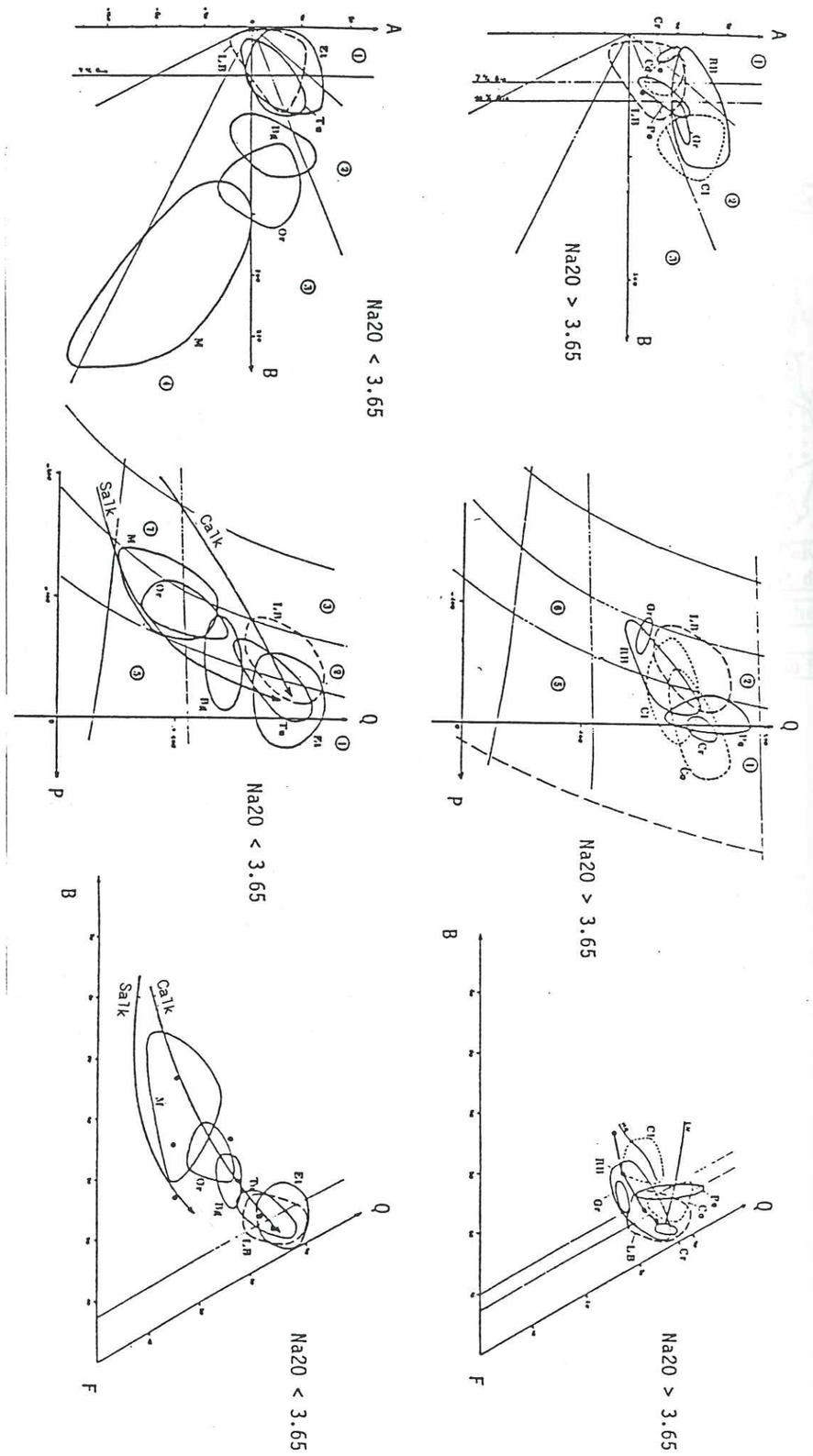

Figure 6.2 Diagrams of a) Coloured minerals
b) Classification
c) Q-B-F Triangle
(After Debon and Lefort, 1988)
Al: Alfrey, Bg: Bourg, Cl: Claphouse, Co: Combeynot, Cr: Crey
Et: Etages and Ailefroide, Gr: Grun, Lb: La Berade,
M: Colle Blanche and Moutiers, Or: Orgieres, Pe: Peou de St
Maurice, Qt: Quatre Tours Rb: Rieou Blanc, Rh: Rochail, Ru: Ramu
Tu: Turbat-Lauranoure.
Calk= Calcalkaline, Salk= Subalkaline

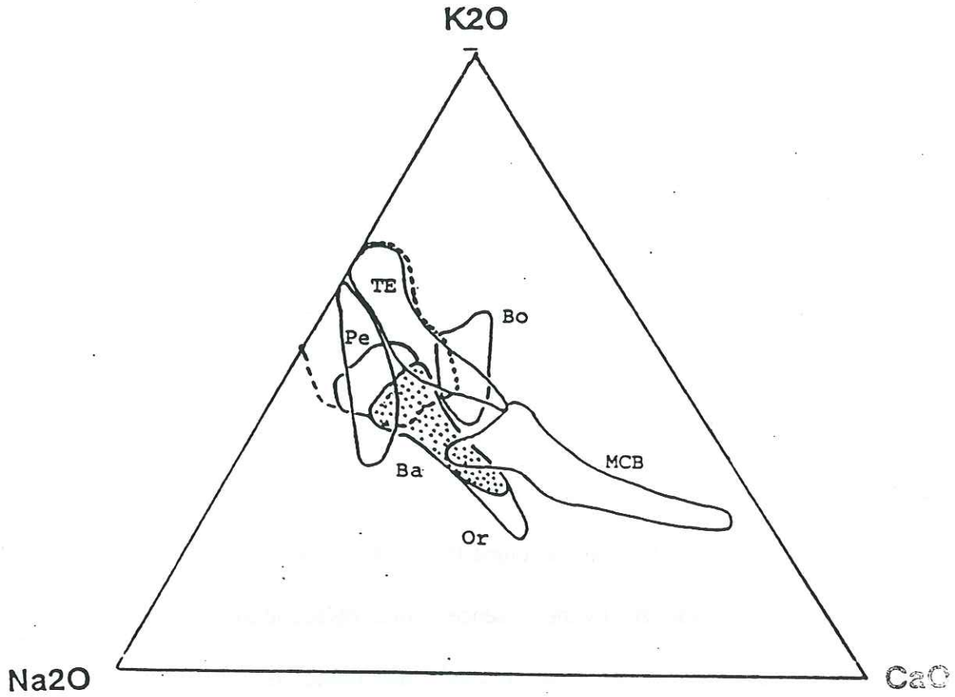

Figure 6.3 $Na_2O/K_2O/CaO$ triangular diagram of the granites from the Haut Dauphine.
(Fields TE: Turbat-Lauranoure, Bo: Bourg, MCB: Colle Blanche-Moutiers Pe: Pelvoux, Ba: Bans, Or: Orgieres.)

The granitoids which make up the alumino-sodic trend are well defined and show little chemical variation within the same intrusion. The same however, cannot be said for the monzonitic group, which show considerable variations, even within the same intrusion. LeFort (1970,1973) underlined this tendency in the granites of Colle Blanche, Moutieres, Bourg and Tourbat-Laurenoure. In an attempt to throw some light on the classification of these intrusions, the PICG-27 working group, using the work and diagrams from Santalier, 1983; Stussi et al., 1983 and De La Roche and Stussi, 1982; again recognized two magmatic associations. The first was termed "subalkaline", into which they grouped the granitoids of Rochail, Valsenestre, Bourg, Orgieres,

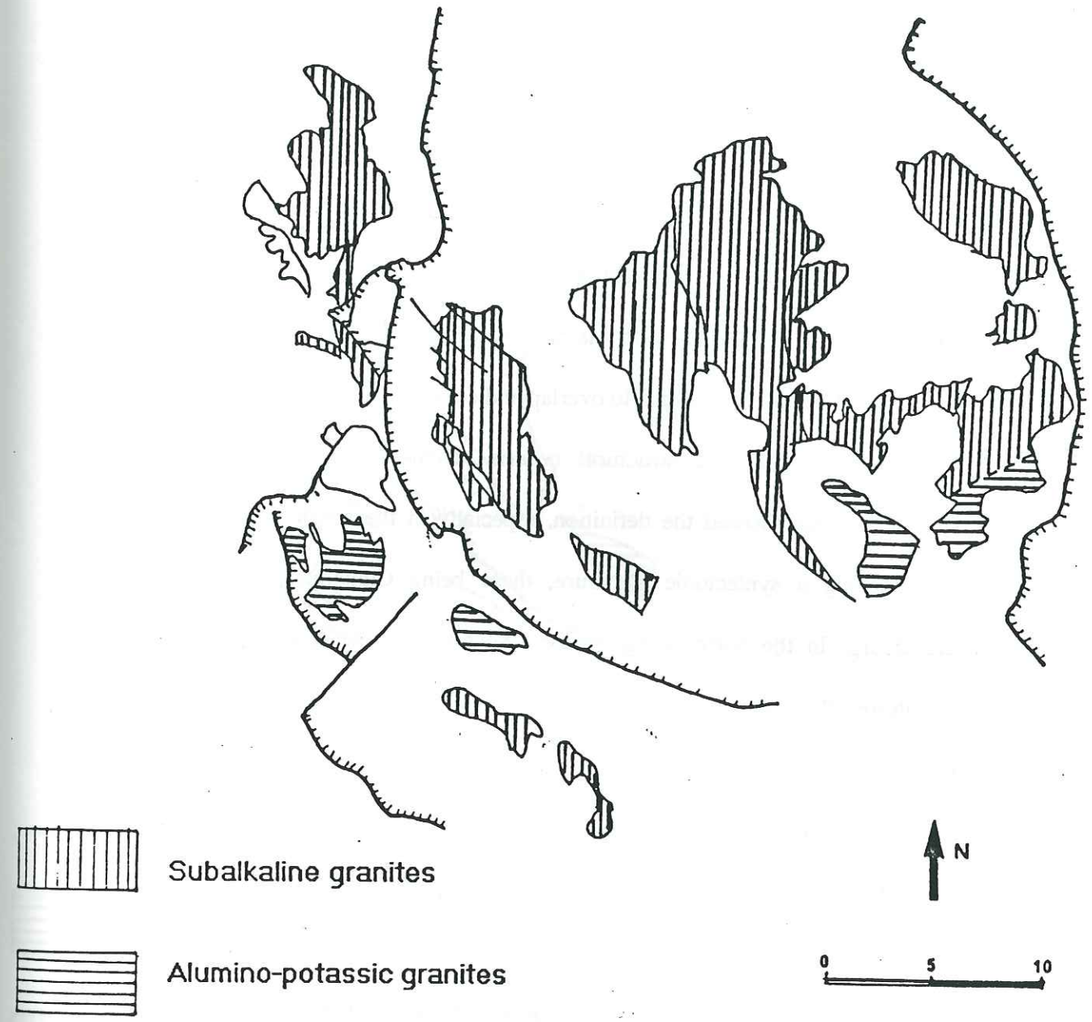

Figure 6.4 Distribution of the granites of the Haut Dauphine, after the classification of Stussi et al., (1983).
(See Figure 6.1 for intusion names and regional geology, and Table 6.1 for basic data.)

Turbat-Lauranoure, Colle Blanche, Moutieres, Les Etages, La Berarde-Promontoire, Combeynot and Pelvoux. The second, termed "alumino-potassic", included the granites of Grun, Petarel, Rieou Blanc and Claphouse. (Figure 6.4)

Whilst these two trends were very close, the authors were able to discriminate between the two, using the couple Al-Na for the first trend and Al-K for the second. However, discrimination using major element chemistry is not entirely satisfactory, especially amongst the more silicic members, as the fields tend to overlap and converge.

The use of geochronological and structural criteria (Demeulmeester, 1981;Giroud et al.,1981;LeFort, 1973) has allowed the definition, especially in the south of the region, of those granitoids having a syntectonic signature, these being Claphouse, Colle Blanche, Moutieres and Bourg. In the north of the region, the granitoids of Rochail, Les Etages, Berarde-Promontoire, Pelvoux and Combeynot,(Pecher, 1970; Giraud and Vivier, 1980; Costarella, 1986) have been assigned to a post-tectonic phase of intrusion.(Figure 6.5)

Comparison of these figures 6.4 and 6.5 highlight certain points. The syn-tectonic granites are, with the exception of Colle Blanche et Moutieres alumino-potassic whilst the post-tectonic granites are sub-alkaline in character.

From these two discrimanatory systems The geographical distribution of these granitoids would appear to be a north-south orientated, but the presence of epi-volcanic facies in the intrusions in the East of the region and their absence in the west, has been interpreted as intrusion at different structural levels (Pecher, 1970; Costarella, 1986). Further the majority of the granitoids found in the western part of the region (Rochail, Quatre Tours/Belle Cote, Peou de St Maurice, Colle Blanche and Moutieres) are associated with a bimodal magmatism of granite and syenite or diorite

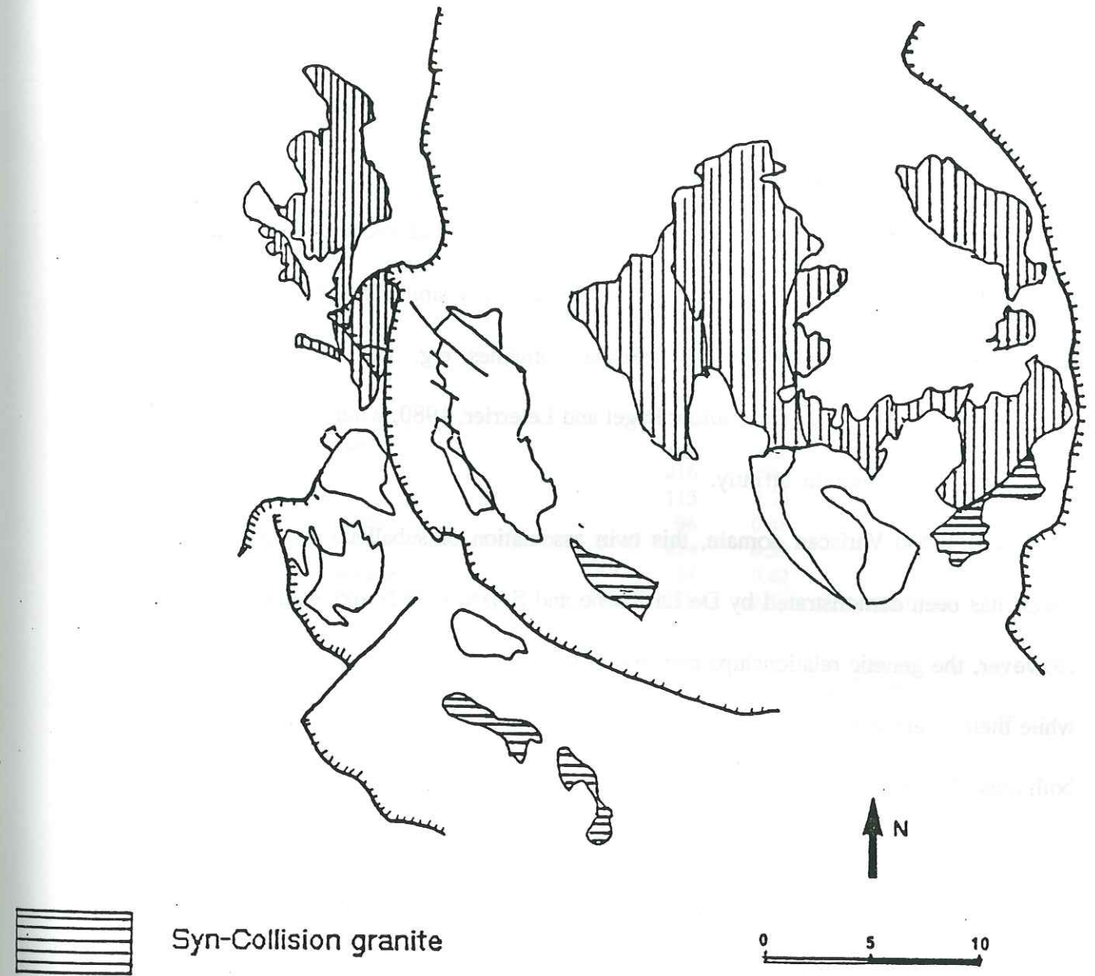

Figure 6.5 Distribution of the granites of the haut Dauphine into 'Pre' and 'Post' tectonic domaines. (after the work of Le Fort, 1973; Giroud et al., 1981 and Demeulmeester, 1986)

(de Boisset et al., 1984; de Boisset, 1986; Banzet and LeFort, 1987), this type of magmatism is also found further to the north, in other massifs of the External Crystalline Alps (Oliver et al., 1981; Aumaitre et al., 1985).

From petrological and geochemical criteria, LeFort, (1973) and Pecher, (1971), showed that the subalkaline association of the Haut Dauphine has many similarities with some subalkaline to potassic series from other French Variscan domaines, e.g. The massif of Ploumanac'h; Barriere, 1977 and The Ballons pluton; Pagel and Leterrier, 1980, where Autran et al., (1980) demonstrated a shoshonitic affinity.

Elsewhere in the Variscan domain, this twin association of subalkale and alumino-potassic trends has been demonstrated by De La Roche and Stussi, (1982) and Autran et al., (1980). However, the genetic relationships between the two associations are not clearly defined, and while their origin is still under discussion, the consensus opinion appears to be that they are both crustal in origin.

6.3 RARE EARTH ELEMENT GEOCHEMISTRY

A number of the granitoids from the Haut Dauphine have been analysed for trace element and REE element data by neutron activation analysis (see Annex 1), some representative values for which are found in Table 6.2.

The chondrite normalised (Nakamura, 1974) REE spectra are plotted in Figure 6.6, these reveal two types of variation between the spectra. 1) A difference in the ratio and hence the fractionation of the LREE over HREE 2) The difference in the relative size of the Eu anomaly.

Sample	Massif	ΣREE	Eu/Eu	(La/Yb)
C2-38	Combeynot	94	0.36	3.75
C21	Combeynot	128	0.28	5.14
COBL	Colle Blanche	194	0.76	19.43
GM100	Peou de St Maurice	86	0.91	18.82
NA33	Turbat -Lauranoure	110	0.67	15.28
NB12	Orgieres	154	0.38	15.28
PA46	Etages	157	0.75	15.42
R4G8	Cray	157	0.25	8.54
RL121	Rochail s.s.	103	1.26	13.25
RL210	Rochail (Clapier)	127	0.87	20.95
RO309	Quatre Tours	100	0.73	13.77
RO508P	Ramu	16	0.32	3.54
RO513	Alfrey	146	0.78	14.39
S8W1	Rieou Blanc (Porph)	142	0.72	15.34
SC6	Bourg	216	0.66	19.06
T3V2	Rieou Blanc (fine)	115	0.36	5.09
T6Q1	Pelvoux-Pic de Clozis	96	0.48	13.33
T6T3	Claphouse	274	0.33	7.16
V272	La Berarde-Promontoire	61	0.62	5.84
VJ20	Valsenestre	152	0.76	11.01

Table 6.2 Rare Earth element characteristics for some granitoids of the Haut Dauphine

Added to this are small relative variations in õREE which when included with the other two criteria allow a discrimination into four major groups.

Group 1:

This group is characterized by relatively low total values (86-127 ppm) and by a large fractionation of LREE to HREE (La/Yb N= 13.25-20.95) and by the almost total absence of a Eu anomaly (Eu/Eu* =0.87-1.26). The members of this group are Rochail, Peou de St Maurice, Alfrey and Quatre Tours.

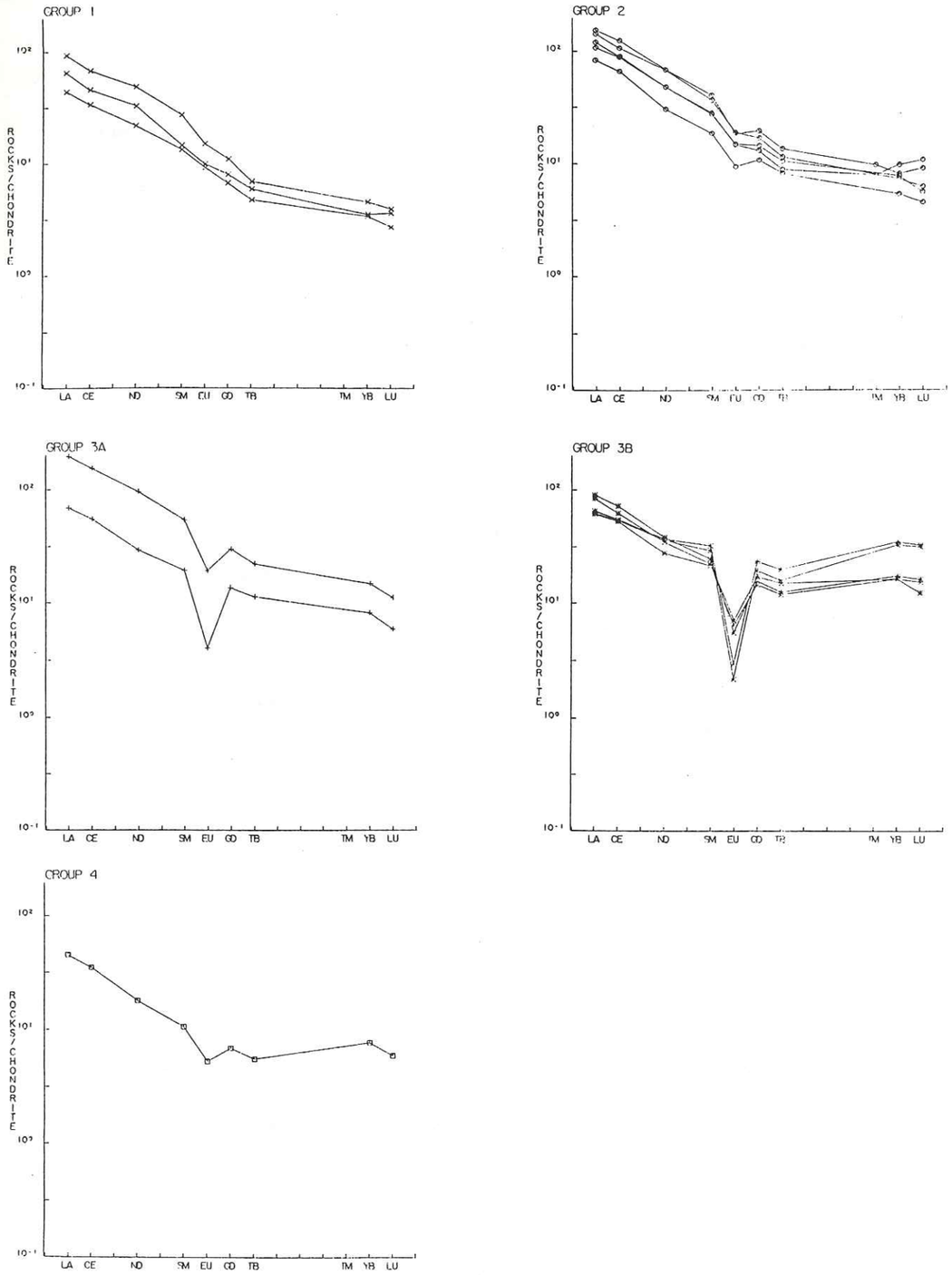

Figure 6.6 Chondrite normalised REE profiles for the granites of the Haut Dauphine. These have been separated into four major groups. (see text for explanation.)

Group 2:

This group includes the granitoids of Turbat-Lauranoure, Bourg, Colle Blanche, Moutieres, Orgieres, Les Etages and Valsenestre, and is defined by a large fractionation index of LREE over HREE (La/Yb N= 11.01-19.43) somewhat higher total values of REE (110 - 216 ppm) and a slight but consistent negative Eu anomaly (Eu/Eu* = 0.66-0.76). The porphyry facies of the Rieou Blanc granitoid also falls into this category.

Group 3:

This group can be subdivided into two groups on the basis of a marked difference in the slope of the chondrite normalised plot. The first, which includes the granitoids of Pelvoux, Pic de Clouzis and Cray, have a La/Yb ratio of 8.54 - 13.33, whilst the second sub group have La/Yb ratios of 5.09 - 8.54. Both sub groups however, show a pronounced negative Eu anomaly with values of Eu/Eu* = 0.25-0.48, whilst the total REE content varies greatly between 94 and 274 ppm, but without showing a further discrimination. These two sub-groups have been labelled 3a and 3b.

Group 4:

Into this last group go, for the moment, just two granites those of La Berarde-Promontoire and Ramu, having low total REE content (16.54 - 61ppm), negative anomalies for Eu (Eu/Eu* = 0.36 - 0.62) and a relatively flat profile with La/Yb of 3.54 - 5.84.

Within the region as a whole, the groups, as defined, form a series of bands running roughly north-south (Figure 6.7), with the granitoids forming Group 1 lying to the west of the region,

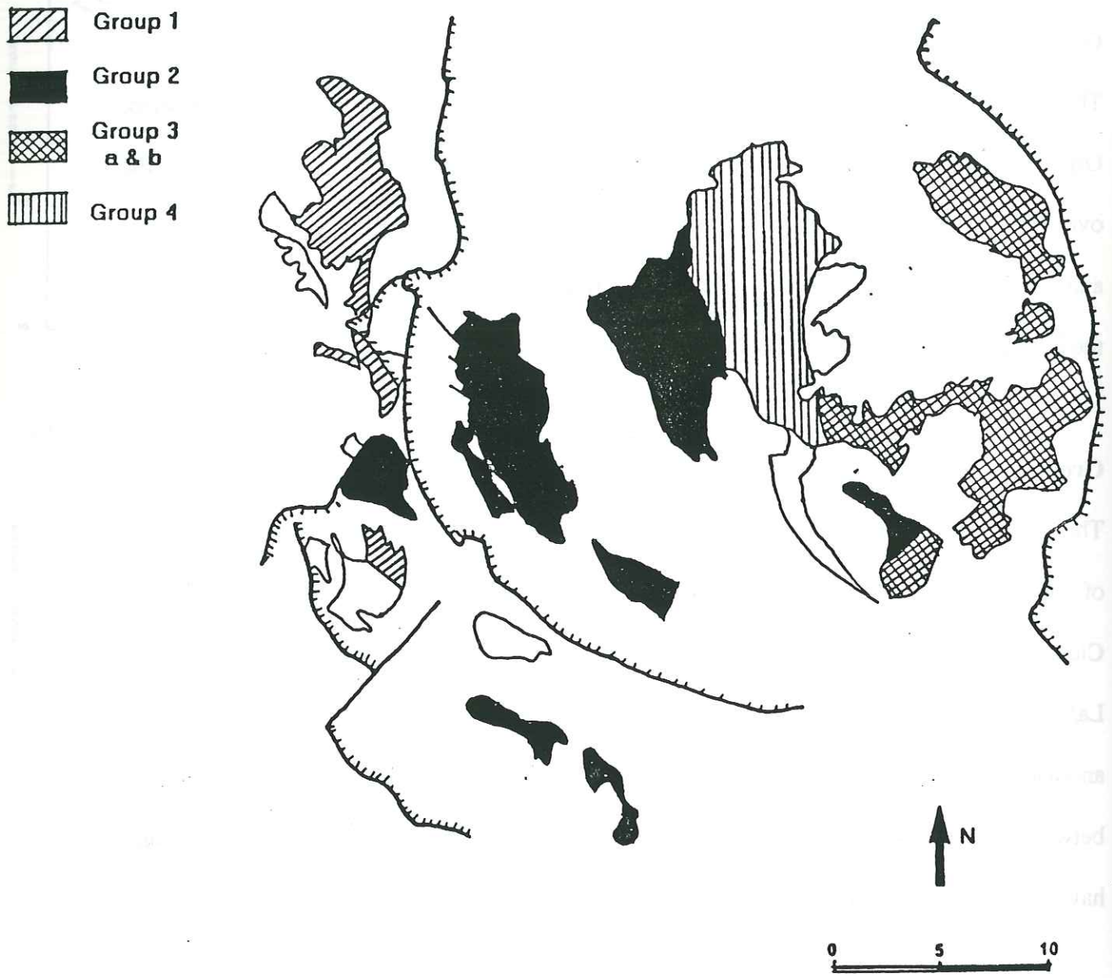

Figure 6.7 Distributio of the granites of the Haut Dauphine according to the four groups defined by the REE geochemistry.

those of Group 2 in the centre and the granitoids forming Group 3 to the East. Group 4 is for the moment an anomaly, but may represent granitoids of high level anatexis or alternatively plutons, which have undergone a greater degree of metamorphism during Alpine orogenic events, with an eventual loss of certain elements in a lost fluid phase. In any event with the exception of this group, the zones established from structural and petrological criteria are in part confirmed by the chemistry of the REE in the different granitoid plutons of the region.

However this is somewhat of a generalisation and there are some minor anomalies that stand in need of further explanation.

1) The porphyry facies of the Rieou Blanc pluton fits in Group 2 Whilst the fine grained facies fits into Group 3b; should these two then be considered as two distinct units with the fine grained facies being associated with the more alkaline rich granites of the eastern edge of the region.

2) The granites of the Etages and Cray are very closly associated in a temporal sense, but have very different REE profiles with Les Etages belonging to Group 2, whilst Crey which is highly aluminous in character, with the presence of cordierite, belongs to Group 3.

On the whole the profiles show similar characteristics to a number of other calc-alkaline and sub-alkaline associations, which also show steep profiles, with pronounced fractionation of LREE with respect to the HREE and important negative Eu anomalies Figure 6.4 (Fourcade and Allegre, 1981).

In particular the profiles of Groups 1 and 2 are very similar to those of the magnesium/potassium rich granitoids of Corsica (Cocherie,1985), to the syeno-granitic complex of Ploumanac'h (Barriere, 1980) and the calc alkaline two mica granite of Aix les Thermes (Fourcade and Allegre, 1981), as well as some of the Corsican granodiorites (Cocherie, 1985) but with a less pronounced fractionation of LREE with respect to HREE.

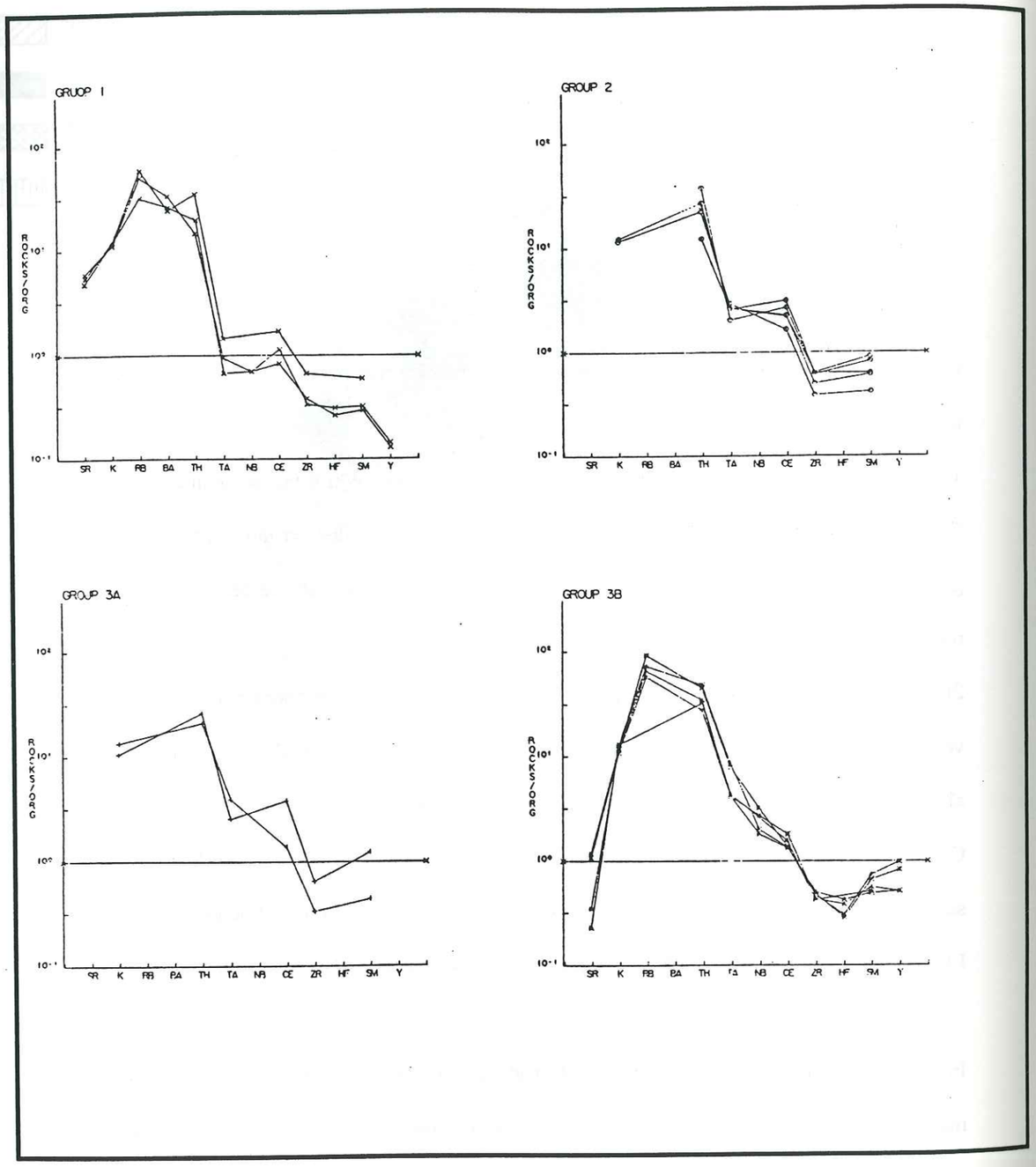

Figure 6.8 Multi-element variation diagrams of the four granite groups (defined by REE geochemistry) for the granites of the haut Dauphine. (Normalization values of ORG are from Pearce et al., 1984.)

The Group 3 granites, with an important negative Eu anomaly, have profiles which are comparable to monzonites of the calc-alkaline series of Corsica (Cocherie, 1985) whilst those the sub-group 3b show important similarities with those of the inter-plate granites of the Isle of Skye (Oliver and Vittoz, unpublished data), considered to have been derived from a mantle source enriched in incompatible elements (Pearce et al., 1984).

6.4 TRACE ELEMENT GEOCHEMISTRY

Variations in abundance for the trace elements Thorium, Hafnium, Cesium, Scandium and Tantulum are very small for the majority of the plutons, with the exception of the Valsenestre granite with a low value of Thorium (9.72), and the intrusive complex of La Berarde-Promontoire which has lower values for all the elements.

These data have been plotted on multi-element variation diagrams normalised to theoretical values of ocean ridge granites (ORG),(Figure 6.8), after Tarney et al., 1981 and Pearce et al., 1984. Groups 1 and 2 are generally characterized by lower values of the more incompatible elements as Tantalum and Thorium, whilst the contrary is true for Group 3 . Within the profiles it can be seen that the ratio of Ta to Ce is marked by an increase between Group 1 to Group 3b, These profiles show close similarities to those defined for granitoids from syn and post collision environments (Pearce et al., 1984). To further test this, the data have been plotted on the discriminant diagram Ta versus Yb (Pearce et al., 1984), (Figure 6.9). This indicates a trend for the Haut Dauphine granitoids from the field of granites generated in a volcanic arc environment (VAG) passing by the field of syn-collision granites to that of within plate granites. The granitoids of Group 1 being of Volcanic arc type and those of Group 3b of within plate type. The zonation of the Haut Dauphine therefore, is in large measure respected.

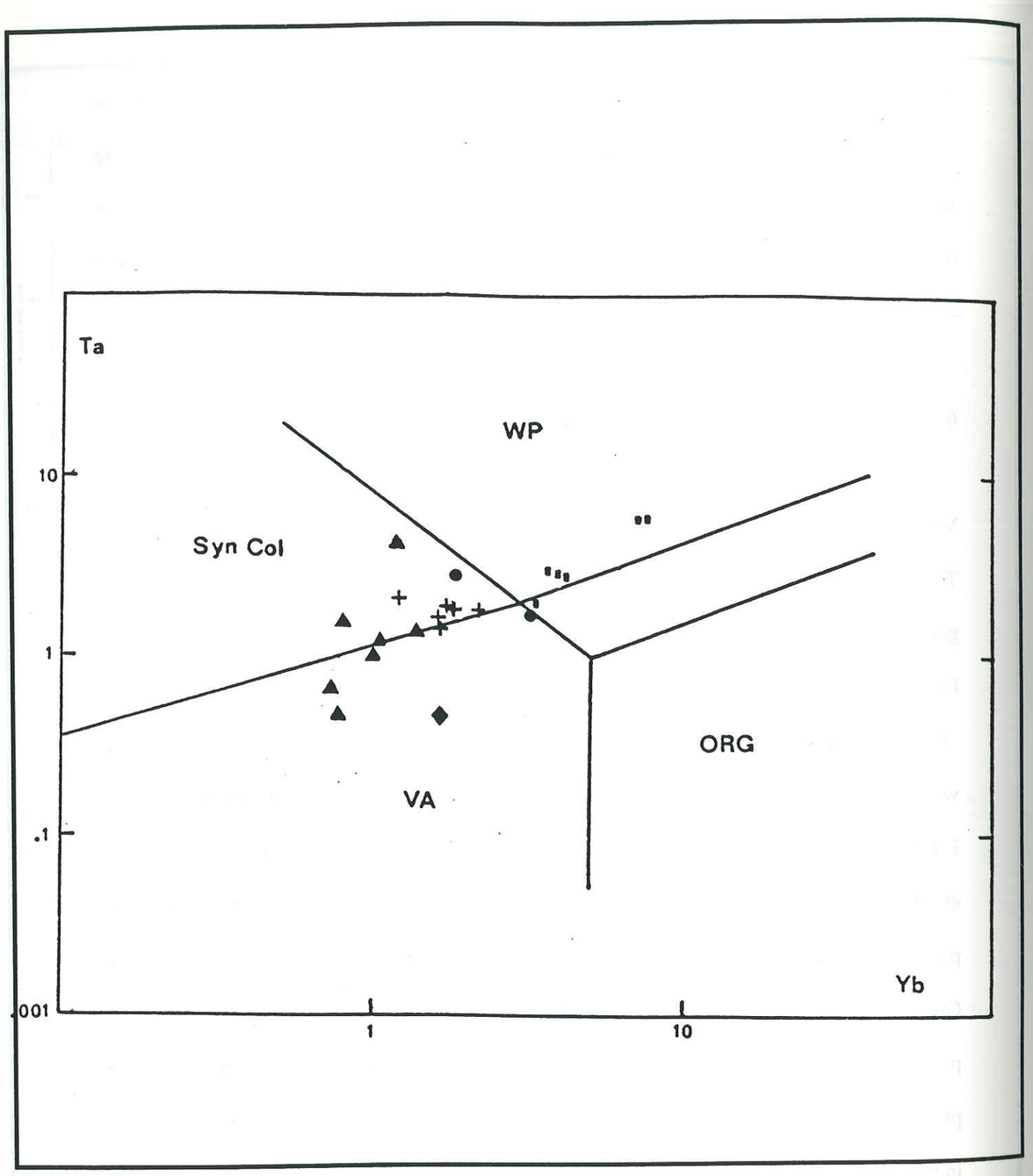

Figure 6.9 Discrimant diagram of Ta versus Yb for the granitoids of the Haut Dauphine.

(Group 1 = ▲, Group 2 = +, Group 3a = ●, Group 3b = ▮, Group 4 = ◆)

6.5 BORON DISTRIBUTIONS

Elemental concentrations of Boron have been determined for a number of the plutons of the Haut Dauphine , by the method of Prompt Gamma Activation analysis (see Annexe 2), and these data are detailed in Table 6.3, and shown schematically on Figure 6.10

Again a close look at these values allows a distribution into a number of groups, this time using derived from values from different tectonic environments (Table 4.2) .

Intrusion	Boron Concentration	Error
Orgieres	4.0	(0.92)
Turbat-Lauranoure	2.0	0.92)
	3.1	(0.87)
Etages	3.0	(0.93)
La Berarde-Promontoire	2.0	(0.88)
	3.3	(0.91)
Combeynot	8.1	(1.0)
Pelvoux-Pic de Clouzis	7.1	(0.91)
Rieou Blanc (Porphyrey)	7.3	(0.94)
Rieou Blanc (Fine grained)	7.0	(0.92)
	7.4	(0.94)
Claphouse	9.7	(0.98)
	6.5	(0.93)
Pic de Valsenestre	9.1	(0.99)
Rochail	15.5	(1.12)
Ramu	13.4	(1.03)
Colle Blanche	13.2	(1.03)
Moutieres	14.1	(1.07)
Quatre Tours	15.5	(1.08)
Alfrey	28.2	(1.68)
Bourg	57.4	(2.99)
	68.2	(3.33)

Table 6.3 Boron concentrations for granites of the Haut Dauphine.

Group 1: < 5 ppm

This group includes the plutons of Orgieres, Turbat-Laurenaure, Les Etages and La Berarde and forms an island situated in the north and centre of the region.

Group 2: 5 to 10 ppm

This group is made up from the intrusions of Combeynot, Pelvoux-Pic de Clouzis, Rieou Blanc and Claphouse, which forms the Eastern Zone. This group also includes the Valsenestre porphyry granite but the fact that this granite shows extensive signs of chloritization and alteration may be a significant factor in its apparent low boron concentration

Group 3: 10 to 30 ppm

This group includes the plutons of Rochail, Colle Blanche, Moutiers, Quatre Tours and Alfrey, forming the Western zone as defined by the REE and trace element geochemistry; as will be demonstrated in section 6.6 this data also accords fairly well with the zircon morphology.

Group 4 : > 30ppm

Finally the Bourg granite is set apart by excessively high values (57 to 68 ppm) of Boron. One explanation of this may be that the granite lies close to a major band of Alpine deformation and has possibly been affected by the circulation of fluids. As yet the mobility of Boron has not been determined, although petrological experiments are under way (Manning and Pichavent, 1983;

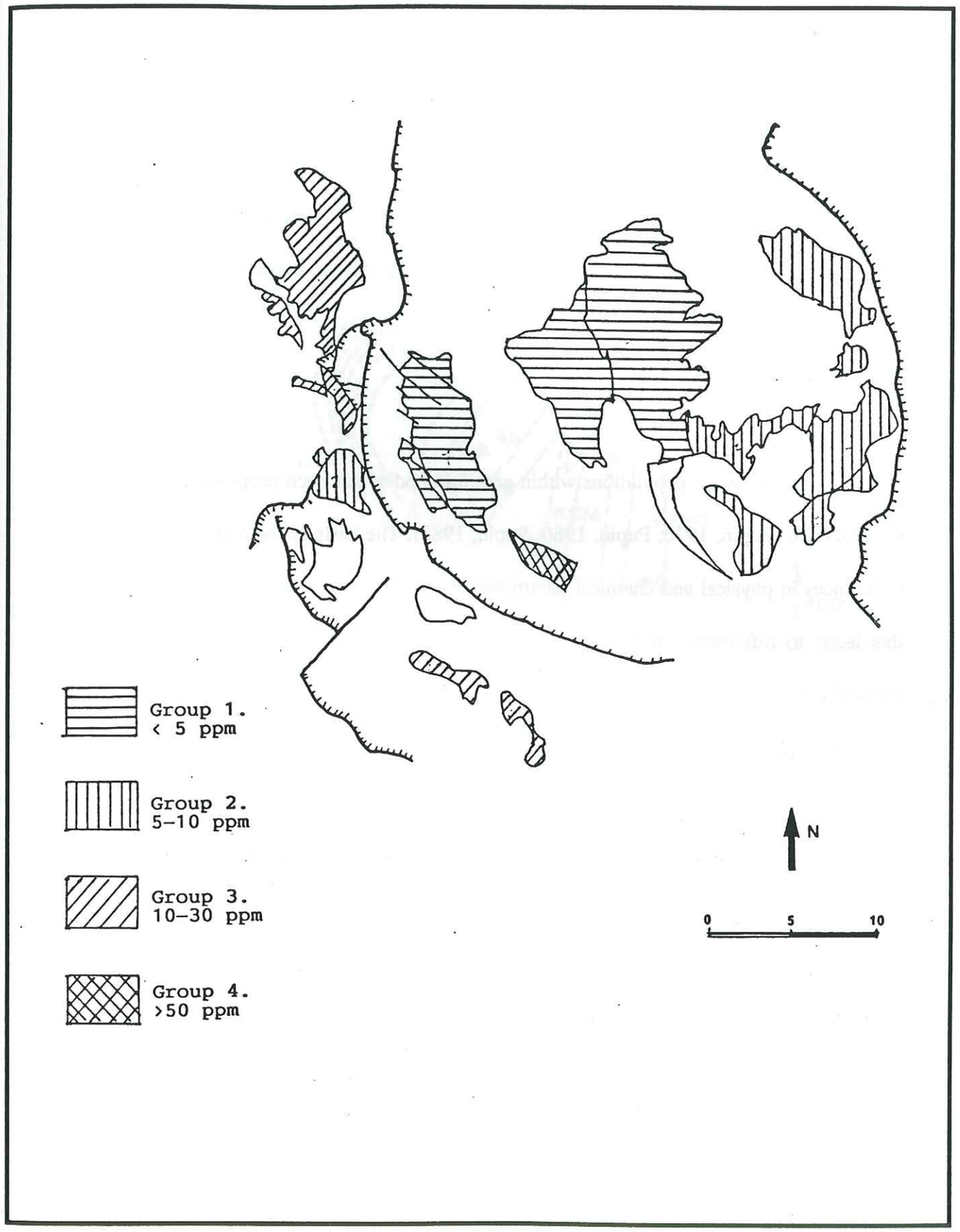

Figure 6.10 Distrubution of groups formed by concentrations of Boron for the granites of the Haut Dauphine.

Pichavant, 1987) to determine both the phase relations and mobility of elements such as Boron and Flourine in magmatic and metamorphic environments.

Values for the basic rocks of the Western zone range from 3 to 12ppm with an average value of 7.5 ppm. Syenites and diorites normally contain from 9 to 14 ppm of Boron (Harder, 1975) and so the values measured for the basic rocks reasonably close to these figures.

6.6 ZIRCON MORPHOLOGY

The typology of zircon populations within granitoid bodies has been proposed as a method of classification (Pupin, 1976; Pupin, 1980; Pupin, 1985). The basis of the method applies to the differences in physical and chemical parameters during the crystallisation of magmatic rocks, this leads to differences in the form of the pinacoids depending on the temperature and alkalinity at the moment of formation .

The granitoids of the Haut Dauphine have been in part studied, using this method, notably by Schade, 1983 and Costarella, 1987. The studies were made on the granites of Combeynot, Pelvoux-Pic de Clouzis, Les Etages and Turbat-Lauranoure (Costarella, 1987) and Orgieres, Bourg and Peterel (Schade, 1983).

These data, together with some new data for Colle Blanche-Moutiers (Banzet, personal communication) and Rochail, are presented in Figure 6.11. From this it can be seen that there are essentially three groups.

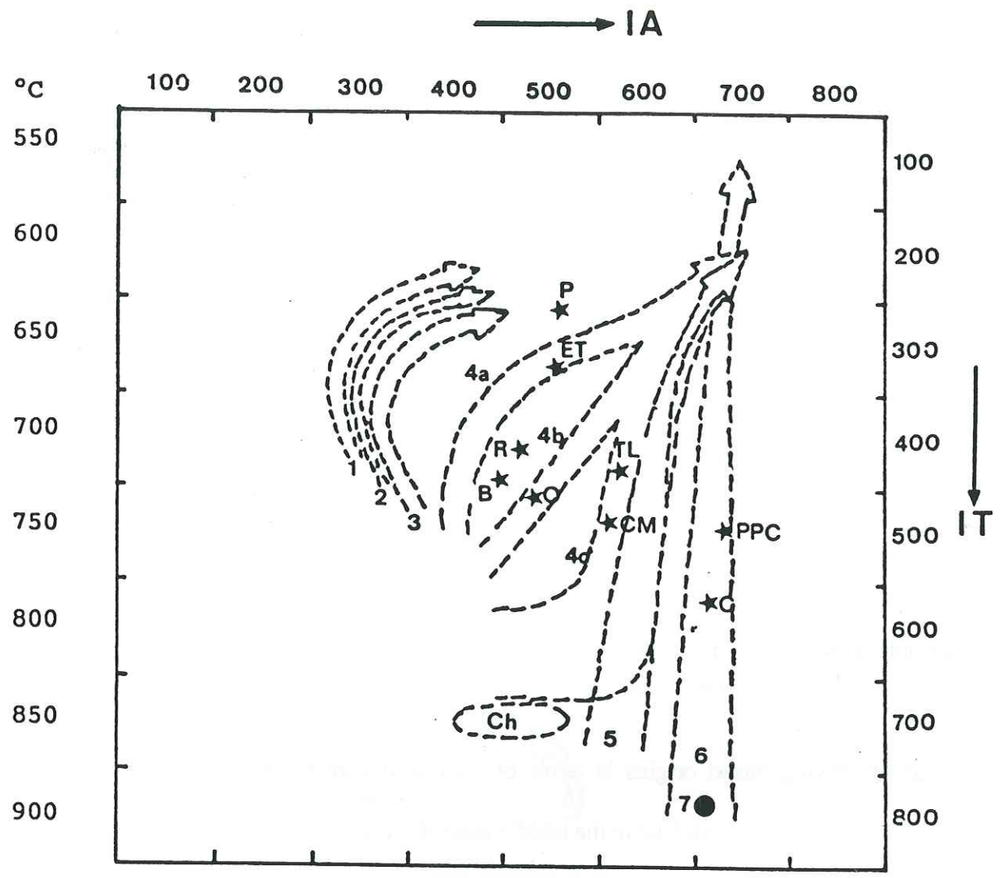

Figure 6.11 Zircon distribution diagram for granites of the Haut Dauphine. (after Pupin, 1980).

(IA = Alkalinity index, IT = Temperature index)

Fields: 1,2 and 3 = crustally derived, 4a,4b and 4c = mixed crustal and mantle origins, 5 = subalkaline mantle derived, 6 = alkaline series granites, 7 = tholeiitic series granites, Ch = Charnokite magmas.

P = Petarel, Et = Etages, R = Rochail, B = Bourg, O = Orgieres, TL = Turbat-Laurenoure, CM = Coll Blanche moutires, C = Combeynot, PPC = Pelvoux-Pic de Clousis.

The first group is represented by a single member, the Peterel granite, the average value plotting in the field of high level crustal granites (Pupin, 1980). The second group consists of the granitoids of Les Etages, Tubat-Laurenoure, Bourg, Orgieres, Rochail and Colle Blanche-Moutieres, which plot in the field of calc-alkaline granites having mixed crustal and mantle origins. Finally the third group represented by the plutons of Combeynot and Pelvoux-Pic de Clouzis have zircon morphologies characteristic of material with mantle origins or at least a large percentage of mantle derived material (Costarella, 1987).

As with the major element, REE and trace element chemistry the three defined groups fall into a zonal pattern Figure 6.12 which shows, running from west to east.

1. Granitoids of essentially crustal origin found in the west of the region.

2. Granitoids having mixed origins in terms of their source material, and showing calc-alkaline chemical affinities which lie in the middle zone of the region .

3. Granitoids having source origins with a high proportion of mantle material and showing alkaline chemical affinities (Costarella, 1987), which form a zone in the east of the region.

It should however be said that a lot of information is not available and a more comprehensive study of the whole of the Haut Dauphine needs to be undertaken.

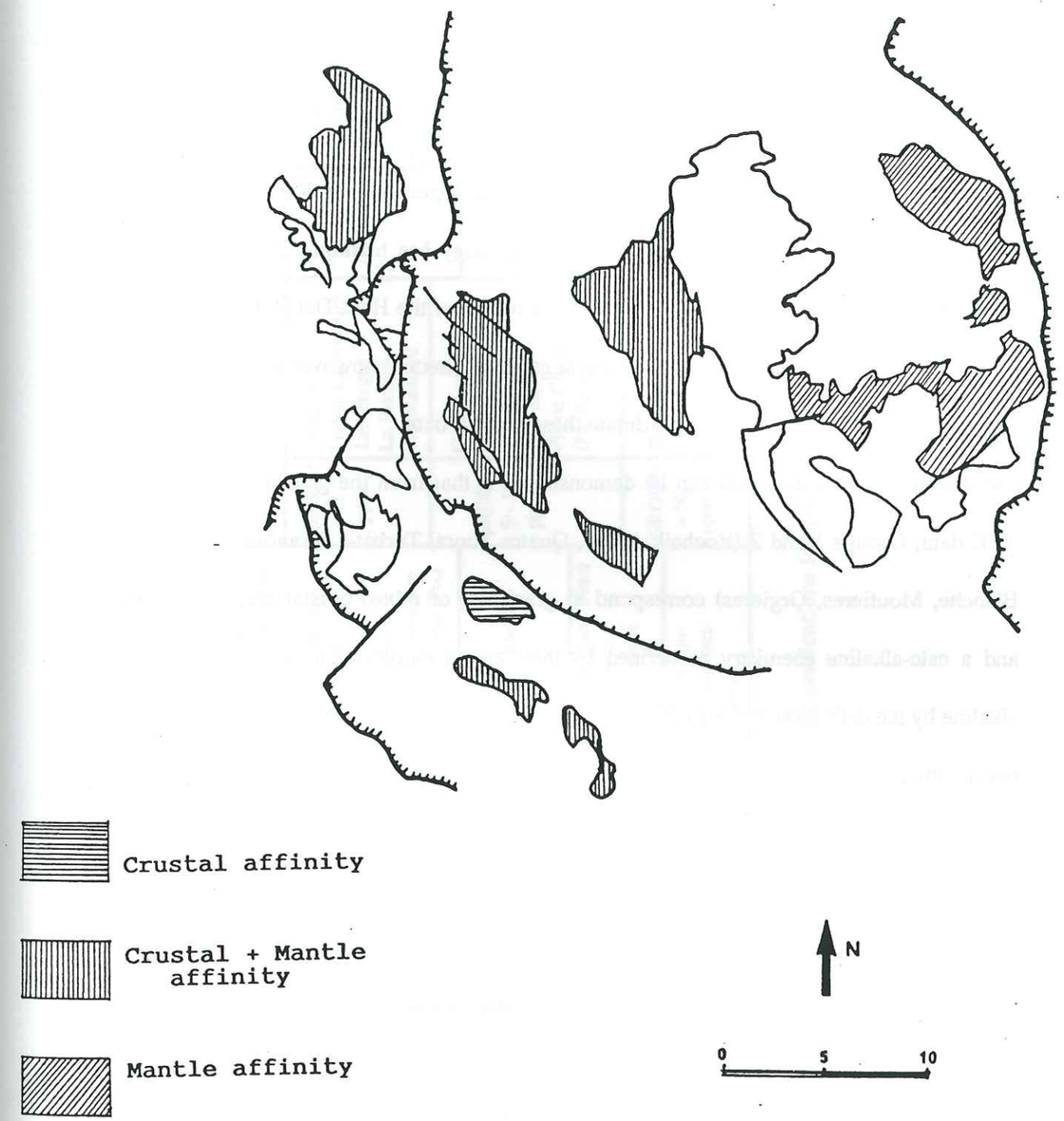

Figure 6.12 Distribution patterns for some granites from the Haut Dauphin from their observed zircon morphology.

6.7 SUMMARY AND CONCLUSIONS

The use of Major element and mineralogical criteria together with Rare Earth and Trace Element data, as well as, the use of Zircon morphology has highlighted a zonation of the granitoid intrusions of Variscan age, found in the region of the Haut Dauphine. Each of these criteria show some sort of zonation which is in general coherant, however minor deviations do occur and Table 6.4 attempts to coordinate these various data.

The essential information that can be demonstrated is that from the grouping defined by the REE data, Groups 1 and 2 (Rochail, Alfrey, Quatre Tours, Turbat-Lauranoure, Bourg, Colle Blanche, Moutieres, Orgieres) correspond to granitoids of mixed crustal and mantle origins and a calc-alkaline chemistry as defined by their zircon morphology, whilst they are sub-alkaline by the definition of the PICG 27 method, these granitoids occupy the west and central part of the region. In the east of the region those granitoids defined by Group 3 (Combeynot, Pelvoux-Pic de Clouzis) are also classified as of mainly mantle origin by their zircon morphology whilst they fall into the alumino-potassic group of the PICG.

The correlation of the Boron geochemistry is not quite so straight forward. However it is interesting to note that with the exception of the Valsenestre porphyry granite, those granitoids in the western zone have boron contents ranging from 12 to 16 ppm with the exception of the Alfrey granite, at nearly 30 ppm, but this granite however, is thought to be slightly older and more fluid rich than the other granites of the western zone, whilst the granites of the eastern zone all have lower values than this within the 5 to 10 ppm range.

Harder, (1975) gives values of 5 to 7 ppm for basic rocks and from 20 to 30 ppm for acidic

	PICG 27		Debon- LeFort		REE + Trace Elements		BORON		ZIRCON MORPHO.
SUB-ALKALINE	Rochail Pic du Valsenestre Bourg Orgieres Turbat-Lauranoure Colle Blanche Moutieres Les Etages La Berarde- Promontoire Combeynot Pelvoux-Pic de Clouzis Alfrey Quatre Tours Ramu	ALUMINO SODIC	Berarde-Promontoire Rieou Blanc Quatre Tours Grun de St Maurice Peou de St Maurice Rochail	GROUP 1	Rochail Peou de St Maurice Quatre Tours Alfrey	GROUP 10-30 ppm	Rochail Colle Blanche Moutieres Quatre Tours Alfrey Ramu	CRUSTAL	Petarel
				GROUP 2	Turbat-Lauranoure Bourg Colle Blanche Moutieres Orgieres Les Etages Pic de Valsenestre Rieoux Blanc (Po.)	GROUP <5 ppm	Orgieres Turbat-Laurenoure Les Etages La Berarde-Promontoire	CRUSTAL + MANTLE	Les Etages Turbat-Laurenoure Bourg Orgieres Colle Blanche Moutires Rochail
ALUMINO-POTASSIC	Grun de St Maurice Petarel Rieou Blanc Claphouse	MONZO-NITIC	Colle Blanche Moutieres Bourg Turbat- Lauranoure Les Etages Pic du Valsenestre	GROUP 3a	Pelvoux-Pic de Clouzis Cray	GROUP 5 - 10 ppm	Combeynot Rieoux Blanc Claphouse Pelvoux-Pic de Clouzis (Pic de Valsenester)	MANTLE	Combeynot Pelvoux-Pic de Clouzis
				GROUP 3b	Rieoux Blanc (fine) Claphouse Combeynot				
				GROUP 4	La Berarde-Promontoire Ramu	GROUP > 50 ppm	Bourg		

Table 6.4 Schematic correlation of data and classifications for the granites of the Haut Dauphine, Western French Alps.

rocks, and measurements made at the ILL corroborate the evidence from the zircon morphology

The main conclusions which can be drawn from this information are:

1) The granitoids of the Haut Dauphine appear to correspond to a zonation which becomes more alkaline in character from West to East

2) Those granitoids forming the Western zone have characteristics close to those described for granites from collision zones (Pearce et al., 1984). This is evidenced by apositive anomaly for Ce and Sm whilst the slope between Hf and Yb is negative (Figure 6.5a), these being good indications of an important crustal component in the make up of these granitoids

3) For the granitoids making up the Eastern zone their trace element chemistry shows little or no selective enrichment and the incompatible elements from Hf to Yb show a mainly flat profile, Pearce et al., (1984) demonstrated these characteristics as belonging to within plate granites and gave as examples the granitoids of the Skaergaard and Mull. For these authors the provenance of these granites was a mantle source enriched in incompatible elements. There is however a slight positive anomaly for Sm for some of these granitoids, which may be an indication of some slight crustal contamination.

CHAPTER 7

GENERAL CONCLUSIONS

7.1 GENERAL SUMMARY

The studied field area has been shown to be a structurally complex region, where crystalline basement in the form of Upper Proterozoic to Lower Paleozoic metamorphosed volcano-sediments have undergone poly-metamorphism. These volcano-sediments have subsequently been intruded by a series of granitic rocks associated with a small basic suite of dikes and intrusions during Variscan times. Rb/Sr and K/Ar dates range from 340 Ma to 310 Ma (Demeulmeester, 1982: Vivier, unpublished data and Chapter 5 op. cit.). During this period, syn-tectonic thrusting and possible strike slip movement have affected the region, and the major result of this deformation has been the creation of mylonitic zones often along the boundaries of allocthonous granite massifs. Following this period, the area suffered erosion (no evidence for deposition of Upper Carboniferous to Lower Permian sediments in this region has been found, although these do exist to the west and further north) and evidence of eroded surfaces in the Alfrey granite, which appears to be in situ, exists (Plate 2.14). This period was followed by crustal extension, and the deposition of quite thick sequences of Lower Mesozoic sediments.

This period was then followed by one of severe crustal shortening, with thrusting from the east, which has led to the failure of the crystalline basement, essentially along existing lines of weakness, and the development of a series of thrust faults, which have resulted in the creation of a series of thrust sheets (Butler et al., 1986). (Fig 2.4 - 2.6)

Within the field area, this has resulted in the overthrusting of the Ramu granite over the Quatre Tours/Belle Cote granite, which has in turn been overthrust onto the Alfrey granite. Field relationships do not unequivocally demonstrate that this type of deformation was unique to the Alpine orogenic event. On the contrary it is probable that some of the observed deformation, in the form of strike-slip tectonics, was coeval with the emplacement of the intrusives, resulting in the creation of mylonitic zones in late Variscan times.

Subsequent deformation during Alpine metamorphic events has given a retro-metamorphic overprint, especially close to the major fracture zones (Demeulmeester, 1982), whereas the Mesozoic cover has suffered intense deformation and mild metamorphism (slate grade).

7.2 GRANITES AND ASSOCIATED ROCKS

7.2.1 Processes of granite formation.

Processes of granite formation can be divided into three main groups.

a) Processes that take place within the source region and which lead to the generation of parental magmas. These include such processes as partial melting and mixing or hybridisation of primary melts within the source region.

b) Processes which operate on the parental magmas, during the period of their emplacement and cooling. These processes include multiple intrusion of magmas, crystal settling and in situ fractionation, assimilation of country rocks and the circulation of late stage volatiles.

c) Processes which vary pressure and temperature constraints, within specific tectonic regimes.

The granites of the Valsenestre region, on the evidence of their geochemistry, fall into two distinct categories. The granites of Alfrey, the Quatre Tours/Belle Cote and Rochail can be considered as sub-alkaline or monzonitic granites after the classification of several workers (Stussi et al., 1983; Debon and LeFort, 1988), and correlate with the other granite intrusions found in the western part of the Haut Dauphine province. The $^{87}Sr/^{86}Sr$ initial ratio for the Rochail and Quatre Tours/Belle Cote granites of 0.705 would appear to be too low for a purely crustal source to be considered, but if coupled with the fact that Rochail at least, shows a marked affinity with volcanic arc domains on discriminant diagrams, it seems possible that the source regions may be found in volcanic arc type rocks from a subduction event prior to the collision event. This could explain this fairly low ratio, without invoking a mantle source input. The Ramu granite has a geochemical signature close to the Group II granites of Harris et al., 1986, and a petrology which suggests, when coupled with field relations, that it is an anatexic granite melting from fairly dry metamorphic crust to give a muscovite rich granite.

7.2.2 Processes of formation of the basic rocks.

The syeno-monzodioritic intrusives appear, from their geochemistry, to be genetically unrelated and it seems most probable that these basic rocks were generated from hydrous upper mantle type sources at temperatures around 800 - 900°C (Hamidullah and Bowes, 1987), which were then forcibly intruded in a volatile rich environment. Subsequent contact with the still hot, overlying granites, has caused a re-equilibration of the primary minerals with the development of essential amphibole and phlogopite followed by K-feldspar. This then implies, the involvment of a basaltic magma with the associated granite. Sabatier, (1980) felt that these types of association and the

high values of the alkali elements were a result of the interaction between granite and basaltic magma, however little or no evidence of this type of reaction has been observed in the studied outcrops, and it is difficult to imagine the large scale movement of K and Na into a basic medium. It is much more probable that these elements are in fact to be found in the highly metasomatised source material of the upper mantle, where small degrees of partial melting give a quite alkaline signature to the melt as envisaged by Thompson, (1984) and Foley et al., (1987).

7.3 TECTONIC REGIME AND ENVIRONMENT OF EMPLACEMENT

Many of the intra Alpine Variscan granites have been studied by a large number of workers and the concensus opinion gives two major periods of granite formation, that of 350 to 330 Ma being considered as the emplacement of granites syn-orogenicly, whilst later granites circa 320 to 280 Ma are considered as post-orogenic. Debon et al., 1994, have recently given an age of 332 ± 13 Ma obtained by Lead isotopes on zircons for the granite of the Sept Laux in the Belledonne range, but this granite has been intruded in a compressive strike slip regime, reminiscent of the Main Donegal granite (Pitcher, 1972; Hutton, 1981), which is not the case for either the Rochail, or Alfrey granites where it appears that emplacement was in a regime of probable extension.

The somewhat younger age tends to place these granites within the post-collision period cited by Finger and Steyrer, (1990, 1991). They argue that the late Carboniferous magmatic activity represents a rather late event in the Variscan cycle, long postdating the initial collision in Devonian times (Matte, 1986). They further argue for a subduction related environment for the production of the I and S-Type granites having concurrant ages within the Moldanubian sector.

Vestiges of late Carboniferous shoshonitic magmatism exist within the province of the Haut Dauphine (Lameyre, 1957, Banzet et al., 1985), and has been ascribed to a Basin and Range type

of environment by these workers. However in several parts of the southern Variscan mountain chain, extensive basement uplift and extensional unroofing have been cited (Krohe and Eisbacher, 1988; Eisbacher et al, 1989; Echtler and Malavielle, 1990; Malaveille et al,. 1990) whilst Ring and Richter, (1994) invoke a high heat source, due to decrease in pressure during exhumation by crustal thinning processes in an extensional regime (Brodie and Rutter, 1987) for the generation of granitic intrusions in the SouthAlpine domaine. This high heat flow would have facilitated melting of the de-pressurised mantle, causing underplating of the crustal pile with the subsequent generation of both I and S type granites, with the injection under high velocities of small amounts of basic magmas probably exploiting normal faults created by the extensional regime.

This then is the prefered model for the generation and emplacement of the granites and their associated basic rocks of at least the western part of the Haut Dauphine magmatic province.

REFERENCES:

ADLINE G. (1982) Les spilites potassiques triasiques de la bordure occidentale du massif des Ecrins-Pelvoux (Alpes français): aspect volcanologique et problèmes de carbonatation. These 3 cycle. Grenoble, 118p.

ALIBERT C., MICHARD A. and ALBAREDE F., 1986, Isotope and trace element geochemistry of of Colerado Plateau volcanics, Geochim. Cosmochim. Acta, 50, pp 2735-2750.

ALLEN J.C., BOETTCHER A.L., MARLAND G. (1975), Amphiboles in andesite and basalt. I: stability as a function of P, T, Fo2. Am. Mineral., 60, pp1069-1085

AMBOLY J., HAMEURT J., ROCCI G. (1967) Relations génétiques entre vaugnérites et kersantites et hypothèse originale sur la gènése des lamprophyres des Vodges. C.R. Acad. Sci, Paris, t. 264, D. p. 25-28.

ANDRE F. (1983) Petrologie structurale et petrogenese des formations plutonique septentrionales du Massif des Ballonns (Vosges, France). Thesis 3eme cycle, Nancy 1, 247p.

ANDRE F., BEBIIEN J. (1983) Mineralogie et petrologie des cumulats gabbro-dioritiques situes en bordure septentrionale du massif des Ballons. (Vosges meridionales, France) : cristallisation d'un magma basique en domaine "orogénique" intracontinental. Bull. Mineral.(1983), 106, 341-351

ARNAUD G. (1980) L'intrusion gabbro-dioritique de St Quay-Portrieux (Cotes du Nord) Thèse 3 cycle, Paris VI, 141 p.

ARNOLD A., 1970, On the history of the Gotthard massif (Central Alps, Switzerland)., Eclogae Geol. Helv., 63, pp 29-30.

ARTH J.G., 1976, Behaviour of trace elements during magmatic processes- a summary of theoretical models and their applications, J. Reaserch U.S. Geol. Surv., 4, pp 41-47.

AUMAITRE R., GIRAUD P., PONCERRY E., VIVIER G. (1985): Les granitoids subalcalins potassique de la Lauziere, Massifs cristallins externes de Belledonne (Alpes francaises), Geologie Alpine, Grenoble, Vol. 61, pp 17-32

AUTRAN A;, STUSSI J.M., PLOQUIN A., ORSINI J.B., (1980): Le plutonisme Caledono-hercynien en France, Contributions du groupe de travail francais.

BAILEY D.K., 1982, Mantle metasomatism - continuing chemical change within the Earth. Nature, 296, pp 525-530.

BAILEY D. K., 1987, Mantle metasomatism - perspective and prospect., in Alkaline Igneous Rocks, Eds. FITTON J. G. and UPTON B.G. J., Geol. Soc. Spec. Pub., 30, pp 1-13.

BANZET G., LE FORT P., 1987, Subalkaline belt of granitoid bearing vaugneritic inclusions in western Haut Dauphine (Externel french Alps): accessory minerals and REE geochemistry, EUG IV, April 1987.

BANZET G. 1988: Interactions croute manteau et genese du plutonism subalcalin du Haute Dauphine occidental (Massifs Cristallins Externes): Vaugnerites, Durbachites et Granitoides megnesio potassiques, Geol. Alpine, Grenoble, Vol. 63, pp 95-112.

BANZET G., LAPIERRE H., LE FORT P. and PECHER A., 1985, Le volcanisme Carbonifere-Superieur du massif des Grandes Rousses (Zone Dauphinoise-Alpes Externes Francais): Un magmatisme a affinites shoshonitique lie a la fracturation crustale tardi-Varisque. Geologie Alpine, 61, pp 33-60.

BARBIER R. 1956 Remarques sur la tectonique et la stratigraphie de la zone dauphinoise orientale au Nord du Pelvoux. Bull. Soc. Geol. Fr., 6 Sé., tVI

BARBIERI A. 1970 Etude pétrographique dela partie orientale du massif des Ecrins-Pelvoux: les granites. Aperçu sur la géochronometrie du massif. Thèse 3 cyclé, Grenoble.

BARD J.P. 1979 Microtexture des roches magmatiques et métamorphiques. Ed. Masson, Paris, 192 p.

BARFETY J. C., GIDON M., LEMOINE M. and MOUTERDE R., 1979, Tectonique syn-sedimentaire Liassique dans les Massifs Crystalins de la zone externe des Alpes occidentales francaises: la faille du Col d'Ornon. C. R. Acad. Sci. Paris, 289, pp 1207-1210.

BARFETTY J. C. and GIDDON M., 1981, Fonctionnement synsedimentaire liasique d'accidents de socle dans la region de Venosc (massif cristallin du Pelvoux, Alpes occidentales). Bull. BRGM, Paris, section I, N° 1, pp 11-12.

BARFETTY J. C. and GIDDON M., 1983, La stratigraphie et la structure de la couverture dauphinoise au Sud du Bourg-d'Oisans: leurs relations avec les deformations synsedimentaires Jurassiques., Geol. Alpine, Grenoble, 59, pp 5-32.

BARFETY J.C. and PECHER A., 1984,

BARFETY J.C.,MONJUVENT G., PECHER A., CARME F., 1988, Notice de la carte geologique de La Mure. Ed. BRGM.

BARRIERE M. (1977) Le complexe de Ploumanach. Massif Armoricain. Thèse 3 cycle, Brest, 1 vol.

BARRIERE M. (1977): le complex de Ploumanac'h, Massif Armoricain. essai sur la mise en place et l'evolution petrologique d'une assocciation plutonique subalcaline tardi-orogenique, These de Doctorat d'Etat, Brest, 291p.

BARTOLI (1973) Etude pétrographique et structurale du Haut Vénéon (Massif du Pelvoux). Thèse 3 cycle, Gronoble.

BATTACHARJI S., 1967, Scale model experiments on flowage differentiation in sills, in Ultramafic and Related Rocks, ed. P.J.Wyllie, Wiley, new York.

BEACH A., 1981a, Thrust structures in the eastern Dauphinoise Zone (French Alps), north of the Pelvoux massif., J. Struct. Geol., 3, 299-308.

BEACH A., 1981b, Thrust tectonics and cover-basement relations on the northern margin of the Pelvoux massif, French Alps., Eclog. Geol. Helv., 74, pp 471-479.

BEBIEN., 1987

BELLAIR P. (1948) Pétrographique et tectonique des masiif centraux dauphinois. Mém. serv. Carte géol. France. 355 p. 1

BELLAIR P.(1938) Sur l'origine du Pelvoux. C.R.A.S. t. 124, P. 189-190.

BELLANGER D. (1980) Vaugnérites et roches associées dans lse Cévennes médianes: quelques aspects pétrologiques et géochimiques. Thèse 3 cycle, Lyon 184 p.

BELLIERE J., 1958, Contributions a l'etude petrogenetique des schistes cristallins du massif des Aiguilles Rouges 5Hte. Savoie). Mem. Soc. Geol. Belg., 81, 204.

BELLIERE J., 1988, On the age of mylonites within the Mont Blanc massif, Geodin. Acta, 2, pp 13-16.

BELLIERE J., STREEL M., 1980, Roche d'age viseen superieur dans le massif des Aiguilles Rouges (Hte Savoie)., C. R. Acad . Sci., Paris, 290D, pp 1341-1343.

BESSON M., FONTEILLES M. (1974) Relations entre les comportements contrastés de l'alumine et du fer dans les différenciation des séries tholeitiques et calc-alcalines. Bull. Soc. Fr. Minéral. Cristallogr. (1974), 97, 445-449

BIJU DUVAL J. (1975) Etude pétrologiques des terrains cristallins de la région du Sirac (Sud du massif des Ecrins-Pelvoux, Haut Dauphiné). Thèse 3 cycle, Grenoble.

BLOOMFIELD A.L.,ARCULUS R.J. (1989) Magma mixing in the San Francisco Volcanic Field, AZ, Cont. Min. Pet., Vol.102, pp 429-453

BODINIER JL., DUPEY C., DOSTAL J., CARME F., 1981, Geochemistry of ophiolites from the Chamrousse complex (Belledonne massif, Alps). Contrib. Min. Pet., 78, pp 379-388 .

BOGDANOFF S., 1980, Analyse structurale dans la partie occidentale de l'Argentera-Mercantour. These, Universite Paris Sud, Orsay, 316p.

BOGDANOFF S., 1986, Evolution de la partie occidentale du massif cristallin externe de l'Argentera. Place dans l'arc alpin. Bull. Bur. Rech. Geol. Min. Geol. Fr., 4, pp 433-453.

BOHOMME M., BUFFIERE J.M., ROBERT M. (1963) Age absolu du granite du massif du Rochail (secteur N.O. du Pelvoux, Isère.) C.R. Acad. Sci, t 256, pp649-2651.
BOISSET T. de, VITTOZ P., VIVIER G., OLIVER R. (1984) Association acide-basique dans le massif du Rochail; Nord-Ouest Pelvoux Massif Cristallins Externes. Relations structurales. 10 R.A.S.T. 1984

BOIVIN P. A (1982) Interactions entre magmas basaltiques et manteau supérieur. Thèse doctorat d'Etat, Clermont, vol.

BONIN B. (1982): Les granites des complexes annulaires, Manuels et Methodes BRGM, N4, 183p.

BONIN B. (1983): Les complexes plutoniques alcalins. Perspectives et hypotheses sur un trait geologique fondamental des zones intraplaques, Geochronique, Vol.4, pp 12-14.

BONIN B., PLATEVOET B., VIALLETTE Y., 1987, The geodynamic significance of alkaline magmatism in the western mediterranean compared with West Africa, in African Geology Reviews., Eds. Bowden P., Kinnard J. A., Geol. J., 22, pp 361-387.

BONIN B., 1987, Reflexions a propos de la repartion des granitoides dans les massif cristallins externes des Alpes françaises., Geol. Alpine, Grenoble, 63, pp 137-149.

BONIN B., BRANDLEIN P., BUSSY F., DESMONS J., EGGENBERGER U., FINGER F., GRAF K., MARRO C., MERCOLLI I., OBERHANSLI R., PLOQUIN A., VON QUADT A., VON RAUMER J., SCHALTEGGER U., STEYRER H.P., VISONA D. and VIVIER G., 1993, Late Variscan Magmatic Evolution of the Alpine Basement., in Pre-mesazoic Geology in the Alps, Eds. J.F. von Raumer and F. Neubauer, Springer Verlag, Berlin, pp 171-201.

BORDET P. and BORDET C, 1963, Belledonne-Gdes Rousse et Aiguilles Rouges-Mont Blanc: quelques donnes nouvelles sur leurs rapports structuraux., in Livre a la mem. Prof. Fallot, Mem. Soc. Geol. Fr., 311-316.

BOUDON J., GAMOND J.F.,GRATIER J.P., ROBERT J.P., DEPARDON J.P., GAY M., RUHLAND M., VIALON P. (1976) L'arc alpin occidental; réorienation des structures primitivement E-W par glissement et érirement dans un système de compression globale N-S. Eclogae Geol. Helv., vol. 69/2 ,p. 509-516

BOUDREAU A.E.,McCALLUM I.S.(1989) Investigations of the Stillwater Complex: Part V. Apatites as indicators of evolving fluid composition. Cont. Min. Pet. Vol. 102, pp 138-153

BRODIE K. H. AND RUTTER E.H., 1987, Deep crustal extensional faulting in the Ivrea Zone of Northern Italy, Tectonophysics, 140, pp 193-212.

BUFFET G., and AUMAITRE R., 1979, Implications tectoniques possibles des filons carbonifere et triasique de la partie Sud et Ouest du massif cristallin des Ecrins-Pelvoux, Geol. Alpine, Grenoble, 55, pp 33-43.

BUFFIERE J.M. 1964 Les formations critallines et cristallophyliennes du massif du Rochail (Secteur Nord-Ouest du Massif du Pelvoux, Isère.) Extrait des travaux du Laboratoire de Géologie de la Faculté des Sciences de Grenoble.

BURNHAM and NEKVASIL, 1986

BURNHAM C.W. 1975 Waters and magmas; a mixing model. Geoch. Cormoch. Acta, no. 39/8.

BURNHAM C. W., 1979,

BUSSEL M.A. 1984 The centered complex of the Rio Huaura: a study of magma mixing and differenciation in high-level magma chambers. In magmatism at a plate edge- the peruvian Andes. John Viley and Sons, ed. New-York. pp128-151.

BUTLER R.W.H., MATTHEWS S. J. and PARISH M., 1986, The NW external Alpine Thrust belt and its implications for the geometry of the western Alpine Orogen., in Collision Tectonics, Eds. Coward M.P. and Ries A.C., Special publication Soc. Geol. Lond. 19, pp 245-260.

CAMBOLY J. (1966) Etude pétrographique et géochimique des granites de la région du Vic Habeautupt (Vosges) et de leurs enclaves. Thèse 3 cycle, Nancy, 1 vol.87 p.

CARME F., 1965, Sur deux formations d'origine volcanique, des schists cristallins anti-houillers de la chaine de Belledonne (Alpes francaises) C. R. Acad. Sci., Paris, 260, 9, pp 6401-6404.

CARME F., 1970, Age brioverien probable de la majeure partie des series supposees devono-dinantiennes et existance d'un cycle orogenique ante- hercynien, sans doute cadomien, dans la chaine de belledonne (Alpes francaises). C. R. Acad. Sci., Paris, 271, d, 631-633.

CARME F., 1973, Precisions nouvelles sur l'ampleur de la tectonique tangantielle hercynienne dans la chaine de Belledonne., C. R. Acad. Sci., Paris, 277D, 2309-2312.

CARME F., 1975, Le massif basique de Chamrousse et du Tabor (chaine de Belledonne, Alpes occidentalles): une variante originale de complexe alpinotype et un jalon majeur d'une ceinture basique brioverienne., C; R; Acad. Sci., Paris, 281D, 223-236.

CARME F. (1978) Les granitoides à affinité monzonitique du complexe granitique du St. Colomban (Chaine de Belledone, Alpes Occidentales.) Etude géochimique et essai d'interprétation génétique.C.R. Acad. Sc. Paris, t. 286, no. 17, p. 1233-1235.

CARME F. and PIN C, 1987, Vue d'ensemble sur le magmatisme pre-orogenique et l'evolution metamorphique et tectonique varisques dans le sud de la chaine de Belledonne (Massifs cristallins externes, Alpes frabcaises)., C. R. Acad. Sci., Paris, 304, II, 19, pp 1177-1180.

CHAMPENOIS M. (1982) Etude d'écaillage en haut Dauphiné occidental: secteur du Clapier du Peyron- Valsenestre. Mém. D.E.A., Nancy,(1982)

CHAPPEL B. W. and STEVENS W. E., 1988, Origin of infracrustal (I-type) granite magmas., Trans. Roy. Soc. Ed. Earth Sciences, 79, pp 71-86.

CHAPPEL B. W. and WHITE A. J., 1974, Two contarsting granite types., Pac. Geol., 8, pp 173-174.

CHAUVEL and JAHN, 1984

CLARKE ET AL., 1983

COCHERIE A. (1978): Geochimie des terres rares dans les granitoides, These 3eme cycle, Rennes, 207p.

COCHERIE A. (1985): Interaction manteau croute: son role dans la genese d'assocciations plutoniques calcoalcalines, contraintes geochimiques (elements en trace et isotopes du strontium et de l'oxygene), These de Doctorat d'Etat, Documents du BRGM, 231p.
COSTARELLA R. (1987): Le complexe annulaire alcalin de combeynot (massifs Cristallins Externe, Alpes francaises), temoin d'un magmetisme en regime distensif. Petrologie et signification geodynamique. These d'universite, Grenoble 1, Mention Sciences de la Terre, 286p.
Costarella, 1987

COUTURIE J.P. (1977) Le massif granitique de la Margeride (Massif Central Français) Ann. Fac. Sci. Clermont, no.62, 319 pp.

CZAMANSKE G.K., ISHIHARA S., ATKIN S.A., 1981, J. Geophys. Res., 86, pp 10431-10469.

CZAMANSKE G.K., WONES D.R. (1973) Oxidation during magmatic differenciation, Finmarka Complex, Oslo Area Norway: part 2- the mafic silicates. Journ. petrol., V. 14, no. 3, pp349-380.

D'ARCO P. (1982) Contribution à l'interprétation géothermométrique des paragénèses calco-alcalines de l'arc des Petites Antilles: critallisation fractionnée de la série du Quill (Ile de Saint Eustache) Thèse 3 cycle, wbrest, 1982.

DAUBREE A. (1967) Classification adoptée pour la classificationdes roches du Muséum d'Histoire Naturelle de Paris. Masson, ed. 1 vol. 47 pp.

de BOISET T., VITTOZ P., VIVIER G., OLIVER R. (1984): Association acide-basique dans le massif du Rochail; NW Pelvoux; massifs cristallins externes. Relations structurales, 10ème R.A.S.T. Bordeaux, p.70.

de BOISSET 1986, Les enclaves basique du granite du Rochail (syenite de Lauvitel), Haut Dauphine, Alpes Francaises, These 3eme cycle, (unpublished), Grenoble.

De SOETE D., GIJBELS R., HOSTE J., Neutron Activation Analysis, Wiley Interscience, London, Publishers.

DEBELMAS J. and KERKHOVE C., 1980, Geologie des Alpes franco-italiennes., Geol. Alpine, Grenoble, 56, pp 21-58.

DEBON F. and LE FORT P., 1982, A chemical - mineralogical classification of common plutonic rocks and associations., Trans. Roy. Soc. Edin., Earth Sciences, 73 pp135-149.

DEBON F., CHOCHERIE A., MENOT RP., VIVIER G. and BARFETY JC., 1994, Datation du plutonisme magnesien varisque des massifs cristallins externes des Alpes: l'example du granite des Sept Laux (massif de Belldonne, France)., C; R; Acad. Sci., Paris, 318 II, pp 1497-1504.

DEBON F. 1975 Les massifs granutoides à structure concentrique de Cauterets-Panticosa (Pyrénées Occidentales) et leurs enclaves. Mém. Sci. de la terre, no.33 Nancy, 1 vol., 420 pp.

DEER W.A., HOWIE R.A., ZUSSMAN J. 1965 Rock forming minerals.John Viley, New-York, 5 vol.

DELONG S.E.,CHATELAIN C. 1989 Complementary trace element fractionation in volcanic and plutonic rocks: imperfect examples from ocean floor basalts and gabbros, Cont. Min.Pet., Vol 102, pp 154-162

DEMEULEMEESTER P. (1982) Contribution à l'étude radiometrique de l'Argon et au Strontium des massifs cristallins externes (Alpes français).Thèse 3 cycle, Grenoble, 1 vol. 228 pp.

DESTHIEUX F., VERNET J. (1968) Les failles intenses du flanc Nord du Rochail. Géol. Alpine, t. 44.

DESTHIEUX F., VERNET J. (1970) Nouvelles données pétrographiques et structurales sur la région du Lauvitel (massif du Pelvoux).Géologie Alpine, t.46, 1970, p.67-76.

DIDIER AND LAMEYRE, 1969 Les granites du Massif Central francais: etude comparée des leucogranites et granomonzodiorites. *Contrib.Miner. Petrol.*, Vol 24, pp219-218

DIDIER J. (1964) Etude pétrographique des enclaves de quelques granites du Massif Central Français. Ann. Fac. Sc. Clermont, no.23 , 254 pp.

DIDIER J. (1973) Granites and their enclaves. Elsevier Publi. Comp. 1 vol, 393 pp.

DIDIER J. (1983) Indications génétiques fournies par la distribution des principaux types d'enclaves dans les granitoides. C.R.A.S. Paris, 296, 765-767

DIDIER J., ROQUES M. (1959) Sur les enclaves des granites du Massif Central Français. C.R.A.S., t. 248, p. 1839.

DODGE et al.,1968

ECHTLER H. AND MALAVIELLE J., 1990, Extensional tectonics, basement uplift and Stephaneo-Permian collapse in a late Variscan metamorphic corecomplex (Montagne Noire, Southern Massif Central). Textonophysics, 177, pp 125-138.
EGGLER D.H. (1972) Amphibole stability in H2O undersatured calc-alkaline melts. Earth planet Sci. lett., 15, 28-34.

EISBACHER G.H., LÜSCHEN E. AND WICKERT F., 1989, Crustal scale thrusting and extension in the Hercynian Schwarswald-Vosges, Central Europe, Tectonics, 8, pp 1-21.

ENGLAND P.C., THOMPSON A.(1986): Some thermal and tectonic models for crustal melting in continental collision zones, Collision tectonics, Geological Society Special Publication N 19 pp. 83-94, Coward M.P. et Ries A.C.(Eds).

ERNST W.G. 1968 Amphiboles. Springer-Verlag-Berlin, New-York, 125 pp.

ESPERANCA S. and HOLLOWAY J. R., 1987, On the origin of some mica-lamprophres: experimental evidence from a mafic minette., Contrib. Min. Pet., 95, pp 207-216.

FABRIES J., CONQUERE F., ARNAUD G. 1984 The mafic silicates in the Saint Quay-Portrieux gabbro-diorite intrusion: cristallisation conditions of a calc-alkaline pluton. Bull. Mineral., 715-736.

FINGER F. and STEYRER H.P, 1991, Reply to comments, Geology, **, pp 1245-1248.

FINGER F. and STEYRER H.P., 1990, I-type granitoids as indicators of alate Paleozoic convergent ocean-continent margin along the southern flank of the central european Variscan orogen, Geology, 18, pp 1207-1210.

FLOYD P.A. and WINCHESTER J. A., 1978, Identification and discrimination of altered and metamorphosed volcanic rocks using imobile elements., Chem. Geol., 21, pp 291-306.

FLUCK P., 1980, Metamorphisme et magmatisme dans les Vosges moyennes d'Alsace. Contributions a l'histoire de la chaine varisque. These, Strasbourg (unpublished), 248p.

FOLEY S.F., VENTURELLI G., GREEN D.H. and TOSCANI L., 1987, The ultra potassic rocks: characteristics, classification and constraints for petrogenetic models, Earth Sci. Rew., 24, pp 81-134.

FONTEILLES M. 1968 Les mécanismes de la métasomatose. Bull. Minéral., vol. 101, pp.166-194.

FOSTER M.D. (1960) Interpretation of the composition of trioctahedral micas. U.S.Geol. Survey Prof. Paper, 354 p.,49 pp.

FOURCADE S., and ALLÈGRE C.J.(1981): Trace elements behavior in granite genesis: A case study. The Calc-Alkaline Plutonic Association from the Querigut Complex(Pyrénées, France),Contrib. Mineral. Petrol., n 76, pp. 177-195.

FOURNET J. (1861) Note sur les roches éruptives modernes du Lyonnais. Bull. Soc. Géol. Fr., 2 série, 18, pp677-678.

FOWLER M.B. (1988) *Geology* Vol.16, pp 1026-1030

FREY F.A., CHAPPELL B. W., ROY S.D., 1978, Fractionation of rare earth elements in the Tuolumne Intrusive Series, Sierra Nevada batholith, California., Geology, 6, pp 239-242.

GAGNY C. (1968) Pétrogénèse du granite des crêtes- Vosges méridionales, France.Thèse ès Sciences, Nantes, 1 vol. 481 pp.

GAGNY C. (1978) Vaugnérites et durbachites sont des cumulats de magma granitique-(l'exemple du magma des crêtes, Vosges).C.R. Acad. Sci, Paris, D., t.287,pp 1361-1364.

GASQUET D. (1979) Etude pétrologique, géochimique et structurale des terrains cristallins de Belledone et du Grand Châtelard traversés par les galeries E.D.F. Arc Isère-Alpes françaises. Thèse 3 cycle, Grenoble, 1979.

GASQUET D., GIRAUD P., PLOQUIN A., VIVIER G., 1981, Geochilie des mylonites et relations entre les Rameaux Internes et Externes du Massif de Belledonne (Alpes francaises) C; R; Acad. Sci.,Paris, 292D, pp 607-610.

GAST P. W., 1968, Trace element fractionation and the origin of theoliitic and alkaline magma types. Geochim. cosmochim. Acta, 32, pp 1057-1086.

GAY N.C. (1968) The motion of rigid particles embedded in a viscousfluid during pure shear deformation of the fluid. Tectonophysics 5, pp 81-88

GIBERGEY P., 1968, Decouverte de "gres a trou" renferment des debris d'organismes dans les schistes noirs du Valbonney (serie cristallo-phyllienne des massifs cristallins externes des Alpes francaises), C. R. Acad. Sci., Paris, 267D, pp 1251-1254.

GIDON M. (1979) Le rôle des étapes successives de deformation dans la tectonique alpine duMassif du Pelvoux. C.R. Acad. Sc. Paris, 288, p.803-806.

GIL IBARGUCHI J.I., BOWDEN P., WHITLEY J.E.(1984): Rare earth element distribution in some Hercynian granitoids from the Finisterre region, NW Spain, Journal of Geology, vol. 92,p.397-416.

GIORGI L. (1979) Contribution à l'étude géologique des terrains cristallins du massif des Grandes Rousses, Isère, France. Thèse 3 cycle, Grenoble, 1 vol.

GIORGI L., GIRAUD P., VACHARD D. (1979) Sur la présence de micro organisme d'âge Cambrien dans les schistes cristallins du versant occidental du Massif Cristallin Externe des Grandes Rousses (Alpes Occidentales). C.R.A.S., t. 288, série D. p 1070-1082

GIORGI L., GIRAUD P., VIVIER G. (1979) La série cristallophylienne du versant occidental du Massif Cristallin Externe des Grandes Rousses. 7 R.A.S.T. Lyon, 1979, 218 p.

GIRAUD P. (1952) Les terrains métamorphiques du Massif des Grandes Rousses. Bull. Soc. Geol. France-6 série- Tome 2, pp 379-402.

GIRAUD P., VIVIER G.(1980): Les granites des massifs Cristallins Externes des Alpes Françaises. Les granitoides de la France, Evolution géologique de la France, 26ème C.G.I., Paris.

GLADNEY E.S., CURTIS D.B., PERRIN D.R., 1985, Determination of selected rare earth elements in 37 international geochemical reference materials by instrumental thermal prompt gamma-ray speectrometry, Geostandards Newsletter, 9, pp 25-30.

GORBATSCHEV R. (1970) Distribution of tetrahedral Al and Si in coexisting biotite and Camphibole. Contrib. Mineral. Petrol., v.28, no.3 pp 251-258.

GOVINDARAJU K., MEVELLE G.(1987): Fully automated dissolution and separation methods for inductively coupled plasma atomic emission spectrometry rock analysis. Application to the determination of rare earth elements, J. of Analy. Atom. Spectro., 2,pp. 615-621.

GRATIER J. P. and VIALON P., 1980, Deformation pattern in a heterogeneous material: folded and cleaved sedimentary cover immediately over-lying a crystalline basement (Oisans, French Alpes), Tectonophysics, 65, pp 151-180.

GRAVIOU P. (1984) Pétrogénèse des magmas calco-alcalins: exemples des granitoïdes Cadomiens de la région Trégorroise (Massif Armoricain). Thèse 3 cycle, Rennes.

GREEN T. H. and RINGWOOD R. E., 1968, Genesis of the calc-alkaline igneous rock suite. Contrib. Min. Pet., 18, pp 105-162.

GREEN T.H., and WATSON E. B., 1982, Cristallization of apatite in Natural Magmas under High Pressure, Hydrous Conditionss, with particular reference to "Ozogenic" rocks series. Contrib.Mineral. Petrol.(1982) 79, 96-109.

GREENLAND L.P.,GOTTFRIED D., TILLING R.I. (1968) Distribution of mznganese between coexisting biotite and amphibole in plutonic rocks. Geoch. Cosmoch. Acta. 1968, vol.32, pp1149-1163.

GROS Y. (1974) Etude pétrologique et structurala du Beaufortin (Nord de Belledonne).Thèse 3 cycle, Grenoble.

HAMEURT J., 1968, Les terrains cristallins et cristollophylliens du versent occidental des Vosges moyennes. Mem. Serv. Carte Geol. Als. Lorr., 26, pp 402.

HAMIDULLAH S. and BOWES D. R., 1988, Petrogenisis of the appinite suite, Appin district, Western Scotland., Acta Univ. Carolinae Geol., 1987(4), pp 295-396.

HANSON G. N., 1978, The application of trace elements to the petrogenesis of igneous rocks of granitic composition., Earth Planet. Sci; Letts., 38, pp 26-43.

HARDER H. 1975 Boron in Igneous Rocks, in Geochemistry of Boron, Ed. Walker C.T., Benchmark Papers in Geology, Dowden, Hutchinson & Ross, INC.,Pennsylvania, Publishers.

HARISSON and WATSON, 1984

HARKER A. (1909) The natural history of igneous rocks. New-York -Macmillan ed.,384 p.

HARRIS N.B.W., PEARCE J.A., TINDLE A.G.(1986): Geochemical characteristics of collision zone magmatism,Collision tectonics, Geological Society Special Publication N 19 pp.67-81, Coward M.P. et Ries A.C. (Eds).

HARRY W.T. (1950) Aluminium reeplacing silicon in some silicate lattices. Min. Mag., 29, 142-149.

HEINRICH E.W. (1946) Studies in yhe mica group: the biotite-phlogopite series. Amer. Journ. Sci. v 244, pp 836-848.

HELLMAN P.L., GREEN T.H. (1979) The role of sphene as an accessory phase in the high pressure partial melting of hydrous mafic compositions Earth and Planetary Sci-Lett. 42 (1979) 191-201.

HELZ R.T. (1973) Phase relations of basalts in their melting range of PH2O: 5kb as a function of oxygen fugacity. Part 1: mafic phases. Journ.Petrol. pp249-302.

HELZ R.T. 1982 Phase relations and compositions of amphiboles produced in studies of the melting behaviour of rocks. In: VEBLEN D.R. RIBBE R.H. (eds) Amphiboles: petrology and experimental phase relations. Mineral Soc. Am. Reviews in Mineralogy, vol. 9B, pp 279-347.

HOLLOWAY J.R., BURNHAM C.W. 1972 Melting relations of basalt with equilibrium water pressure less than total pressure. J. Petrol. 13, 1-29

HOLUB F. V., 1977, Petrology of inclusions as akey to petrogenesis of the durbachitic rocks from Czechoslovakia. Tschermaks. Men. pet. Mitt., 24, pp 133-150.

HUTTON D., 1981, The Main Donegal granite: lateral wedging in a syn-magmatic shear zone. J. Struct. Geol., 3, 93.

IRVING A.J., 1978, A review of experimental studies of crystal/liquid trace element partitioning., Geochim. Cosmochim. Acta, 42, 743-770.

JAKES P., WHITE A.J.R. (1972) Major and trace elements abundances in volcanic rocks of orogenic areas. Geol. Soc. Amer. Bull; 83 pp 29-40

JAUPART C., BRANDEIS G., ALLEGRE C.J. (1984) Sur l'existence d'une couche stagnante à la base des chambres magmatiques convectives. 10 R.A.S.T. Bordeaux 1984

JOHANNSEN A. (1931-1939) A descriptive photography of the igneous rocks. Univ. Chicago Press-Illinois. Part II, 5 ed., 1958.

JUNG J., BROUSSE R. (1959) Classification modale des roches éruptives utilisant les données fournies par les compteur depoints. Masson ed. I vol. 122 pp.

KAWAKATSU K. and YAMAGUCHI Y. (1987) Successive zoning of amphiboles during progressive oxydation in thje Daiti-Yokota granitic complex, San-In belt, Southwest Japan, Geochimica Cosmochimica Acta, Vol 51, pp 535-540.

KROHE A. and EISBACHER G.H., 1988, Oblique crustal detachment in the Variscan Schwarzwald, southwestern Germany, Geologishe Rundschau, 77, pp 25-44.

LA ROCHE H. de (1964) Sur l'expression graphique des relations entre la composition chimique et de la composition minéralogique quantitative des roches cristallines. Sci. de la terre - Nancy t. IX, no.3,pp 293-337.

LA ROCHE H. de, LETERRIER J. (1973) Transposition du tetraèdre minéralogique de Yoder et Tilley dans un diagramme chimique de classification des roches basaltiques. C.R. Acad. Sci., Paris t. 276,D, pp3115-3118.

LA ROCHE H de., 1976, Sur la contributiondes donnees chimiques a une systematique generale des roches ignees. Sci. de la Terre, 21, pp 17-35.

LA ROCHE H., STUSSI J.M.1982:A contribution to the development of regional geochemical mapping based on the example of the French Variscan Granitoids, ECC, Environment and raw materials Research Programmes, Section "Geochemical Methods",Project 02040-Contract N 013-79-4-MPP-F

LACOMBE J.C. 1970 Etude pétrographique de la partie orientale du massif des Ecrins, Pelvoux; le complexe volcano-sédimentaire.Thèse 3 cycle, Grenoble.

LACROIX A. 1893 Les enclaves des roches volcaniques. Protat ed., Mâcon, 770 p.

LACROIX A. 1917 La composition chimique de la vaugnérite et la position de cette roche dans la systématique . Bull. Soc. Fr., Min., t. 11, p.158-162.

LAMEYRE J. (1958) La partie Nord du massif des Grandes Rousses (TLG,t.34)

LAMEYRE J. (1980) Les magmas granitiques: leurs comportements, leurs associations et leurs sources. Mém. h. sér. Soc. Géol. de France, 1980 no. 10

LAMEYRE J. et BOWDEN P. (1982) Plutonic Rock Type Series: discrimination of various granitoides series and related rocks. J. Volcan. Geoth. Res., 14, p.169-186

LAMEYRE J.,AUTRAN A. (1980) Les granitoïdes de France- extrait de: Evolutions géologiques de la France. Mém. BRGM no.107,pp 51-97

LAMEYRE, J., 1957, Le complexe volcanique de la partie nord du synclinal Hercynien oriental du massif des Grandes Rousses, C. R. Somm. Soc Geol. France, 9, p 157.

LAPORTE ,1987

LAPPARENT A. de (1893) Traité de géologie. Ed. Masson - 3 ed., 2 vol. 1645 pp.

LATOUCHE L. and BOGDANOFF S., 1987, Evolution precoce du Massif de l'Argentera: apport des eclogites et des granulites. Geol. Alpine, Grenoble, 63, pp 151-164.

LAURENT R., 1968, Etude geologique et petrographique de l'extremite meridionale du Massif des Aiguilles Rouges (Htes. Savoie) Arch. Sci. Geneve, 20, 2, pp 223-254.

LAURENT J.C., 1993, Les episodes magmatiques filoniens basique du Massif des Ecrins-Pelvoux entre Carbonifere et Lias., These, Universite de Grenoble, (unpublished), 240p.

LE FORT P. (1970): Geologie du haut Dauphine cristallins (Alpes Francaises). Etude petrologique et structurale de la partie occidentale, These Sci. de la Terre, Memoires, nancy, N25, 373p.

LE FORT P.,PECHER A. (1971) Présentation d'un schéma structural du Haute Dauphiné cristallin. C.R.A.S. Tome 273, pp 3-5.

LE FORT P. (1973) Géologie du Haute Dauphiné (Alpes françaises) Etude pétrologique et structurale de la partie occidentale. Sc. de la terre - Nancy - Mém. 25.

LE FORT P.,PECHER A. (1981) Présentation d'un schéma structural du Haute Dauphiné pour l'excursion sur les granitoïdes du cristallin externe des Alpes françaises, Sept. 1981.

LE MAITRE R. W., 1989, A Classification of Igneous Rocks and Glossary of terms. Blackwell, Oxford.

LEAKE B.E. (1965) The relationship between tetrahedral aluminium and the maximum possible octahedral aluminium in natural calciferous and subcalciferous amphiboles. Amer.Mineral.,vol.50,no.7-8,pp843-851.

LEAKE B.E. (1968) A catalog of analyzed calciferous and subcalciferous amphiboles together with their nomenclature and associated minerals. Geol. Soc. Amer. Spec. Paper no.98,210 pp;

LEAKE B.E. (1978) Nomenclature of amphiboles. Amer. Mineral. vol.63, page 1023-1052 (1978)

LEMOINE M.,GIDON M.,BARFETY J.M. (1981) Les Massifs Cristallins Externes des Alpes occidentales: d'anciens blocs basculés nés au lias lors du rifting tethysien. C.R. Acad.Sci.Paris.t.292 (1981).

LETERRIER J. (1972) Etude pétrographique et géochimique du massif granitique du Quétigut (Ariège) Thèse ès Sciences, Nancy, I vol. 292 pp;

LETERRIER J.,DEBON F. (1978) Caractères chimiques comparés des roches granitiques et de leurs enclaves microgrenues. Implications génétiques. Bull. Soc. Geol. France, 1978 (7), txx, no.1,p 3. 20.

LIEGEOIS J. P. and DUCHESNE J.C., 1981, The lac Cornu retrograded eglogites (Aiguilles Rouges Massifs, Western Alpes, France): evidence of crustal origin and metasomatic alteration., Lithos, 14, pp 35-48.

LORY Ch. (1981) Sur les schistes cristallins des Alpes occidentales et sur le rôle des failles dans la structure géologique de cette région. Bull. Soc. Géol. Fr. (3) 9, p.652-679.

MACARTHY T.S.and HASTY R.A., 1976, Trace element distribution patterns and their relationship to the crystalization of granitic melts. Geochim. Cosmochim. Acta, 40, pp 1351-1358.

MACDONALD R.,THORPE R.S., GASKARTH J.W., GRINDROD A.R., 1985, Multi-component origin of Caledonian lamprophyres of northern England., Min. Mag., 49, pp 485-494.

MALAVEILLE J., GUIHOT P., COSTA S., and LARDEAUX J.M., 1990, Collapse of the thickened crust in the French massif Central: Mont Pilat extensional shear zone and St Etienne late Carboniferous basin, tectonophysics, 177, 139-149.

MARRE J.(1975) L'écoulement magmatique des matériaux homogènes dans le complexe éruptif de Quérigut (Pyrénées, France).Pétrologie 1, pp 17-36.

MARRE J. (1982) Méthode d'analyse structurale des granitoïdes. Manuels et méthodes, vol. 3., BRGM.

MATTE P., 1986, La chaine varisque parmi les chaines paleozoiques peri-atlantique, modele d'evolution et position des grandes bloques continentaux au Permo-Carbonifere., Bull. Soc. Geol. Fr., 8, II, 1, pp 9-24.

McCARTHY T.S.and GROVES D.I., 1979, The Blue Tier batholith, North eastern Tasmania. A cumulate-like product of fractional crystallisation. Cont. Min. Pet., 71, pp 193-209.

MEEN J.K.,EGGLER D.H. (1989) Chemical and isotopic compositions of Absaroka granitoids, Southwestern Montana, Cont. Min. Pet., Vol. 102, pp 462-477

MENOT R.P., 1987, Magmatismes et structuration orogenique paleozoique de la chaine de Belle donne (Massifs Cristallins externes). Le domaine Sud- occidental., Geol. Alpine, Grenoble, 63, pp 55-93.

MENOT R.P., PEUCATJ.J., SCARENZI D., PIBOULE M., 1988, 496 Ma age of plagiogranites in the Chamrousse ophiolite complex (External Crystalline Massifs in the French Alpes): evidence of a Lower Paleozic oceanization. Earth Plan. Sci. Lett., 88 (1-2), pp 82-92.

MENOT R.P.,BONHOMME M.G.,VIVIER G. (1985) Upper visean cooling ages of amphiboles - isotopic evidence of a late variscan nappe tectonic in the Belledonne massif (French External Alps). Terra Cognita, vol.5, no.2-3, D.18, 1985.

MENOT R.P.,VIVIER G.(1986) Décrochements et chevauchements varisques dans le massif de Belledonne 11 R.A.S.T. 1986.

MERCOLLI I. and OBERHANSLI R., 1988, Variscan tectonic evolution in the Central Alps: a working hypothesis. Schweiz Min. Pet. Mitt., 68(3), pp 491-500.

MERGOIL DANIEL J. (1970) Les feldspaths potassiques dans les roches métamorphiques du Massif Central Français. Ann. Fac. Sci. Clermont,

MICHEL LEVY A., LACROIX A. (1887) Sur le granite à amphibole de Vaugneray (vaugnérite du Fournet)Bull. Soc. Fr. Minéral.Paris, tx, pp 27-31

MICHEL R., BUFFIERE J.M. 1963a Caractères pétrographiques et pétrochimiques du granite du Massif du Rochail (secteur NW du massif du Pelvoux, Isère). C.R.A.S. 256, p 1812.

MICHEL R.,BUFFIERE J.M. 1963b Sur la nature et l'origine de la syénite du Lauvitel (Massif du Rochail, secteur NW du Pelvoux,Isère) C.R.A.S. 256, p 225-227.

MICHON G. (1979) Typologie des vaugnéritesdes Monts du Lyonnais et du Haut Vivarais, Massif Central français. Thèse 3 cycle, Lyon, 1 vol.

MICHON G. (1984) Les vaugnérites de l'Est du Massif Central français. Apport de l'analyse statistique multivariée. 10 R.A.S.T. Bordeaux (1984).

MITCHELL ET AL., 1987

MONIE P., MALUSKI H., 1983, Donnees chronologiques $^{39}Ar/^{40}Ar$ sur le socle ante-Permien du massif de l'Argentera - Mercontour (Alpes Maretimes, France), Bull; Soc. Geol. Fr., 7, XXV, pp 247-257.

MONTEL J.M. and WEISBROD A., 1986, Characteristics and evolution of "Vaugneritic magmas", an analytical and experimental approach, on the example of the Ceven medianes (French massif Central) Bull. Min. Fr., 109, pp 575-587.

MOORE A.C. (1976) Untergrowth of prehnite and biotite. Mineral. Mag., v.40, pp526-529.

MUELLER R. (1972) On the stability of biotite; a discussion. Am. Mineral, 57, N 162 pp 300-316.

NACHIT H., RAZAFIMAHEFA N., STUSSI J.M., CARRON J.P.(1985) Composition chimique des biotites et typologie magmatique des granitoïdes. C.R. Acad. Sc. Paris, t. 301, Série II, no.11

NAKAMURA N. (1974): Determination of REE, Ba, Fe, Mg, Na and K in carbanceous and ordinary chondrites Geoch. Cosmo. Acta, Vol. 38, pp 757-776.

NOCKHOLDS S.R. (1947) The relation between chemical composition and paragenesis in the biotite micas of igneous rocks. Amer. Journ. Sci., v. 245, pp 401-420.

OBERHANSLI R., SCHENKER F., MERCOLLI I., 1988, Indications of Variscan nappe tectoniques in the Arr massif. Schweiz. Min. Pet.Mitt., 68(3), pp 509-520.

OBERHANSLI R., 1986, Geochemistry of meta-lamprophyres from the Central Swiss Alps., Schweiz. mineral.petrogr. Mitt., 66, pp 315-342.

ODLING N.W.A., 1994, An experimental simulation of upper mantle metasomatism., Am. Min., 79, pp 148-153.

OHNENSTETTER M., ROSSI P. (1987): Signification des complexes basiques-ultrabasiques associes aux granitoides dans l'evolution de la chaine varisque du Sud de l'europe, Bull. Soc. Geol. France, T.III N5, pp 801-810.

OLIVER R.A., VITTOZ P., de BOISSET T., VIVVIER G., 1981, Bimodal magmatism in the French Western Alps, J. Open Univ. Geol. Soc., 4, pp 1-6.

OLIVER R.A., VITTOZ P., VIVIER G., KERR S.A., HOYLER F., 1988, The measurement of low elemental concentrations in geolgical reference materials by neutron capture prompt gamma-ray spectroscopy., Inst. Phys. Conf. Ser. 88, Capture Gamma-ray spectroscopy 1987, EdsAbrahams K. and van Assche P., pp 599-603.

OLIVER R.A., ROBINSON S., VITTOZ P., VIVIER G., 1989, The method of Instrumental Activation Analysis as practiced at the ILL, together with the abundance of 16 elements in twenty one international standard reference materials measured by this method. ILL Technical report, 900L15T, 11p.

OLIVER R.A.,VITTOZ P.,BOISSET T. de,VIVIER G.,KERR S.A. (1985) Bimodal magmatism in the Western French Alps. Journal of the Open University Geological Society.,

OLIVER R.A.,VITTOZ P.,BOISSET T. de,VIVIER G.,KERR S.A.,HOYLER F. (1988) The measurement of low elemental concentrations in geoligical reference materials by neutron capture prompt gamma-ray spectroscopy. in Capture Gamma-ray Spectroscopy 1987, Inst. of Phys. Conf. Series No.88, K. Abrahams and P. Van Asche Eds.

ORSINI J.B. (1976) Les granitoïdes hercyniens corso-sardes; mise en évidence de deux associations magmatiques. Bull. Soc. Geol. Fr., 18, pp.1203-1206.

ORSINI J.B. (1980) Le batholite Corso-Sarde: anatomie d'un batholite hercynien. Composition, structure, orginisation d'ensemble, sa place dans la chaine varisque française. Thèse,Marseille, 390 p.

OZOCAK R. (1965) Etude pétrographique des schistes cristallins et des granites de la haute vallée du Vénéon (Massif du Pelvoux). Thèse 3 cycle, Grenoble.

PAGEL M.,LETERRIER J. (1980) The subalkaline potassic magmatism of the Ballons Massif (Southern Vosges, France): shoshonitic affinity. Lithos, 13, p.1-10.

PAGEL M., 1981, Facteur de distibution et de concentration de l'uranium et du thorium dans quellques granites de la chaine hercyniene d'Europe. These d'Etat, INPL, 566p.

PALM Q.A.(1970) Vaugnérites et amphibolites. Deux types de roches amphiboliques dans les Cévennes à la hauteur de Largentière (Ardèche). Bull. Soc. Géol. Fr. t.4, pp 627-641.

PAQUETTE J.L., 1987, Comportiment des systeme isotopique U-Pb et Sm-Nd dans le metamorphisme eclogitic. Chaine hercynienne et chaine Alpine., Cent. Amorc. d'Etude Struct. Soc., Rennes, 14, pp 1-189.

PAQUETTE J.L., MENOT RP., PEUCAT JJ., 1989, Sm-Nd and U-Pb zircon study of eclogites from the Alpine External massifs (Western Alpes): evidence for crustal contamination., Earth Plan. Sci. Lett., 96 (1-2), pp 181-198.

PEARCE J.A. and CANN J.R., 1973, Tectonic setting of basic volcanic rocks, determined using trace element analysis. Earth Plant. Sci. Lett., 19, pp 290-300.

PEARCE J.A., 1983 Role of the sub-continental lithosphere in magma genesis at active continental margins. in Hawksworth CJ and Norry M.J. Eds. Continental basalts and Mantle Xenoliths, Shiva, Cheshire, U.K., pp 230-249

PEARCE J.A., HARRIS N.B.W., TINDLE A.G. (1984): Trace element discrimination diagrams for the tectonic interpretation of granitic rocks, J. Pet., Vol. 25, pp 956-983.

PEARCE J.A., BENDER J.F., DELONG S.E.,KIDD W.S.F., LOW P.J., GUNER Y., SAROGLU F., YILLMAZ Y., MOORBATH S., MITCHELL J.G., 1990, Genesis of collision volcanism in Eastern Anatolia, Turkey., J. Vol. Geo. Therm. Reas., 44, pp 189-229.

PECCERILLO A., POLI G., TOLOMEO L., 1984, Genesis evolution and tectonic significance of K-rich volcanics from the Alban hills (Roman co-magmatic region) as inferred from trace element geochemistry., Cont. Min. Pet., 36, pp 230-240.

PECHER A. (1970) Etude pétrographique des schistes cristallins et des granites de la haute vallée du Vénéon (Massif du Pelvoux) Thèse 3 cycle, Grenoble.

PÉCHER A. (1971): Données nouvelles sur les granites paléozoiques du massif des Ecrins-Pelvoux (Alpes du Haut Dauphiné, France), Géologie Alpine, n 47, pp.91-102.

PECHER A. (1986) Notice de la carte géologique de la Mure -- A paraître.

PEISACH M. 1981 Prompt Techniques pp 93-111, in Nondestructive Activation Analysis, Ed. Amiel S., Elsivier Scientific Puplishing Co. NewYork, Publishers.

PETERLONGO J.M. (1960) Les terrains cristallins des Monts du Lyonnais (Massif Central français). Ann. Fac. Clermont,no.4, I vol. 187 pp.

PHAROAH T. and PEARCE J.A., 1984,

PITCHER W.S.AND BERGER A.R.,1972, The Geology of Donegal: a study of Granite Emplacement and Unroofing, Wiley Interscience, London, pp 4-35.

PITCHER W.S. 1993 The Nature and Origin of Granite, *BlackiePress*.

PONCERRY E. (1981) Contribution à l'étude géologique des granitoïdes de Valloreine, Beaufort, Lauzière, de leur encaissant et des minéralisations uranifères associées. Alpes françaises. Thèse 3 cycle, Grenoble.

PUPIN J.P.(1976): Signification des caractères morphologiques du zircon commun des roches en pétrologie. Base de la méthode typologique. Applications, Thèse de doctorat d'état, Nice 394 p.

PUPIN J.P.(1980): Zircon and granite petrology, Contrib. Mineral. Petrol., n73 pp.348-359.

PUPIN J.P., TURCO G. (1981) Le zircon, minéral commun significatif des roches endogènes et exogènes. Bull. Minéral. (1981), 104, 724-731.

RAASE P. (1974) Al and Ti contents of hornblende, indicators of pressure and temperature of regional metamorphism. Cotr. Mineral. Petrol., v. 45, no.3, pp 231-236.

RAMSAY J.G. (1967) Folding and fracturing rocks. Mac. Graw Hill, New-York, 568 p.

RICHE A. (1887) Etude géologique sur le Plateau du Lyonnais à l'occasion de l'établissement du chemin de fer de Lyon à Vaugneray et à Mornant. Pitrat, ed. Lyon, 1 vol. 90 pp.

RING U. AND RICHTER C., 1994, The Variscan structural and metamorphic evolution of the eastern South alpine besement, J. Geol. Soc., 151, pp 755-766.

ROBINSON P.,ROSS M.,JAFFE M.W. (1971) Composition of the anthophyllite gedrite series, comparisons of gedrite and hornblende, and the anthophyllite-gedrite solvus. Ann. Mineral, 56, pp 1005-1041.

ROCK N.M.S., GASKARTH J.W., and RUNDLE C.C., 1986, Late Caledonian dyke swarms in southern Scotland: a regional zone of primitive k-rich lamprophyrs and associated vents. J. Geol., 94, pp 505-522.

ROUBAULT M. (1963) Détermination des minéraux des Roches. Ed. Lamarre - Poinat - Paris.

SABATIER H. (1978) Remarques préliminaires sur quelques vaugnérites du Massif Central. C.R. Acad. Sci. Paris, t.286 (9/1/78) série D, 9.

SABATIER H. (1980) Vaugnérites et granites: une association particulière de roches grenues acides et basiques. Bull. Mineral (1980) 103, 507-522.

SANTALLIER D. co-ordinator (1983): Main metamorphic features of the paleozoic orogen in France, Contribution of the french working group, IGCP n 27.

SCHADE J. (1983): Le synclinal de St Martin de Belleville et son Permien uranifère (zone houillère briançonnaise- Alpes de Savoie), Thèse 3ème cycle, Grenoble, 250 p.
SCHILLING, 1971

SIDDENS A.W.B., 1983, Finite strain patterns in some Alpine nappes. J. Struct. Geol., 5, pp 441-448.

SIMEON Y. (1979) Etude pétrologique, géochimique et structurale du massif de Belledonne entre l'Arc et l'Isère (Alpes françaises). Thèse 3 cycle, Grenoble.

STOUT J.H. (1972) Phase petrology and mineral chemistry of coexisting amphiboles from Telemark, Norway. Journ, Petrol., 13, pp 99-145.

STRECKEISEN A. 1973 Classification and nomenclature of plutonic rocks. Recommendations (I.V.G.S.). N. Jb. Mineral - Mh, H4, pp149-164.

STRECKEISEN A. 1976)Classification of the common igneous rocks by means of their chemical composition. b. Miner. Mh, H1, pp 1-15.

STUSSI J.M. PLOQUIN A. (1983): Chronology and typology of the Caledono-Hercynian plutonism in France, Contribution of the french working group, IGCP n 27.

SUN and HANSON, 1975

SWANSON S.E., 1977, Amer. Miner., 62 pp 966-978.

TARNEY J. and JONES,C.E., 1994, Trace element geochemistry of orogenic igneous rocks and crustal growth models., J. Geol. Soc. London, 151, pp 558-868.

TERMIER P. 1896 Sur le sphène de la syénite du Lauvitel. B.S.F. Min. t. 19, p 81-85.

TERMIER P. 1897 Sur le graduel appauvrissement en chaux des roches éruptives basiques de la région du Pelvoux. C.R.A.S. t. 114, p. 637-666.

TERMIER P. 1900 Le Massif du Pelvoux et le Briançonnais. Livret guide du VIII Congrès Géologique Internatioal.

THOMPSON R.N., MORRISON M.A., HENDRY G.L., PARRY S.J., 1984, An assessment of the relative roles of crust and mantle in magma genesis: an elemental approach., Phil. Trans. R. Soc. Lond., A310, 549-590.

TINDLE A.G., PEARCE J.A., 1981, Petrogenetic modelling of in situ fractional crystallization in the zoned Loch doon pluton, Scotland. Contrib. Min. Pet., 78, pp 196-207.

TINDLE A.G., 1982, Petrogenesis of the Loch Doon Granitic intrusion, Southern Uplands of Scotland. Phd Thesis, The Open University, UK, (unpublished). 327p.

TRÖGER W.E. (1935) Spezielle Petrographie des Eruptivesteine. Deutschen Mineral. Gesellschaft. 1 vol., 342 pp.

TUTTLE O.F., and BOWEN N.L., 1958, Origin of granite in the light of experimental studies in the system $NaAlSi_3O_8$ - $KAlSi_3O_8$ - SiO_2 - H_2O., Geol. Soc. Amer. Mem., 74, 153p.

VELDE D., 1971, Les kersantites - etude des lamprophyres a plagioclases et biotites., Bull; Soc. Fr. Crist., 94, pp 411-426.

VENTURELLI G., THORPE R.S., DAL PIAZ G.V., DEL MORO A., POTTS J.P., 1984, Petrogenesis of calc-alkaline shoshonitic and associated ultra potassic Oligocene volcanic rocks from the North Western Alpes, Italy., Contr. Min. Pet., 86, pp 209-220.

VITTOZ P., COSTARELLA R., VIVIER G., OLIVER R.A., 1987 , Typologie des granitoides hercyniens et zonation magmatique dans le massif du Haut Dauphine., Geol. Alpine, 63, pp 119-136.

VIVIER G., MENOT R.P., GIRAUD P., 1987, Magmatismes et structuration orogenique Paleozoique de la chaine de Belldonne., Geol. Alpine, Grenoble, 63, pp 25-53.

VON RAUMER J.F., 1984a, The Hercynian basement in the Helvetic realm. Western and central Alps., Mem. Soc. Geol. Ital., 29, pp 57-69.

VON RAUMER J.F., 1984b The External Massifs, relics of Variscan Basement in the Alps. Geol. Rundsch., 73, pp 1-31.

VON RAUMER J.F., 1987, Les massifs du Mont Blanc et des Aiguilles Rouges: temoin de la formation de croute varisque dans les Alpes Occidentales., Geol. Alpine, Grenoble, 63, pp 7-24.

VON RAUMER J.F., 1988, Caledonian - Variscan structures in the Alps: an introduction., Schweiz. Min. Pet., 68, pp 291-299.

VON RAUMER J.F., and MENOT RP., 1989, Evolution Paleozoique du socle ouest alpin et place des Massifs Cristallins Externes dans l'orogene Varisque., C. R. Acad. Sci., Paris, 309, II, pp 397-402.

WATTERS B.R. and PEARCE J.A., 1987, Metavolcanic rocks of the La Ronge Domain in the Churchill Province, Saskatchewan., in Geochemistry and Mineralization or Proterozoic Volcanic Suites, Eds. Pharoah T.C. Beckinsale R.D. Rickard D., Special Pub. Soc Geol Lond., 33, pp 167-182.

WHITE A.R. and CHAPPEL B.W., 1977, Ultrametamorphism and granitoid genesis., Tectonophysics, 43, pp 7-22.

WHITE A.J.R. and CHAPPEL B.W., 1988, Some supracrustal (S-type) granites of the Lachlan Fold Belt., Trans R. Soc. Edin., Earth Sciences, 79, 169-182.

WINKLER and SCHULTES, 1982

WONES D.R. (1981) Mafic silicates as indicators of intensive variables in granitic magmas. Mining Geology, Vol 31 pp 191-212.

WYLIE P.J., 1983, Experimental and thermal constraints on the deep-seated parantage of some granitoid magmas in subduction zones., in Migmatites, Melting and Metamorphism, Eds. Atherton M.P. and Gribble C.D., Shiva, Cheshire, UK, pp 37-53.

APPENDICES

INSTITUT

MAX VON LAUE - PAUL LANGEVIN

90OL15T

THE METHOD OF INSTRUMENTAL ACTIVATION ANALYSIS AS PRACTICED AT THE ILL, TOGETHER WITH THE ABUNDANCE OF 16 ELEMENTS IN TWENTY ONE INTERNATIONAL STANDARD REFERENCE MATERIALS MEASURED BY THIS METHOD.

Richard A. OLIVER* , Stephen ROBINSON*,
Pascal VITTOZ+, Gerard VIVIER++

* ILL

156 X - 38042 GRENOBLE Cedex - France

INTRODUCTION

This report describes the methods used for the measurement of a number of Rare Earth and Trace elements, essentially in geological samples which have been developed over a number of years at the Institut Laue -Langevin, Grenoble.

The measurements are made by the process known generally as Instrumental Activation Analysis (INAA), using the emisson of gamma rays after beta decay of unstable atoms following thermal neutron capture.

We also detail the results from Twenty one internationally recognised and one unrecognised, or in house, standard reference materials which have been analysed for sixteen rare earth and trace elements using the described method, the determined elements being La, Ce, Nd, Sm, Eu, Tb, Tm, Yb, Lu, U, Th, Hf, Cs, Sc, Ta and Ba.

EXPERIMENTAL CONDITIONS AND METHODS

Two hundred milligrams of powdered sample, having a size of less than forty microns and which has been Teemaed in agate rings, are weighed into round polythene capsules of two centimeters diamater and five millimeters thickness (see Fig. 1) and

hermatically sealed. Small iron flux monitors (99.999% purity) of approximately thirty milligrames weight are attached to each capsule using 'Scotch Tape. Batches of samples together with standard reference materials and blanks are then simultaneously irradiated in a high thermal flux at the T1 position of the High Flux reactor for a period of two hours. The thermal neutron flux is approximatley 1.5 x 10^{13} Neutrons $cm^{-2}s^{-1}$ and the thermal to rapid ratio is of the order of 10^{-6} to 10^{-7}.

All the irradiated capusules, together with the flux monitors are subsequently counted using a hyper pure Germanium LEPS detector, coupled to a Canberra multi-channel analyser based on a 286AT pc system. Spectra for each sample and standard are obtained for a 3600 seconds count after a seven day cooling off period, and a second 9000 seconds count after twenty six days. The elements La, Nd, Sm, Lu and U with fairly short half lives are determined from the first counting, whilst the elements Ce, Eu, Tb, Tm, Yb, Th, Hf, Cs, Sc, Ta and Ba having longer half lives are determined from the second counting.

The spectra are first treated automatically by the peak fitting programme 'dbGamma' (Canberra Electronics, 1988) on a PC micro-computer and are subsequently corrected using an interactive programme 'FIT' (Vittoz in press).

Background corrected peak areas are obtained for peaks of interest, by summing a fixed number of channels around a chosen point to left and right of the peak, the corrected channels are then summed over the number of channels within the peak.

Details of half-lives, peak energies used and possible contamination for each element are listed in table 1. and lower limits of detection, as defined in De Soete et al., 1972, for four major classes of crystalline rocks are listed in Table 2.

RESULTS FOR STANDARD REFERENCE MATERIALS

The geological reference materials that have been measured are listed in Table 3., together with their split and position number where known. Whin Sill, a fine grained doleritic sill from the North of England, sampled from a large fallen block within the confines of the High Force quarry, High Force, Co Durham, is the measured in house standard. The determined elemental concentrations are also shown in Table 3. and are normally from a single determination, exept when indicated in parenthesis. The quoted errors are purely statistical (1 sigma) on the measured data.

DISCUSSION

1. Rare Earth Elements

The values obtained for the recognised reference materials have been compared with the 'Working values' given by Govindaraju, 1984.

In general our values are in good agreement with those given, with the notable exception of Cerium, which shows consistently smaller values. However other values given for this element, in various publications (Gladney et al., 1982: Gladney et al., 1985: Abbey, 1983: Govindaraju and de la Roche, 1977:

Govindaraju, 1979,1980,1982,1984a,1984b: Bornhurst and Balagna, 1979: Potts et al., 1981) show a spread which is greater than the difference between our values and those of the 'Working values'. Two notable exceptions to this are, G-2 and SDC-1 whose values for Cerium fall outside this criterium.

The measured values for the less well known reference materials GL-O, FK-N, MA-n, and Mica-Fe are given as an indication only, as these materials have either very small (GL-O, FK-N, MA-N) or extremly large (Mica-Fe) elemental abundances, and other published data for these materials are sparse.

2. Trace Elements

Again, in general, good agreement is found between our measured values and the 'Working values' for the trace elements Th, Hf, Cs, Sc and Ta. Uranium shows some variation, but this can be explained by the fact that this element tends to concentrate in exotic minerals e.g. uranite, uraninite, xenotime, allenite etc., and depending on the distribution of these minerals within what is, in effect, a very small sample (200mg) they can markedly affect the values determined.

Barium has been listed, but we consider these values to give only an order of magnitude determination, as Ba, due in the main to its small thermal neutron capture cross section, does not appear to analyse very well by this method.

Finally we list the values for an 'in house' standard, Whin Sill, which we propose hear as a possible standard reference material, as the abundances of rare earth and trace elements appear to be very homogeneous. Comparetive values are taken from Potts (personal communication).

CONCLUSIONS

We have presented the methods employed, together with the data acquired in support of the method, on twenty one internationally recognised standard materials, as well as one in house standard, which we propose to establish as a standard material. This being the data acquired, over a number of years operation, of the Instrumental Neutron Activation Analysis facility at the Institut Laue-Langevin, Grenoble, France.

REFERENCES

Abbey S.,1983:Studies in "standard samples" of silicate rocks and minerals 1969-1982, Geological Survey of Canada, Paper 83-15, 114p.

Bornhorst Th.G. and Balagna G.P., 1979: Instrumental neutron activation analysis of French geochemical reference samples, Geostandards Newsletters, Vol.3, pp 177-180.

Canberra Electronics, 1988: dbGamma V5.0

De Soete D., Gijbels R. and Hoste J.,1972: Neutron Activation Analysis, Chemical Analysis No.34, John Wiley & Sons, London and New York.

Gladney E.S. and Goode W.E.,1981:Elemental concentrations of eight United States Geological Survey rock standards - A review, Geostandards Newsletter, Vol. 5, pp 31-64.

Gladney E.S., Curtis D.B., Perrin D.R., 1985:Determination of selected rare earth elements in 37 international geochemical reference materials by instrumental thermal prompt gamma-ray spectrometry, geostandards Newsletter, Vol. 9, pp 25-30.

Govindaraju and de la Roche, 1977: Rapport (1966-1976) sur les elements en traces dans trois roches standards du Centre de Recherches Petrographiques et Geochimiques/ Basalte BR, Granites GA et GH, Geostandards Newsletter, Vol. 1, pp 67-100.

Govindaraju K., 1979: Report (1968-1978) on two mica reference samples: Biotite Mica-Fe and Phlogopite Mica-Mg, Geostandards Newsletter, Vol. 3, pp 3-24.

Govindaraju K., 1980: Report (1980) on three GIT-IWG rock reference samples: Anorthosite from Greenland, AN-G: Basalt d'Essay-la-Cote BE-N; Granite de beauvoir, MA-N, Geostandards Newsletter, Vol. ', pp 23-31.

Govindaraju K., 1982: Report (1967-1981) on four ANRT rock reference samples: Diorite DR-N; Serpentine UB-N; Bauxite BX-N and Disthene DT-N, Geostandards Newsletter, Vol. 6, pp 99-159.

Govindaraju K., 1984a: Report (1973-1983) on two ANRT geochemical reference samples: Granite GS-N and Potash Feldspar FK-N, Geostandards Newsletter, Vol. 8, pp

Govindaraju K., 1984b: Compilation of 'Working Values' for 170 International Reference samples of mainly silicate rocks and minerals, Geostandards Newsletter, Vol. 8 Special Issue.

Potts P.J. Thorpe O.W. and Watson J., 1981: Determination of the rare earth elemet abundances in 29 International rock standards by Instrumental activation analysis: a critical appraisal of calibration errors, Chemical Geology, Vol. 34, pp 331-335.

Vittoz (in press) Fit, an interactive peak fitting programme for gamma-ray spectroscopy, submitted to Computers in Physics.

Element	Nuclide observed	Half-life	Gamma-ray energy Kev	Interferences	Peak used for correction Kev	Correction factor
Ba	181-Ba	11.5 d	216.1	160-Tb	86.7	0.08806
Ce	141-Ce	32.5 d	145.4			
Cs	134-Cs	2.06 y	604.7			
Eu	152-Eu	13.2 y	121.78			
			1407.92			
Gd	153-Gd	236 d	97.5	233-Pa,182-Ta	311.9,67.75	2.3474,0.2252
			103.2	233-Pa	311.9	0.08759
Hf	181-Hf	43 d	482.16			
La	140-La	1.68 d	487	146-Nd	91	0.00052
			1596.2			
Lu	177-Lu	6.75 d	208.34	177-Yb	63.5	0.0033
Nd	147-Nd	10.98 d	91			
Sc	46-Sc	83.9 d	889.3			
Sm	153-Sm	1.94 d	69.66	153-Gd	97.5	0.11147
			103.2	153-Gd,233-Pa	97.5,311.9	0.677,0.08759
Ta	182-Ta	115 d	67.75			
Tb	160-Tb	73 d	86.76	233-Pa	311.9	0.27727
			879.31			
Th	233-Pa	27.4 d	311.9			
Tm	170-Tm	129 d	84.4	182-Ta,XKα-Pb possible	67.5	0.05128, -
U	239-Np	2.35 d	106.4			
Yb	169-Yb	30.6 d	63.5			

TABLE 1: Elements determined,nuclides observed with half-life, gamma-ray energy used and possible interferences.

	Acid	Intermediate	Basic	Ultrabasic
La	1.09	1.27	1.40	0.65
Ce	0.60	0.35	1.04	0.47
Nd	1.88	1.88	2.30	0.89
Sm	0.56	0.06	0.74	0.20
Eu	0.06	0.14	0.15	0.10
Tb	0.02	0.15	0.09	0.05
Tm	0.04	0.04	0.06	0.02
Yb	0.10	0.13	0.16	0.07
Lu	0.03	0.06	0.05	0.02
U	1.54	2.06	1.59	–
Th	0.33	0.32	0.35	–
Hf	0.62	0.39	0.62	0.25
Sc	0.07	0.09	0.09	0.05
Cs	1.24	0.74	1.24	–
Ta	0.16	0.07	0.16	0.03
Ba	97.00	133.00	152.00	–

Table 2. Lower limits of detection for the major classes of crystalline rocks.

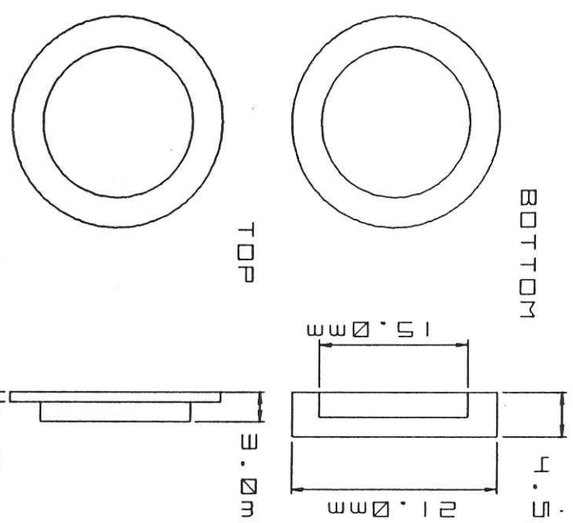

Fig. 1 Standard polyethelyne capsule for INAA

Sample Ref.	BCR-1			AGV-1 S46 P30			G-2 S109 P5			N-1			STM-1 S33 P26			SDC-1 S13 P17			GSP-1 S77 P4			
	TW	+/-	Ref	TW	+/-	Ref	TW	+/-	Ref	TW	+/-	Ref	TW	+/-	Ref	TW	+/-	Ref	TW	+/-	Ref	
n	4		(5)	1		(5)	3		(5)	1		(5)	1		(6)	1		(6)	1		(5)	n
La	26.06	0.40	25.00	38.39	2.29	37.00	86.21	4.34	90.00	11.43	0.52	11.00	158.54	2.19	150.00	47.70	1.11	42.00	180.68	2.46	185.00	La
Ce	53.93	1.57	53.70	68.87	0.44	66.00	148.36	3.57	160.00	21.81	0.50	23.00	240.92	1.37	260.00	84.70	0.63	92.00	364.35	2.02	400.00	Ce
Nd	28.65	0.76	28.70	32.78	0.76	34.00	50.68	3.51	55.00	13.55	1.34	15.00	80.40	4.21	78.00	38.81	2.33	38.00	183.72	9.15	190.00	Nd
Sm	6.77	0.08	6.60	5.66	0.15	5.90	7.40	1.16	7.20	3.26	0.04	3.50	12.89	0.11	13.00	8.36	0.80	8.30	26.66	0.18	26.80	Sm
Eu	1.93	0.14	1.96	1.67	0.07	1.66	1.26	0.07	1.40	1.08	0.05	1.11	3.23	0.10	3.70	1.53	0.05	1.70	1.93	0.06	2.40	Eu
Tb	1.04	0.01	1.05	0.70	0.05	0.70	0.42	0.05	0.48	0.65	0.04	0.65	1.40	0.06	1.60	1.10	0.05	1.20	1.01	0.05	1.36	Tb
Tm	–	–	0.59	–	–	–	–	–	–	0.35	0.06	0.34	0.55	0.09	–	0.63	0.08	0.70	0.39	0.06	0.45	Tm
Yb	3.76	0.18	3.39	1.73	0.04	1.70	0.77	0.07	0.80	2.34	0.07	2.10	4.91	0.09	4.30	5.04	0.09	4.20	1.60	0.05	1.70	Yb
Lu	0.53	0.11	0.51	0.25	0.01	0.28	0.11	0.00	0.11	0.32	0.02	0.34	0.61	0.04	–	0.64	0.04	–	0.23	0.02	0.22	Lu
U	1.75	0.47	1.72	1.34	0.39	1.89	1.49	0.81	2.04	0.41	0.16	0.57	6.58	0.49	9.10	2.45	0.31	3.00	1.99	0.38	2.20	U
Th	5.78	0.12	6.04	6.37	0.09	6.50	24.54	1.23	24.60	2.13	0.17	2.40	29.77	0.25	31.00	11.87	0.16	12.00	97.45	0.73	105.00	Th
Hf	4.76	0.11	4.90	5.10	0.14	5.10	7.78	0.44	7.90	2.64	0.17	2.60	27.76	0.58	27.00	8.31	0.21	8.10	14.66	0.32	15.00	Hf
Sc	32.31	1.08	33.00	11.63	0.05	12.10	3.46	0.12	3.50	35.25	0.11	35.00	0.48	0.01	0.70	14.96	0.05	15.00	5.39	0.02	6.10	Sc
Cs	0.91	0.10	0.97	–	0.12	1.30	1.36	0.19	1.33	0.98	0.13	0.95	1.51	0.06	1.50	3.73	0.11	3.90	1.07	0.06	1.00	Cs
Ta	0.83	0.07	0.79	0.80	0.01	0.92	0.81	0.04	0.88	0.50	0.01	0.50	17.94	0.12	18.00	1.29	0.01	1.30	–	0.01	0.90	Ta
Ba	725	75	678	1095	121	1220	–	–	1880	–	–	162.00	–	–	560.00	–		650.00	–	–	1310.00	Ba

TABLE 3: Rare earth and trace element determinations by INAA.
(n is the number of determinations for each standard)

Sample Ref.	BHVO-1 S21 P27			GA 1214A2			GH 604			BR 2538A2			DR-N 4043A			GL-O 16131			UB-N 6247A			
	TH	+/-	Ref	TH	+/-	Ref	TH	+/-	Ref	TH	+/-	Ref	TH	+/-	Ref	TH	+/-	Ref	TH	+/-	Ref	
n	1		(6)	8		(7)	3		(7)	5		(7)	1		(10)	1		(13)	1		(10)	n
La	18.62	0.59	17.00	41.08	0.74	38.00	24.69	1.00	25.00	80.51	2.80	80.00	22.05	1.83	21.00	20.02	0.39	20.00	0.48	0.19	-	La
Ce	33.78	0.52	39.00	74.36	1.78	70.00	59.82	1.68	50.00	140.38	4.27	140.00	43.81	0.40	46.00	48.08	0.44	22.00	1.16	0.30	-	Ce
Nd	28.43	1.98	24.00	29.06	1.09	25.00	30.85	4.59	25.00	63.00	0.73	60.00	22.14	0.65	22.00	27.37	1.81	32.00	0.64	0.70	-	Nd
Sm	6.11	0.05	6.10	5.12	0.15	5.00	9.63	0.31	10.00	11.36	0.50	12.00	5.20	0.14	5.30	5.61	0.04	6.10	0.20	0.01	-	Sm
Eu	2.08	0.07	2.00	1.01	0.03	-	0.11	0.02	0.11	3.55	0.08	3.70	1.42	0.07	1.50	1.19	0.04	1.28	0.07	0.02	-	Eu
Tb	0.98	0.05	1.00	0.53	0.06	-	1.19	0.22	2.00	1.44	0.10	-	0.78	0.06	0.80	0.66	0.03	0.62	0.03	0.02	-	Tb
Tm	0.45	0.07	0.30	0.26	0.02	-	0.93	0.14	1.50	0.55	0.08	-	-	-	-	0.26	0.04	-	-	0.03	-	Tm
Yb	2.51	0.07	1.90	2.26	0.28	2.00	8.80	0.55	8.00	2.11	0.30	2.00	3.05	0.07	2.80	0.85	0.04	0.73	1.16	0.04	-	Yb
Lu	0.31	0.03	-	0.31	0.03	-	1.09	0.04	1.17	0.25	0.02	0.24	0.42	0.02	-	0.12	0.02	0.12	0.04	0.01	-	Lu
U	0.52	0.17	0.40	4.56	1.17	4.00	15.67	2.44	18.00	2.12	0.47	3:00	1.69	0.42	1.50	0.67	0.12	-	0.10	0.10	-	U
Th	1.12	0.16	1.00	16.70	0.92	17.00	76.21	4.15	90.00	10.73	0.62	12.00	4.73	0.10	5.00	3.26	0.11	4.30	-	-	-	Th
Hf	4.71	0.18	4.30	4.18	0.31	-	6.33	0.64	6.50	5.70	0.48	-	2.94	0.14	2.70	1.07	0.10	1.20	0.07	0.10	-	Hf
Sc	29.84	0.10	31.00	6.86	0.29	7.00	0.73	0.00	1.00	21.98	0.68	26.00	27.24	0.10	28.00	7.62	0.03	8.30	10.00	0.04	13.60	Sc
Cs	0.14	0.14	0.15	6.34	1.37	6.00	2.46	0.11	2.50	0.71	0.17	1.30	5.99	0.27	6.00	3.25	0.10	4.50	8.25	0.15	11.00	Cs
Ta	1.18	0.01	1.10	1.32	0.08	-	4.47	0.20	4.20	5.55	0.16	-	0.44	0.02	0.70	0.25	0.01	-	0.06	0.01	-	Ta
Ba	-	-	135.00	817.00	64.00	850.00	-	-	22.00	1103.00	105	1050	424.00	98.00	385.00	210.00	256.00	-	-	-	-	Ba

TABLE 3 (Cont'd) : Rare earth and trace element determinations by INAA.
(n is the number of determinations for each standard)

Sample Ref.	FK-N 14022			Mica-Fe			AL-I 20911			AN-G 18368			BE-N 17016			MA-N 19194			Ailsa Craig 604			Mhin Sill 2538A2			
	TH	+/-	Ref	TH	+/-	Ref	TH	+/-	Ref	TH	+/-	Ref	TH	+/-	Ref	TH	+/-	Ref	TH	+/-	Ref	TH	+/-	Ref	
n	1		(12)	1		(8)	1		(11)	1		(9)	5		(9)	1		(9)	9		(14)	10		(15)	n
La	1.40	0.40	1.00	230.99	8.84	190.00	9.98	0.34	9.90	2.07	0.70	2.00	83.91	1.68	82.00	-	-	1.00	59.31	2.44	60.00	27.64	1.09	25.30	La
Ce	0.89	0.16	1.30	509.85	5.63	370.00	21.47	0.25	21.00	4.58	0.15	4.70	153.24	2.60	152.00	3.98	0.51	10.00	151.91	9.06	160.00	58.74	2.16	58.00	Ce
Nd	1.51	0.93	-	260.75	17.33	-	9.82	1.23	10.00	1.94	0.27	2.00	68.18	3.22	70.00	5.71	0.56	-	93.60	4.48	95.00	32.16	1.26	32.00	Nd
Sm	0.08	0.02	0.07	39.74	0.83	-	3.08	0.03	2.74	0.69	0.05	0.70	11.93	0.38	12.00	0.24	0.02	-	24.23	0.53	25.00	7.30	0.23	7.20	Sm
Eu	0.56	0.07	0.42	0.75	0.09	-	0.20	0.01	0.19	0.30	0.03	0.37	3.80	0.73	3.60	-	-	-	1.85	0.06	2.00	2.00	0.06	2.17	Eu
Tb	-	-	-	1.41	0.23	-	0.28	0.02	0.30	0.19	0.02	0.20	1.35	0.19	1.30	-	-	-	4.52	0.32	5.00	1.08	0.06	1.07	Tb
Tm	-	-	-	-	-	-	0.07	0.03	-	-	-	-	-	-	-	-	-	-	2.13	-	3.00	0.57	0.11	0.42	Tm
Yb	-	-	0.04	3.74	0.16	-	0.92	0.03	0.78	0.93	0.03	0.85	1.81	0.13	1.80	-	-	-	19.95	1.08	18.00	2.82	0.10	2.48	Yb
Lu	-	-	-	0.61	0.10	-	0.15	0.02	0.11	0.14	0.01	0.12	0.27	0.02	0.24	-	-	-	2.33	0.10	3.00	0.39	0.03	0.38	Lu
U	-	-	0.15	115.25	33.55	60.00	5.67	0.31	5.80	-	-	-	2.67	0.43	2.40	11.93	1.14	12.00	2.78	0.59	5.00	0.70	0.18	-	U
Th	-	-	0.40	192.61	2.66	150.00	9.12	0.10	9.50	-	-	-	11.43	0.57	11.00	1.52	0.15	1.00	17.91	0.95	20.00	2.93	0.23	2.97	Th
Hf	-	-	0.13	23.01	1.07	17.00	2.42	0.07	2.60	0.37	0.08	0.38	5.85	0.36	5.40	3.48	0.17	4.50	27.01	1.15	25.00	5.18	0.14	4.70	Hf
Sc	-	-	0.05	14.74	0.10	-	1.74	0.01	1.74	9.65	0.04	10.00	22.64	1.13	22.00	0.15	0.02	0.24	0.11	0.01	-	27.23	0.98	29.00	Sc
Cs	6.94	0.37	7.00	180.69	8.37	200.00	0.34	0.04	0.34	-	-	-	0.75	0.15	0.80	533.00	12.47	640.00	2.99	0.43	3.00	1.63	0.20	1.30	Cs
Ta	0.33	0.01	0.28	31.31	0.63	34.00	1.65	0.01	1.85	0.16	0.01	0.20	5.38	0.36	5.50	59.93	0.54	306.00	6.95	0.35	5.00	1.75	0.83	1.22	Ta
Ba	-	-	200.00	-	-	145.00	-	-	85.00	-	-	34.00	1029.0	154.00	1025.0	-	-	42.00	345.00	15.86	-	436.00	33.00	300.00	Ba

TABLE 3 (Cont'd.) : Rare earth and trace element determinations by INAA.
(n is the number of determinations for each standard)

The measured elemental concentrations are compared in table 2. with the 1984 compilation of working values by Govindaraju (8) and the most recent PGAA values of Anderson (9) and Gladney (10-11). The general agreement between these data is very satisfactory. In particular our data for boron support those of Anderson for most of the GRM where previous values either differed or were not known at all.
Twelve French GRM have also been analysed for B, Sm, and Gd. Existing information concerning these elements is very sparce (8) which therefore justified their measurement.

Table 2. Boron, Samarium and Gadolinium concentrations in eleven USGS geological reference materials

USGS reference material	Boron		Samarium		Gadolinium	
	This work	Others	This work	Others	This work	Others
W-1	12.5+1.3	13 (8)	3.2+0.8	3.5 (8)	4.3+0.9	4 (8)
G-2	3.0+1.2	2 (8) 2.6+0.7(9)	6.7+0.8	7.2 (8) 7.6+0.1(9)	4.4+0.8	4.1 (8) 4.3 (9)
AGV-1	8.42+0.56	6/7 (8) 8.7+0.8(9) 8.3+0.8(10)	5.7+0.9	5.9 (8) 6.4+0.2(9)	5.0+1.0	5.2 (8) 5.1 (9)
SCO-1	78.5+2.01	66 (8) 86+4(9) 78+7(10)	5.1+1.0	5.1 (8) 5.5+0.2(9) 5+0.5(9)	4.7+0.9	4.2 (8) 5.1 (9) 5.1 (9)
GSP-1	2.35+1.6	- 1.5+0.5(9) 0.81+0.16(10)	26.2+1.2	26.8 (8) 27.6+(9) 27+2(9)	12.2+0.9	13 (8) 13 (9) 12.8(11)
BHVO1	3.8+0.98	- 3.5+0.4(9) 2.1+0.2(10)	6.1+0.8	6.1 (8)	6.9+0.9	6.0 (8)
SDC-1	13.95+1.04	- 14+0.9(9) 13+1.0(10)	8.1+0.8	8.3 (8)	6.9+0.9	7.2 (8)
SGR-1	56.5+1.36	50 (8) 57.9+1.6(10) 55+5(10)	2.5+1.0	2.8 (8)	2.6+1.0	-
STM-1	8.1+1.1	- 9+2(9) 5.6+0.6(10)	12.0+0.9	13 (8)	9.2+0.8	10 (8)
MAG-1	138.6+2.29	130(8) 150+4(9) 136.7+1.6(10)	7.1+1.0	8.1 (8)	5.6+1.0	6.6 (8)
RGM-1	29+1.15	31 (8) 31+2(9) 29+3(10)	3.9+0.8	4.3 (8)	4.3+0.9	-

The measured elemental concentrations are shown in Table 3. and are again based on single sample measurements and should therefore be treated as preliminary values. For Samarium where some values are quoted in the literature our measured results are in relatively good agreement. Finally Table 4. indicates detection limits for B, Sm and Gd. Detection limit is defined here as the concentration of an element which would yield a net signal of 2/B counts, where B is the background underlying the peak of interest. The detection limits have been calculated for a granite matrix (USGS G-2) of 500mg weight and for a measurement time of 2350 seconds.

4.CONCLUSIONS

A facility for PGAA installed on a thermal neutron guide at the ILL High Flux Reactor has been described. The performance of the facility has been assessed by the measurement of B, Sm and Gd concentrations in eleven USGS geological reference materials.

The agreement between our data and earlier values is generally good. Twelve French geological reference materials have also been analysed for the same trace elements and preliminary values for their concentrations are reported. The results demonstrate that the ILL facility is capable of providing high sensitivity analyses for B, Sm and Gd, mainly due to the experimental geometry based on a neutron guide which results in a relatively high flux/low background environment.

French reference sample	Boron this work	(7)	Samarium this work	(7)	Gadolinium this work	(7)
GA	28.2±1.3	20	4.4±0.8	5	4.0±0.8	-
GH	3.8±1.3	-	10.0±1.4	10	10.2±1.4	-
BR	7.4±1.3	10	12.4±1.7	12	10.0±0.9	-
Mica-Fe	-	-	32.7±1.5	-	20.2±0.8	-
Mica-Mg	4.1±1.3	-	-	-	-	-
DR-N	18.0±1.3	-	5.3±1.5	5.3	5.5±0.9	3.5
UB-N	169±3	145	-	-	-	-
DT-N	17.6±1.3	-	8.4±0.8	-	7.2±0.8	-
GS-N	12.6±1.3	-	7.7±0.8	8.2	5.5±0.9	-
GL-O	421±5	-	5.5±1.4	-	4.6±1.0	-
BE-N	7.3±1.3	-	11.4±1.0	12	9.5±1.3	9
MA-N	19.4±1.3	17	-	-	-	-

Table 3. Preliminary boron, samarium and gadolinium concentrations in twelve French geological reference samples

Element	Gamma-ray energy (keV)	Detection limit in granite G-2 ($\mu g\ g^{-1}$)
B	478	0.22
Sm	334	0.15
	439	0.24
Gd	181	0.09
	199	0.36

Table 4. Elemental detection limits for a 500 mg granite matrix

5.ACKNOWLEDGEMENTS

The authors are indebted to the ILL for support to perform this study. The financial assistance of the University of Grenoble is also gratefully acknowledged.

6.REFERENCES

(1) S.A.Kerr, R.A.Oliver, P.Vittoz, G.Vivier, F.Hoyler, T.D.MacMahon, N.I.Ward (1986)
Proceedings of 7th MTAA,Ed. H.Levi, (1986)
Elemental concentrations in geochemical reference samples by neutron capture prompt gamma-ray spectroscopy.

(2) D.L.Anderson, M.P.Failey, W.H.Zoller, G.E.Gordon (1981)
Facility for non-destructive analysis for major and trace elements using neutron-capture gamma-ray spectrometry, Journal of Radioanalytical Chemistry, 63:97-119
(3) S.A.Kerr, W.V.Prestwich, T.J.Kennet, D.M.Shaw (1980)
The determination of boron in sedimentary rocks by neutron irradiation and prompt gamma-ray spectrometry, Journal of Radioanalytical Chemistry, 557:525
(4) E.G.Gordon et al (1981)
Technical report ORO-5173-020', University of Maryland, College Park. Ma..

(5) B.P.Maier (Ed.) (1983)
Neutron Research facilities at the ILL-HFR, Institut Laue-La
ngevin, Grenoble

(6) A.G.Hanna, R.M.Brugger and M.D.Glascock (1981)
The prompt gamma neutron activation analysis facility at MURR, Nuclear instruments and Methods, 188:619-627
(7) M.A.Lone,R.A.Leavitt, D.A.Harrison (1981)
Prompt gamma-rays from thermal neutron capture, Atomic Data and Nuclear Data Tables,26:511-559
(8) K.Govindaraju (1984)
1984 compilation of working values and sample description for 170 international reference samples of mainly silicate rocks and minerals, Geostandards Newsletter,8: Special Issue
(9) D.L.Anderson, Y.Sun, M.P.Failey and W.H.Zoller (1985)
Neutron capture prompt gamma-ray multielement analysis of twenty two geological standards, Geostandards Newsletter, 9:219-228
(10) E.S.Gladney D.B.Curtis D.R.Perrin (1984)
Determination of boron in 35 international geochemical reference materials by thermal neutron capture prompt gamma-ray spectrometry, Geostandards Newsletter,8:43-46
(11) E.S.Gladney, D.B.Curtis, D.R.Perrin (1985)
Determination of selected rare earth elements in 37 international geochemical reference materials by instrumental thermal neutron prompt gamma-ray spectrometry, Geostandards Newsletter, 9:25-30

The measurements of low elemental concentrations in geological reference materials by neutron capture prompt gamma-ray spectroscopy

R A Olivier, P Vittoz, G Vivier, S A Kerr and F Hoyler

Institut Max von Laue - Paul Langevin, Grenoble, France
Institut Dolomieu, CNRS L.A.69, University of Grenoble
Grenoble, France.
University of Surrey, Guildford, Surrey, U.K.
(Present address:BP Research Center, Sunbury on Thames, UK.)
University of Tubingen, Tubingen, R.F.A..

1.INTRODUCTION

Over the last decade, the technique of neutron capture prompt gamma-ray activation analysis (PGAA) has evolved as a powerful instrumental analytical tool, complementary to that of instrumental activation analysis (INAA). PGAA is generally useful for major element analysis but it is capable of performing analysis for a limited number of trace elements with large capture cross sections, such as B, Cd, Sm, Gd. The elemental sensitivity which can be achieved with the PGAA technique is directly dependent on the irradiating neutron flux, therefore reactor based instruments are preferred for trace element applications (1-4).
The purpose of this paper is to describe a facility which has recently been developed for PGAA at the High Flux Reactor of the Institut Laue-Langevin (ILL) at Grenoble, France. An experimental programme is in progress to evaluate the efficiencyof the facility,in order to provide elemental analysis of a wide variety of geological materials. As part of this programme, a number of geochemical reference materials(GRM) from the United States Geological Survey (USGS) have been analysed and results are presented here for measured concentrations of B, Sm, and Gd. At the same time a number of geochemical reference materials from the French CRPG have been analysed, and these results are also presented.For the majority of these materials our values are the first to be published, we therefore tentativly propose these as recommended values.

2.EXPERIMENTAL

The ILL-HFR operates at a thermal power of 57 MW and provides high intensity neutron beams predominantly for neutron scattering and diffraction instruments. In order to extend the experimental facilities available at the HFR (5), a number of neutron beams are carried by internal reflection within curved neutron guides into an adjacent experimental hall. The guides have differing radii of curvature which determine the maximum neutron energies propagated along each guide.
The PGAA experiments described here were performed at the last but one position of a thermal neutron guide (#H22) with a radius of curvature of 27 km.

The curved guide ends at a distance approximatly 110 meters from the reactor core after which the neutron beam travels a further 2 meters through straight evacuated beam tubes to the experimental position. The advantage of performing PGAA experiments at such a position are the absence of fast neutrons which are effectively removed by the curvature of the guide, the low background radiation levels due to the large distance from the reactor and finally the ease with which the neutron beam may be collimated thus enabling the detector to be positioned relatively close to the sample position.

The final experimental arrangement is shown in Fig. 1. The neutron beam emerges from an upstream experiment where a 6LiF collimator reduces the beam to a 25mm diameter circle. An evacuated beam tube of aluminium with 4μm zirconium foil windows, extends to the sample position, and continues to the beam stop of the next downstream experiment position.

The sample position is surrounded by plates of 6LiF with appropriate windows for the entry and exit of the neutron beam, as well as for the detection of the emitted prompt gamma-rays. The measured flux density at the sample position is 3.5 x 10^8 n cm-2 s-1.

Powder samples of less than 40μm particle size, typically weighing 500mg, are contained in thin walled (<0.5 mm) teflon tubing (8 mm outside diameter) closed at each end by a teflon plug. The tubes are supported in a jig which allows the measurement geometry to be accurately reproduced.

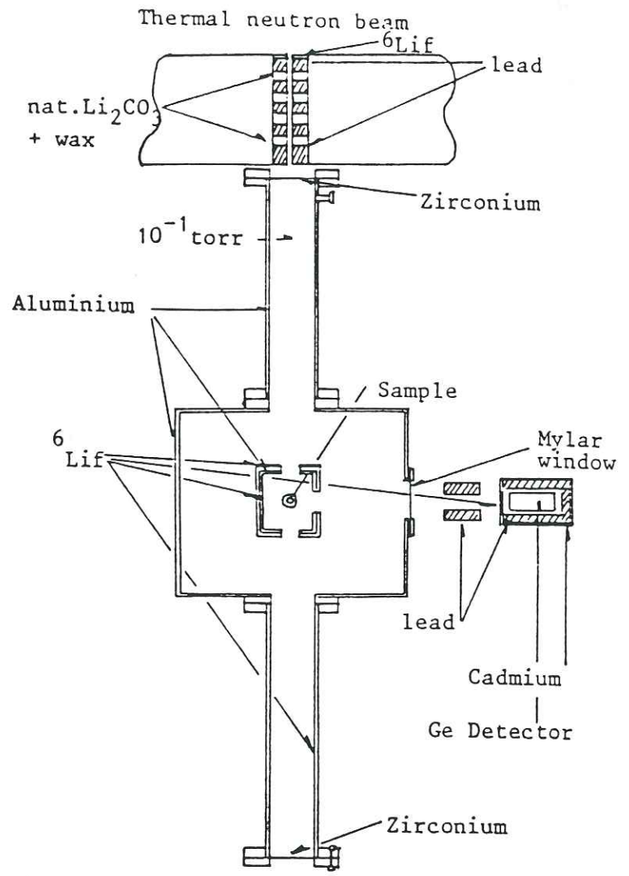

Figure 1. Schematic plan view of the PGAA experimental arrangement on the H22(S51) thermal neutron guide at ILL

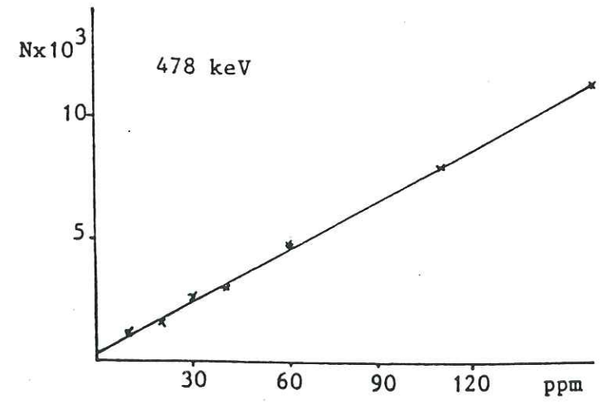

Figure 2. Calibration curve using the 478 keV Doppler broadened peak for Boron

The detector end face is positioned approximately 50 cm from the sample irradiation position. The whole of the detector is protected from extraneous gamma-rays and scattered neutrons by succesive layers of 2 mm of cadmium, 5 cm of lead, and 1 mm of copper, with the exception of the aperture which allows the detector to view the sample, this aperture being covered by a layer of 3 mm of 6LiF and 1 mm of copper.
Gamma-ray spectra are accumulated on an in house multi-parameter MCA for counting times of typically 1 hour and are corrected for dead-time by the use of a low frequency pulser. The neutron flux is monitored by detecting capture gamma-rays from a fine (0.1 mm diameter) Au wire, permanently positioned beside the sample.

Elemental sensitivities are determined by the method of addition (3), that is, a range of quantities of each element in solution form are pipetted into replicate samples of two geological reference materials. The aliquots are selected to cover the anticipated range of concentrations in the samples under study. A plot of measured count rate versus the added quantity of Boron is shown in Fig. 2.

This has been checked for linearity by performing a weighted linear least squares analysis. The obtained gradient is therefore the calibrated sensitivity of the technique for each element and is used to determine the concentrations in the studied samples.

3.RESULTS AND DISCUSSIONS

Table 1 lists the gamma-ray lines which were used for the determination of B, Sm, and Gd in the GRM under study. The characteristically Doppler broadened 478 keV boron peak suffers from a strong interfering gamma-ray at 472 keV due to Na, which had to be corrected for, in all the measurements. A possible Fe interference at 479.5 keV (7) was also investigated but found to be negligible for the samples studied,including those samples with high values of< Fe as Fe-Mica, BE-N etc.

Table 1. A comparison of elemental sensitivities observed at three different PGAA facilities

Element	Gamma-ray energy (keV)	Sensitivity (counts s^{-1} μg^{-1}) ILL (This work)	NBS (Maryland) (4)	MURR (Missouri) (5)
B	478	2700	530	759
Sm	334	3700	640	740
	439	1900	320	363
Gd	181	6900	680	956
	199	1600	-	-

Table 1 also details the sensitivity values which were obtained by the addition method at ILL, together with published sensitivities for the PGAA facilities at NBS Maryland (2) and MURR Missouri (6), which are included for comparison. The greater sensitivity of the ILL facility is principally due the ability to place the detector much closer to the sample position than is possible at either NBS or MURR.
Eleven USGS reference materials have been analysed for B, Sm, and Gd using the ILL facility and the preliminary results of these measurements are detailed in Table 2.

We have termed these results as preliminary since only two samples of each GRM were analysed, except for SCO-1 where four determinations were made and AGV-1 where ten determinations were made. The quoted errors however include an assessment of both statistical and systematic uncertainties, based on three independant sensitivity calibrations for each element and nineteen replicate analyses.

ELEMENTAL CONCENTRATIONS IN GEOCHEMICAL REFERENCE SAMPLES BY NEUTRON CAPTURE PROMPT GAMMA-RAY SPECTROSCOPY

S A Kerr, R A Oliver, P Vittoz, G Vivier, F Hoyler
Institut Laue-Langevin, BP156X, 38042 Grenoble Cedex, France

T D MacMahon, N I Ward
Imperial College Reactor Centre, Silwood Park, Ascot, Berks, UK

Abstract

A facility for neutron capture prompt gamma-ray activation analysis, installed on a curved thermal neutron guide at the ILL High Flux Reactor, is described. Elemental sensitivities for B, Sm and Gd have been measured. The performance of the facility has been assessed by the measurement of these trace elements in eleven USGS geochemical reference samples and comparison of the results with existing values. Preliminary concentrations of B, Sm and Gd are also reported for twelve French GRS.

INTRODUCTION

Over the last decade, the technique of neutron capture prompt gamma-ray activation analysis (PGAA) has evolved as a powerful instrumental analytical technique, complementary to that of instrumental neutron activation analysis (INAA). PGAA is generally useful for major element analysis but it is capable of performing trace analysis for a limited number of elements with large neutron capture cross-sections, such as B, Cd, Sm and Gd. Since the elemental sensitivity which can be achieved with the PGAA technique is directly dependent on the irradiating neutron flux, reactor based instruments are preferred for trace element applications /1-4/.

The purpose of this paper is to describe a facility which has recently been developed for PGAA at the High Flux Reactor (HFR) of the Institut Laue-Langevin (ILL) in Grenoble, France. An experimental programme is in progress to evaluate the facility and to provide elemental analyses of a wide variety of geological materials. As part of this programme, a number of geochemical reference samples (GRS) from the USGS and France have been analysed and preliminary results are presented here for the measured concentrations of B, Sm and Gd. For the purpose of comparison, independent measurements on a number of the same GRS have also been performed on an existing PGAA facility /5/ at the Imperial College Reactor Centre (ICRC) at Ascot, UK; the results of which are also presented.

EXPERIMENTAL

The ILL-HFR operates at a thermal power of 57 MW and provides high intensity neutron beams predominantly for neutron scattering and diffraction instruments. In order to extend the experimental facilities available on the HFR /6/, nine neutron beams are carried by internal reflection within curved neutron guides into an adjacent experimental hall. The guides have differing radii of curvature which determine the maximum neutron energies propagated along each guide.

The PGAA experiments described here were performed at the end position of a thermal neutron guide (#H22) with a radius of curvature of 27 km. The curved guide ends at a distance of approximately 110 m from the reactor core after which the neutron beam travels a further 4 m through straight evacuated

beam tubes to the end experimental position. The advantage of performing PGAA experiments at such a position are the absence of fast neutrons which are effectively removed by the curvature of the guide, the low background radiation levels due to the large distance from the reactor and finally the ease with which the neutron beam may be collimated thus enabling the detector to be positioned relatively close to the irradiated sample.

The experimental arrangement is shown in Fig. 1. The neutron beam emerges from an up-stream experiment and ^{6}LiF collimators reduce the beam dimension to 12 mm high × 10 mm wide. An evacuated beam tube surrounded by ~ 3 cm of paraffin wax loaded with 50% $^{nat}Li_2CO_3$ extends to the sample position. The measured neutron flux density at the sample position is 1.3×10^{6} n cm^{-2}s^{-1}.

Powder samples, typically weighing 500 mg, are contained in thin walled (0.5 mm) teflon tubing (9 mm outside diameter) closed at each end by a teflon plug. The tubes are supported in a jig which enables the measurement geometry to be accurately reproduced. Gamma-ray spectrometry is performed with a specially constructed high purity Ge detector supplied by Canberra in which the usual boron implanted contact has been replaced by an evaporated gold substrate, resulting in a 'boron-free' detector. The 23% efficiency coaxial detector has an energy resolution of 1.75 keV and a peak to Compton ratio of 60:1 for gamma-rays of 1.3 MeV. The detector end face is positioned 18 cm from the sample irradiation position and is protected from scattered neutrons by 4 mm of ^{6}LiF. Apart from the aperture which allows the detector to 'view' the sample, the detector is surrounded by a minimum thickness of 3 cm $^{nat}Li_2CO_3$/wax and 5 cm lead.

Gamma-ray spectra are accumulated on a Canberra Series 80 MCA for counting times typically ~ 1 hour and are corrected for dead-time and pulse pile-up effects by the use of a low frequency pulser. The neutron flux is monitored by two independent methods: firstly by detecting capture gamma-rays from a fine (0.2 mm diameter) Ni wire permanently positioned beside the sample, and secondly, by recording integrated counts from a Li-glass scintillation detector mounted close to the ^{6}LiF collimators.

Elemental sensitivities are determined by the method of addition /2/; that is, a range of quantities of each element in solution form are pipetted into replicate samples of a GRS. The aliquots added are selected to cover the concentration range anticipated in the samples under study. Plots of measured count rate versus the quantity of element added are obtained and checked for linearity by performing a weighted linear least-squares analysis. The gradient thus obtained is the calibrated sensitivity of the technique for each element and is used to determine concentrations in the remaining GRS.

A subset of the samples and standards prepared for the ILL experiments have also been measured using the PGAA facility at ICRC which consists of a Compton suppressed Ge(Li) spectrometer positioned on an external neutron beam of the 100 kW 'Consort' swimming pool reactor. The thermal neutron flux density at the sample position is ~ 2×10^{6}n cm^{-2}s^{-1}. The spectrometer has an energy resolution of 3.1 keV at 1.3 MeV and a peak to Compton ratio of 170:1 at 662 keV. Further details of the facility are published elsewhere /5/. A typical sample counting time is 10000s.

RESULTS AND DISCUSSION

Table 1 lists the gamma-ray lines which were used for the determination of B, Sm and Gd in the GRS. The characteristically Doppler broadened 478 keV boron peak suffers from a strong interfering gamma-ray at 472 keV due to Na, which had to be corrected for in all the measurements. A possible Fe interference (479.5 keV) /7/ was also investigated but found to be negligible for the samples studied. At ICRC the Sm 439 keV and Gd 199 keV lines were unusable because of interfering gamma-rays resulting form the capture of scattered

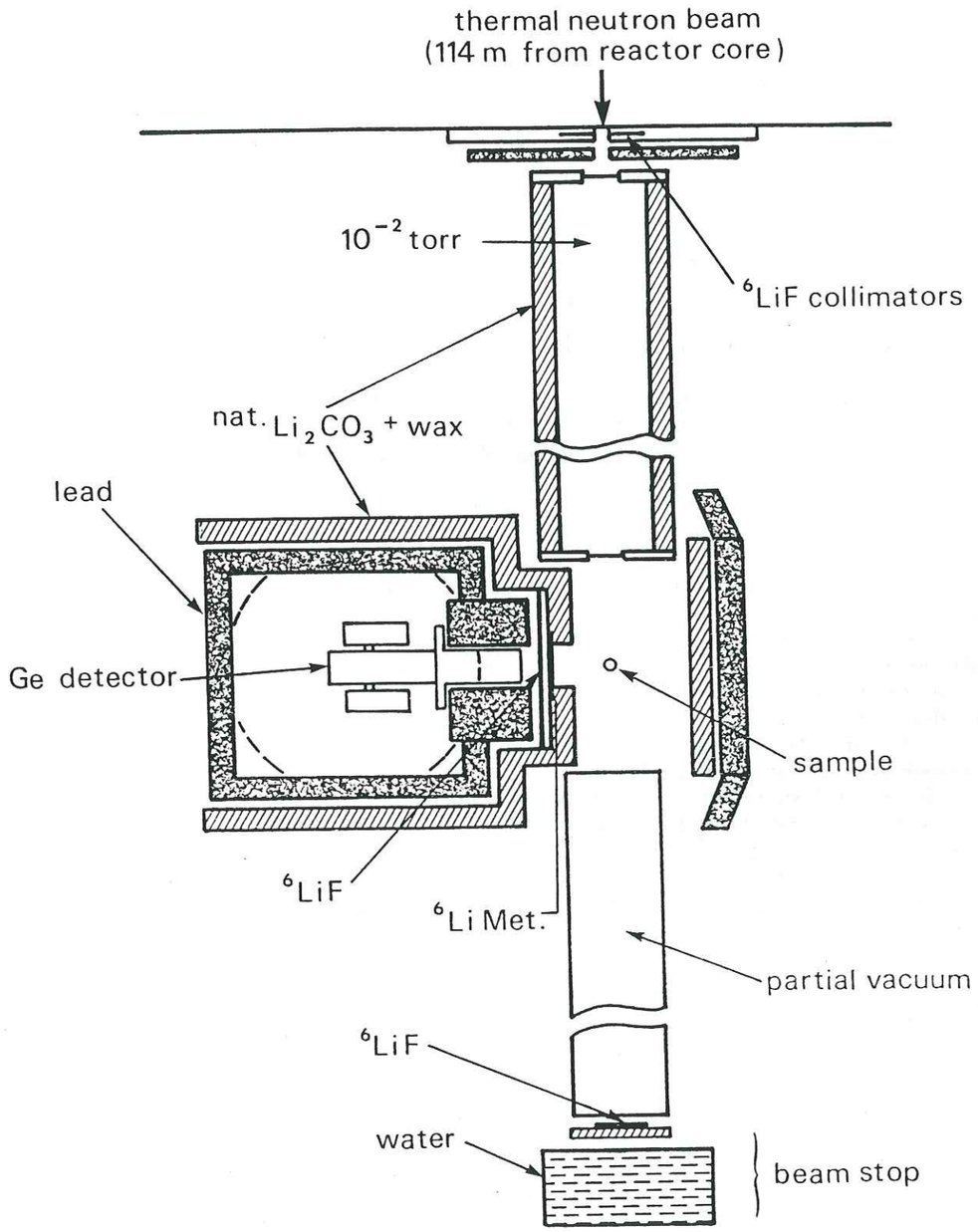

Figure 1. Schematic plan view of the PGAA experimental arrangement at the end position of thermal neutron guide H22 at the ILL-HFR.

Element	Gamma-ray energy (keV)	Sensitivity (counts $s^{-1}mg^{-1}$)			
		ILL (this work)	ICRC (this work)	NBS (Maryland) /3/	MURR (Missouri) /4/
B	478	2700	6.4	530	759
Sm	334	3700	13.	640	740
	439	1900	-	320	363
Gd	181	6900	21.	680	956
	199	1600	-	-	-

Table 1: A comparison of elemental sensitivities observed at four different PGAA facilities.

neutrons within the detector materials, namely I(442.9 keV) /7/ and Ge(197.8 keV) /8/, respectively.

Table I also details the sensitivity values which were obtained by the addition method at ILL and ICRC, together with published sensitivities for the PGAA facilities at NBS (Maryland) /3/ and MURR (Missouri) /4/, which are included for comparison. The greater sensitivity of the ILL facility is principally due to the ability to place the detector much closer to the sample position than is possible at either NBS or MURR.

Eleven USGS reference samples have been analysed for B, Sm and Gd using the ILL facility and the preliminary results of these measurements are summarised in Table 2. The results are termed preliminary since only one sample of each GRS was analysed, although the quoted errors include an assessment of both statistical and systematic uncertainties, based on three independent sensitivity calibrations for each element and nineteen replicate analyses.

The measured elemental concentrations are compared in Table 2 with the 1984 compilation of working values by Govindaraju /9/ and the more recent PGAA measurements of Anderson /10/. The general agreement between these data is very satisfactory. In particular, our data for boron support those of Anderson for most of the GRS where previous values either differed or were not known at all.

Twelve French GRS have also been analysed for B, Sm and Gd. Existing information concerning these elements is very sparse /9/ and therefore justified their measurement at both ILL and ICRC in order to provide independent comparative results. The measured elemental concentrations are shown in Table 3 and are again based on single sample measurements and should therefore be treated as preliminary values. A general correspondence is obtained between the ILL and ICRC results, but the ICRC data are of substantially lower precision, due to the much lower neutron flux density at the facility, and therefore serve only as a useful control check of the more precise ILL results. For samarium, where some working values are known /9/, agreement with the ILL results is good. In view of these considerations, the ILL values should be taken as the most reliable of the measurements in Table 3 for the French GRS.

Finally Table 4 compares detection limits for B, Sm and Gd between the ILL and ICRC facilities. Detection limit is defined here as the concentration of an element which would yield a net signal of $2\sqrt{B}$ counts, where B is the background underlying the peak of interest. The detection limits are calculated

USGS reference standard	Boron		Samarium		Gadolinium	
	This work	/9/ /10/	This work	/9/ /10/	This work	/9/ /10/
W-1	12.5±1.3	13 -	3.2±.8	3.5 -	4.3±.9	4 -
G-2	2.3±1.2	2 2.6±.7	6.7±.8	7.2 7.6±.1	4.4±.8	4.1 4.3±.3
AGV-1	8.9±1.6	6-7 8.7±.8	5.7±.9	5.9 6.3±.2	5.0±1.0	5.2 5.1±.3
BHVO-1	3.0±1.3	- 3.5±.4	6.1±.8	6.1 6.5±.3	6.9±.9	6.0 6.4±.5
STM-1	7.6±1.3	- 9±2	12.0±.9	13 13.3±.3	9.2±.8	10 10.3±.3
RGM-1	28.2±1.4	31 31±2	3.9±.8	4.3 4.15±.14	4.3±.9	- 3.73±.08
SGR-1	58.6±1.7	50 57.9±1.6	2.5±1.0	2.8 2.6±.2	2.6±1.0	- 2.2±.1
GSP-1	2.0±1.3	- 1.5±.5	26.2±1.2	26.8 27.6±1.2	12.2±.9	13 13.0±1.2
MAG-1	145±3	130 150±4	7.1±1.0	8.1 7.6±.2	5.6±1.0	6.6 6.4±.4
SDC-1	13.2±1.3	- 14.0±.9	8.1±.8	8.3 8.7±.3	6.9±.9	7.2 7.5±.8
SCo-1	80±2	66 86±4	5.1±1.0	5.1 5.5±.2	4.7±.9	4.2 5.1±.3

Table 2. Boron, samarium and gadolinium concentrations in eleven USGS-GRS.

for a granite matrix (USGS-G2) of 500 mg and for measurement times of 2350s and 10000s at ILL and ICRC respectively. Missing values in the table are due to interference problems described earlier in the text.

It is instructive to compare the detection limits obtained in this work with those from a much earlier PGAA experime nt also performed at the ILL by Henkelmann and Born /11/. Those measurements were performed on a 'cold' neutron guide; that is, one having a spherical container of liquid deuterium located within the reactor moderator and against the entrance window to the guide resulting in a high flux of 'subthermal' energy (~ 1-4 meV) neutrons. Since the average capture cross-sections for most elements are higher by a factor of ~ 2-3 for 'cold' compared to 'thermal' neutrons, this represents a significant gain in sensitivity. The neutron flux density reported was 1.5×10^{10} n cm^{-2} s^{-1}

GRS	Boron This work ILL / ICRC	/9/	Samarium This work ILL / ICRC	/9/	Gadolinium This work ILL	/9/
GA	28.2±1.3 22±5	20	4.4±.8 3±2	5	4.0±.8	-
GH	3.8±1.3 4±2	-	10.0±1.4 7±2	10	10.2±1.4	-
BR	7.4±1.3 -	10	12.4±1.7 9±2	12	10.0±.9	-
MICA-Fe	- -	-	32.7±1.5 23±5	-	20.2±.8	-
MICA-Mg	4.1±1.3 11±4	-	-	-	-	-
DR-N	18.0±1.3 25±5	-	5.3±1.5 4±2	5.3	5.5±.9	3.5
UB-N	169±3 118±24	145	-	-	-	-
DT-N	17.6±1.3 16±4	-	8.4±.8 -	-	7.2±.8	-
GS-N	12.6±1.3 30±6	-	7.7±.8 4±2	8.2	5.5±.9	-
GL-O	421±5 356±71	-	5.5±1.4 5±2	-	4.6±1.0	-
BE-N	7.3±1.3 15±3	-	11.4±1.0 -	12	9.5±1.3	9
MA-N	19.4±1.3 12±3	17	-	-	-	-

Table 3. Preliminary boron, samarium and gadolinium concentrations in twelve French GRS.

and the detection limits obtained for B, Sm and Gd were 0.2×10^{-3}, 0.15×10^{-3} and 0.1×10^{-3} μg, respectively. These results indicate that substantial increases in sensitivity, possibly by a factor of 1000, may be achieved at a high flux experimental position on a 'cold' guide.

CONCLUSIONS

A facility for PGAA installed on a thermal neutron guide at the ILL High Flux Reactor has been described. The performance of the facility has been assessed by the measurement of B, Sm Gd concentrations in eleven USGS-GRS.

Element	Gamma-ray energy (keV)	Detection limit (μg g^{-1}) in granite ILL (t_c = 2350s)	ICRC (t_c = 10000s)
B	478	0.22	6.6
Sm	334	0.15	2.2
	439	0.24	-
Gd	181	0.09	3.6
	199	0.36	-

Table 4. Elemental detection limits for a 500 mg granite matrix measured at ILL and ICRC.

The agreement between our data and earlier values is generally good. A further twelve French GRS have also been analysed for the same trace elements and preliminary values for their concentrations are reported. The results demonstrate that the ILL facility is capable of providing high sensitivity analyses for B, Sm and Gd, mainly due to the experimental geometry based on a neutron guide which results in a relatively high flux/low background environment.

ACKNOWLEDGEMENTS

The authors are indebted to the ILL and ICRC for support to perform this study. The financial assistance of the Universite de Grenoble is also gratefully acknowledged.

REFERENCES

/1/ M P Failey, D L Anderson, W H Zoller, G E Gordon, Anal. Chem. **51** (1979) 2209.

/2/ S A Kerr, W V Prestwich, T J Kennett, D M Shaw, J. Radioanal. Chem. **57** (1980) 525.

/3/ D L Anderson, M P Failey, W H Zoller, W B Walters, G E Gordon, R M Lindstrom, J. Radioanal. Chem. **63** (1981) 97.

/4/ A G Hanna, R M Brugger, M D Glascock, Nucl. Instrum. & Meths. **188** (1981) 619.

/5/ G D Burholt and T D MacMahon, J. Radioanal. Chem. **53** (1979) 365.

/6/ B P Maier (ed.) 'Neutron Research Facilities at the ILL-HFR' (1983) Institut Laue-Langevin, Grenoble.

/7/ M A Lone, R A Leavitt, D A Harrison, At Data & Nucl. Data Tab. **26** (1981) 511.

/8/ R L Bunting, J J Kraushaar, Nucl. Instrum. & Meth. **118** (1974) 565.

/9/ K. Govindaraju, Geostandands Newsletter **8** (1984) 3.

/10/ D L Anderson, Y Sun, M P Failey, W H Zoller, Geostandands Newsletter **9** (1985) 219.

/11/ R Henkelmann, H T Born, J. Radioanal. Chem. **16** (1973) 473.

Author affiliations

SAK	-	Nucl. Geophys. Sect., BP Research Centre, Sunbury on Thames, Middlesex, UK.
NIW, SAK (formerly)	-	University of Surrey, Guildford, Surrey, UK.
RAO, FH	-	Institut Laue-Langevin, Grenoble, France.
PV, GV	-	Institut Dolomieu, Universite de Grenoble, France.
TDM	-	Imperial College Reactor Centre, Ascot, Berks, UK.

DETERMINATION OF B, SM AND GD IN TWENTY-THREE GEOLOGICAL REFERENCE MATERIALS BY NEUTRON-CAPTURE PROMPT GAMMA-RAY ACTIVATION ANALYSIS (PGAA)

P. VITTOZ*, R.A. OLIVER**, G. VIVIER*, S.A. KERR*** and F. HOYLER**

* Institut Dolomieu, U.A. 69 CNRS, University of Grenoble, France
** Institut Laue-Langevin, Grenoble, France
*** Nuclear Geophysic Section, BP Research Centre, Sunbury on Thames, Middlesex, UK.

Eleven USGS geological reference materials and twelve French geological reference materials have been measured for B, Sm and Gd concentrations by prompt-gamma activation analysis. For those materials that have already been analysed, our data is in agreement with published recommended values. These values constitute the first measured data for several French geological reference materials

Complementary to Instrumental Neutron Activation Analysis(INAA), Neutron Capture Prompt Gamma-Ray Activation Analysis (PGAA) has become a viable method for the analysis of a number of major and trace elements with large neutron capture cross section such as Al, Mg, Fe, Gd, Sm or B...

We report here the measured concentrations of Sm, Gd and B for twenty-three geological reference samples using PGAA. All the analyses were carried out at the High Flux Reactor of the Institut Laue-Langevin, Grenoble.

EXPERIMENTAL

Prompt Gamma Activation experiments have been carried out at the High Flux Reactor facility of the Institut Laue-Langevin to determine the best experimental configuration and have been reported by Kerr et al. (1986) (1). The final experimental arrangement (Figure 1) was installed at the end position of the thermal neutron guide H22 which has a radius curvature of 27 km at a distance of 114 meters from the reactor core. This position offers several advantages which are:

a) A well thermalised neutron beam
b) A low level of fast neutrons due to the curvature of the neutron guide
c) Low reactor and guide generated background gamma levels.

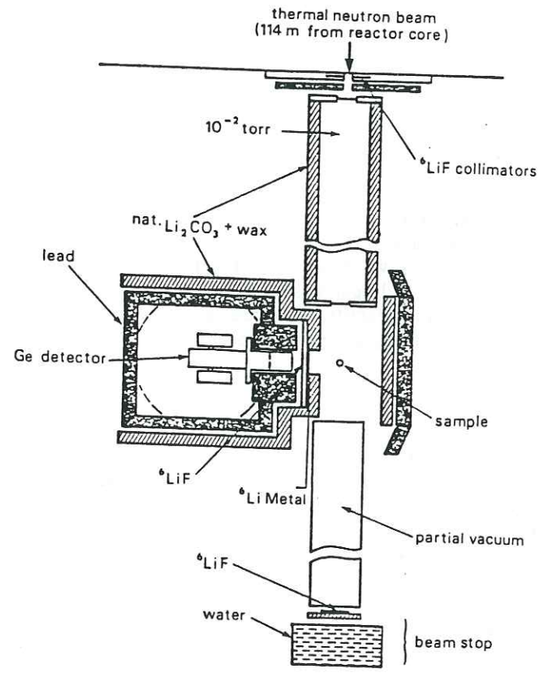

Figure 1. Schematic plan view of the PGAA experimental arrangement at the end position of thermal neutron guide H22 at the ILL-HFR

Problems were posed by interference from scattered and diffused neutrons as well as from extraneous gamma rays (2). To overcome this, the neutrons were guided to the target chamber through a tube of plexiglass, the walls of which had been coated with an approximatelly 3 cm

thick mixture of 50% parrafin wax and 50% $LiCO_3$. The tube was maintained at a vacuum of better than 10^{-2} torr, and the neutrons traversed two Mylar windows of approximatelly 40 μm thickness. The samples were supported in a jig which enables the measurement geometry to be accurately reproduced. The neutron beam was then evacuated through a plexiglass box, kept at a small depression, to a beam stop of $LiCO_3$ and water. The detector, positioned close to the irradiated sample, was surrounded by 5 cm of lead, which in turn was covered by a $LiCO_3$+wax shield. The detector window was protected by a 4 mm thick enriched ^6LiF plate and a 4 mm thick ^6Li metal plate.

The prompt gamma spectra were collected with a high purity Ge detector (23% efficiency) supplied by Canberra Electronics, the usual implanted boron contact having been replaced by an evaporate gold substrate, resulting in a detector with very low concentrations of boron.

Data reduction was performed on the ILL DEC 10 computing facility.

A set of two geological reference samples were spiked with a solution of Gd, Sm and B. The elemental concentrations were then determined by a method of addition (3). A linear regression of the measured count rate versus the quantity of element added was then carried out by performing a weighted linear least-squares analysis.

Each sample was counted for a period of one hour, together with blank and background counts. Monitoring of the neutron flux was provided by a neutron counter (a Li-glass scintillation detector) positioned at the beam head and a thin Ni wire suspended in the beam at the sample position.

RESULTS AND DISCUSSION

The gamma-ray lines and the related sensitivities are listed in Table 1, also listed are values obtained at NBS (Maryland, 4) and MURR (Missouri, 5) for comparison. The greater sensitivity of the ILL facility is principally due to the ability to place the detector much closer to the sample position, because of the reduced background from fast neutrons and reactor generated gamma rays.

The characteristically Doppler broadened 478 keV boron peak suffers from a strong interfering gamma-ray at 472 keV due to Na, which had to be corrected for in all the measurements. A possible Fe interference (479.5 keV) (6) was also investigated but found to be negligible for the samples studied, including those samples with high percentages of Fe as Mica-Fe, BE-N etc. .

Table 1. A comparison of elemental sensitivities observed at three different PGAA facilities

Element	Gamma-ray energy (keV)	Sensitivity (counts s^{-1} μg^{-1}) ILL (This work)	NBS (Maryland) (4)	MURR (Missouri) (5)
B	478	2700	530	759
Sm	334	3700	640	740
	439	1900	320	363
Gd	181	6900	680	956
	199	1600	-	-

Calibration curves using the 181 keV decay line for gadolinium, the 333 keV prompt line for samarium and the 478 keV Doppler broadened line for boron are shown in Figure 2.

Eleven USGS reference samples have been analysed for B, Sm and Gd and the preliminary results of these measurements are summarised in Table 2. The results are termed preliminary since only one sample of each geological reference sample was analysed, although the quoted errors include an assessment of both statistical and systematic uncertainties, based on three independent sensitivity calibrations for each element and nineteen replicate analysis.

The measured elemental concentrations are compared in Table 2 with the 1984 compilation of working values by Govindaraju (7) and other published values (8-14). The general agreement between these data is very satisfactory. In particular, our data for boron support those of Anderson for most of the geological reference samples where previous values either differed or were not known at all.

Twelve French geological reference samples have also been analysed for B, Sm and Gd. Existing information concerning these elements is very sparce (7) and therefore justified their measurement. The measured elemental concentrations are shown in Table 3 and are again based on single sample measurements and should therefore be treated as preliminary values. For samarium, where some working values are known (7), agreement with our results is good.

Finally, Table 4 indicates detection limits for B, Sm and Gd. Detection limit is defined here as the concentration of an element which would yield a net signal of $2\sigma_B$ counts, where B is the background underlying the peak of interest. The detection limits are calculated for a granite matrix (USGS G-2) of 500 mg and for a measurement time of 2350 s.

Table 2. Boron, samarium and gadolinium concentrations in eleven USGS geological reference samples

USGS reference sample	Boron This work	Boron Others	Samarium this work	Samarium Others	Gadolinium this work	Gadolinium Others
W-1	12.5±1.3	13[7] -	3.2±0.8	3.5[7] -	4.3±0.9	4[7] -
G-2	2.3±1.2	2[7] 2.6±0.7[8] 2.6±0.1[9] 1.3[10]	6.7±0.8	7.2[7] 7.6±0.1[8] 6.71±0.33[9]	4.4±0.8	4.1[7] 4.3±0.3[8] 3.3±0.03[9]
AGV-1	8.9±1.6	6-7[7] 8.7±0.8[8] 5.9±0.1[9] 8.6[10] 8.3±0.8[11] 7.8[12]	5.7±0.9	5.9[7] 6.4±0.2[8] 5.3±0.2[9]	5.0±1.0	5.2[7] 5.1±0.3[8] 3.67±0.03[9]
BHVO-1	3.0±1.3	- 3.5±0.4[8] 2.1[10] 2.1±0.2[11]	6.1±0.8	6.1[7] 6.5±0.3[8] 5.5±0.5[13]	6.9±0.9	6.0[7] 6.4±0.5[8] 6.4±0.6[13]
STM-1	7.6±1.3	- 9±2[8] 6.1[10] 5.6±0.6[11]	12.0±0.9	13[7] 13.3±0.3[8] 12.8±1.2[13]	9.2±0.8	10[7] 10.3±0.3[8] 9.7±0.9[13]
RGM-1	28.2±1.4	31[7] 31±2[8] 28[10] 29±3[11]	3.9±0.8	4.3[7] 4.15±.14[8] 3.9±0.4[13]	4.3±0.9	- 3.73±0.08[8] 3.7±0.4[13]
SGR-1	58.6±1.7	50[7] 57.9±1.6[8] 55[10] 55±5[11]	2.5±1.0	2.8[7] 2.6±0.2[8] 2.6±0.3[13]	2.6±1.0	- 2.2±0.1[8] 2.2±0.3[13]
GSP-1	2.0±1.3	- 1.5±0.5[8] 0.7±0.2[9] 0.9[10] 0.81±0.16[11] 1[12]	26.2±1.2	26.8[7] 27.6±1.2[8] 24±0.3[9] 27±2[13]	12.2±0.9	13[7] 13.0±1.2[8] 9.64±0.09[9] 12.9[12] 12.8±1.3[13]
MAG-1	145±3	130[7] 150±4[8] 142[10] 136.7±1.6[14]	7.1±1.0	8.1[7] 7.6±0.2[8] 6.4±0.6[13]	5.6±1.0	6.6[7] 6.4±0.4[8] 15.6±0.5[13]
SDC-1	13.2±1.3	- 14.0±0.9[8] 12.2[10] 13±1[11]	8.1±0.8	8.3[7] 8.7±0.3[8] 7.9±0.8[13]	6.9±0.9	7.2[7] 7.5±0.8[8] 7.±0.7[13]
SCo-1	80±2	66[7] 86±4[8] 76[10] 78±7[11] 77.3±0.7[14]	5.1±1.0	5.1[7] 5.5±0.2[8] 5±0.5[13]	4.7±0.9	4.2[7] 5.1±0.3[8] 5.1±0.7[13]

Table 3. Preliminary boron, samarium and gadolinium concentrations in twelve French geological reference samples

French reference sample	Boron this work	(7)	Samarium this work	(7)	Gadolinium this work	(7)
GA	28.2±1.3	20	4.4±0.8	5	4.0±0.8	-
GH	3.8±1.3	-	10.0±1.4	10	10.2±1.4	-
BR	7.4±1.3	10	12.4±1.7	12	10.0±0.9	-
Mica-Fe	-	-	32.7±1.5	-	20.2±0.8	-
Mica-Mg	4.1±1.3	-	-	-	-	-
DR-N	18.0±1.3	-	5.3±1.5	5.3	5.5±0.9	3.5
UB-N	169±3	145	-	-	-	-
DT-N	17.6±1.3	-	8.4±0.8	-	7.2±0.8	-
GS-N	12.6±1.3	-	7.7±0.8	8.2	5.5±0.9	-
GL-O	421±5	-	5.5±1.4	-	4.6±1.0	-
BE-N	7.3±1.3	-	11.4±1.0	12	9.5±1.3	9
MA-N	19.4±1.3	17	-	-	-	-

Table 4. Elemental detection limits for a 500 mg granite matrix

Element	Gamma-ray energy (keV)	Detection limit in granite G-2 (μg g^{-1})
B	478	0.22
Sm	334	0.15
	439	0.24
Gd	181	0.09
	199	0.36

CONCLUSIONS

A facility for PGAA installed on a thermal neutron guide at the ILL High Flux Reactor has been described.

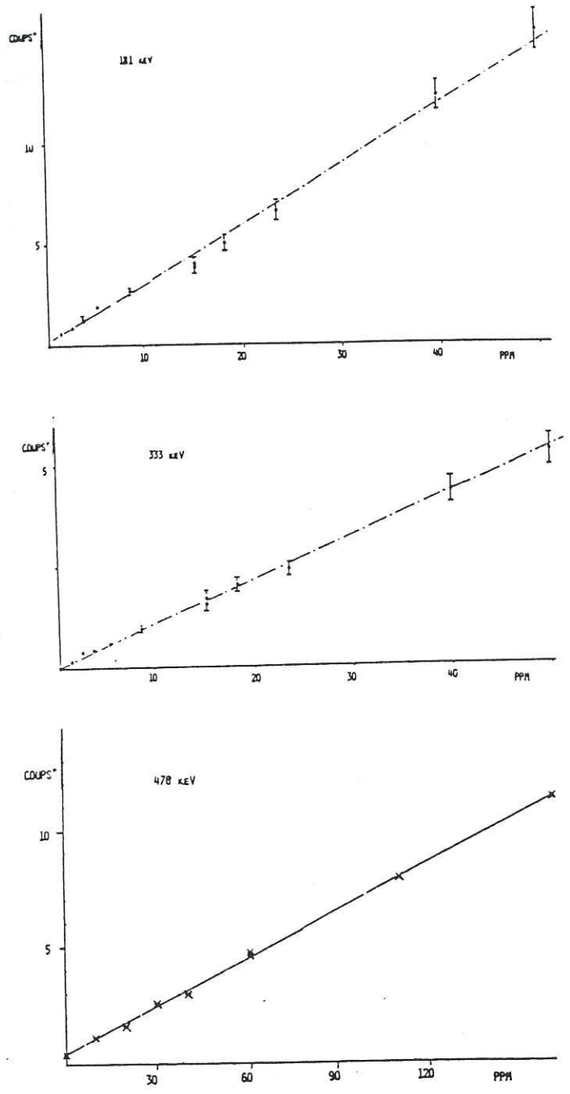

Figure 2. Calibration curves using the 181 keV decay line for gadolinium, the 333 keV prompt line for samarium and the 478 keV Doppler broadened line for boron

The performance of the facility has been assessed by the measurement of B, Sm and Gd concentrations in eleven USGS geological reference samples. The agreement between our data and earlier values is generally good. Twelve French geological reference samples have also been analysed for the same trace elements and preliminary values for their concentrations are reported. The results demonstrate that the ILL facility is capable of providing high sensitivity analyses for B, Sm and Gd, mainly due to the experimental geometry based on a neutron guide which results in a relatively high flux/low background environement.

ACKNOWLEDGEMENTS

The authors are indebted to the ILL for support to perform this study. The financial assistance of the University of Grenoble is also gratefully acknowledged.

RESUME

Une installation d'analyse par mesure des rayonnements gamma-prompt émis après capture de neutron a permis la mesure des concentrations en B, Sm et Gd sur onze échantillons géologiques de référence de l'USGS et sur douze échantillons géologiques de référence français. Pour les échantillons géologiques de référence déjà analysés, les résultats sont en accord avec les valeurs recommandées. Pour la plupart des échantillons géologiques de référence français, ces valeurs représentent les premières données.

REFERENCES

(1) S.A. Kerr, R.A. Oliver, P. Vittoz, G. Vivier and F. Hoyler (1986)
Elemental concentrations in geochemical reference samples by neutron capture prompt gamma-ray spectroscopy, Proceeding of the 1986 world meeting of modern trends in activation analysis, Copenhagen, June 1986 (In press).

(2) E.G. Gordon et al (1981)
Technical report ORO-5173-O20.

(3) S.A. Kerr, W.V. Prestwich, T.J. Kennet and D.M. Shaw (1980)
The determination of boron in sedimentary rocks by neutron irradiation and prompt gamma-ray spectrometry, Journal of Radioanalytical Chemistry, 57: 525.

(4) D.L. Anderson, M.P. Failey, W.H. Zoller, W.B. Walters, G.E. Gordon and R.M. Lindstrom (1981)
Facility for non-destructive analysis for major and trace elements using neutron-capture gamma-ray spectrometry, Journal of Radioanalytical Chemistry, 63: 97-119.

(5) A.G. Hanna, R.M. Brugger and M.D. Glascock (1981)
The prompt gamma neutron activation analysis facility at Murr, Nuclear Instruments and Methods, 188: 619-627.

(6) M.A. Lone, R.A. Leavitt and D.A. Harrison (1981)
Prompt gamma rays from thermal-neutron capture, Atomic Data and Nuclear Data Tables, 26: 511-559.

(7) K. Govindaraju (1984)
1984 compilation of working values and sample description for 170 international reference samples of mainly silicate rocks and minerals, Geostandards Newsletter, 8: Special Issue.

(8) D.L. Anderson, Y. Sun, M. P. Failey and W.H. Zoller (1985)
Neutron-capture prompt gamma-ray multielement analysis of twenty-two geological standards, Geostandards Newsletter, 9: 219-228.

(9) G.E. Gordon, W.B. Walters, W.H. Zoller, D.L. Anderson and M.P. Failey (1979)
Nondestructive determination of trace element concentrations, Technical Report ORO-5173-008, Dept. of Chemistry, University of Maryland, College Park, MD.

(10) M.D. Higgins (1984)
Abundance of boron in international Geochemical standards by prompt gamma neutron activation analysis, Geostandards Newsletter, 8: 31-34.

(11) E.S. Gladney, D.B. Curtis and D.R. Perrin (1984)
Determination of boron in 35 International geochemical reference materials by thermal neutron capture prompt gamma-ray spectrometry, Geostandards Newsletter, 8: 43-46.

(12) M.A. Gautier, E.S. Gladney and D.R Perrin (1985)
Quality assurance for health and environmental chemistry 1984, Los Alamos National Laboratory report LA-10508-MS.

(13) E.S. Gladney, D.B. Curtis and D.R. Perrin (1985)
Determination of selected rare earth elements in 37 international geochemical reference materials by instrumental thermal neutron prompt gamma-ray spectrometry, Geostandards Newsletter, 9: 25-30.

(14) M.G. Truscott, and D.M. Shaw (1984)
Boron in chert and precambrian siliceous iron formations, Geochimica et Cosmochimica Acta, 48: 2313-2320.

Table 4.1a Major and trace elements for the Quatre Tours/Belle Cote granite

	RO503	RO507	RO651	RO309	RO657	RO311	RO220	RO310	RO653B
SiO2	62.63	65.78	69.61	70.82	70.83	71.23	71.67	71.72	71.72
Al2O3	15.33	18.65	16.26	15.26	15.43	15.78	15.14	14.83	15.28
Fe2O3	4.34	1.51	2.45	1.73	1.78	1.39	1.51	1.45	1.74
MgO	4.46	0.95	1.71	1.14	1.36	0.68	0.81	0.88	0.99
CaO	0.96	1.12	0.89	0.01	1.04	0.60	0.62	0.54	0.93
Na2O	2.83	4.63	3.00	4.41	4.39	4.60	3.20	4.33	4.01
K2O	4.34	5.61	3.60	4.93	4.41	4.52	4.60	4.52	4.06
TiO2	0.66	0.24	0.41	0.28	0.30	0.24	0.05	0.26	0.27
MnO	0.06	0.04	0.05	0.03	0.06	0.04	0.02	0.04	0.06
P2O5	0.51	0.13	0.21		0.30		0.21		0.14
LOI	2.83	0.83	1.81	1.07	0.10	0.85	0.91	0.84	0.80
TOTAL	98.95	99.49	100.00	99.68	100.00	99.93	98.74	99.41	100.00
Y	14.00	10.00	3.00	12.00	9.00	11.00	4.00	11.00	3.00
Sr	518.00	908.00	552.00	407.00	442.00	354.00	537.00	520.00	387.00
Rb	135.00	227.00	147.00	203.00	196.00	164.00	175.00	166.00	168.00
Zr	242.00	177.00	161.00	132.00	153.00	91.00	116.00	122.00	126.00
Nb	16.40	11.00	9.00	12.00	12.00	9.00	4.00	12.00	11.00
Ba	2762.00	2086.00	1273.00	1366.00	1316.00	1249.00		1172.00	1025.00
Co	137.00	89.00	6.52			39.00	2.40	28.00	3.46
Cu	22.00	12.00	2.00	27.00	4.00	16.00	9.00	21.00	4.00
Cr	227.00	68.00	46.00		26.00	12.00		21.00	24.00
Ni	95.00	22.00	20.00		13.00		27.00		11.00
V	79.00	65.00	36.00	41.00	24.00	20.00		30.00	21.00
U	7.20	15.05	1.78	4.25		3.86	4.00	15.50	1.17
Th	53.60	19.47	19.45	29.60		17.00	23.40	21.80	14.42
Hf	7.58	5.08	3.79	4.30		2.84	3.99	3.75	3.22
Sc	12.95	3.14	5.19	3.81		3.19	3.28	3.27	4.06
Cs	3.68	8.01	4.74	3.84		4.35	3.55	4.48	5.66
Ta	1.44	1.18	1.08	1.60		2.19	0.15	1.46	1.41
La	51.42	13.35	26.09	24.76		12.53	16.89	19.54	16.63
Ce	100.60	23.64	51.30	49.35		23.87	31.55	41.71	33.42
Nd	50.27	13.71	20.11	21.00		12.07	14.16	19.30	11.90
Sm	8.73	2.71	2.35	3.45		2.45	2.23	3.45	2.34
Eu	1.31	0.72	0.87	0.53		0.40	0.69	0.51	0.62
Gd	4.84	1.83	4.20	2.30		1.44	4.22	1.91	2.14
Tb	0.38	0.21	0.92	0.26		0.13	0.94	0.15	0.34
Yb	1.15	1.18	0.67	0.62		0.94	0.40	0.75	0.94
Lu	0.19	0.14	0.17	0.10		0.12	0.07	0.11	0.21
La/Yb	44.71	11.31	38.94	39.94		13.33	42.23	26.05	17.69
Tot. REE	214.05	55.66	102.48	100.07		52.51	66.93	85.52	66.40

Table 4.1a (contd.)

	RO675B	RO655	RO656	RO132	RO210	RO218	RO124	RO133	RO652
SiO2	71.85	71.96	72.00	72.31	72.37	72.43	72.48	73.59	73.85
Al2O3	14.16	15.35	15.43	13.67	15.07	14.86	14.95	16.36	14.31
Fe2O3	2.89	1.49	1.56	3.60	0.75	1.72	1.30	0.53	0.53
MgO	2.30	1.08	0.84	2.00	0.31	0.85	0.91	0.43	0.25
CaO	0.48	0.92	1.01	0.11	0.35	0.36	0.74	0.23	0.72
Na2O	4.10	3.80	4.25	1.62	4.68	3.85	4.68	2.84	3.20
K2O	2.94	4.40	3.93	5.61	5.16	4.70	4.46	6.13	5.77
TiO2	0.40	0.25	0.27	0.16	0.11	0.20	0.08	0.24	0.05
MnO	0.06	0.03	0.05	0.03	0.04	0.03	0.02		0.04
P2O5	0.18	0.12	0.15	0.52	0.07	0.11	0.20	0.06	0.27
LOI	0.63	0.60	0.50	1.89	0.55	0.92	1.13	1.21	1.01
TOTAL	100.00	100.00	100.00	101.52	99.44	100.03	100.95	101.62	100.00
Y	10.00	3.00	10.00	26.00	25.00	17.00	12.00	11.00	1.00
Sr	360.00	601.00	445.00	63.00	294.00	421.00	474.00	47.00	147.00
Rb	148.00	164.00	155.00	196.00	165.00	182.00	183.00	311.00	257.00
Zr	118.00	152.00	138.00	205.00	476.00	116.00	118.00	41.00	47.00
Nb	13.00	10.00	13.00	15.00	40.00	10.00	9.50	16.00	15.00
Ba	898.00	1093.00	1072.00	1000.00			1700.00	200.00	314.00
Co	7.38	27.14	1.36	8.35	12.49	6.80	2.47	0.83	1.14
Cu	4.00	3.00	2.00	37.00	10.00	3.00		8.00	4.00
Cr	62.00	27.00	19.00						7.00
Ni	34.00	12.00	9.00			23.00			5.00
V	41.00	22.00	20.00						8.00
U	1.78	5.26	5.75	4.00	58.00	6.26		7.00	1.67
Th	16.24	28.61	41.80	17.60	51.61	55.60	24.00	3.00	2.95
Hf	3.39	5.00	9.22	5.50	12.93	9.74	3.54	1.36	1.27
Sc	5.82	11.12	14.98	9.29	13.50	8.99			2.42
Cs	1.99	7.53	14.88						6.75
Ta	3.94	1.26	1.38	1.14	3.35	1.60	0.97	2.59	4.49
La	13.09	26.31	52.10	35.15	63.83	51.28	19.60	3.28	3.98
Ce	29.72	61.05	120.58	64.50	130.03	103.20	46.70	11.70	8.34
Nd	18.23	23.09	56.37	29.02	76.11	42.34	22.30	5.43	3.53
Sm	2.92	4.22	10.49	5.01	14.05	9.08	2.63	1.56	0.97
Eu	0.66	1.44	1.57	0.87	2.60	1.63	0.74	0.24	0.27
Gd	4.71	6.96	12.44	3.77	9.26	8.06	1.65	1.44	1.38
Tb	1.00	1.49	2.33	0.50	1.03	1.25	0.17	0.23	0.28
Yb	0.88	0.86	1.03	2.44	1.96	3.50	1.26	1.11	0.96
Lu	0.16	0.27	0.23	0.39	0.32	0.35	0.17	0.31	0.13
La/Yb	14.88	30.59	50.58	14.41	32.57	14.65	15.56	2.95	4.15
Tot. REE	66.66	118.73	244.70	137.88	289.93	212.63	93.57	23.86	18.46

Table 4.1a (contd.)

	RO675A	RO653A	RO501	RO209	RO502	RO215	RO208	RO134	RO505
SiO2	73.92	74.40	74.56	74.58	74.68	75.71	77.42	79.12	88.65
Al2O3	13.61	13.99	15.59	14.05	16.13	13.17	10.70	11.75	6.16
Fe2O3	0.98	0.58	1.29	1.07	1.56	1.88	1.05	0.02	0.52
MgO	0.68	0.25	1.22	0.40	1.71	0.65	0.62	0.24	0.44
CaO	0.83	1.17	0.14	0.17	0.43	0.32	1.58	0.03	0.09
Na2O	3.13	3.61	3.74	3.00	3.76	3.96	1.04	3.61	1.31
K2O	6.58	4.70	4.94	5.00	4.84	3.60	4.67	4.94	2.32
TiO2	0.15	0.06	0.23		0.27	0.09	0.02	0.30	0.09
MnO	0.03	0.05	0.02	0.02	0.03		0.10		
P2O5	0.09	0.17	0.16	0.12	0.16	0.20	0.11	0.10	0.01
LOI		1.00		0.72		0.84	2.26	0.74	0.57
TOTAL	100.00	100.00	101.89	99.21	103.57	100.46	99.57	100.85	100.16
Y	0.00	1.00	5.00	12.00	7.00	31.00	10.00	9.00	3.00
Sr	310.00	206.00	411.00	215.00	454.00	169.00	144.00	196.00	79.00
Rb	225.00	204.00	167.00	185.00	168.00	143.00	187.00	183.00	105.00
Zr	61.00	55.00	119.00	38.00	114.00	117.00	48.00	70.00	47.00
Nb	6.00	13.00	10.20	7.00	8.60	17.00	5.00	8.00	3.60
Ba	934.00	481.00	1433.00		1488.00			1200.00	530.00
Co	2.82	1.08	81.00	1.34	87.00	1.43	1.47	0.28	49.00
Cu	4.00	2.00	4.00	6.00	5.00	6.00		8.00	5.00
Cr	16.00	7.00	56.00		56.00				52.00
Ni	10.00	4.00	13.00		18.00	24.00			7.00
V	16.00	9.00	61.00		61.00				49.00
U	2.04	0.77	2.08	1.80	7.27	7.00		5.00	3.20
Th	10.33	4.25	22.40	10.00	41.90	15.96	12.04	17.40	9.32
Hf	0.87	1.61	3.90	0.90	5.75	4.32	1.91	2.14	1.55
Sc	2.43	2.40	2.72	2.66	3.87	5.61	2.48	1.43	1.49
Cs	2.35	8.39	4.80		4.18				3.57
Ta	0.63	3.94	1.10	0.84	1.02	2.28	0.40	0.61	0.41
La	7.53	5.66	20.10	11.22	19.41	25.81	13.88	17.18	12.58
Ce	15.94	12.42	36.75	21.19	34.22	45.87	28.28	28.88	19.28
Nd	8.74	3.77	15.39	8.40	17.39	19.48	11.71	12.40	8.52
Sm	0.72	0.95	2.53	1.77	2.83	4.69	2.23	2.53	1.32
Eu	0.53	0.39	0.42	0.41	0.64	0.60	0.59	0.48	0.26
Gd	2.23	1.58	1.86	2.12	1.63	3.61	1.74	1.72	0.81
Tb	0.55	0.34	0.24	0.40	0.14	0.49	0.24	0.20	0.08
Yb	0.55	1.01	0.53	2.06	1.07	2.98	0.90	0.49	0.39
Lu	0.14	0.14	0.08	0.21	0.17	0.32	0.15	0.10	0.04
La/Yb	13.69	5.60	37.92	5.45	18.14	8.66	15.42	35.06	32.26
Tot. REE	34.70	24.68	76.04	45.66	75.87	100.24	57.98	62.26	42.47

Table 4.1b Major and trace elements for the Alfrey granite

	RO513	RO118	RO258	RO257	RO256	RO119
SiO2	70.77	71.74	72.39	72.69	76.49	76.95
Al2O3	14.73	15.45	13.33	15.53	13.82	12.86
Fe2O3	1.88	1.47	2.72	0.92	0.96	1.08
MgO	0.74	0.91	1.45	0.61	0.68	0.70
CaO	0.84	0.65	1.37	0.72	0.53	0.12
Na2O	4.12	3.98	3.06	4.40	3.97	3.24
K2O	4.36	4.65	4.21	4.93	3.71	4.51
TiO2	0.37	0.21	0.40	0.16	0.15	0.13
MnO	0.02	0.04	0.06	0.03	0.02	0.03
P2O5	0.17	0.24	0.20	0.06	0.09	0.13
Loi	1.47	1.41	2.02	1.01	1.03	1.40
TOTAL	99.47	100.75	101.21	101.06	101.45	101.15
Y	10	9	22	11	10	14
Sr	443	338	303	464	502	132
Rb	170	193	222	191	204	164
Zr	167	109	138	103	114	75
Nb	10	12	20	10	10	10
Ba	1484	1600	1309	1157	1224	1000
Co	96		4.5	1.76	0.63	2.35
Cu	26	4			6.6	8
Cr	63					
Ni	21					
V	63					
U	6.93	4	12.74	5.55	2	6
Th	32.18	14	23	12.8	14.9	19.2
Hf	5.48	3.1	3.4	2.79	2.75	2.2
Sc	4.55		6.5	2.66	2.78	3.18
Cs	4.93					
Ta	0.91	1.61	1.32	0.95	1.31	0.87
La	40.07	19.4	30.5	14.84	16.2	21.52
Ce	58.99	41.3	56.66	28.09	33.05	39.79
Nd	39.11	17.1	23.97	10.85	15.1	18.77
Sm	5.57	2.64	4.49	2.08	2.21	3.54
Eu	0.83	0.69	0.63	0.62	0.48	0.45
Gd	2.86	1.98	3.67	1.72	1.73	2.23
Tb	0.18	0.26	0.53	0.25	0.24	0.23
Yb	0.96	0.9	1.62	0.78	1.1	1.04
Lu	0.14	0.17	0.17	0.1	0.12	0.21
La/Yb	41.74	21.56	18.83	19.03	14.73	20.69
Tot.REE	145.85	82.46	118.57	57.61	68.5	85.55

Figure 4.1c Major and trace elements for the Ramu granite

	RO512	RO104	RO101	RO508	RO102	RO508P	RO508D
SiO2	72.40	72.90	73.67	73.69	74.29	75.22	75.30
Al2O3	14.66	14.20	14.23	14.49	14.61	14.19	14.60
Fe2O3	1.37	1.00	0.67	0.76	0.76	1.13	0.77
MgO	0.67	0.42	0.45	0.29	0.32	0.34	-
CaO	0.69	0.68	0.65	0.65	0.69	0.58	0.63
Na2O	4.47	5.31	5.21	5.36	5.19	4.30	4.36
K2O	4.13	4.26	4.27	4.70	3.51	3.30	4.54
TiO2	0.18	0.61	0.64	0.70	0.71	0.80	0.60
MnO	0.30	0.50	0.30	0.50	0.50	0.30	0.50
P2O5	0.60	0.29	0.50	0.17	0.34	0.32	0.28
LOI	1.12	0.51	1.35	0.47	0.62	0.63	0.50
TOTAL	99.78	100.68	98.94	100.70	101.54	99.85	100.82
Y	16.00	15.00	12.00	12.00	13.00	12.00	14.00
Sr	410.00	420.00	400.00	115.00	521.00	555.00	410.00
Rb	163.00	473.00	445.00	427.00	471.00	451.00	428.00
Zr	112.00	20.00	25.00	40.00	22.00	22.00	18.00
Nb	7.20	10.00	9.00	11.20	11.00	10.00	9.00
Ba	1274.00	380.00	521.00	439.00	441.00	340.00	434.00
Co	82.00			72.00			
Cu	4.00			6.00			
Cr	56.00			53.00			
Ni	9.00			6.00			
V	6.00			50.00			
U	5.68	1.72	2.14	2.87	1.52	2.55	1.49
Th	22.81	2.15	3.54	5.14	2.66	2.56	2.46
Hf	3.78	1.50	1.71	1.51	1.23	1.40	1.22
Sc	2.35	1.60	2.12	2.35	1.55	1.62	1.40
Cs	5.10	5.32	4.95	5.00	5.11	6.91	0.30
Ta	0.92	3.60	2.97	3.90	3.52	2.23	3.70
La	17.53	3.71	4.25	6.30	6.15	3.58	3.40
Ce	33.57	8.12	8.54	13.20	12.56	7.13	6.43
Nd	14.73	3.51	3.95	5.34	5.78	3.33	2.76
Sm	3.00	0.89	1.10	1.42	1.36	0.95	0.89
Eu	0.58	0.24	0.26	0.29	0.31	0.24	0.23
Gd	2.01	1.06	1.15	1.42	1.32	1.05	0.99
Tb	0.23	0.20	0.20	0.24	0.22	0.19	0.18
Yb	1.43	1.09	1.20	1.51	1.43	1.10	0.78
Lu	0.21	0.19	0.22	0.20	0.21	0.11	0.09
La/YB	12.26	3.4	3.54	4.17	4.3	3.25	4.36
Tot.REE	85.55	19.01	20.87	34.09	29.34	20.93	20.11

Figure 4.1d Major and trace elements for the Rochail granite

	RL402	RL112	RL203	RL223	RL210	RL202	RL201	RL412	RL101
SiO2	63.26	67.67	67.82	68.16	68.68	68.85	69.1	69.94	70.56
Al2O3	16.23	15.25	15.79	15.12	15.17	15.72	15.4	15.69	15.18
Fe2O3	3.55	4.97	2.08	2.23	2.04	1.91	2.17	1.73	1.79
MgO	2.42	1.56	1.46	1.45	1.23	1.35	1.51	0.81	0.76
CaO	2.16	0.25	1.38	1.03	1.45	1.15	1.38	0.83	0.63
Na2O	3.92	3.41	4.38	4.26	4.08	4.29	3.8	3.77	3.89
K2O	5.77	3.73	4.81	4.53	4.86	4.78	4.78	5.35	4.98
TiO2	0.98	0.7	0.41	0.5	0.33	0.38	0.41	0.34	0.29
MnO	0.08	0.07	0.04	0.05	0.04	0.03	0.04	0.03	0.04
P2O5	1.14	0.16	0.23	0.26	0.29	0.17	0.29	0.2	0.13
LOI	0.10	2.22	1.91	1.39	1.17	1.02	1.44	0.91	0.99
TOTAL	99.61	99.99	100.31	98.98	99.34	99.65	100.32	99.6	99.24
Y			12			13	12		10
Sr	945		567		546	649	532	716	620
Rb	285		211		237	231	174	218	184
Zr			175			167	170		145
Nb			11			14	12		12
Ba	2149		1377		1211	1560	1194	1174	1182
Co									4
Cu	115		68		71	69	77	58	45
Cr									
Ni	44				14				
V	114				12	12		132	11
U	5.9	6.65		8.14	5.25	5.42	7.81		
Th	34.53	26.24		27.81	22.25	22.69	34.66	23.07	
Hf	8.37	6.19		6.01	4.98	5.35	4.56	4.82	
Sc	8.74	4.3		5.21	2.76	4.53	3.87		
Cs	25.68	7.94		9.43	6.44	7.64	8.67		
Ta	1.33	0.86		1.01	0.71	0.93	0.7	0.94	
La	35.16	25.06		30.62	15.7	25.2	41.19	33.34	
Ce	90.98	52.38		58.64	34.35	51.78	78.9	63.03	
Nd	34.32	27.49		30.22	21.27	26.92	31.36	24.64	
Sm	9.61	4.87		5.37	4.24	4.36	4.88	3.1	
Eu	1.48	1.07		1.12	0.95	0.96	0.77	0.92	
Gd	5.58	2.83		3.39	2.69	2.81	3.26	2.66	
Tb	0.49	0.25		0.35	0.28	0.3	0.37	0.4	
Yb	1.29	0.86		0.98	0.81	0.89	0.54	0.8	
Lu	0.16	0.13		0.13	0.09	0.12	0.08	0.19	
La/Yb	27.26	29.14		31.24	19.38	28.31	76.28	41.68	
Tot. REE	173.49	112.11		127.43	77.69	110.53	158.09	126.42	

Figure 4.1d (contd.)

	RL127	RL213	RO207	RL108	RL207	RL110	RL121	RL111
SiO2	70.96	71.1	71.43	71.68	71.81	72.38	72.66	73.16
Al2O3	14.36	14.75	14.87	14.63	14.89	15.15	15.34	14.09
Fe2O3	1.58	2.1	0.98	1.64	1.26	1.14	1.03	0.91
MgO	0.96	1.18	0.39	0.94	0.59	0.31	0.47	0.35
CaO	0.5	1.3	0.63	0.13	0.73	0.01	0.25	0.31
Na2O	3.82	3.89	4.46	3.92	3.86	4.77	4.67	4.32
K2O	4.81	3.73	5.49	5.02	4.92	4.29	4.45	4.9
TiO2	0.22	0.41	0.53	0.31	0.19	0.15	0.22	0.05
MnO	0.03	0.04	0.07	0.04	0.03	0.02	0.03	0.04
P2O5	0.06	0.26	0.11	0.15	0.08	0.14	0.23	0.1
LOI	1.43	1.23	0.4	1.12	1.04	1.1	0.67	0.75
TOTAL	98.73	99.99	99.36	99.58	99.4	99.46	100.02	98.98
Y			10	9	10	8	9	
Sr			146	361	377	446	593	
Rb			341	195	185	172	202	
Zr			35	143	100	101	89	
Nb			15	9	9	8	7	
Ba				1104	992	1829	1676	
Co			1.75	4		3		
Cu			7	67	66	46	48	
Cr							10	
Ni								
V				39		28	27	
Zn								
U			6.5		4.21		0.45	
Th			2	23.96	15.01	20.18	11.63	
Hf			1.31	5.2	3.63	4.18	3.42	
Sc			3.13		3		2.64	
Cs					9.3		4.66	
Ta			5.77	0.75	0.74	0.65	0.66	
La			3.3	47.18	21.62	25.49	14.42	
Ce			9.4	81.98	39.53	49.45	29.06	
Nd			5.04	31.08	16.6	23.09	13.56	
Sm			1.26	4.05	2.69	2.99	2.63	
Eu			0.12	0.95	0.57	0.9	0.69	
Gd			1.49	2.43	1.75	1.87	1.9	
Tb			0.28	0.23	0.19	0.19	0.24	
Yb			1	0.96	0.71	0.86	0.73	
Lu			0.06	0.15	0.12	0.14	0.09	
La/Yb			3.3	49.15	30.45	29.64	19.75	
Tot. REE			20.46	166.58	82.03	103.11	61.42	

Figure 4.1d (contd.)

	RL109	RL100
SiO2	73.4	74.18
Al2O3	15.01	13.86
Fe2O3	1.01	0.75
MgO	0.15	0.22
CaO	0.19	0.25
Na2O	4.41	3.61
K2O	4.85	5.97
TiO2	0.21	0.04
MnO	0.02	0.02
P2O5	0.06	0.09
LOI	0.92	0.62
TOTAL	100.23	99.61
Y	7	10
Sr	404	303
Rb	196	181
Zr	76	57
Nb	7	10
Ba	810	652
Co	2	1
Cu	33	42
Cr		
Ni		
V	11	26
U		
Th	8.27	9.15
Hf	2.81	2.25
Sc		
Cs		
Ta	0.48	0.74
La	13.77	7.73
Ce	24.76	21.91
Nd	11.11	11.26
Sm	1.89	1.92
Eu	0.52	0.47
Gd	1.53	1.86
Tb	0.22	0.31
Yb	0.83	1.01
Lu	0.1	0.21
La/Yb	16.59	7.65
Tot. REE	53.2	44.82

Table 4.2a Major and trace element analyses for the Quatre Tours diorite

	RO506	RO514	RO503B	RO659	RO125	RO660	RO662	RO504	RO661	RO658
SiO2	47.75	53.72	58.26	59.20	59.40	59.53	60.20	61.25	61.85	62.34
Al2O3	10.42	12.62	15.86	13.08	14.23	13.75	13.54	15.00	13.76	14.17
Fe2O3	3.76	6.36	5.99	6.86	4.37	6.67	6.33	4.99	5.64	5.45
Mgo	5.55	6.47	6.10	6.59	3.41	6.48	6.00	4.44	5.51	5.47
CaO	9.25	5.88	1.40	4.52	3.60	4.51	4.45	1.26	4.09	3.59
Na2O	1.11	1.65	1.29	2.55	2.33	3.42	3.29	2.57	3.44	3.45
K2O	5.42	6.63	4.97	5.53	7.88	4.09	4.65	4.49	4.25	4.16
TiO2	1.49	1.74	1.05	0.89	0.70	0.86	0.82	1.09	0.79	0.74
MnO	0.31	0.14	0.07	0.10	0.06	0.10	0.10	0.04	0.09	0.09
P2O5	1.18	1.36	0.83	0.66	1.30	0.58	0.61	0.80	0.57	0.53
LOI	12.74	3.14	3.72	0.00	1.96	0.00	0.00	3.01	0.00	0.00
Total	98.98	99.71	99.54	100.00	99.24	100.00	100.00	98.94	100.00	100.00
Y	41.00	36.00	20.00	24.00	31.00	21.00	24.00	16.00	17.00	17.00
Sr	620.00	671.00	511.00	799.00	833.00	962.00	1055.00	259.00	1023.00	954.00
Rb	524.00	435.00	146.00	225.00	498.00	172.00	179.00	199.00	166.00	186.00
Zr	429.00	679.00	435.00	381.00	548.00	308.00	353.00	210.00	295.00	281.00
Nb	29.00	37.00	29.20	24.00	36.00	19.00	25.00	22.60	17.00	18.00
Ba	2204.00	2747.00	3177.00	4188.00	2700.00	2777.00	3850.00	2160.00	2619.00	2378.00
Co	171.00	189.00	161.00		14.30			145.00		
Cu	24.00	133.00	35.00	24.00	23.00	60.00	37.00	37.00	50.00	17.00
Cr	493.00	384.00	411.00	306.00		300.00	232.00	319.00	245.00	250.00
Ni	115.00	201.00	164.00	108.00		113.00	100.00	62.00	100.00	99.00
V	167.00	203.00	137.00	125.00		119.00	109.00	169.00	101.00	94.00
Zn				78.00		73.00	72.00		69.00	72.00
U	17.40	11.43	11.75	7.00	13.00	7.83	8.12	24.87	4.00	7.48
Th	47.47	73.97	73.00	17.63	73.40	28.23	44.21	38.74	34.25	31.75
Hf	10.95	18.62	13.33	3.90	15.80	6.11	7.81	6.94	8.46	6.24
Sc	18.14	20.04	19.35	4.00	0.00	16.01	15.44	21.61	16.77	14.68
Cs	5.64	20.09	2.75	5.30	0.00	8.38	7.42	6.32	8.21	3.60
Ta	1.82	2.48	2.48	4.94	2.45	1.19	1.98	1.13	1.05	1.49
La	84.60	96.59	64.10	18.20	67.60	49.74	70.16	61.52	46.79	40.60
Ce	171.90	221.20	145.92	40.85	179.30	97.99	142.65	101.12	113.91	87.57
Nd	117.20	124.92	78.46	15.75	105.90	46.04	66.20	49.92	53.39	46.58
Sm	22.25	22.60	14.56	2.57	20.18	8.89	11.56	8.04	10.11	8.64
Eu	0.89	4.02	2.07	0.76	3.31	2.10	2.65	1.43	2.17	2.06
Gd	10.92	11.94	7.13	1.86	12.21	8.28	12.21	4.24	11.15	5.73
Tb	0.57	0.82	0.37	0.35	1.17	1.56	2.30	0.29	2.10	1.08
Yb	1.51	1.85	1.43	1.21	1.26	1.26	1.33	1.39	1.23	1.28
Lu	0.24	0.29	0.40	0.17	0.40	0.20	0.29	0.15	0.19	0.18
TotalREE	410.10	484.20	314.40	81.72	391.30	216.10	309.30	228.10	241.00	193.70
La/Yb	56.03	52.21	44.83	15.04	53.65	39.48	52.75	44.26	38.04	31.72

Table 4.2b Major and trace element analyses for the Belle Cote syenites.

	RO307	RO308	RO317	RO313	RO314	RO315	RO219	RO312	RO213
SiO2	45.18	47.79	49.50	49.77	50.33	51.04	51.11	51.88	52.11
Al2O3	14.46	14.60	11.66	9.81	11.63	10.04	9.95	10.27	11.93
Fe2O3	7.73	9.97	8.31	9.19	8.67	7.76	8.14	8.32	7.85
Mgo	5.69	7.37	10.23	12.79	10.07	9.95	12.34	11.51	7.40
CaO	7.84	4.31	7.00	8.29	7.84	9.17	7.97	7.82	5.43
Na2O	1.85	1.98	1.58	1.31	1.70	1.75	1.21	1.30	1.29
K2O	5.11	3.96	5.71	4.65	5.34	4.57	4.46	5.29	6.78
TiO2	2.39	2.57	2.19	1.56	1.84	1.81	1.48	1.46	1.16
MnO	0.17	0.09	0.11	0.15	0.14	0.13	0.14	0.13	0.12
P2O5	1.87	1.54	1.56	0.63	0.94	1.49	0.50	0.36	1.91
LOI	7.93	5.80	1.12	1.04	1.05	0.98	1.72	1.01	1.73
Total	100.22	99.98	98.97	99.19	99.55	98.69	99.02	99.35	97.71
Y	37.00	37.00		22.00			23.00	19.00	36.00
Sr	847.00	640.00	530.00	374.00	637.00	517.00	399.00	362.00	521.00
Rb	195.00	127.00	401.00	356.00	414.00	254.00	295.00	332.00	311.00
Zr	626.00	776.00		222.00			194.00	207.00	420.00
Nb	42.00	44.00		14.00			15.00	12.00	30.00
Ba	2392.00	2360.00	2742.00	1258.00	1877.00	2198.00		1434.00	3111.00
Co	22.00	25.00	0.00	32.00	17.00	38.00		76.00	44.20
Cu	13.00	12.00	35.00	99.00		69.00	18.00	606.00	43.00
Cr	307.00	296.00	539.00	917.00	519.00	552.00		130.00	
Ni	168.00	198.00	264.00	716.00	310.00	321.00	99.00		93.00
V	193.00	217.00	212.00	215.00	209.00	197.00			
Zn									
U	8.91	5.50		4.08			4.00	4.80	9.30
Th	38.50	44.30		22.20			23.00	22.90	51.80
Hf	16.50	19.40		6.39				6.10	13.60
Sc	26.00	24.60		28.35				26.80	21.64
Cs	9.60	7.15		7.58				6.20	8.81
Ta	2.94	2.73		0.36				0.29	1.86
La	72.32	81.87	50.09	17.34	44.62	35.93	25.50	19.05	73.50
Ce	196.02	207.68	134.19	49.07	114.90	81.54	78.30	48.69	187.60
Nd	126.79	127.82	94.07	47.46	77.03	48.71	48.40	42.70	137.10
Sm	23.32	23.62	18.80	11.43	15.12	9.13	11.27	8.57	27.07
Eu	3.90	3.87	3.36	2.10	2.79	1.93	2.03	1.77	4.68
Gd	13.75	13.52	11.70	7.40	9.55	5.67	8.12	5.41	16.17
Tb	1.25	1.15	1.18	0.80	0.99	0.57	1.02	0.56	1.51
Yb	2.25	2.36	1.47	1.51	1.61	0.96	1.45	0.98	2.40
Lu	0.35	0.34	0.27	0.24	0.21	0.18	0.27	0.14	0.31
TotalREE	440.00	462.20	315.10	137.40	266.80	184.60	176.40	127.90	450.30
La/Yb	31.14	34.69	34.07	11.48	27.71	37.43	17.59	19.44	30.63

Table 4.2b (contd.)

	RO316	RO672	RO671A	RO217	RO671B	RO674
SiO2	52.02	54.87	56.64	58.07	61.88	62.56
Al2O3	9.69	16.48	13.83	17.07	16.76	19.91
Fe2O3	7.38	7.49	7.25	4.60	3.51	2.21
Mgo	9.77	5.22	6.06	3.97	2.97	1.50
CaO	9.22	4.60	4.42	3.21	2.71	2.02
Na2O	1.84	3.15	1.97	4.97	4.28	5.40
K2O	4.50	5.87	7.52	5.26	6.68	5.65
TiO2	1.70	1.32	1.31	0.46	0.66	0.43
MnO	0.13	0.10	0.10	0.08	0.06	0.03
P2O5	1.40	0.89	0.90	0.87	0.48	0.29
LOI	0.96			1.03		
Total	98.61	100.00	100.00	99.59	100.00	100.00
Y		46.00	50.00	18.00	21.00	4.00
Sr	491.00	1156.00	857.00	129.00	1052.00	1242.00
Rb	201.00	269.00	310.00	244.00	236.00	240.00
Zr		632.00	705.00	290.00	326.00	253.00
Nb		30.00	40.00	13.00	15.00	5.00
Ba	2132.00	3743.00	3363.00		3864.00	2650.00
Co	16.00	26.23	24.16	14.90	12.42	0.00
Cu	75.00	45.00	43.00	16.00	22.00	9.00
Cr	488.00	124.00	314.00		122.00	44.00
Ni	273.00	113.00	149.00	56.00	56.00	24.00
V	174.00	131.00	132.00		61.00	39.00
Zn		98.00	87.00		47.00	39.00
U		6.89	10.62	6.00	4.14	8.00
Th		33.07	63.37	25.50	18.49	48.00
Hf		17.65	19.69	7.73	7.66	
Sc		20.71	20.51	11.10	9.58	1.00
Cs		10.09	22.69	0.00	11.57	
Ta		1.39	3.54	0.97	1.23	
La	49.65	64.93	99.50	35.70	30.10	12.00
Ce	131.28	182.38	255.80	73.85	86.68	37.00
Nd	90.05	113.29	142.41	46.72	54.40	21.00
Sm	18.13	20.87	24.96	8.19	8.17	
Eu	3.08	4.37	4.89	2.07	1.83	
Gd	11.14	3.09	4.08	5.58	1.40	
Tb	1.10	2.69	3.95	0.66	1.43	
Yb	1.30	2.47	2.41	1.25	1.01	
Lu	0.22	0.38	0.60	0.23	0.19	
TotalREE	306.00	327.83	437.69	174.20	154.48	
La/Yb	38.19	26.29	41.28	28.56	29.80	

Table 4.2c Major and trace element analyses for the Cascade de Lauvitel syenites.

	RL118	RL103	RL131	RL119	RL105	RL102	RL106	RL120	RL104
SiO2	50.10	50.12	50.45	50.59	50.96	51.08	51.14	51.61	52.89
Al2O3	11.41	11.03	15.05	12.12	11.64	12.76	11.80	13.54	15.18
Fe2O3	9.48	9.69	5.95	8.93	7.87	8.05	8.87	5.63	6.85
Mgo	8.16	10.32	3.98	8.09	8.17	7.25	6.91	5.01	4.91
CaO	7.72	6.96	5.48	6.41	5.87	5.77	6.81	6.77	3.98
Na2O	1.16	1.39	2.81	1.25	1.68	1.58	1.72	1.53	2.06
K2O	5.11	5.54	6.02	6.66	7.31	6.77	6.07	7.84	8.48
TiO2	2.13	2.02	1.60	1.99	2.21	2.29	2.56	1.88	2.12
MnO	0.15	0.13	0.22	0.15	0.13	0.14	0.15	0.18	0.08
P2O5	1.16	1.14	0.87	1.18	1.40	1.07	1.25	0.99	1.17
LOI	2.99	1.82	6.70	2.63	1.26	2.54	2.54	4.39	1.49
Total	99.57	100.16	99.13	100.00	98.50	99.30	99.82	99.37	99.21
Y	32.00	31.00		30.00	32.00	40.00	39.00	33.00	40.00
Sr	591.00	403.00	959.00	621.00	641.00	860.00	519.00	871.00	1418.00
Rb	216.00	321.00	289.00	373.00	511.00	341.00	327.00	401.00	354.00
Zr	309.00	213.00		252.00	566.00	664.00	409.00	403.00	923.00
Nb	21.00	27.00		25.00	34.00	39.00	32.00	26.00	60.00
Ba	2533.00	1568.00	2385.00	2535.00	2787.00	3175.00	2159.00	2782.00	4045.00
Co	12.00	46.00		0.00	39.00	35.00			
Cu	444.00	443.00	75.00	350.00	324.00	354.00	328.00	313.00	150.00
Cr	66.00	11.00	21.00	11.00	17.00	30.00	39.00	0.00	86.00
Ni	206.00	269.00	46.00	195.00	179.00	158.00	137.00	121.00	66.00
V	213.00	140.00	196.00	179.00	240.00	182.00	270.00	180.00	161.00
Zn									
U	7.90							9.22	1.09
Th	29.73	31.38			81.59	35.11		36.42	42.64
Hf	9.37	7.50			18.69	20.19		11.02	26.71
Sc	29.55							19.37	18.99
Cs	12.00							19.80	11.39
Ta	1.65	1.43			1.87	2.75		2.09	4.45
La	47.41	86.62			116.85	105.76		49.49	99.30
Ce	125.91	209.44			274.27	266.36		142.78	259.70
Nd	82.32	121.44			156.18	156.67		110.12	150.00
Sm	17.86	29.41			35.19	35.08		25.48	25.60
Eu	3.43	4.55			5.39	4.98		4.27	5.17
Gd	11.53	17.07			23.13	19.66		15.11	16.47
Tb	1.24	1.50			2.56	1.59		1.39	1.76
Yb	1.88	2.92			2.87	4.15		2.00	2.53
Lu	0.33	0.93			0.74	0.69		0.34	0.38
TotalREE	291.90	473.40			617.20	594.90		351.00	560.90
La/Yb	25.22	29.66			40.71	25.48		24.75	39.25

Table 4.2c (contd.)

	RL130	RL124	RL123	RL129	RL107	RL116
SiO2	55.41	55.49	55.72	57.97	61.19	62.61
Al2O3	13.06	12.92	16.75	15.46	19.22	14.99
Fe2O3	6.97	6.86	4.41	4.82	3.10	3.07
Mgo	7.01	7.14	3.03	3.75	1.93	2.96
CaO	4.48	4.54	3.66	2.95	1.61	2.67
Na2O	1.79	1.95	2.90	3.16	4.70	2.97
K2O	7.13	6.77	7.29	6.20	5.69	8.20
TiO2	1.84	1.78	1.73	1.25	0.69	0.76
MnO	0.10	0.10	0.13	0.08	0.04	0.06
P2O5	1.07	0.98	0.81	0.69	0.46	0.47
LOI	1.52	1.32	3.88	2.20	1.47	1.17
Total	100.38	99.85	100.31	98.53	100.10	99.93
Y		33.00	26.00		18.00	
Sr	792.00	665.00	1096.00	941.00	755.00	1127.00
Rb	426.00	393.00	321.00	369.00	316.00	445.00
Zr		547.00	489.00		96.00	0.00
Nb		37.00	31.00		13.00	0.00
Ba	2442.00	2239.00	2595.00	2240.00	1281.00	3131.00
Co	12.00					
Cu	400.00	390.00	159.00	158.00	83.00	150.00
Cr	18.00	18.00	19.00	12.00		31.00
Ni	217.00	203.00	44.00	63.00		50.00
V	163.00	151.00	170.00	103.00	81.00	63.00
Zn						
U						
Th						
Hf						
Sc						
Cs						
Ta						
La						
Ce						
Nd						
Sm						
Eu						
Gd						
Tb						
Yb						
Lu						
TotalREE						
La/Yb						

Table 4.2d Major and trace element analyses for the Refuge des Sources and Les Gauchoirs syenites

	RL407	RL204	RL209	RL405	RL214	RL211	RL404	RL205	RL206
SiO2	50.41	54.18	54.41	54.84	57.17	57.31	57.34	58.38	58.41
Al2O3	10.88	14.17	14.67	13.85	13.64	13.83	14.05	13.48	13.38
Fe2O3	7.82	7.69	8.05	6.85	7.11	5.43	5.88	5.03	4.84
Mgo	11.57	5.96	5.16	5.86	5.08	4.81	5.40	3.93	4.46
CaO	6.22	3.87	4.66	4.94	4.30	3.70	4.16	4.14	3.32
Na2O	1.45	2.93	3.41	2.07	2.59	2.16	3.19	2.35	2.03
K2O	5.74	4.95	4.62	7.26	5.89	6.36	6.26	6.53	6.85
TiO2	1.92	1.88	1.66	1.79	1.62	1.48	1.48	1.49	1.55
MnO	0.14	0.15	0.20	0.13	0.14	0.08	0.09	0.12	0.09
P2O5	1.52	1.12	1.12	1.13	0.98	0.92	1.18	1.02	1.01
LOI	1.67	3.00	2.12	0.87	1.61	3.81	0.95	3.23	3.54
Total	99.34	99.90	100.08	99.59	100.13	99.89	99.98	99.70	99.48
Y		34.00	46.00		39.00	24.00		27.00	24.00
Sr	889.00	390.00	376.00	585.00	332.00	666.00	925.00	595.00	493.00
Rb	401.00	346.00	370.00	431.00	342.00	288.00	383.00	328.00	282.00
Zr		595.00	493.00		543.00	353.00		537.00	534.00
Nb		45.00	51.00		46.00	31.00		37.00	36.00
Ba	3549.00	1231.00	923.00	3053.00	1287.00	1924.00	2379.00	2065.00	1872.00
Co				13.00					
Cu	854.00	282.00	212.00	228.00	234.00	282.00	246.00	226.00	270.00
Cr		14.00					52.00		
Ni	456.00	102.00	90.00	137.00	81.00	105.00	108.00	61.00	71.00
V	265.00	149.00	151.00	144.00	110.00	105.00	146.00	97.00	111.00
Zn									
U	15.66	14.01	20.21	14.16			10.13	12.22	12.23
Th	57.01	79.81	59.19	50.82			57.80	80.16	76.71
Hf	16.07	22.24	16.86	15.74			16.10	19.51	18.10
Sc	19.58	24.88	29.47	19.21			15.79	18.20	16.15
Cs	35.22	23.53	24.65	15.99			26.77	20.15	11.50
Ta	1.16	3.02	3.23	2.27			2.32	2.86	2.34
La	112.96	74.89	69.50	75.37			62.79	70.77	63.60
Ce	279.53	183.11	178.77	188.74			167.92	164.68	145.30
Nd	174.90	114.75	103.97	110.12			113.85	100.08	93.23
Sm	28.18	19.72	18.49	18.76			21.38	18.43	17.09
Eu	5.95	3.70	3.59	4.19			3.54	3.34	3.01
Gd	15.98	11.78	12.39	11.15			11.88	10.27	8.78
Tb	1.33	1.10	1.41	1.03			0.94	0.82	0.55
Yb	1.77	2.69	3.59	2.20			1.72	1.93	1.69
Lu	0.28	0.42	0.54	0.30			0.30	0.26	0.31
TotalREE	620.9	412.20	392.20	411.9			384.3	370.60	333.60
La/Yb	63.82	27.84	19.36	34.26			36.51	36.67	37.63

Table 4.2d (contd.)

	RL212	RL215	RL216	RL402	RL219	RL218
SiO2	59.35	62.59	63.25	63.26	63.27	63.72
Al2O3	13.25	14.20	14.58	16.23	14.00	13.59
Fe2O3	5.51	3.96	4.05	3.55	4.16	4.41
Mgo	4.44	2.75	3.33	2.42	3.28	3.52
CaO	4.23	2.85	2.91	2.16	3.18	2.51
Na2O	2.28	2.41	3.22	3.92	2.60	2.62
K2O	7.13	7.90	5.95	5.00	6.96	6.32
TiO2	1.44	1.34	1.02	0.77	0.98	1.13
MnO	0.10	0.07	0.08	0.08	0.10	0.09
P2O5	0.89	0.62	0.62	0.98	0.65	0.72
LOI	1.52	1.46	1.28	1.14	1.24	1.77
Total	100.14	100.15	100.29	99.51	100.42	100.40
Y	25.00					
Sr	529.00	560.00	467.00	945.00	380.00	355.00
Rb	381.00	411.00	347.00	285.00	338.00	349.00
Zr	472.00					
Nb	31.00					
Ba	1714.00	1876.00	1674.00	2149.00	1754.00	1742.00
Co						
Cu	240.00	140.00	171.00	115.00	158.00	190.00
Cr						
Ni	81.00	43.00	51.00	44.00	68.00	57.00
V	97.00	56.00	45.00	114.00	54.00	60.00
Zn						
U	5.90					
Th	34.53					
Hf	8.37					
Sc	8.74					
Cs	25.68					
Ta	1.33					
La	35.16					
Ce	90.98					
Nd	34.32					
Sm	9.61					
Eu	1.48					
Gd	5.58					
Tb	0.49					
Yb	1.29					
Lu	0.16					
TotalREE	179.1					
La/Yb	27.26					